University of Strathclyde
Department of Bioengineering

A Wound Infection Monitoring System

Malcolm Farrow, MEng

A thesis presented in the fulfilment of the requirements
for the degree of Doctor of Engineering

December 2010

This thesis is the result of the author's original research. It has been composed by the author and has not been previously submitted for examination which has led to the award of a degree.

Signed:  Date: 10/8/2011

Abstract

Infection control is a key aspect of wound management strategies. An infected wound results in chemical imbalances in the wound and may lead to prolonged healing times and wound surface degradation. Wound dressings changes may result in damage to healing tissues and an increased risk of infection.

This thesis presents details of a measurement system based on sensors that can be placed at the wound-dressing interface and potentially monitor the bacteria in real time. Two systems were developed, one to grow bacteria in suspension and the second to encourage biofilms to grow on the electrode surfaces. Both systems allow the electrical impedance to be measured and were used to evaluate the impedance characteristics of bacterial growth with two sensor materials, silver-silver chloride and carbon. The bacteria *Staphylococcus aureus* and *Staphylococcus epidermidis* were selected as species commonly isolated from wounds.

The growth of bacteria was confirmed by plate counting methods from the suspensions and by microscopy staining techniques of the biofilms. The impedance data was analysed for discernible differences in the impedance profiles to distinguish the absence and/or presence of bacteria. Equivalent circuit modelling was performed to provide further information on the physical processes occurring within the systems.

The main findings were that the impedance profiles of silver-silver chloride sensors in bacterial suspensions could detect the presence of high cell densities. However, the electrodes tended to inhibit the growth of bacteria and also prevented biofilms forming on the electrode surfaces. The *Staphylococcus aureus* strains adhered to the carbon sensors and in at least one strain the impedance profiles had discernible differences. All the strains with carbon sensors produced noticeable differences in the equivalent circuit model analysis. These results show that there is potential to create a real-time infection monitor for wounds.

Acknowledgements

Firstly I would like to thank my supervisors Professors Patricia Connolly and Iain Hunter for their advice, enthusiasm and support throughout my EngD. I would like to acknowledge the EPSRC for providing the funding for the Doctoral Training Centre in Medical Devices that allows for interdisciplinary research in this field. I would also like to thank the technicians, in particular Brian Cartlidge for his advice and assistance in the experiments and David Robb who helped in the construction of the test rigs. A thank you also to fellow students and staff in both the department of bioengineering and the microbiology group for all their efforts. Finally I would like to thank my friends and family for all their support.

Symbols

$\|Z\|$	Impedance magnitude
A	Plate area
A	Cross-sectional area of current flow
c	Ionic concentration
C	Capacitance
C_{GC}	Gouy and Chapman capacitance
C_H	Helmholtz double layer capacitance
C_s	Stern capacitance
d	Plate separation
e	Electronic charge
F	Faraday's constant
I	Current
I_s	Ionic strength
I_{out}	Output current
j	Imaginary number
k	Boltzmann constant
k^{-1}	Debye length
l	Length of material
n	Ion concentration
R	Resistance
t	Time
T	Temperature
u	Ion mobility
V	Voltage
V_{in}	Input voltage
X	Reactance
Z	Impedance
z	Valence of ion species
Z'	Real component of impedance
Z''	Imaginary component of impedance
ε	Dielectric permittivity
ε_o	Permittivity of free space
ε_r	Relative permittivity of the material
θ	Phase angle
ρ	Resistivity
σ	Conductivity
ψ	Potential
ω	Angular frequency

Abbreviations

Ag-AgCl	Silver-silver chloride
CFU	Colony forming units
CLSM	Confocal laser scanning microscopy
CRP	C-reactive protein
DEP	Dielectrophoresis
DNA	Deoxyribonucleic acid
ECM	Extracellular matrix
ELISA	Enzyme-linked immunosorbent assay
EPS	Extracellular polymeric substance
EWMA	European wound management association
HAI	Hospital acquired infections
KCl	Postassium chloride
MHB	Mueller-Hinton broth
MMP	Matrix metalloproteinase
MRSA	Methicillin resistance *Staphylococcus aureus*
PBS	Phosphate buffered saline
PCR	Polymerase chain reaction
PMN	Polymorphonuclear leukocytes
PTFE	Polytetrafluoroethylene
RNA	Ribonucleic acid
SAM	Self-assembled monolayer
SEM	Scanning electron microscope
TIME	A framework for wound management

Contents

List of tables

List of figures

1 Wounds, infection and detection of bacteria

Wounds in the skin provide an ideal environment for bacteria to inhabit which can lead, by stages, to an established infection when the human immune system struggles to reduce the numbers of bacteria. Infected wounds create complications, for example, they heal more slowly and the type of bacterial infection has to be identified to allow the correct treatment of antibiotics to be given. In some cases wound infection can lead to serious complications including sepsis or limb amputation. Current methods to detect infected wounds and identify bacteria are invasive, increase the chance of infection and are also slow, costly and labour intensive. This may delay both the wound healing and the time treatment can be started.

This thesis presents the results of a preliminary investigation into the development of a medical device that will address the problems of detecting infection and provide better management of infected wounds. The layout of this thesis follows a traditional structure with the literature review in chapter 1, the materials and methods in chapter 2, the results in chapters 3 and 4 and finally the discussion in chapter 5.

The field of wound care and detecting infection covers an extensive range of topics. Chapter 1 begins with an overview of bacteria including their structure, growth and biofilms. Next a summary of wounds and wound healing is described. The bacteria and wounds are then brought together in the topic of infected wounds. This leads on to the current diagnosis and treatment of wounds and infected wounds plus the microflora commonly isolated from wounds. The current detection of infection has limitations and therefore a significant proportion of research is investigating potential diagnostic tools that would lead to improved treatment of wounds. One potential diagnostic tool is biological impedance and this topic is expanded with its theory and techniques, particularly its use in tissue and bacteria studies. The final topic is current devices and electrodes that are used in wounds. Combining these topics brings the field to the objectives of this investigation.

1.1 Bacteria

Bacteria are single-celled microscopic organisms that are capable of performing the essential tasks for sustaining independent life. These include growth, energy production and reproduction. A micrograph of one species of bacteria, *Staphylococcus aureus*, is illustrated in Figure 1-1. This section provides an overview of the structure of bacteria, their growth and formation of biofilms.

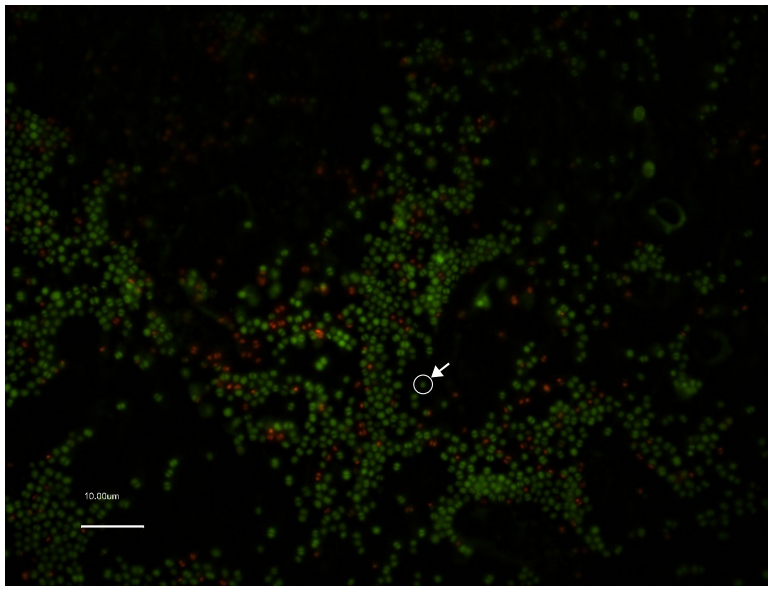

Figure 1-1. A micrograph of *Staphylococcus aureus* stained with a LIVE/DEAD *Bac*Light stain. The bacteria have been grown on a polyethylene surface. The green colour indicates healthy cells and the red colour damaged cells. Each circle is an individual bacteria as illustrated by the white ring and arrow. The scale bar indicates 10μm.

1.1.1 Structure of bacteria

The cell morphology of bacteria varies, however there are a number of key shapes: a coccus is a round bacterium; a rod is a cylindrical shape; and a spirillium is a curved rod shaped bacteria. In addition bacteria may have distinct shapes, for example, spirochetes are tightly coiled bacteria, there may be extensions in the form of tubes and stalks, and filamentous bacteria are long thin cells. Cells on average are between 1 and 10μm in diameter. Examples of bacteria include *Staphylococcus aureus* which are cocci, form clusters and are approximately 0.8μm in diameter, and *Escherichia coli* are rods and are approximately 1 x 2μm in size.

Bacterial cells contain a number of key structures, illustrated in Figure 1-2. The protective shell of a bacterium consists of a cytoplasmic membrane and a cell wall. The cytoplasmic membrane consists of phospholipid bi-lipid molecules with various proteins involved in the synthesis of substances, transport of ions and molecules, energy systems and sensors. The cell wall provides protection, shape and structure to the bacterium. In addition some bacteria have a protective capsule or slim layer surrounding the cell wall. Inside the cytoplasmic membrane is the cytoplasm which consists mainly of water with ribosomes, nutrients, ions, enzymes, molecules and waste products. These are involved in synthesis, maintenance and metabolism. The nucleoid, commonly a loop of DNA, holds the information necessary for cell function and growth.

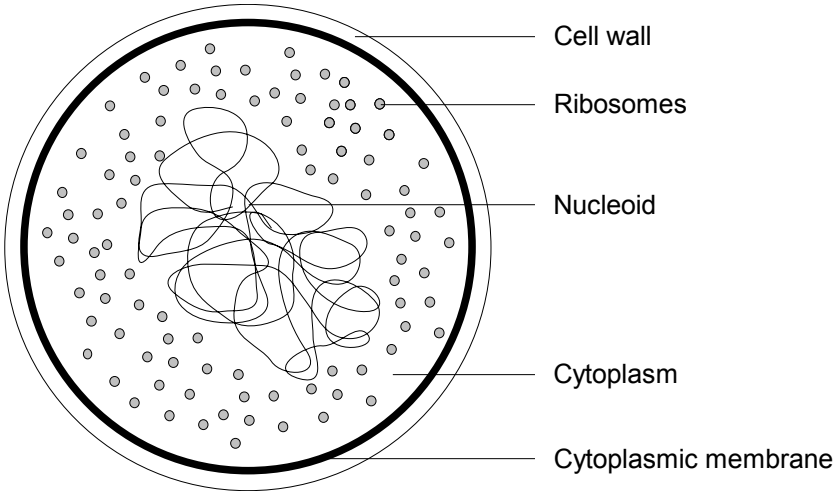

Figure 1-2. The main components of a bacterial cell.

The structure of the cell wall is used to divide bacteria into two classifications, Gram-positive and Gram-negative, which are based on the results of the Gram stain test. The differences are illustrated in Figure 1-3. The main component of cell walls is peptidoglycan, a polysaccharide containing sugar derivatives and amino acids. The peptidoglycan form a repeating structure in three dimensions. Gram-positive bacteria have a thick wall, 30-100nm, made of peptidoglycans and containing teichoic acids and proteins. In contrast Gram-negative bacteria have a thin wall, 20-30nm, which has an inner layer made from peptidoglycan and an outer membrane composed of an inner phosphlipid layer and an outer lipopolysaccharide layer, where the polysaccharide is connected to the lipid.

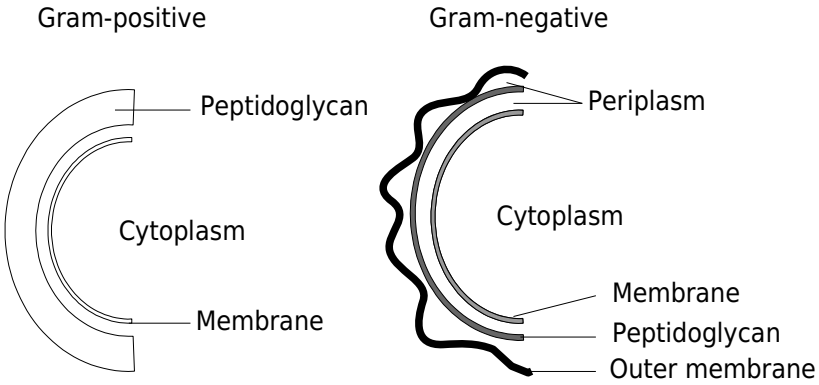

Figure 1-3. The differences between Gram-positive and Gram-negative cell walls.

1.1.2 Growth cycle of bacteria

The growth of bacteria occurs by binary fission which is the process of a cell splitting into two new cells and this results in an increase in population numbers. The time taken for the cell population to double is known as the generation time and is dependent on genetics and environmental factors, for example temperature and available nutrition. The generation times vary between 10 minutes for a few bacteria up to several days for eukaryotic microorganisms. Typical generation times in laboratory cultures are: 21 minutes for *Escherichia coli*, 28 minutes for

Staphylococcus aureus and 35 minutes for *Pseudomonas aeruginosa* (Prescott *et al.*, 2002). The generation times tend to be longer in the natural environment. Cell growth may result in the formation of cell chains, 3D structures or round clusters.

The growth cycle has four stages as illustrated in Figure 1-4. The lag phase allows the bacteria to adjust to their new environment and prepare themselves for growth. In the exponential phase the cell population doubles every generation. Once the available nutrient necessary for growth reduces or the volume of waste products increases the stationary phase occurs during which their is no net growth. Finally in the death phase the cells die.

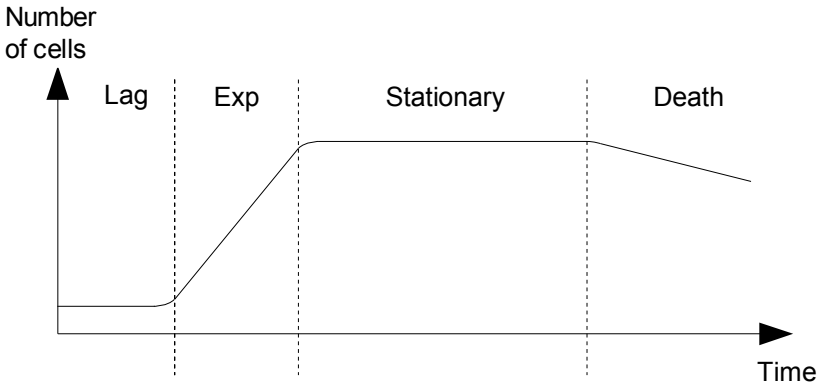

Figure 1-4. The growth cycle of bacteria.

1.1.3 Biofilms

In the natural environment bacteria form colonies known as biofilms, first described by Costerton *et al*. (1978). Biofilms have been defined as a "structured community of bacterial cells enclosed in a self-produced polymeric matrix and adherent to an inert or living surface" (Costerton *et al.*, 1999). There is no generic biofilm in terms of formation, architecture or specific molecular contents.

An example of the growth sequence of biofilms is illustrated in Figure 1-5. Planktonic bacteria encounter a surface and explore it (Costerton *et al.*, 2003). If a suitable place is located the cells attach with cell surface components. Attachment causes the extracellular matrix genes to be up regulated, for example *Staphylococcus*

epidermidis may produce accumulation associated protein or polysaccharide intercellular adhesin (Mack *et al.*, 2007). The cells first form a monolayer which then evolves into microcolonies.

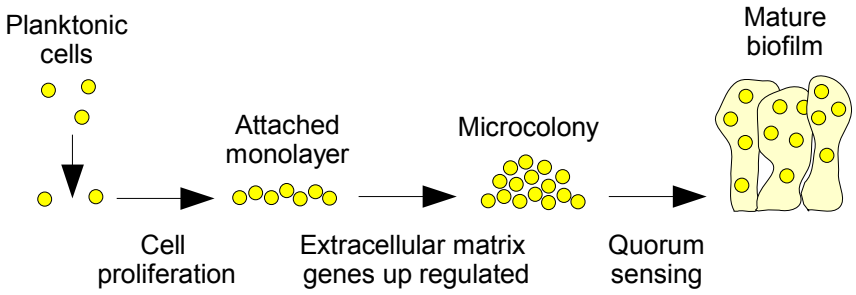

Figure 1-5. Stages of biofilm growth. Figure based on an illustration from Costerton *et al.*, 1999.

Quorum sensing systems provide cell-to-cell communication mechanisms which trigger the formation of mature biofilms. In *Staphylococcus aureus* the main quorum sensing system is the *agr* system. The formation of *Staphylococcus aureus* biofilms is more pronounced when the *agr* system is suppressed either in a mutant strain or by quorum sensing blockers (Vuong *et al.*, 2000). To allow colonisation of further areas the biofilm may disperse cells. The *agr* system in *Staphylococcus aureus* may control the changing from planktonic to biofilm states and in reverse, for example it was found that the *agr* system must be inhibited to form a biofilm and reactivated to lead to biofilm dispersal (Boles & Horswill, 2008).

The current advanced techniques to study biofilms include confocal laser scanning microscope (CLSM), magnetic resonance imaging and scanning transmission X-ray microscope (Neu *et al.*, 2010). The most common technique is CLSM where fluorescent stains are used to show cells, cell viability and components of the extracellular matrix (Donlan, 2002). An example of an imaged biofilm is illustrated in Figure 1-6. In addition CLSM can be used to study the structure, microhabits, activity and processes within biofilms, plus quantification of volumes and structures (Neu *et al.*, 2010).

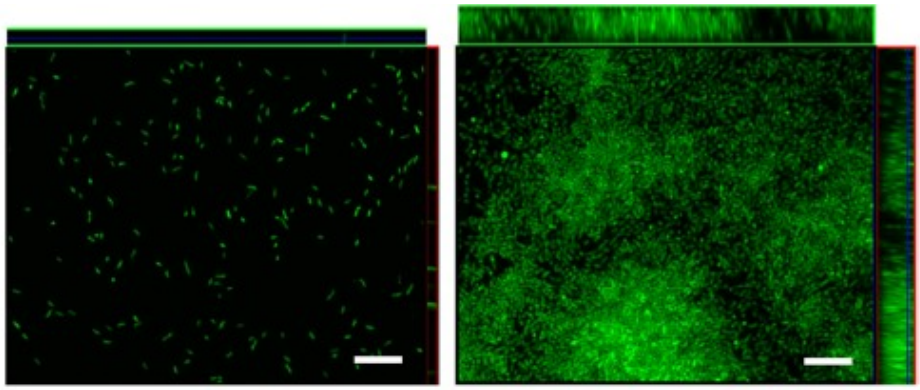

Figure 1-6. Images of monolayer (left) and multilayer biofilms (right). Biofilms were stained with Syto9 and visualised using confocal scanning laser microscopy. Scale bar is 10μm. Images from Karatan & Watnick, 2009 and reproduced with the permission of the American Society for Microbiology.

The architecture of biofilms is influenced by hydrodynamics, nutrients, cell motility and intercellular communications (Flemming & Wingender, 2010). In addition the production, quantity and contents of the extracellular matrix alters the structure of the biofilm. Three models of the structure have been proposed and include: the water channel model where mushroom shaped colonies form with significant channels for fluids; the dense biofilm model consists mostly of a two dimensional structure and has no obvious signs of fluid channels; and the heterogeneous mosaic which contains a basal layer of cells with stacked colonies rising like beads on a chain (Wimpenny & Colasanti, 1997). However the number of morphologies is likely to be more extensive than these three models.

A study of numerous biofilms showed significant variation between species and within species (Bridier *et al.*, 2010). *Escherichia coli* formed rough biofilms with small aggregates and were of variable thickness. *Pseudomonas aeruginosa* produced mushroom shaped clusters. *Staphylococcus aureus* either created flat and compact structures or consisted of patchy coverage with areas of denser growth where clumps formed. Therefore morphologies can include smooth, flat, rough, fluffy, filamentous and mushroom like macrocolonies with water filled voids (Flemming & Wingender, 2010).

The contents of most biofilms consists of less than 10% cells and over 90% extracellular matrix (Flemming & Wingender, 2010). The matrix is known as extracellular polymeric substances (EPS) and contains polysaccharides, proteins, nucleic acids, lipids and other biopolymers. Currently there is a poor understanding of the interaction and matrix integrity of these polymers at a molecular level (Karatan & Watnick, 2009).

Exopolysaccharides (sugar derivatives) are a significant portion of the EPS (Frolund *et al.*, 1996) and are long molecules that are connected to the cell surface and into a complex network between the cells. Proteins are either enzymes or structural proteins The enzymes degrade biopolymers to provide energy sources or to modify the biofilm. The structural proteins promote biofilm formation to link the cell surface to the EPS. Extracellular DNA is a major structural component in many biofilms and could also aid in gene transfers. The majority of EPS components are involved in the adhesion, aggregation and cohesion within biofilms. The other major component is water and channels within the biofilm provide nutrients and waste removal (Stoodley *et al.*, 1994).

The main function of the biofilm is to provide a protective environment for the cells in harsh environments. In clinical terms biofilms have an innate resistance to antimicrobial agents, an increased gene transfer allowing cells to become resistant and the human immune system is less effective against them (Percival & Bowler, 2004). Studies have shown that biofilms are less susceptible to antibiotics due to: impaired penetration of the antibiotics; reduced metabolic rates of bacteria, a changed micro-environment; a different gene expression; communication between cells, known as quorum sensing, which allows adaptation to the environment and the development of different phenotypes (Percival & Bowler, 2004). In summary bacteria are single-celled microorganisms that have a variety of cell structure and morphologies. In the natural environment bacteria form biofilms which are structured communities that enhance their chances of survival. The ability of bacteria to adapt to their environment makes them a significant problem in human health.

1.2 Wounds and infection

Human skin comprises three layers: the epidermis consisting of superficial epithelial cells; the dermis which is connective tissues; and the subcutaneous tissues which separate the dermis from the deep tissues and other organs. Also present in skin are additional structures which include hair, glands and blood vessels. The main components of the skin are illustrated in Figure 1-7. The skin layers fulfil many important functions, one of which is to provide a protective barrier against the invasion of bacteria into the underlying tissues and organs. If this barrier is removed, for example in the case of wounds, then the potential for infection is greatly increased. Wounds provide a moist, warm and nutritious environment for the colonisation and proliferation of bacteria (Bowler *et al.*, 2001). Measures to prevent and limit the spread of infection are essential, especially since it is not possible to eradicate bacteria from wounds (Kingsley, 2001).

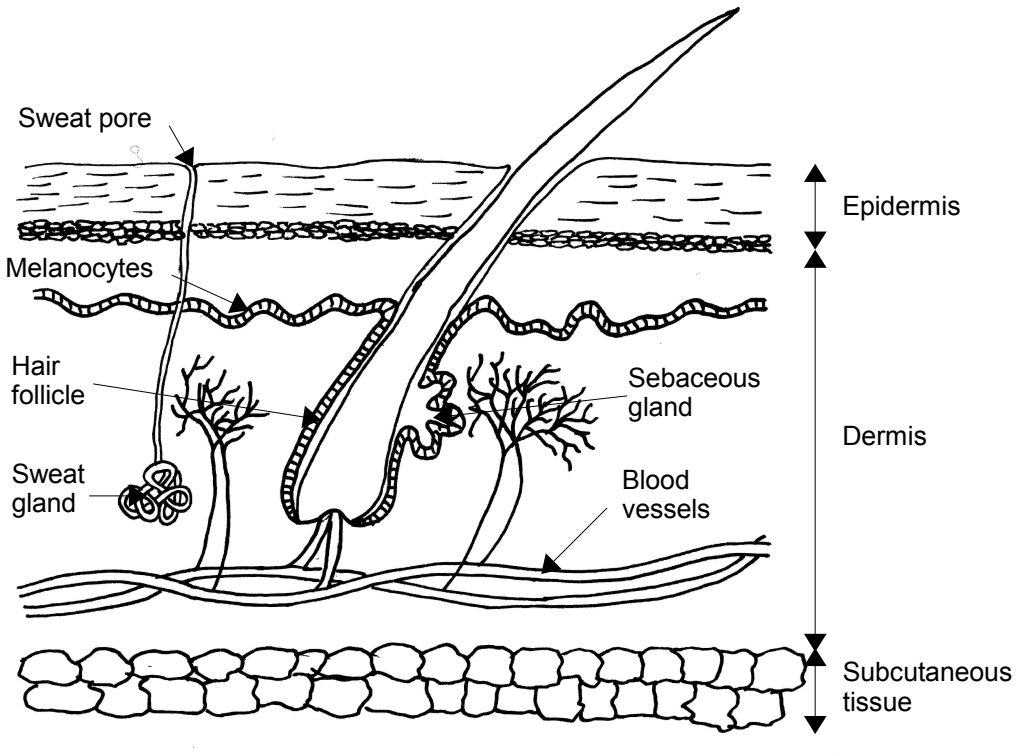

Figure 1-7. The main components of human skin.

1.2.1 Types of wounds

Wounds result from a wide variety of injuries to the skin and are categorised by the medical profession into two types: acute wounds, those which are primary injuries and normally heal within a specific time frame; and chronic wounds, those which are secondary injuries caused by a primary disease and where healing is abnormal. Typical acute wounds include minor cuts, abrasions, bites, burns, surgical wounds and traumatic injuries. Chronic wound examples are: leg ulcers, foot ulcers and pressure ulcers. Illustrated in Figure 1-8 are examples of wounds. The stages of wound healing are discussed in Section 1.2.3 and the stages of infection in Section 1.2.5

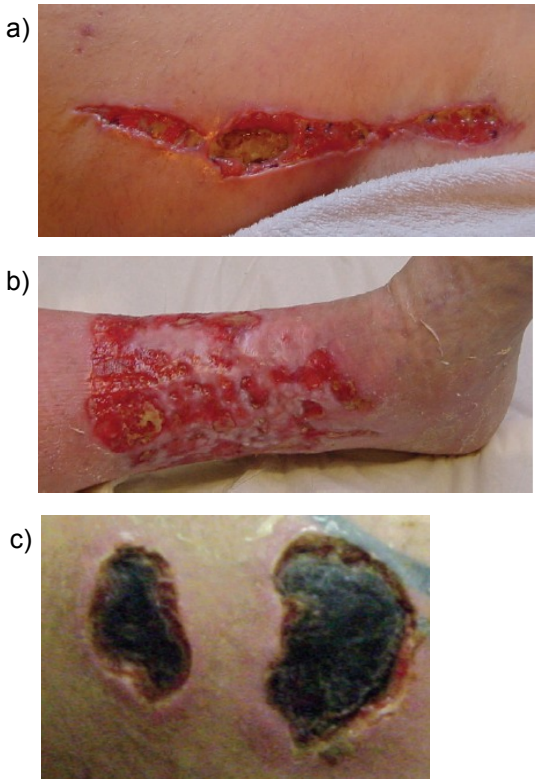

Figure 1-8. Images of different wound types: a) Surgical wound; b) Leg ulcer; and c) Burns. Images sourced from www.wounds-uk.com/wound-essentials.shtml

1.2.2 Incidence and costs of wound care

There are a significant number of wounds in a given population and many become infected. This produces a large cost involved in the healthcare of wounds. The exact incidence and costs of wound care, plus additional costs incurred when wounds become infected, are difficult to determine due to differences in wound care within and between countries and differences in decisions regarding which costs are included as part of wound care. To provide a sample of the wound care costs a selection of figures are presented. Posnett and Franks (2007) reviewed the literature and estimated the incidence and costs of common chronic wounds for the year 2005/2006. The incidence and costs are summarised in Table 1-1.

Table 1-1. **Estimated incidence and costs of chronic wounds in the UK in 2005/2006.** Data from Posnett & Franks, 2007.

Wound Type	Incidence	Cost per patient	Total annual cost
Venous leg ulcer	108,600	£1,549-£1,822	£168 million - 198 million
Pressure ulcer	370,000 - 460,000	£4,300-£6,400	£1.76 billion - 2.64 billion
Diabetic ulcer	63,700	£4,710	£300 million
		Total cost	£2.3 billion - 3.1 billion

Posnett and Franks (2007) estimated that approximately 100,000 cases of venous leg ulcers occurred in 2005/2006 and by multiplying by the cost per patient arrived at the total annual cost. However the actual incidence and hence the cost will be higher since the estimates did not include the under 65 year olds. The prevalence of diabetes in the UK population in 2002/2003 was 2.3%, of which 4.55% had active foot ulcers (Gordois *et al.*, 2003). Posnett and Franks (2007) used these figures to estimate the incidence and cost of diabetic ulcers for the year 2005/2006. However other estimates of the prevalence of diabetes have placed it as high as 5.3% in the UK (Amos *et al.*, 1997) which would increase costs, while another study placed active foot ulcers in diabetics at only 1.4% which would reduce costs (Kumar *et al.*, 1994). Overall the total estimated cost of chronic wound care in the UK for the year 2005/2006 was £2.3 billion to £3.1 billion and this is likely to increase as the UK population increases (Posnett & Franks, 2007).

In addition to the chronic wound care costs there are costs associated with other wound types, for example burns, which add to the overall wound care cost. It is estimated that 250,000 people in the UK suffer burn injuries every year with approximately 175,000 people attending accident and emergency departments (National Burn Care Review, 2001). Out of these, 13,000 are admitted to hospital and 1,000 require fluid resuscitation due to the severity of burns. The cost of burns varies depending on the severity; in an English hospital 144 patients were admitted with uncomplicated, minor paediatric scalds in the year 2002/2003, each case costing £1,850 resulting in a total cost for the year of £266,400 (Griffiths *et al.*, 2006). In comparison the cost of major burn care for three patients in Wales varied between £82,000 and £517,000 per patient (Hemington-Gorse *et al.*, 2009).

To provide an example of the incidence of infected wounds the percentage of wound types and infected wounds for a survey of NHS organisations in Hull and East Riding of Yorkshire, England are illustrated in Figure 1-9 (Drew *et al.*, 2007). The number of patients included in the study was 1,644 with a total of 2,300 wounds. The percentage of patients with surgical or trauma wounds was 43%, with leg or foot ulcers was 38.8% and with pressure ulcers was 18.1%. The percentage of wounds infected were 14.3% of surgical and trauma wounds, 13.3% of leg and foot ulcers and 10.4% of pressure ulcers, which results in an average of 12.8% of wounds infected.

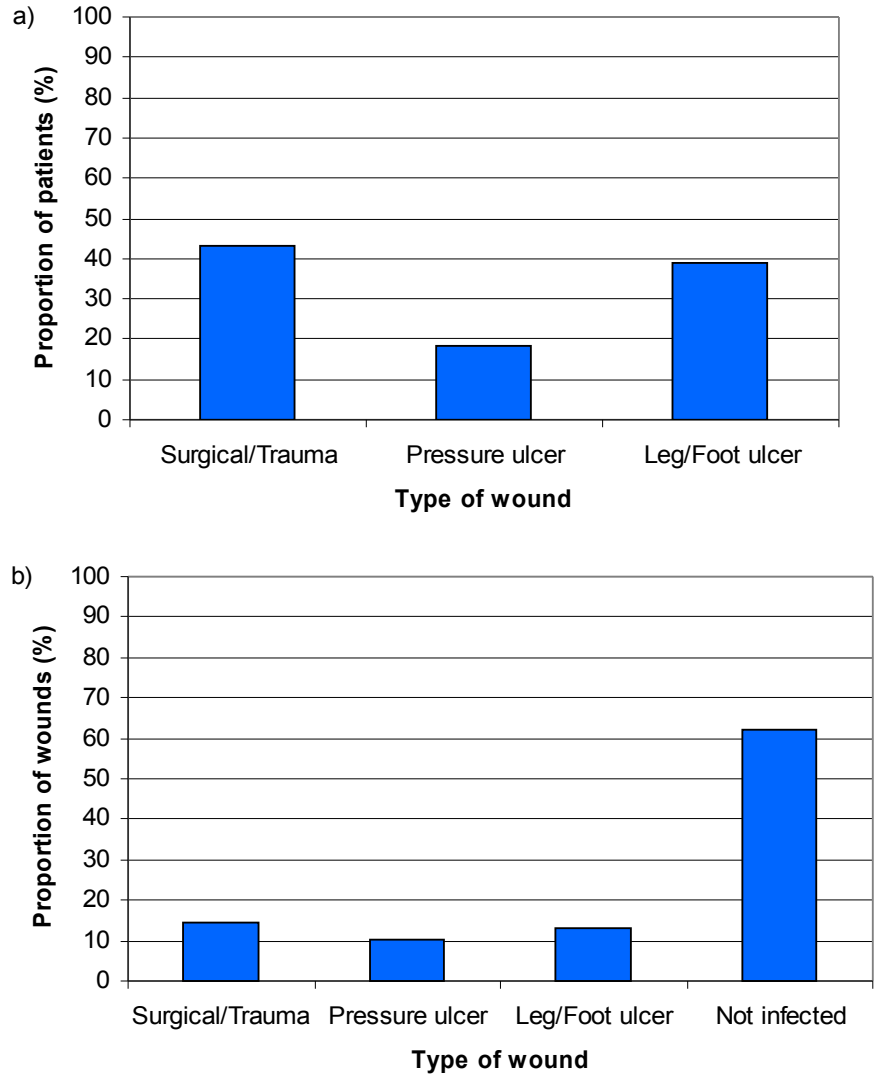

Figure 1-9. Wound types and wound infection in an NHS area: a) The percentage of patients with certain types of wounds; b) The percentage of each type of wound that was infected. Data from Drew *et al.*, 2007.

Healthcare centres are a significant source of infection for wounds and these infections are known as Hospital Associated Infections (HAI). A Scottish survey in 2005/2006 indicates that the prevalence of HAIs among patients was 9.50% for acute hospitals and 7.32% for non-acute hospitals (Reilly *et al.*, 2008). Of these HAIs 15.8% and 3.0% were surgical site infections in acute and non-acute hospitals respectively, and 11.0% and 26.8% were soft tissue or skin infections (Figure 1-10a). A survey of HAIs for England, Wales, Northern Ireland and the Republic of Ireland

in 2006 indicates that the prevalence among patients was between 5.43% and 8.19% (Smyth *et al.*, 2008). The percentage of these HAIs that were surgical site infections was between 0.5% and 11.7%, and those that were soft tissue or skin infections was between 11.0% and 26.8% (Figure 1-10b).

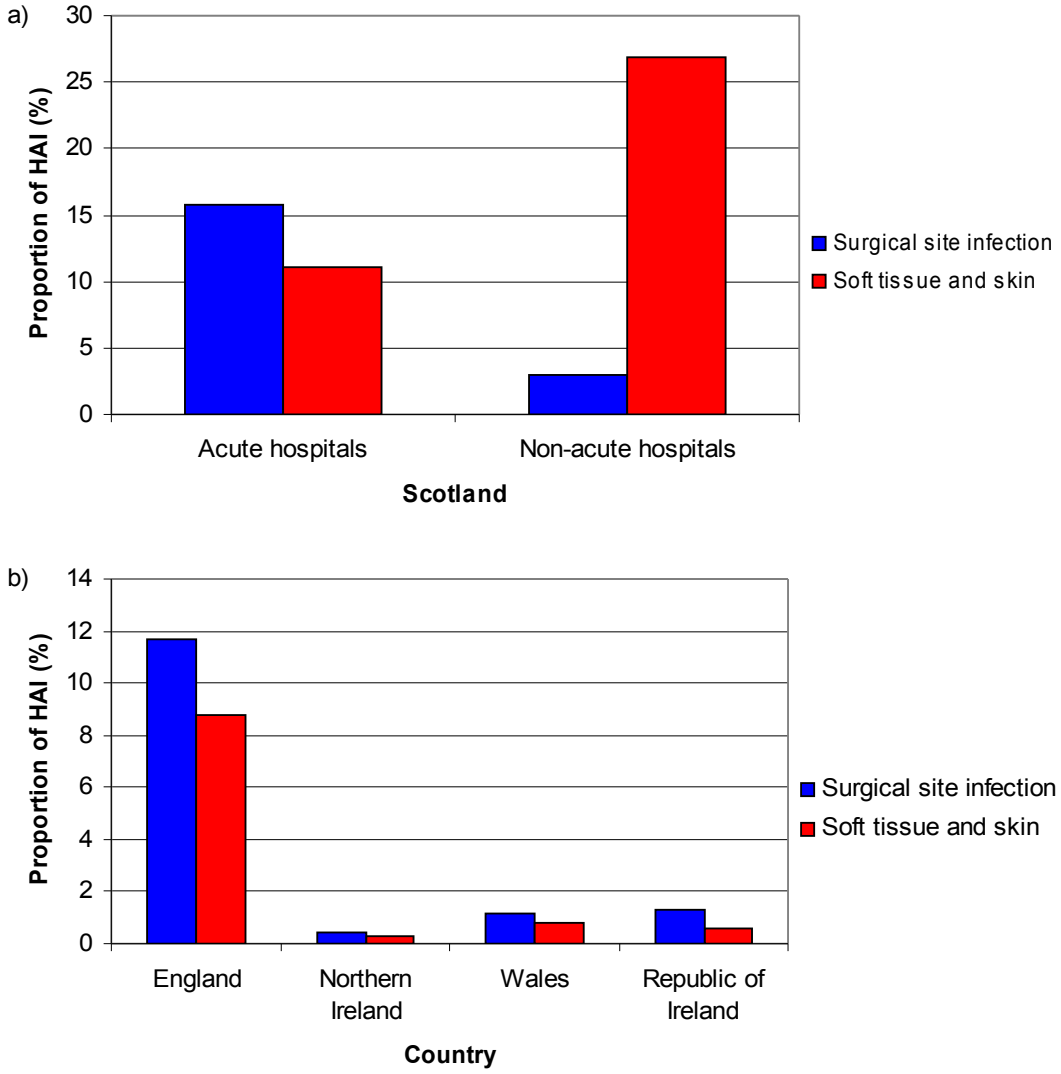

Figure 1-10. The proportion of hospital acquired infections (HAI) for surgical wounds, and skin and soft tissues: a) In Scotland. Data from Reilly *et al.*, 2008; b) In the UK except Scotland. Data from Smyth *et al.*, 2008.

Infected wounds delay healing, create longer treatments times and often require antibiotics. Both of these increase the costs associated with healing. An example of the additional costs when wounds become infected is provided by a study in an English district hospital which concluded that surgical wounds cost £3,246 per case with an additional £1,618 per case due to hospital acquired infections (Plowman *et al.*, 2001). Similarly for skin wounds the costs per patient was £3,418 plus an additional £1,790 due to infection. However it is unclear what type of diagnosis were included in the skin classification. Plowman *et al.* (2001) extrapolated from these figures and estimated the cost of hospital acquired infection for the whole of England in 2001 and placed it at £62.37 million for surgical wound infection and £41.37 million for skin infections.

Despite not knowing the exact incidence and costs of wound care, the figures shown here clearly show that there are a significant number of wounds and that these are expensive to treat especially when they become infected. This creates a significant strain on the UK healthcare system, not just in cost but also in patient welfare. Therefore there is a real need to detect infection quickly for patient well-being, and cheaply to reduce the financial burden of wound care.

1.2.3 Normal stages of wound healing

To explain how wounds become infected, the normal wound healing process must be described first. Acute wounds normally heal through four phases: haemostasis, inflammation, proliferation and remodelling, which occur within a specific time frame dependent on the severity of the wound. The main events in each of the four phases are illustrated in Figure 1-11. Chin *et al.* (2005), and Johnstone *et al.*(2007) provide a more detailed account of these phases.

Haemostasis occurs immediately and consists of three stages to stop the bleeding from damaged blood vessels (Martini, 2006). The vascular stage involves the contraction of blood vessels to reduce their diameter, the release of chemical factors and local hormones, and increased "stickiness" of endothelial cell membranes. The platelet stage involves platelets sticking to endothelial surfaces and collagen fibres, plus the release of a variety of substances which promote the aggregation of platelets and confine the platelet plug to the area of injury. Finally the coagulation stage is a complex sequence of events leading to the conversion of fibrinogen to insoluble protein fibrin which forms part of the blood clot along with blood cells and platelets.

Within 24 hours the inflammation phase begins which prepares the wound for re-growth by removing foreign and devitalised tissues. The common signs of inflammation are redness, heat, swelling and pain, caused by the secretion of enzymes, histamine and amines from mast cells. The platelet mediators and the coagulation cascade activate neutrophils which perform phagocytosis, kill bacteria with free oxygen radicals and remove foreign and devitalised tissues. Monocytes also enter the injured tissue and become macrophages which ingest and kill bacteria, remove devitalised tissues, and also secrete various growth factors and cytokines that activate fibroblasts that will build the new tissue matrix. This phase may last up to two weeks. As the wound progresses to the next stage of healing the number of macrophages decreases.

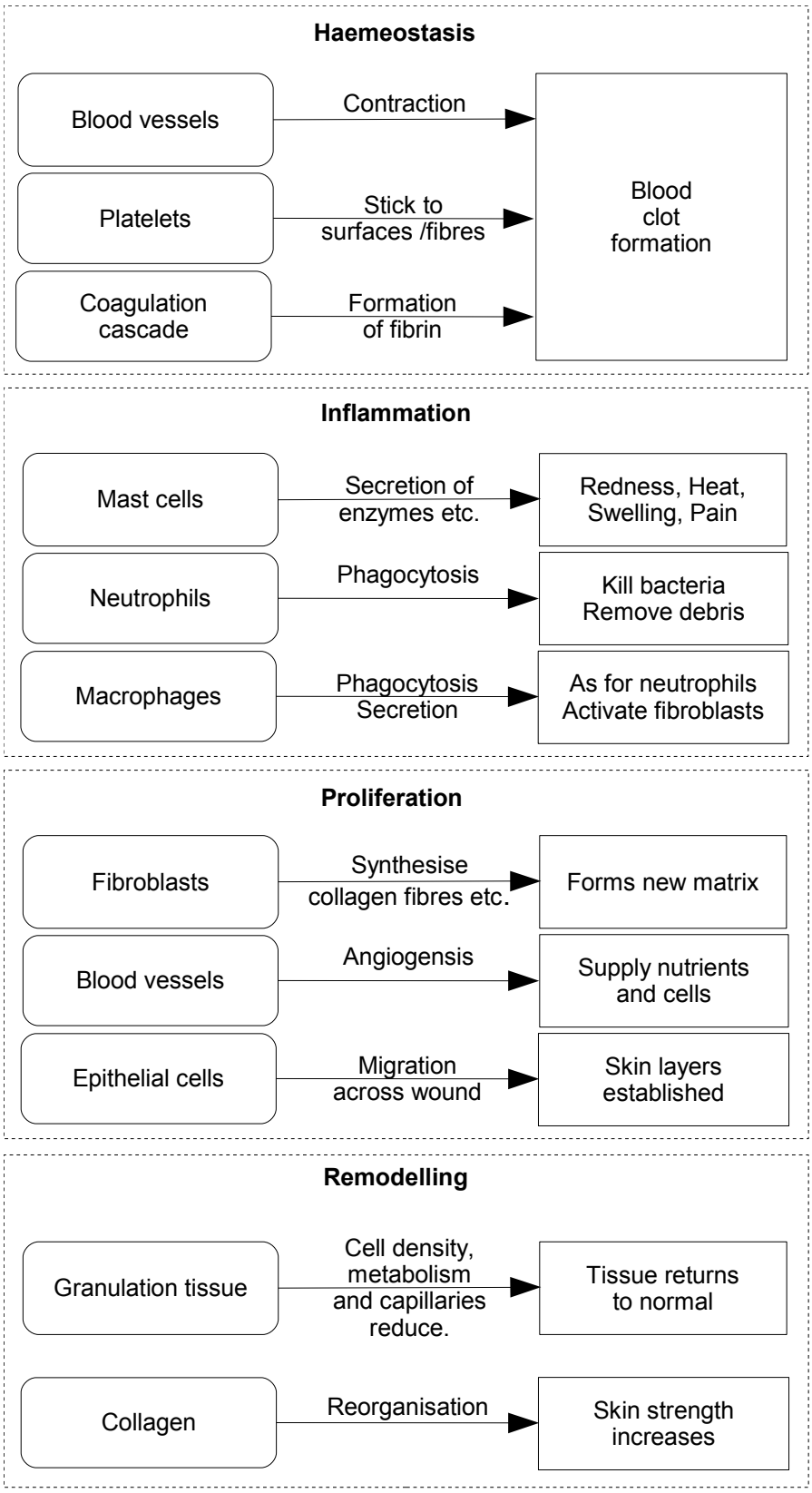

Figure 1-11. The main events occurring in the four phases of normal wound healing.

The injured area regrows in the proliferation phase. A new matrix is formed by fibroblasts synthesising collagen fibres, proteoglycans and fibronectin. Granulation tissue forms and is a temporary replacement of the normal dermis. The morphology and pink colour of granulation tissue is the result of angiogenesis, a process which replaces damaged capillaries with a dense network of capillaries to allow the supply of fibroblasts, macrophages and nutrients to the growth area. Epithelialisation occurs in parallel with the contraction and deposition of cells and involves epithelial cells migrating into the wound, connecting with other advancing cells, additional cells supplied by the basal layer; resulting in the skin layers re-establishing over time.

The final phase of remodelling occurs over several months and involves the granulation tissue maturing and tissue strength increasing as the collagen reorganises itself. The cell density, metabolic activity and number of capillaries also reduce as the healing process reaches its end.

Clinical intervention can help the healing process, depending on the type of wound. There are three clinical methods by which wounds are healed (Johnstone *et al.*, 2007): in primary intention the wound edges are held together by sutures, staples or glue; with secondary intention the wound is left open to allow the formation of granulation tissue and epithelialisation; and tertiary intention is a combination in which the wound is left open for several days to remove contamination before bringing the edges together. The clinical healing methods and the typical wounds they are used on are summarised in Table 1-2.

Table 1-2. Clinical classifications of wound healing. Data from Johnstone *et al.*, 2007.

Type	Description	Typical wounds
Primary intention	Edges brought together immediately.	Surgical wounds
Secondary intention	Left open to heal naturally.	Leg ulcers
Tertiary intention	Left open for several days before edges brought together.	Contaminated wounds

1.2.4 Chronic wound healing

Chronic wounds are the result of underlying medical conditions, for example venous disease, and the primary cause must be treated to help heal the wounds and reduce the re-occurrence of the wound. The different types of chronic wounds each have a main factor in non-healing: Diabetic ulcers have a combination of necrosis and infection; venous ulcers fail to re-epithelialise; and pressure ulcers have a loss of subcutaneous tissues (Falanga, 1993). In addition there are numerous other factors that impair healing including foreign bodies, tissue maceration, ischaemia, infection, age, malnutrition, diabetes and renal disease (Harding *et al.*, 2002).

On a cellular level chronic wound healing is delayed due to an imbalance in the chemicals involved in the healing and destructive processes (Bjarnsholt *et al.*, 2008), for example, in key proteases, cytokines, endocrine hormones and growth factors (Chin *et al.*, 2005), (Lobmann *et al.*, 2005). Chronic wound fluid reduces proliferation of keratinocytes, fibroblasts and endothelial cells (Schultz *et al.*, 2003). The inflammatory phase is prolonged by bacterial endotoxins, fragments of extracellular matrix (ECM) and cell detritus (Lobmann *et al.*, 2005). This causes the number of neutrophils to increase and produce pro-inflammatory cytokines that stimulate matrix metalloproteinases (MMP). The altered levels of MMPs cause fibroblasts to behave differently and cause the ECM to form incorrectly (Cook *et al.*, 2000a). Also the fibroblasts do not respond to growth factors which may be a cause of the re-epithielisation failure (Hasan *et al.*, 1997).

1.2.5 Infected wounds

Once a wound is present it will become contaminated either by microbes from the host's body, from airborne dust or water droplets, or from contact with clothes, equipment and carers (Cooper & Lawrence, 1996). The level of infection in a wound can be described as a five stage process from a sterile wound when first created, through colonisation to infection, in which the bacteria overwhelm the immune system and can lead to systemic infection, sepsis, and death (Kingsley, 2001). The

stages are described in Table 1-3. A wound that heals normally only reaches either the contamination or colonisation stages. If critical colonisation is reached then the wound becomes infected.

Table 1-3. The five stages of wound infection. Data from Kingsley, 2001.

Stage of infection	Description
Sterile	Very short period after the wound is created where there are no bacteria in the wound, unless wound is created by a contaminated source.
Contamination	The wound becomes contaminated with bacteria, however there is very little bacterial growth.
Colonisation	This is the normal situation in which bacterial growth is kept in check by the host's immune system.
Critical colonisation	The point at which the immune system begins to fail in keeping the bacteria in check.
Infection	The host's immune system is overwhelmed, local cellulitis forms and ulcers deteriorate.

The three factors that determine the stage of infection are bacterial numbers, virulence and host resistance (Schultz *et al.*, 2003). The importance of bacterial numbers is still debated with numbers for critical colonisation ranging between 10^4 and 10^6 colony forming units (CFU) per gram of tissue. An example is split-thickness skin grafts were applied to 30 wounds and due to the skin graft not surviving at first a total of 81 failed and 30 successful skin grafts were performed (Robson & Krizek, 1973). In 95% of the unsuccessful skin grafts the wounds contained over 10^5 CFU per gram of tissue, while 100% of the wounds with successful skin grafts contained less than 10^5 CFU per gram of tissue. In another study of 80 wounds, 20% had greater than 10^5 CFU per gram of tissue (Robson *et al.*, 1973). Wound infections

occurred in 9 of these 16 wounds. More recently the prevalence of infection was higher when the bacteria levels were greater or equal to 10^4 CFU per tissue gram in 28 wounds (Breidenbach & Trager, 1995).

Therefore wounds with bacterial levels greater than 10^4 CFU per tissue gram are more likely to have an infection, however it is not an absolute certainty and wounds with lower numbers can also became infected. An example is beta-haemolytic streptococci that can cause infections at levels of 10^2 to 10^3 CFU per gram of tissue (Schultz *et al.*, 2003). Therefore the virulence of the bacteria and the host's resistance are more significant in causing infections. Virulence is the degree of pathogenicity of microorganisms in terms of ability to invade tissues and cause fatalities. Virulence factors aid pathogens to invade hosts by promoting adhesion, suppressing the host's immune system and obtaining nutrition.

The risk factors for host resistance are numerous and include: the patient's health in terms of their immune system, diseases, tissue viability and wound type, depth and location; access to the healthcare system; and the actual treatment provided (Bowler *et al.*, 2001); (Kingsley, 2001).

In assessing wounds for infection the physical signs are highly important due to the delay in receiving reports from sampling and the fact that the presence of bacteria does not necessarily indicate infection. Clinical signs of infection are: unchangeable wound edges; an increase in serous exudate; granulation tissue that is bright red in appearance; is friable and may bleed easily; unpleasant odour; breakdown in wound tissue and increased necrosis (Schultz *et al.*, 2003). Based on physical signs of infection the European Wound Management Association (EWMA) have defined four clinical stages of infection based on the management strategy which is required and these are listed in Table 1-4 (European Wound Management Association (EWMA), 2006). The treatments are discussed further in Section 1.2.7.

Table 1-4. Clinical stages of wound infection. Data from European Wound Management Association (EWMA), 2006.

Stage	Signs of infection	Healing progress	Suggested treatment
1	Subtle. Some odour, pain or exudate.	Normal progress	Topical antimicrobial. Adjust if poor response. (Antibiotic)
2	Increasing. Increasing odour, pain or exudate.	No longer progressing normally	Topical antimicrobial. Adjust if poor response. (Antibiotic)
3	Local infection. Pus discharge, swelling, pain, erythema, warmth.	Surrounding tissue involved; unhealthy or deteriorating	Topical antimicrobial and/or broad-spectrum antibiotics. Adjust if poor response and microbiology report available
4	Local and systemic infection. Pyrexia and raised white blood cell count	Surrounding tissue evidence that may lead to sepsis and organ failure	Broad spectrum antimicrobial. Adjust if poor response and microbiology report available

The classification of burns by the healthcare profession is also based on physical signs of infection. The four categories of burn wound infections are: burn wound impetigo, characterised by the loss of epithelium from re-epithelialised surfaces; burn-related surgical wound infection, which occurs when excised burn and donor sites are not re-epithelialised; burn wound cellulitis, in which the infection extends into the surrounding skin and soft tissue; and when the infection spreads in an unexcised burn wound it is classed as an invasive infection (Church *et al.*, 2006); (Pruitt *et al.*, 1998). Surgical site infections (SSI) are classified by their location and defined as infections that occur within 30 days of a surgical procedure or within one year if an implant is left in place (Mangram *et al.*, 1999). These infections are classified as superficial, deep incisional infection, or infection of the organs or body spaces. An example of an infected surgical wound is illustrated in Figure 1-12.

Figure 1-12. An example of an infected surgical wound. Image sourced from www.wounds-uk.com/wound-essentials.shtml

The physical signs of infection are caused by changes at the cellular level and these alter the normal healing process. Bacteria at low levels may aid healing by producing proteolytic enzymes that aid wound debridement and stimulate neutrophils to release proteases (Pollack, 1984); (Stone *et al.*, 1980). At higher levels bacterial endotoxins prolong the inflammatory phase similarly to processes in chronic wounds, hence the number of neutrophils and MMPs increase causing alterations in the normal healing process (Lobmann *et al.*, 2005). Bacteria release MMPs and other pro-inflammatory mediators that delay wound healing. They also stimulate angiogenesis which causes deficient or corrupt matrix to form. Neutrophils increase in numbers and release cytolytic enzymes and oxygen free radicals that result in tissue destruction (Schultz *et al.*, 2003).

It has also been found that *Pseudomonas aeruginosa* produces rhamnolipid which reduces the host defences by lysis of polymorphonuclear leukocytes (PMN) (Jensen *et al.*, 2007). Lysis of PMNs would result in antimicrobial and tissue-devastating compounds. This may lead to increased levels of MMPs, hence more PMNs and more tissue destruction (Bjarnsholt *et al.*, 2008).

1.2.6 Biofilms in wounds

Studies have only recently started to investigate biofilms in wounds and therefore the evidence for biofilm formation is limited (James *et al.*, 2008). Some examples include, the volume of aggregates of *Pseudomonas aeruginosa* and *Staphylococcus aureus* varied in relation to the depth of the wound in 22 chronic wounds (Kirketerp-Moller *et al.*, 2008). Biofilms containing *Staphylococcus aureus*, *Escherichia coli*, *Pseudomonas aeruginosa* and mixed anaerobes were found in 7 out of 12 wounds (Deva *et al.*, 2007). Images of 50 chronic and 16 acute wounds showed that in chronic wounds Gram-positive cocci in large aggregates with extra-polysaccial substance predominated, while in contrast the acute wounds contained individual cells in small microcolonies (James *et al.*, 2008). Therefore concluding that chronic wounds were more likely to contain biofilms. An example of the micrographs showing biofilms in wounds is illustrated in Figure 1-13.

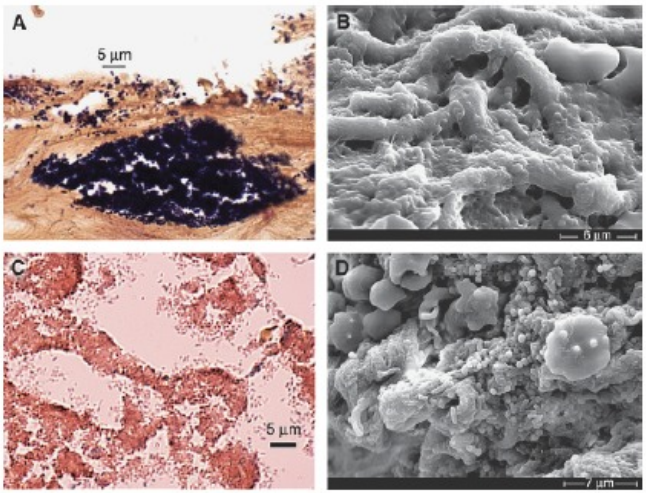

Figure 1-13. Examples of microscopic images from chronic wounds: (a) Photomicrograph of a Gram-stained thin section from a pressure ulcer specimen showing a biofilm formed by Gram-positive cocci near the tissue surface; (b) Scanning electron micrograph of pressure ulcer specimen showing a biofilm of coccoid bacterial cells colonizing collagen bundles within the wound. The bacterial cells are blanketed in extracellular polymeric substance, which had collapsed onto the cells during the dehydration steps of specimen preparation; (c) Photomicrograph of a Gram-stained thin section from a diabetic foot ulcer specimen showing a biofilm formed by Gram-negative rods near the tissue surface; (d) Scanning electron micrograph of pressure ulcer specimen showing bacteria of different morphotypes (rods and cocci) colonizing the wound within close proximity. All images taken from James *et al.*, 2008 and reproduced with the permission of John Wiley and Sons.

Biofilms may lead to a prolonged inflammatory phase due to the ineffectiveness of PMNs against the extracellular matrix of biofilms (Deva *et al.*, 2007). It has also been shown that the formation of biofilms in cutaneous wounds of mice prevented the normal re-epithelialisation of the wounds (Schierle *et al.*, 2009). Images from the control wounds and the wounds containing biofilms are illustrated in Figure 1-14. Normal healing occurred when the biofilm was disrupted by quorum sensing blockers but topical antibiotics were not shown to disrupt the biofilm.

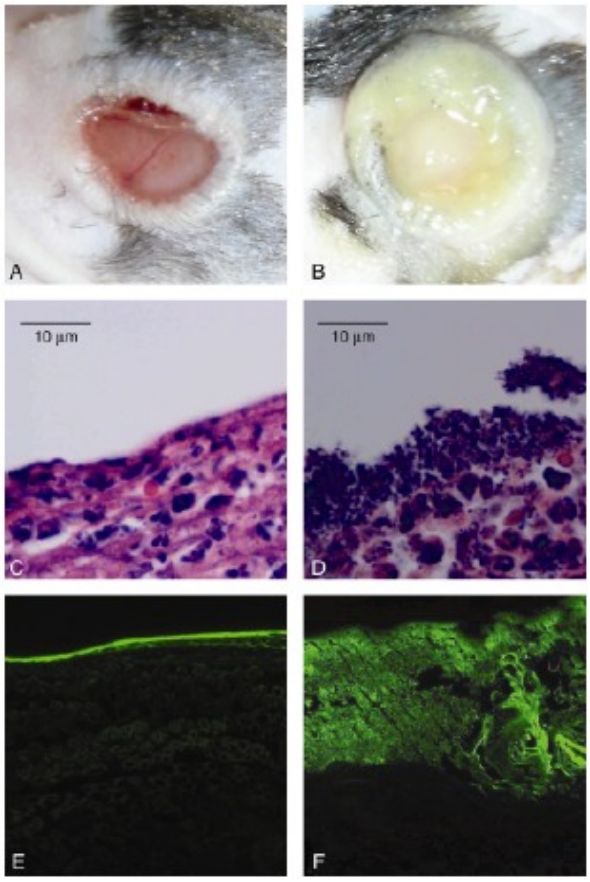

Figure 1-14. Examples of microscopic images from chronic wounds: (a) Gross appearance of uninfected control wounds; (b) Gross appearance of wound colonized by biofilms; (c) Gram stain of uninfected control wounds; (d) Gram stain of biofilm in wound bed; (e) BODIPY-stained uninfected control wound; (f) BODIPY-stained wound bed. All images taken from Schierle *et al.*, 2009 and reproduced with the permission of John Wiley and Sons.

1.2.7 Wound management

Wound management involves the assessment, treatment and re-evaluation of the treatment to ensure that the wound heals whether or not it becomes infected. The first step is to assess the wound and decide whether to perform basic or advanced wound care. The management of acute wounds is based on debridement and appropriate dressings. Debridement removes necrotic tissue and bacteria which could potentially delay healing, and the correct choice of dressing provides a moist environment that enhances the healing process. Chronic wounds and wounds that are failing to heal require more advanced techniques to re-establish the normal stages of wound healing (Section 1.2.3), by trying to change the altered cellular and molecular processes that occur in chronic wounds (Section 1.2.5) .

The wound bed is an important aspect in wound healing since this is the physical and chemical base that the wound has to heal from. Firstly any underlying diseases must be treated, and an adequate blood supply to the wound should be ensured, and the wound history and characteristics should be assessed and monitored (Schultz *et al.*, 2003). The wound bed should then be managed by debridement, exudate management and controlling the bacteria. A framework for the preparation of the wound bed to form a systematic management of non-healing wounds was developed by the International Wound Bed Advisory Board (Schultz *et al.*, 2003). This framework was given an acronym TIME (Flanagan, 2003) and these terms were further developed by the European Wound Management Association (EWMA) (European Wound Management Association (EWMA), 2004). The TIME framework is listed in Table 1-5 and links clinical observations, cellular abnormalities, clinical treatments and their cellular effects.

Table 1-5. The TIME framework for wound bed preparation. Data from European Wound Management Association (EWMA), 2004.

TIME elements	Pathophysiology	Suggested treatment	Clinical result
Tissue management	Defective matrix and debris inhibit healing	Debridement	Viable wound base
Inflammation and infection control	High bacterial counts/prolonged inflammation	Topical or systemic: antimicrobials Anti-inflammatories Protease inhibitors	Bacterial balance and reduced inflammation
Moisture balance	Desiccation or maceration	Moisture balancing dressings Negative pressure Remove fluid	Correct moisture balance
Epithelial (edge) advancement	Epithelial cells not migrating. Wound cells not responsive	Re-asses cause. Corrective therapies	Advancing epidermal margin

The first of the four elements in the TIME framework is tissue management where necrotic and compromised tissue are removed by debridement to allow healthy tissue to grow. The control of inflammation and infection requires microbial loads to be treated promptly to reduce their negative effects. Wound infection control is discussed further in Section 1.2.9. The moisture in the wound must be kept in balance to prevent desiccation or maceration of the wound and surrounding tissues. If the epithelium is not advancing across the wound due to inhibited keratinocyte migration by wound matrix problems, ischaemia or regulatory defects then re-assessment of causes or corrective treatment are given. The TIME framework is not linear and some or all elements will be used one or more times before the wound heals.

In the effort to improve wound management the Wound Healing Society have developed a set of guidelines for the treatment of chronic wounds. These guidelines are published as a series of papers which include a set of guidelines with supporting evidence in the form of published literature, and these papers are listed in Table 1-6. The guidelines cover all aspects of chronic wound management and include diagnosis, treatment, surgery, adjunctive therapies to promote wound healing and preparation for treatment. In addition the pressure ulcer guidelines cover positioning and supporting patients, and information on nutrition. The guidelines concur with the elements of the TIME framework in the relevant subdivisions of the guidelines, for example infection control.

Table 1-6. Chronic wound guideline papers.

Wound Type	Reference
Chronic wound introduction	(Robson & Barbul, 2006)
Venous ulcers	(Robson *et al.*, 2006)
Diabetic ulcers	(Steed *et al.*, 2006)
Pressure ulcers	(Whitney *et al.*, 2006)
Arterial ulcers	(Hopf *et al.*, 2006)

1.2.8 Wound management – Dressings

There are numerous different dressings currently available, each designed to enhance wound healing in a variety of ways. A recent study critically reviewed the literature on dressings and selected studies based on the following criteria: complete healing, pain, ease of use, wound trauma on removal, absorption and containment of exudates and prevention of infection (Chaby *et al.*, 2007). The main conclusion was that the evidence to support which dressings to use in healing, managing and preventing infection is not strong. For acute wounds the evidence supports that hydrofiber dressings promote quick healing and that glycerine-impregnated or foam dressings do not delay healing where as hydraluronic and silver dressings do. For chronic wounds: hydrocolloid dressings are better than gauze; alginate dressings promote debridement of necrotic tissue; and healing rates are similar when hydrocolloids or foam dressings are used.

Pain, exudate control and dressing tolerance were the most important criteria for dressing selection found by a companion study to investigate which dressings are most used and accepted by the healthcare personnel (Vaneau *et al.*, 2007). This study concluded that for chronic wounds healthcare personnel used: hydrogels for debridement; foam and low adherent dressings at the granulation stage; hydrocolloid and low adherence dressings at the epithelilisation stage; aliginated dressings for haemorrhagic wounds; and dressings with activated charcoal for malodourous wounds. However the purposes that specific dressings are typically used for by healthcare personnel do not agree with the strongest evidence supporting that dressing for a particular purpose (Chaby *et al.*, 2007). The ideal properties of dressings for use on chronic wounds specified in the Wound Healing Society chronic wound guidelines are listed in Table 1-7.

Table 1-7. Chronic wound guidelines for dressings.

Dressing Property	Venous	Diabetic	Pressure	Arterial
Maintains a moist environment	●	●	●	●
Manages exudate	●	●	●	●
Protects from further damage	●	●	●	●
Cost effective and appropriate	●	●	●	●
Used with compression bandages	●			

1.2.9 Wound management – Infection

The main issues with infected wounds are to correctly diagnose, remove necrotic tissues and to treat the infection (Kuehn, 2007). All the elements in the TIME framework described in Section 1.2.7 aid in the management of infected wounds. All possible alternative causes for delayed healing should be eliminated before microbial involvement be suspected. The sampling of wounds for diagnostic purposes should be performed to confirm an infection, when antimicrobial treatment has not succeeded, the patient requires screening or healing has stopped and other potential causes have been treated (European Wound Management Association (EWMA), 2006). The sampling of infected wounds is discussed in Section 1.2.10.

The European Wound Management Association (EWMA) stages of clinical infection described in Section 1.2.5 and Table 1-4 provide a management strategy based on the clinical signs of infection. In stage 1 no intervention is required and basic wound management of debridement and appropriate dressings should be used. In stage 2 the use of topical antimicrobials may be required to restore the bacterial balance. In stages 3 and 4 the use of combined topical antimicrobial and systemic antibiotics may be required. Frequent reassessments are required to ensure the correct level of treatment is provided at all times.

The Wound Healing Society guidelines (Table 1-6) regarding infected venous, diabetic, pressure and arterial ulcers are summarised in Table 1-8. They are in general agreement with the TIME framework and the EWMA stages of clinical infection with debridement, testing to determine the species and the use of antimicrobials and antibiotics only when necessary

Table 1-8. Brief description of guidelines for infected chronic wounds.

Treatment Option	Venous	Diabetic	Pressure	Arterial
Remove necrotic and devitalised tissue	●	●	●	●
Determine species by tissue biopsy or swab	●	●	●	
Use tropical antimicrobial agents when greater than $1x10^6$ colony forming units per gram of tissue	●	●	●	●
Use systemic antibiotics when surrounding tissue infected	●			
Use systemic antibiotics if infection not confined to granulating wound		●		
Treat distant infections with antibiotics			●	
Reduce bacteria to less than $1x10^5$ colony forming units per gram of tissue	●	●	●	●
Osteomyelitilis may occur which requires correct diagnosis and treatment		●		
Treat neuro-ischemic ulcers with short systemic antibiotics				●
Adequate oxygen will prevent and control infection				●
Tropical antimicrobial dressings in chronically infected wounds				●

1.2.10 Wound management – Sampling and diagnosis

Once a wound is suspected of infection, a sample from the wound must be taken to diagnose the species and volume of bacteria to allow the correct treatment to be given. Bowler *et al.* (1999) recommends that only clinically infected or deteriorating wounds be sampled as these wounds will provide information that will help treatment while swabbing of other wounds will waste time and resources.

The sampling of infected wounds and identification of bacterial species in the UK is defined in the national standards from the UK Health Protection Agency. For skin, superficial and non-surgical wounds (Health Protection Agency, 2009a) samples should preferably be taken before antimicrobial therapy. Pus or exudate samples are preferred to swabs, however in practice superficial swabs are the most common. The transport of the media to the laboratory should be rapid and samples carried in suitable media to maintain the bacteria. Samples are cultured on blood agar and other media in specific cases. For absesses and deep-seated infections (Health Protection Agency, 2009b) the procedure is similar except more identification tests are performed initially since the number of possible microorganisms present is usually larger.

The species present and their susceptibility should be found and reported within 16 to 72 hours and a further report may be issued if anaerobic species are being cultured. Better results are obtained if the laboratory personnel know information about the wound, for example, type, position, clinical infection, necrosis, malodours and whether antimicrobial therapy is being undertaken. Testing for anaerobic species is not usually performed unless the wound is malodorous and/or purulent as the tests are more difficult to perform. Bowler *et al.* (1999) states that anaerobic species should not be overlooked as *Clostrium* species can be highly virulent. Reports from the laboratory tend to single out *Staphylococcus aureus*, *Pseudomonas aeruginosa*, beta-hemolytic streptococci as pathogens, and states the occurrence of anaerobic species when present. If *Clostrium* species are present these are specifically reported.

The identification of the bacteria (Health Protection Agency, 2008) is performed in three stages. Firstly the investigator makes a choice based on experience and then performs a number of tests for confirmation. If this does not succeed then a battery of tests in commercial identification systems is employed. Finally if the identification is still elusive then a step by step process to obtain the fundamental characteristics of the bacteria is performed. The microscopic appearance, cultural appearance and growth requirements are used for identification purposes at all stages.

The most common susceptibility procedure (Health Protection Agency, 2006) in the UK is disc diffusion. An agar plate is inoculated and paper discs containing the antimicrobial/antibiotic agent are placed on top. The agent diffuses into the medium and causes zones of inhibition in the growth of the bacteria. This determines the susceptibility or resistance of the species.

1.2.11 Summary of wounds and infections

Wound healing is a complex series of events which are hindered when bacteria proliferate and cause an infection. The management of wounds is complicated with wound assessment, decisions on the most suitable treatment, the continual reassessment of the treatment and dealing with the patients welfare. This whole process is further complicated by infections that prolong wound healing, cause additional pain to the patient and add to the multitude of possible treatment options. Current research in the wound care field aims to improve wound management at all stages to increase patient welfare and reduce the financial burden of wounds and associated infections.

1.3 The microflora of infected wounds

The bacterial species that are medically important with respect to wounds are a small proportion of the vast numbers of microbes that exist on the Earth. The bacterial species that are typically isolated from wounds varies with demographic location, purpose of investigation, methods used to detect the bacteria and differences in the patients age, sex, wound type and location (Gadepalli *et al.*, 2006); (Goldstein *et al.*, 1996). Also the predominant species is likely to change over time as shown by a study on the microflora of burns and therefore the age of the wound when sampled will affect the bacterial species isolated (Vindenes & Bjerknes, 1995). This section presents an overview of the bacterial species commonly isolated from wounds and presents a number of studies that recorded the bacterial species isolated from various wound types.

1.3.1 Characteristics of typical bacteria isolated from wounds

The characteristics of bacterial species typically isolated from wounds are listed in Tables 1-9 to 1-11, Gram-positive aerobic species, Gram-negative aerobic species, and anaerobic species respectively. The summary includes the structure of the colonies, virulence factors, where they reside, how they spread and the diseases they may cause in the wounds.

Table 1-9. Summary of Gram-positive aerobic species commonly isolated from wounds. Adapted from Murray *et al.*, 2005.

***Corynebacterium* species** • Irregular shape, Gram-positive rods, mostly facultative anaerobes. • Produce toxins, adhere to foreign bodies and have antibiotic resistance. • Most infections are endogenous. • Can cause wound infections and sepsis.
Enterococci species: • Gram-positive, facultative anaerobic cocci arranged in pairs or short chains. • Surface adhesions, effects host processes and have antibiotic resistance. • Can survive on surfaces for long periods. • Present in digestive tract and infects endogenous or via person contact. • Can cause wound infections and sepsis.
Staphylococci species: for example *Staphylococcus aureus* • Spherical facultative anaerobic Gram-positive, grow in clusters. • Protective capsule and slime layer. • Produce toxins and enzymes, plus adhesion proteins. • Present as normal skin flora and transfers via persons or materials. • *Staphylococcus aureus* contains coagulase, other species do not.
Streptococci species: for example *Streptococcus pyogenes* • Diverse collection, therefore precise details vary from species to species. • Gram-positive, facultative anaerobic cocci in pairs or chains. • Protective capsule, adhesion substance and substance that lyse blood cells. • Present in the respiratory tract and transiently on skin. • Spreads through respiratory droplets or breaks in the skin. • Can cause cellulitis, deep skin destruction and sepsis.

Table 1-10. Summary of Gram-negative aerobic species commonly isolated from wounds. Adapted from Murray *et al.*, 2005.

Enterobacteriaceae family: for example *Escherichia coli*, *Enterobacter* species, *Klebsiella* species, *Proteus* species. • Gram-negative rods. • Present in the environment and digestive tract. • Can be pathogens, opportunistic pathogens or obtain virulence via gene transfer. • Protective capsule and other substances to disguise itself. • Produce toxins and resistance to many antibiotics. • Can cause wound, soft tissue infection and sepsis (depends on species).
Pseudomonas* species: for example *Pseudomonas aeruginosa • Small, aerobic Gram-negative rods, often in pairs. • Protective capsule and adhesion molecules. • Produce toxins and destructive enzymes and antibiotic resistance • Present in the environment, especially moist environments. • Infects wounds and leads to vascular damage, tissue necrosis and sepsis.

Table 1-11. Summary of anaerobic species commonly isolated from wounds. Adapted from Murray *et al.*, 2005.

Bacteroides* species: for example, *Bacteroides fragilis • Pleomorphic in shape and size, Gram-negative • Present in the digestive tract. • Capsule protects against phagocytosis and enhances adherence to host. • Produce enzymes that destroy tissues and some strains produce toxins. • Can cause soft tissue infections and sepsis.
Clostridium* species: for example *Clostridium perfringens • Large, rectangular, Gram-positive rods. • Produce variety of toxins, haemolytic enzymes. • Present in the digestive tract. • Type A responsible for most infections. • Can cause cellulitis with localised edema and erythema, may lead to sepsis.

1.3.2 The microflora of burn wounds

The bacterial species commonly isolated from burn wounds are listed in Table 1-12. *Staphyloccus aureus* and *Pseudomonas* species were consistently the most common species isolated with coagualse-negative staphylococci and various species of the *Enterbacteriumceae* family the next most common. A number of species were isolated from only one of the three studies and included species of *Streptococcus*, *Bacteroides* and *Acinitobacter.*

In a study to determine how the species of bacteria changed over time it was found that *Staphylococcus aureus*, streptococci species and Coagulase-negative staphylococci species were predominant to begin with and then decreased over time, whereas *Pseudomonas aeruginosa* and bacteria from the Enterobacteriaceae family started at low levels and became more dominant as time progressed (Vindenes & Bjerknes, 1995).

Table 1-12. Common bacteria isolated from burn wounds. Data from Appelgren *et al.*, 2002; Mousa, 1997; and Santucci *et al.*, 2003.

Gram-positive aerobes	
- *Staphylococcus aureus*	- Coagulase-negative staphylococci
- *Streptococcus*	- *Enterococcus*
Gram-negative aerobes	
- *Escherichia coli*	- *Proteus*
- *Enterobacter*	- *Acinetobacter*
- *Citrobacter*	- *Pseudomonas*
- *Klebsiella*	
Anaerobes	
- *Bactoroides*	- *Fusobacterium*
- *Clostrium*	- *Preptrostreptococcus*

1.3.3 The microflora of surgical site infections

The bacterial species isolated from surgical site infections depends on the location of the surgical wound and hence the type of surgical operation performed. The types of bacteria isolated from different operations are listed in Table 1-13.

Table 1-13. The common surgical site infection pathogens found depending on the type of surgical operation. Modified from Mangram *et al.*, 1999.

Bacterial species	Operations
• *Staphylococcus aureus* • Coagulase-negative staphylococci	• Placement of all grafts, prostheses or implants • Neurosurgery • Breast • Vascular
• *Staphylococcus aureus* • Coagulase-negative staphylococci • Streptococci • Gram-negative bacilli	• Ophthalmic
• *Staphylococcus aureus* • Coagulase-negative staphylococci • Gram-negative bacilli	• Orthopedic
• *Staphylococcus aureus* • Coagulase-negative staphylococci • *Streptococcus pneumoniae* • Gram-negative bacilli	• Noncaricic thoracic
• Gram-negative bacilli • Anaerobes	• Appendectomy • Bililary tract • Colorectal
• Gram-negative bacilli • Streptococci • Oropharyngeal anaerobes	• Gastroduodenal
• *Staphylococcus aureus* • Streptococci • Oropharyngeal anaerobes	• Head and neck involving oropharyngeal mucosa
• Gram-negative bacilli • Enterococci • Group B streptococi • Anaerobes	• Obstetric and gynecologic
• Gram-negative bacilli	• Urologic

1.3.4 The microflora in chronic wounds

The bacterial species commonly isolated from chronic ulcers are listed in Table 1-14

Table 1-14. Common bacteria isolated from chronic wounds. The circles indicate the number of studies that the bacterial species were reported in: ● - Isolated; ○ - May have been isolated however not specified. Diabetic ulcer data from: Dang *et al.*, 2003; Gadepalli *et al.*, 2006; and Tentolouris *et al.*, 1999. Leg ulcer data from: Brook & Frazier, 1998; and Lim *et al.*, 2006. Pressure ulcer data from: Daltrey *et al.*, 1981; Heym *et al.*, 2004; and Peromet *et al.*, 1973.

Chronic Wound Type / Bacterial Species	Diabetic Ulcer	Pressure Ulcer	Leg Ulcer
Gram-positive aerobes	●●●	●●●	●●
- *Staphylococcus aureus*	●●●	●●●	●●
- *Streptococcus*	●●	●●●	●●
- Coagulase-negative staphylococci	●●●	●●●	●●
- *Corynebacterium*	●	●	●
- *Enterococcus*	●●	●	●
- *Micrococcus*	●	●	●
- Other		●	
Gram-negative aerobes	●●●	●●●	●●
- *Escherichia coli*	●○	●●○	○○
- *Enterobacter*	●●○	●○	○○
- *Citrobacter*	●○	●●○	○○
- *Klebsiella*	●○	●●○	○○
- *Morganella*		●●○	○○
- *Proteus*	●○	●○	○○
- *Acinetobacter*	●	●●	●●
- *Pseudomonas*	●●●	●●●	●●
- Other		●●	
Anaerobes	●●●	●●	●
- *Bactoroides*	●○○	●●	○
- *Clostrium*	●○○	●●	○
- *Fusobacturium*		●●	○
- *Preptrostreptococcus*	●○○		○
- Other	●○○	●●	○

1.3.5 The microflora of diabetic foot ulcers

Aerobic bacteria are the most common with a significant proportion being Gram-positive bacteria, particularly *Staphylococcus aureus.* The importance of anaerobic bacteria should not be discounted and was first reported in relation to diabetic foot ulcers by Louie *et al*. (1976). They also reported that their was no difference in the microflora between a healing ulcer and a deteriorating ulcer, and suggested that other factors were responsible for the healing rates, for example, quality of care, stage of disease and treatment of diabetes. In contrast a more recent study has shown that the number of Methicillin-Resistant *Staphylococcus aureus (*MRSA) cases was significantly higher in infected diabetic foot ulcer than non infected foot ulcers, 61.1% and 12.5% of *Staphylococcus aureus* isolates respectively (Tentolouris *et al.*, 2006).

Dang *et al*. (2003) investigated pathogens in diabetic foot ulcers in 1998 and then performed a repeat study using a routine with less antibiotic use in 2001. It confirmed that the previous use of antibiotics increases the risk of MRSA occurring, that the number of cases of MRSA was rising while the proportion of *Staphylococcus aureus* cases remained similar and that more research was required to discover how MRSA is acquired and how to reduce the problem. There was 15.2% MRSA cases in 1998 compared with 30.2% in 2001. The findings that MRSA was more common in patients previously treated with antibiotics was also shown by Tentolouris (Tentolouris *et al.*, 1999). In addition this study showed that healing times were prolonged by MRSA even though the morphology of the wound did not change.

1.3.6 The microflora of leg ulcers

Brook *et al.* (1998) investigated the link between pathogens and non healing ulcers between 1981 and 1989, however a correlation between the two was not found. Most of the wounds were polymicrobial and several matched the normal skin flora and bacteria from the digestive tract.

Bowler and Davis (1999) investigated the microflora of infected and non-infected leg ulcers and found that the numbers of anaerobic species per wound was significantly greater in infected wounds than in non infected wounds. However they found that there was no obvious correlation between common faculative pathogens and infected wounds, for example the numbers of *Staphylococcus aureus* was greater in non-infected wounds and in infected wounds that contained no anaerobes. Therefore clinically the interaction between species may be significantly more important than isolating individual species.

Davis *et al.* (2007) compared the bacteria isolated from non-infected wounds using surface swabs and tissue biopsies and found that there was a higher correlation between aerobic species than for anaerobic species. There was no correlation between the species and the length of healing, the large variations in bacteria species indicated that the species is less important than other factors and that swab analysis was better at predicting when wounds would not heal. Similarly Lim *et al.* (2006) found that there was a low correlation between sampling methods, full correlation only occurred in 46.2% of samples, only one bacteria was similar in 25.6% and there was no correlation in 28.2%.

1.3.7 The mircoflora of pressure ulcers

Peromet *et al.* (1973) investigated the microflora of pressure ulcer patients and found that all the wounds contained aerobic species, however only the higher ulcer stages contained anaerobic bacteria. In summary the microflora depended on the stage of the ulcer with the higher stages often including those species normally found on the skin and in the digestive tract. Anaerobic species were important in that they could lead to bacteremia, for example *Clostridium* species and *Bacteroides* species.

Daltrey *et al.* (1981) investigated the bacteria species and their effect on healing rates and noticed that necrotic ulcers tended to have higher levels of *Proteus mirabilis*, *Pseudomonas aeruginosa* and *Bacteriodes* species. Other than this no correlation between the bacteria species and the rate of healing was found, for example there was no difference between those ulcers containing only *Staphylococcus aureus* even though only some of them were clinically infected. Heym *et al.* (2004) compared the differences between deep tissue samples taken pre-surgery and samples taken from the drainage fluids post-surgery of spinal cord injured patients with pressure ulcers (Heym *et al.*, 2004). It was found that there was a good correlation between the two sampling methods and both gave a good indicator of the potential of deep tissue infection.

1.3.8 Summary of wound microflora

There are many factors that influence the microflora of wounds, however most studies indicate that *Staphylococcus aureus*, *Pseudomonas aeruginosa* and *s*treptococci species are the most common. One of the key factors is how the samples are analysed which is highlighted in a study that compared the results from bacteria in venous leg ulcers, diabetic foot ulcers and pressure ulcers by culturing techniques and DNA sequencing (Dowd *et al.*, 2008). Contrasting differences in the microflora were found for the different methods with the conclusion that the use of molecular techniques rather than culturing techniques would lead to a greater understanding of the wound microflora and the wound's ecology. This in turn would allow better treatment and management of the chronic wounds.

1.4 Methods to detect bacteria

The management of wound healing would be enhanced by faster methods to detect the bacteria commonly isolated from wounds. The correct antibiotic treatment would be provided sooner, the appropriate dressing could be selected to control the infection, and other treatment methods , for example debridment could be employed at the appropiate times.

In recent years a large volume of research has been devoted to bacterial detection methods, not just in the clinical field but also in food and environment (Lazcka *et al.*, 2007). This section provides an overview of bacterial detection: conventional methods, for example plating and culturing; more recent methods like polymerase chain reaction (PCR) and immunoassays; and current methods in development which include biosensors, DNA microarrays and microfluidic devices. The basic principles and a few examples of the various methods will be given. For further information readers are directed to (Lazcka *et al.*, 2007), (Deisingh & Thompson, 2002) and (Deisingh & Thompson, 2004).

1.4.1 Conventional methods

Plating and culturing methods are still extensively used due to their high sensitivity and selectivity, and are considered to be the gold standard in bacterial detection. Bacteria are grown on selective and diagnostic media that prevent or enhance growth. It may also cause a colour change in specific species or strains. Microscopy is the main method for direct counting and may be enhanced by the staining of bacteria with dyes, in particular fluorescent dyes. These tests need to be carried out by trained personnel in a microbiology facility.

Other enumeration methods include: Most Probable Numbers where replicate tubes containing three different sample sizes and the numbers are found by reference tables and computer programs; differences in bacterial species' abilities to ferment sugars, glycosides and alcohols allow biochemical tests to be conducted; and flow cytometry allows the number and size of bacteria to be found by measuring the resistance changes across a narrow channel that the bacteria are forced through.

1.4.2 Recent techniques

Diagnosis of infectious diseases, identifying genetic fingerprints and detecting genetic diseases are some of the applications that make use of the polymerase chain reaction (PCR) (Turner *et al.*, 1997). The PCR method is used to amplify target sequences in DNA that have been extracted from bacteria and the detection of these sequences allows species to be identified. The conventional PCR method uses a series of thermal steps that denature, anneal and polymerise the DNA repetitively for twenty to forty cycles, and this produces a significant amplification of the target sequence.

Quantitative real-time PCR was a further development to overcome some of the problems of conventional PCR. These disadvantages included the need for post processing to quantify amounts, product carry-over producing false positives and PCR inhibition producing false negatives (Abu Al-Soud & Radstrom, 1998); (Kaltenboeck & Wang, 2005). Real-time PCR correlates the PCR product concentration to the fluorescence intensity and various fluorescent chemistry detection systems are available (Higuchi *et al.*, 1992). The simplest fluorescent system is DNA binding dyes that emit fluorescence once bound to DNA (Wong & Medrano, 2005). As the amount of DNA increases due to the PCR amplification, the amount of fluorescent increases. The advantages of real-time PCR are the ease of use, less time is required and there is a high sensitivity and specificity (Kaltenboeck & Wang, 2005).

A second recent technique to improve bacterial detection is an enzyme-linked immunosorbent assay (ELISA), a biochemical method to detect the presence of an antibody or antigen in a sample (Crowther, 2001). The sandwich ELISA is the method used to detect bacteria and the main steps are illustrated in Figure 1-15, which include binding an antibody to a surface, adding the sample with the antigen which then binds to the antibody; adding the enzyme linked antibody that also binds to the antigen; and finally adding the chemical which the enzyme converts to a colour, fluorescent or electrochemical signal that is then measured.

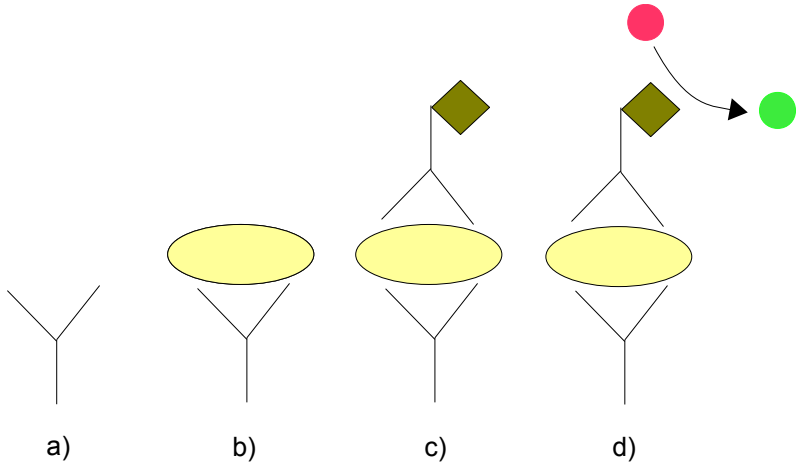

Figure 1-15. The basic steps in the sandwich ELISA: a) bind antibody to plate; b) bacteria bind to the antibody; c) enzyme linked antibody binds to bacteria; d) chemical added that is converted by the enzyme to a detectable signal.

To aid in the specificity of detection methods immunomagnetic separation has been used to isolate specific organisms from mixed cultures (Olsvik *et al.*, 1994); (Safarik *et al.*, 1995). The general technique involves placing super-paramagnetic particles coated in antibodies into the mixed culture. The specific bacteria bind to the particles which are then removed with a magnetic separator. Bacteria are then detected by standard methods, for example plating and fluorescent microscopy, or by combining with ELISA or PCR methods.

1.4.3 Current research on rapid detection methods

The conventional methods are slow and labour intensive while the more recent methods can still be time consuming, expensive and labour intensive (Deisingh & Thompson, 2004). Current research is focused on rapid methods to detect bacteria or their by-products, for example odours produced by bacteria. The sensing systems have two components, the target molecule or cell, which is the substance that needs to be detected and the transducer that converts the detected substance into a signal that can be measured. Biosensors in addition have a third component which is a biological recognition substance which aids in the capture of the target molecule or cell. There are a vast number of different transducers and includes electrochemical, optical and high frequency sensors. The most common transducers and their typical operation are listed in Table 1-15.

Biosensors contain one of three types of biological recognition substances, enzymes, antibodies or nucleic acids (Lazcka *et al.*, 2007) of which antibodies are the most common in bacteria detection. Antibodies are immobilised onto the surface of the sensors either by adsorption onto gold, the avidin-botin system or by self-assembled monolayers (SAMs). Adsorption on to gold is quick and simple, however antibodies are randomly attached. The avidin-biotin system uses biotinylated antibodies bound to an avidin coated surface. SAMs commonly bind disulphides or thiols to the sensor surface and the antibody is attached to the other end of these molecules.

Table 1-15. The most common sensor types and their operation. Data from Turner & Magan, 2004.

Sensor Type	Operation
Conducting polymer sensors	The target substance interacts with polymers, which changes the resistance of the polymer and hence the measured signal.
Metal oxide sensors	The oxide contains adsorbed oxygen species which interact with target substances and changes the conductivity of the oxide. Selectivity changed by temperature and composition of oxide.
Metal oxide silicon field effect sensors	Similar to the metal oxide sensors, however the signal is changed due to potential changes when the target substance interacts with a catalytic surface.
Piezoelectric crystals	The target molecules are absorbed by acetyl cellulose or lecithin membranes and this changes the magnitude of the resonance frequency, which is related to the mass of the target substance. Selectivity can be altered based on the thickness of the membranes.
Surface acoustic-wave devices	Similar to the piezoelectric sensors where the resonance frequency of waves emitted along the surface of a crystal by an electric field from surface electrodes are changed.
Electrical impedance sensors	The impedance of an alternating current changes in the presence of target substances.
Electrochemical sensors	The target molecules are oxidised or reduced at the electrodes and the generated voltage is measured.
Surface plasmon resonance	The target substances alter the optical properties of polymer surfaces.
Optical sensors	A light source excites the target substance and a signal is measured in the resulting absorbance, reflectance, fluorescence or chemiluminescence.

To provide an example of the types of detection systems currently being developed a number of sensors will be described in more detail. Pasche *et al.* (2009) developed an optical sensor designed to monitor wound healing in real time by measuring either the pH or the concentration of protein present in an infection, the C-reactive protein (CRP). The operation of the sensor is illustrated in Figure 1-16. White light propagates along the waveguide in two directions which creates two spectral peaks. The waveguide has either a pH sensitive hydrogel or a functional layer that interacts

with CRP. Alterations in the pH or the presence of CRP modify the light via the sensitive or functional layer causing the spectral peaks to change. These changes in the peaks are related to the pH or the quantity of CRP. In vitro testing has proved the concept is viable.

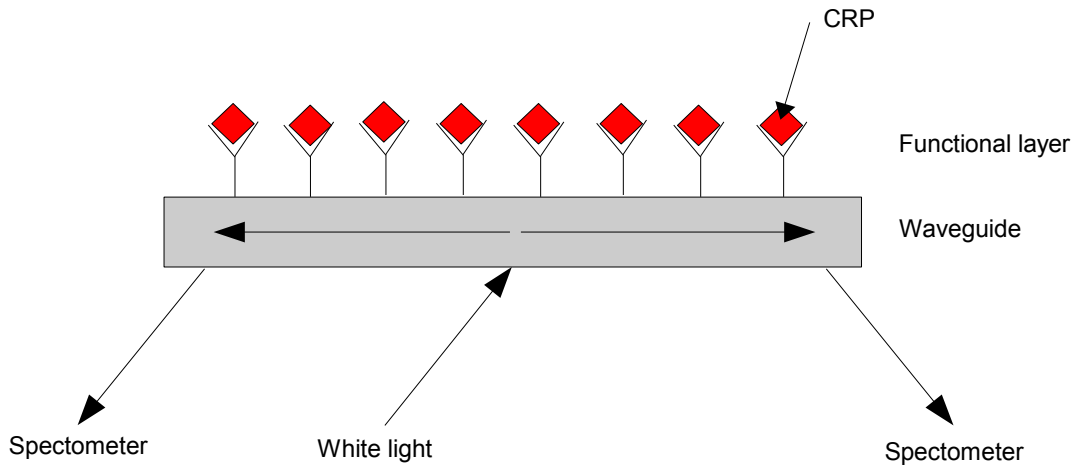

Figure 1-16. The CRP optical sensor.

An example of a biosensor using amperometric and immunoassay technology contained within a flow tube is illustrated in Figure 1-17 (Abdel-Hamid *et al.*, 1999). Bacterial cells are passed through the system and captured on a membrane. Loose cells are removed with a wash step. The antibody-cell complex is completed by washing through a conjugate solution and then washing the system again. Finally a hydrogen-peroxide and sodium iodine solution is added and the reaction with the enzyme produces an increase in electrons. The corresponding current measured is proportional to the numbers of bacteria. The system can detect *Escherichia coli* and Salmonella species within 35 minutes.

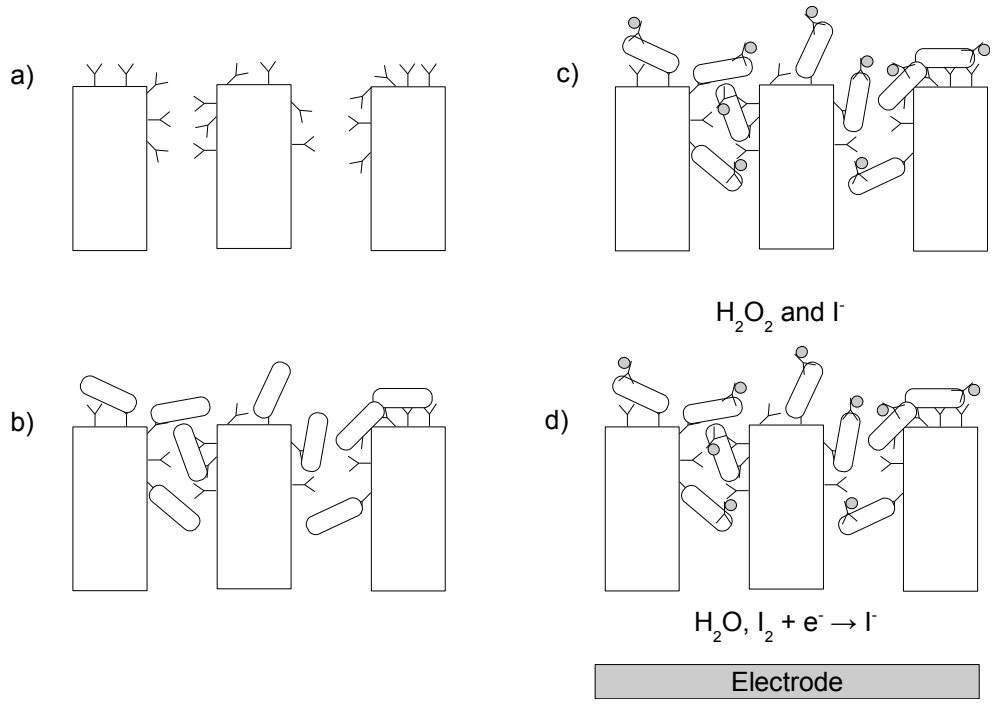

Figure 1-17. The amperometic immunoassay steps. a) The mesh with the immobilised antibody, b) Addition of the bacteria that bind to the antibody. c) Addition of the enzyme linked antibody. d) Addition of the solution that reacts and caused a change in the current that flows between the electrodes (Abdel-Hamid *et al.*, 1999).

Another amperometric sensor detects the RNA extracted from *Escherichia coli* (Gau *et al.*, 2001). A microelectromechanical system was used to fabricate a detector array with multiple electrodes. The protein steptavidin was immoblised onto the surface by SAMs. Then an assay procedure was performed which washed through the ribosome RNA and the single strand DNA signal molecules. If the *Escherichia coli* RNA was present then a DNA – RNA hybrisation complex formed on the electrodes and the signal enzyme, peroxidase, would release more electrons. The corresponding current could be correlated with the number of bacteria. The procedure could be performed within 40 minutes and could detect down to 1000 CFU ml^{-1}.

Electronic noses detect odours by using the volatile molecules as the target substance and have been used with the majority of the transducers listed in Table 1-15 (Turner & Magan, 2004). Arrays of sensors are used to allow detection of many smells in single devices. More recent electronic noses have incorporated biological recognition

substances to aid in immobilising the target molecules (Lee & Park, 2010). The main problems in the medical field are creating instruments with adequate sensitivity, selectivity, reproducibility and stability, and in producing experimental procedures to create specific responses and allow the identification of odours (Casalinuovo *et al.*, 2006).

Electronic noses could indicate whether samples are infected or not and whether pathogens exist. Studies of infections include leg infections, urinary tract infections, sinusitis pneumonia, tuberculosis and ear, nose and mouth infections. Parry *et al.* (1995) demonstrated that an electronic nose could differentiate between leg ulcer samples that contained β-haemolytic streptococci and those that did not due to the specific odours produced by these species.

Trill (2006) investigated various biosensors that detected infection in wounds by monitoring the levels of certain substances related to bacteria metabolism and these included a glucose sensor, hydrogen peroxide biosensor and ethanol biosensor, however the ability of these sensors to distinguish *Staphylococcus aureus* was not accurate and therefore the research turned to investigating electronic noses. A mixed metal oxide semiconductor gas sensor with temperature and humidity sensors was developed and the results indicate that it can detect and discriminate between *Staphylococcus aureus*, *Escherichia coli*, *Streptococcus pyogenes*, *Klebsiella pneumoniae* and *Pseudomonas aeruginosa*.

Many of the sensors are also being placed in microfluidic devices. The advantage of these are reduced costs, mass production, nano-litre volumes, improved mixing and transport, and multi-analyte analysis (Lazcka *et al.*, 2007). Another avenue being researched is the analysis of large numbers of genes in microarrays where DNA is labelled and then bound to thousands of immobilised complementary DNA within a microarray (Deisingh & Thompson, 2002). The locations of the DNA within the microarray can indicate the genes present and if specific genes correspond to a specific bacteria then the bacteria can be identified.

Gomez and colleagues described one of the first microfluidic devices illustrated in Figure 1-18 (Gomez *et al.*, 2001); (Gomez *et al.*, 2002). The bacteria cells were removed from an overnight culture and re-suspended in a very low ionic buffer (Tris-Gly-Dext). The cells were incubated for a further two hours to release ions into the media and then the solution was placed into the mircofluidic device and impedance measurements were performed between 100Hz and 1MHz. (Further details on electrical impedance methods are described in Section 1.5.) There was a small difference between the impedance of live and heat killed cells of *Listeria innocua* and *Escherichia coli*.

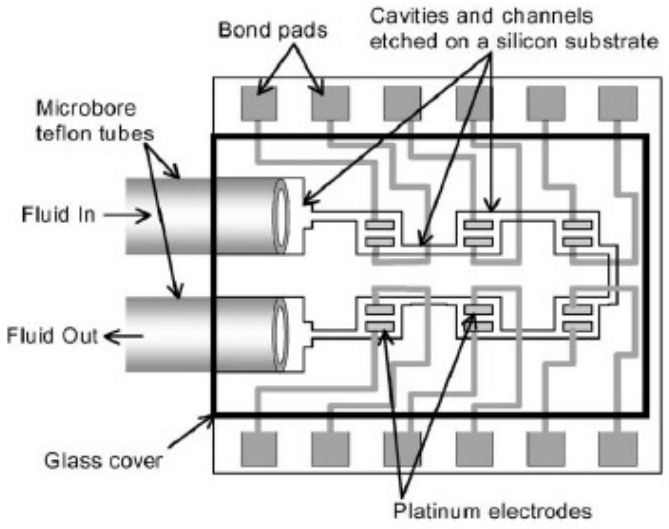

Figure 1-18. Simplified schematic of a microfludic device. Image taken from Gomez *et al.*, 2002 and reproduced with the permission of Elsevier.

Suehiro and colleagues performed a number of investigations into combining impedance detection, microfludic devices and additional technologies to aid the detection of bacteria. Firstly positive dielectrophoresis (DEP) was combined with an interdigitated microelectrode array within a microfluidic chamber (Suehiro *et al.*, 1999). DEP is the electrokinetic motion of dielectrically polarised particles in non-uniform electric fields. This helped trap the bacterial cells in chains between the electrodes and by using a theoretical model the cell numbers could be quantified. To enhance the detection of bacteria this was then combined with

electropermeabilization of the cells which causes the bacteria to release additional ions (Suehiro *et al.*, 2003b). This increases the conductance of the media and hence the impedance decreases.

In a second investigation an antibody solution was added to the microfluidic chamber which caused the target bacteria to aggregate (Suehiro *et al.*, 2003a). The DEP effect was greater on the target bacteria due to their larger size and hence were held in place while the non-target bacteria were washed away. Finally the DEP technique was combined with immobilised antibody which captured the target bacteria within the microfludic chamber (Suehiro *et al.*, 2006).

Biosensors and electrical impedance sensors, especially if incorporated into microfluidic devices are the future of rapid detection of bacteria. Also possible are gene microarrays and combining existing technologies with microfluidic devices, for example, PCR (Deisingh & Thompson, 2002). The difficulties in realising these technologies lie in commercialising ideas developed in the laboratory and achieving consistent, reliable and sensitive results (Deisingh & Thompson, 2004).

1.5 Biological impedance

Electrical impedance is the opposition to the change that occurs when a time varying current is applied in an electrical circuit. By using electrical impedance spectroscopy the electrical properties of a biological system can be characterised. This section provides an overview of electrical impedance spectroscopy, divided into electrochemistry and biological impedance systems. For further reading, Bockris and Reddy provide a good account of electrochemical theory (Bockris & Reddy, 1970) and Kell and Davey, and Foster and Schwan provide a good account of the impedance technique (Foster & Schwan, 1989); (Kell & Davey, 1990).

1.5.1 Electrochemistry

A basic electrochemical cell consists of an electrolyte, two electrodes placed in the solution and connected into an electrical circuit. The electrolyte contains ions that have solvation shells of water molecules surrounding them due to the attraction of the water molecule dipole to the charged ion, as illustrated in Figure 1-19a. When an electrode is placed in the electrolyte a solvation shealth of water molecules forms around the electrode due to the attraction between the free electrons and the water molecule dipole. The electrostatic attraction of the free electrons also draws the positive ions to the electrode surface which creates an interface between the electrode and the bulk electrolyte.

Various theories to model this interface have been proposed including a fixed double layer model proposed by Helmholtz in which there is an inner layer of water molecules surrounding the electrode with ions sitting between the inner layer and the outer layer as shown in Figure 1-19b. Other theories suggest that the double layer is not fixed and that the ions spread out gradually into the bulk solution, or a combination of a fixed layer followed by a gradual spreading out of the ions. Using the fixed double layer model the difference between the negatively charged free electrons and the positively charged ions creates a separation of charge which produces a potential difference and this situation is analogous to a capacitor with the water molecules representing the dielectric material.

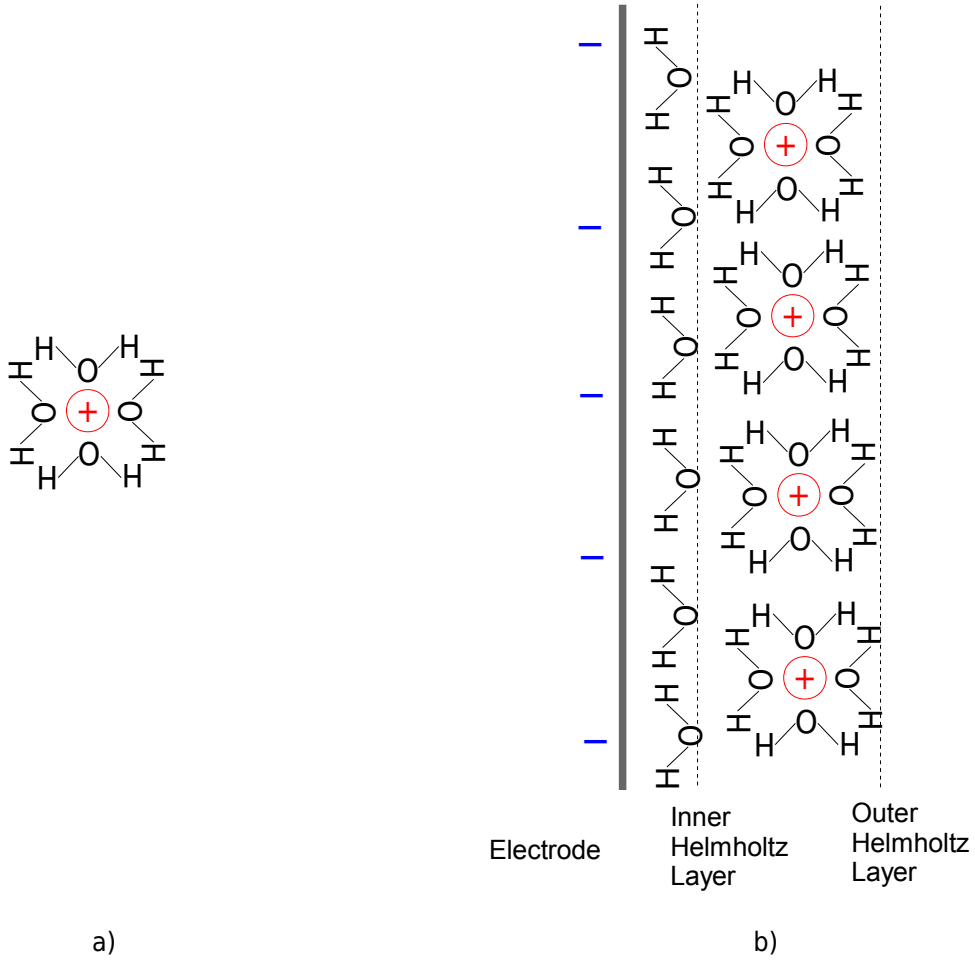

Figure 1-19. Solvation shealth and Helmholtz double layer: a) Solvation shealth of water molecules surrounding a positive ion in an electrolyte; b) Double layer formation on surface of electrode formed by water molecules and ions with solvation shealths.

The Helmholtz double layer capacitance, C_H can be expressed by Equation 1-1 where ε is the dielectric permittivity and d is the distance between the plates.

$$C_H = \frac{1}{\varepsilon 4 \Pi d} \tag{1-1}$$

Gouy and Chapman suggested that the ionic charge in the liquid decreases exponentially with increasing distance from the electrode. The ions in this model are affected by the electrode charge and the thermal buffering of particles in the solution. The capacitance C_{GC} for this model is expressed by Equation 1-2 where ε is the

dielectric permitivitty, z is the valence of ion species, e is the electronic charge, n is the ion concentration, ψ is the potential, k is the Boltzmann constant and T is the temperature.

$$C_{GC} = \sqrt{\frac{\varepsilon z^2 e^2 n}{2\pi k T}} \cosh\left(\frac{ze\Psi}{kT}\right) \tag{1-2}$$

Stern proposed that the capacitance is modelled by the Helmholtz model plus the Gouy-Chapman model where the charge separation is linear close to the electrode surfaces and varies exponentially further away. Therefore the Stern capacitance C_S can be expressed by Equation 1-3 where C_H and C_{GC} are Equations 1-1 and 1-2.

$$C_S = C_H + C_{GC} \tag{1-3}$$

In an electrochemical cell electrons carry the current in the wires and the electrodes, and ions carry the current in the electrolyte, as illustrated in Figure 1-20. Using a DC voltage the transfer between electrons and ions occurs at the electrode surface through redox reactions. At equilibrium the rate of oxidation equals the rate of reduction and no current flows.

By applying a voltage between the electrodes, an electric field is created across the solution and this potential difference across the solution attracts the ions to the electrodes and redox reactions take place producing a net current flow around the circuit. The positive electrode, the anode attracts negative ions performing oxidation and removing electrons. The negative electrode, the cathode attracts positive ions performing reduction by supplying electrons. This leads to concentration differences in which the positive ions and negative ions move in opposite directions and the electrolyte concentration changes as elements are removed from the solution. The redox reactions using a direct current and with silver-silver chloride electrodes in a solution containing chloride ions are shown in Equations 1-4 to 1-6.

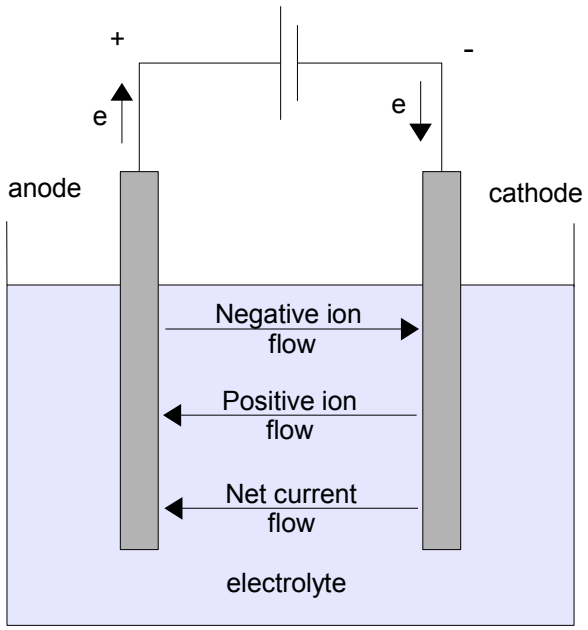

Figure 1-20. Typical electrochemical cell with direct current, showing electron and ion movements.

Cathode reaction $2Ag^{+} + 2e^{-} \rightarrow 2Ag$ (1-4)

Anode reaction $2Cl^{-} \rightarrow Cl_2 + 2e^{-}$ (1-5)

Total reaction $2Ag^{+} + 2Cl^{-} \rightarrow 2AgCl$ (1-6)

A constant direct current requires the transfer of electrons between the electrodes and the electrolyte by the redox reactions described previously, however using an alternating current in an electrochemical cell does not require these reactions to take place for a current to flow. In this situation the double layer effect at the electrode-electrolyte interface (Figure 1-19b) behaves as a capacitor and allows a current flow on both sides without the transfer of charge across the dielectric. There will be some transfer of electrons across the interface, and this is due to the double layer effect not being a perfect electrical capacitor.

1.5.2 Impedance

To measure the impedance of a system requires a sine wave generator, current meter and electrochemical cell as shown in Figure 1-21. A sine wave with a small magnitude (Eqn. 1-7) is applied across the two electrodes which produces a current flow (Eqn. 1-8) which is proportional to the input voltage.

$$V_{in} = Vsin(\omega t) \quad (1\text{-}7)$$

$$I_{out} = Isin(\omega t) \quad (1\text{-}8)$$

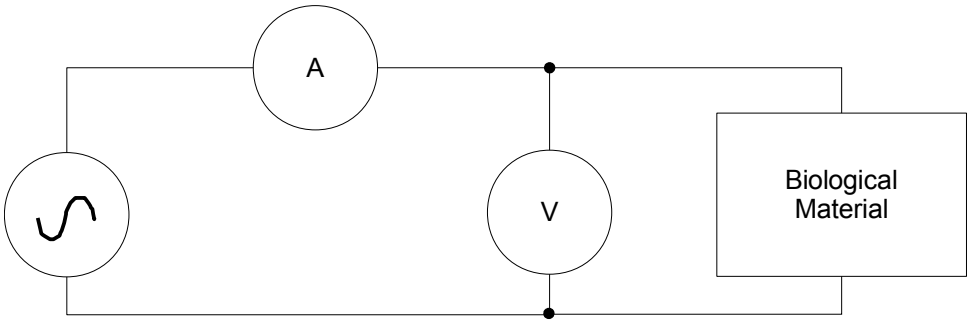

Figure 1-21. A typical impedance system to measure the electrical characteristics of a biological system: a sine wave is applied to the test material which produces a current flow and the impedance is calculated from the measured voltage and current.

The system is classified as linear since the output is proportional to the input, hence the impedance can be calculated from the input voltage and the resulting output current (Eqn. 1-9). By varying the frequency of the input signal and measuring the output signal, the frequency response of the system can be found.

$$Z = \frac{V_{in}}{I_{out}} \quad (1\text{-}9)$$

Impedance is a complex quantity defined by Equation 1-10 where Z' is the resistance and Z'' is the reactance, and are graphically represented in Figure 1-22.

$$Z = R + jX = Z' + Z'' \quad (1\text{-}10)$$

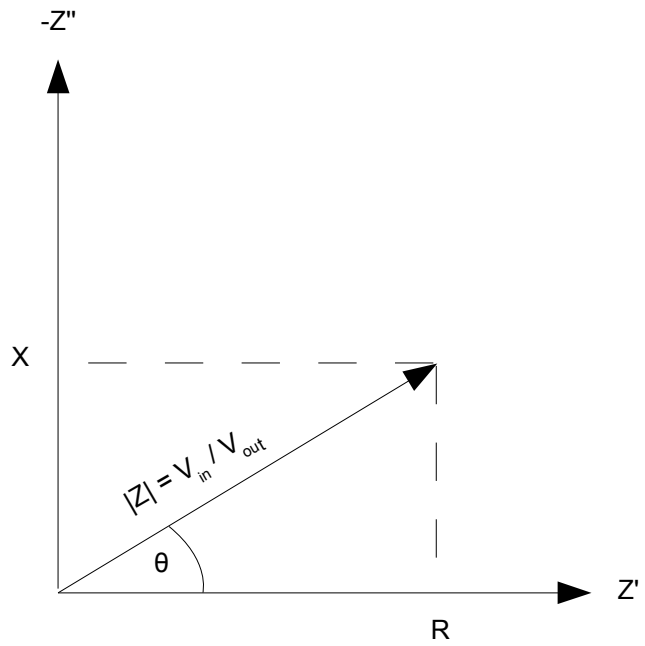

Figure 1-22. Electrical impedance represented as a complex quantity.

The impedance modulus, |Z|, and the phase angle, θ, can either be calculated from (Eqns. 1-11 and 1-12) or used to find the resistance, Z', and the reactance, Z" (Eqns. 1-13 and 1-14).

$$|Z| = \sqrt{(Z')^2 + (Z'')^2} \tag{1-11}$$

$$\theta = \arctan\left(\frac{Z''}{Z'}\right) \tag{1-12}$$

$$Z' = |Z|\cos(\theta) \tag{1-13}$$

$$Z'' = |Z|\sin(\theta) \tag{1-14}$$

The impedance of an electrical circuit is defined by the resistors, capacitors and inductors in the circuit. Resistance, R, is defined by Equation 1-15 where l is the length, A is the cross sectional area of current flow and ρ is the resistivity of the material.

$$R = \rho \frac{A}{l} \tag{1-15}$$

Capacitance (C) is defined by Equation 1-16 where A is the plate area, d is the plate separation, ε_0 is the permittivity of free space and ε_r is the relative permittivity of the material.

$$C = \frac{\varepsilon_0 \varepsilon_r A}{d} \tag{1-16}$$

The voltage across a resistor is proportional to the current through it as defined by Ohm's law (Eqn. 1-17).

$$V = IR \tag{1-17}$$

When a voltage (V) is applied to a capacitor with a capacitance (C), the current (I) is proportionally to the rate of change of the voltage (Eqn. 1-18).

$$I = C \frac{dV}{dt} \tag{1-18}$$

The reactance (X) of a component is the ratio of the magnitudes of voltage across it (|V|) and the current through it (|I|) (Eqn. 1-19).

$$X = \frac{|V|}{|I|} \tag{1-19}$$

Applying a sine wave (Eqn. 1-20), where A is the amplitude, ω is the angular frequency and t is the time, to a capacitor (C) would produce an output current that would lead the input voltage by 90^0 (or π/2) (Eqn. 1-21).

$$V_C = A\sin(\omega t) \tag{1-20}$$

$$I_C = C\omega A\cos(\omega t) = C\omega A\sin(\omega t + \pi/2) \tag{1-21}$$

Using Equations 1-19, 1-20 and 1-21 the reactance of a capacitor (X_C) can be calculated (Eqn. 1-22).

$$X_c = \frac{1}{\omega C} \tag{1-22}$$

Similarly when a current is applied in an inductor (L) the voltage (V_L) is proportionately to the rate of change of the current (Eqn. 1-23).

$$V_L = L\frac{dI}{dt} \tag{1-23}$$

Applying an alternating current (Eqn. 1-24), where A is the amplitude, ω is the angular frequency and t is the time, to an inductor (L) would produce an output voltage that would lead the input current by 90^o (or π/2) (Eqn. 1-25).

$$I_L = A\sin(\omega t) \tag{1-24}$$

$$V_L = L\omega A\cos(\omega t) = L\omega A\sin(\omega t + \pi/2) \tag{1-25}$$

Using equations 1-19, 1-24 and 1-25 the reactance of an inductor can be calculated (Eqn. 1-26).

$$X_c = \omega L \tag{1-26}$$

Using Equation 1-10 the impedance of a resistor, Z_R, capacitor, Z_C, and inductor, Z_l are defined in Equations 1-27, 1-28 and 1-29.

$$Z_R = R \tag{1-27}$$

$$Z_C = \frac{1}{j\omega C} \tag{1-28}$$

$$Z_R = j\omega L \tag{1-29}$$

Therefore resistors are frequency independent, and capacitive and inductive reactances are frequency dependent. For capacitors as the angular frequency approaches zero the impedance approaches infinity, thus the capacitor acts as an open circuit. As the angular frequency approaches infinity the impedance approaches zero, thus the capacitor acts as a short circuit. Inductors behave in an opposite manner to capacitors, as the angular frequency approaches zero, the impedance approaches zero and as the angular frequency reaches infinity, the impedance approaches infinity.

1.5.3 Biological impedance

The impedance characteristics of an electrochemical cell can be modelled by combinations of resistors and capacitors. Inductance is not often observed except in certain situations, for example at high frequencies the wires may produce some inductance. The simplest electrochemical cell consisting of two electrodes and an ionic solution can be modelled with a resistor, R_s, in series with a parallel resistor, R_{dl}, and capacitor, C_{dl} (Figure 1-23) (Cole, 1928). The resistor R_s represents the bulk solution which is purely resistive since the flow of ions is similar to that of metals. The electrode-electrolyte interface is represented by the components R_{dl} and C_{dl}, which represent the charge transfer resistance and the double layer formed at the boundary.

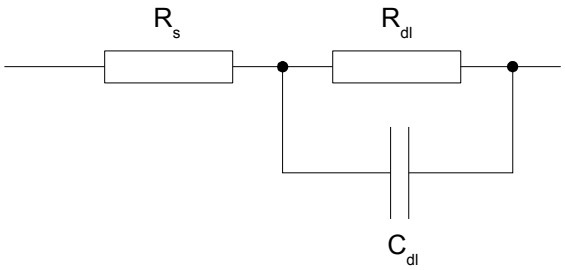

Figure 1-23. Electrical equivalent model for electrochemical cell.

The impedance for this circuit is shown in Equation 1-30 and rearranging produces Equation 1-31.

$$Z = R_s + \frac{1}{\frac{1}{R_{dl}} + j\omega C_{dl}} \tag{1-30}$$

$$Z = \frac{R_s + R_{dl} + j\omega R_s R_{dl} C_{dl}}{1 + j\omega C_{dl}} \tag{1-31}$$

The impedance of a typical electrochemical cell can be represented graphically on Nyquist plots and Bode plots as illustrated in Figure 1-24. The components of the circuit model are represented at certain points within these plots. The impedance

magnitude plot has a high plateau which represents the resistance of the solution and the low frequency plateau represents the solution resistance plus the double layer resistance. The frequency dependent section between the plateaus is called a dispersion and is caused by the double layer effect which blocks low frequencies and passes high frequencies, hence as the frequency increases the impedance decreases. In terms of the circuit model at high frequencies the capacitor, C_{dl}, acts as a short circuit and therefore the total impedance is represented only by the solution resistance, R_s, and at low frequencies the capacitor acts as an open circuit hence the total impedance is the sum of the two resistors, R_s and R_{dl}.

A more complex circuit model for the electrochemical cell and ionic solution is the Randles equivalent circuit illustrated in Figure 1-25 (Kell & Davey, 1990). The components R_s, R_{dl} and C_{dl} represent the same physical components as in Figure 1-23. The components R_w and C_w represent the Warburg impedance which involves the diffusion of the electroactive materials to and from the reaction zone.

In a system that contains biological materials and cells the electrical behaviour is more complex than that described by the electrochemical cell with an ionic solution. The structure of the cells and the cell membranes produce additional electrical characteristics of the system (Foster & Schwan, 1989). These can also be explained by comparing them to the behaviour of capacitors. As the frequency of the applied sine wave is increased in a capacitor, there is less time for the charge to build up and impede the current flow. Hence as the frequency increases the impedance decreases. In a biological system the additional components add further pseudo-capacitance to the electrical system and therefore the impedance magnitude has a series of dispersions.

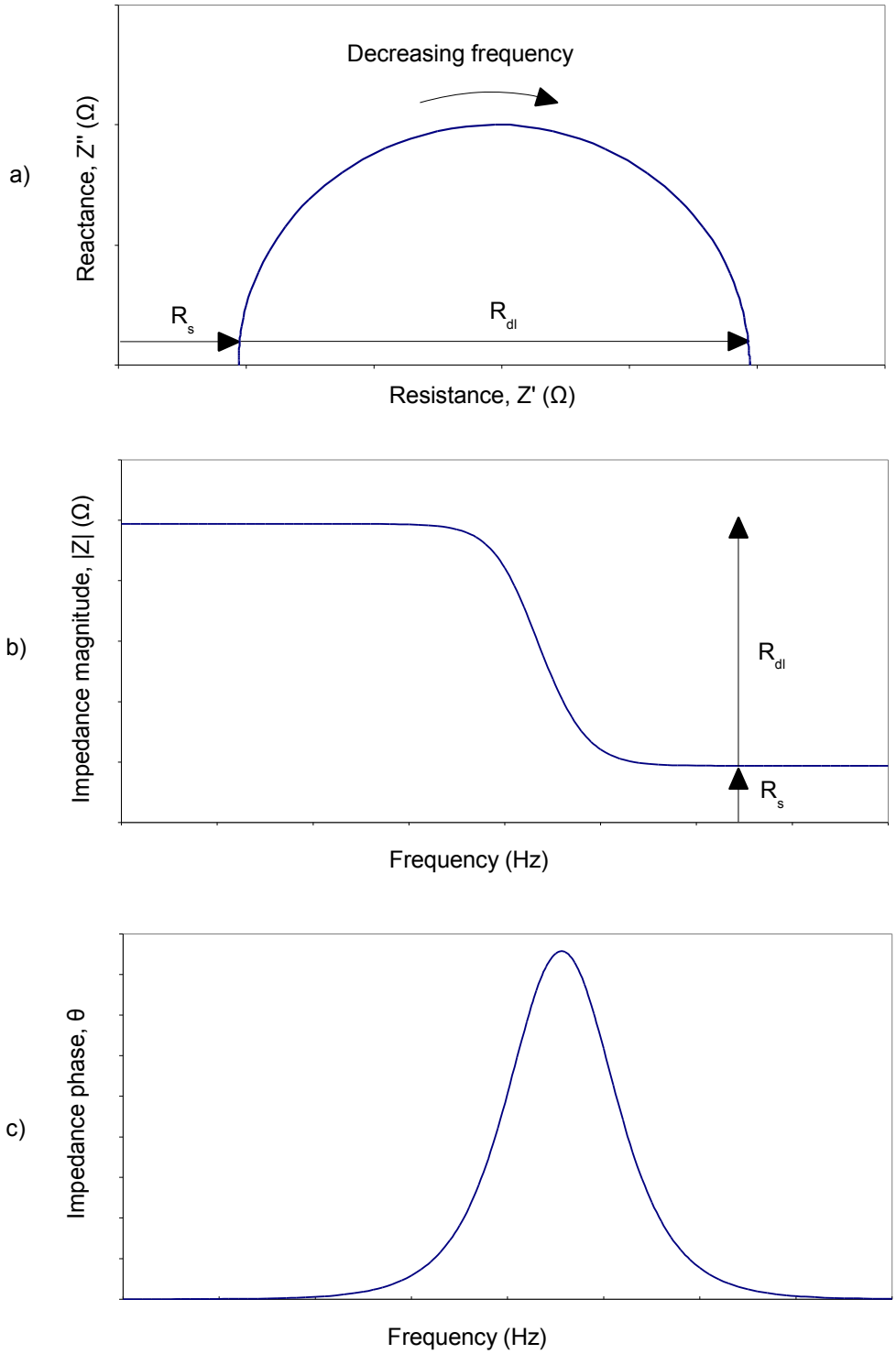

Figure 1-24. Typical frequency response of electrical circuit model: a) Semicircular arc on complex plot; b) Impedance magnitude plot; c) Impedance phase plot.

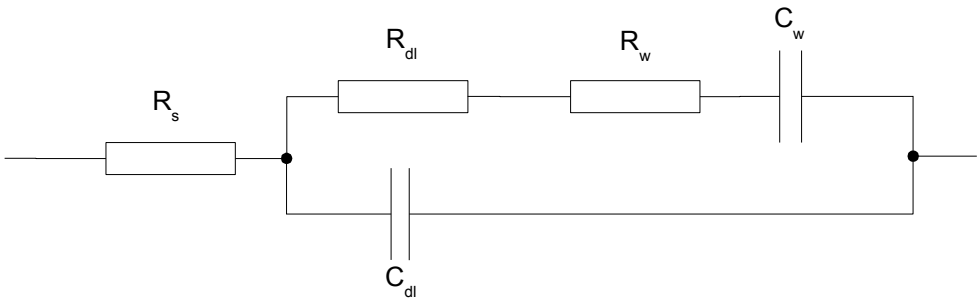

Figure 1-25. The Randles equivalent circuit for an electrochemical cell.

Examples of the causes of these dispersions are interfacial polarisation, dipolar mechanisms and counter-ion polarisation effects (Foster & Schwan, 1989). The interfacial polarisation produces a dispersion due to the charging of interfaces within the bulk material, for example in dilute suspensions of cells where there is no interaction between cells the current flows around the cells at low frequencies. However, at high frequencies the current flows through the cells and there is a larger area carrying the current which reduces the impedance and produces a dispersion. At higher concentrations of cell suspensions the dispersion occurs over a broader frequency range due to the interaction of cells. A similar effect is seen in tissues where the current flows in the extracellular fluids at low frequencies and flows through the cells at higher frequencies.

The dipolar mechanisms include the partial orientation of dipoles, for example proteins at 1 to 10 MHz, polar side chains on molecules at 0.1 to 1 GHz and water at 20 GHz (Foster & Schwan, 1989). The counter-ion polarisation effect is the ionic diffusion within the electrical double layer surrounding the electrodes and these can be large at low frequencies.

The impedance of biological systems is therefore a function of frequency; a series of plateaus between infinite impedance and zero impedance with dispersion regions, as illustrated in Figure 1-26. The dispersions are named with Greek letters: the α dispersion is caused by the tangential flow of ions along cell surfaces; the β dispersion is the build up of charge at the cell membranes; the β1 dispersion is due to the rotation of proteins; the δ dispersion is due to the rotation of sidechains on

molecules and bound water; and the γ dispersion is due to the rotation of small molecules with dipoles, for example water (Foster & Schwan, 1989); (Kell & Davey, 1990).

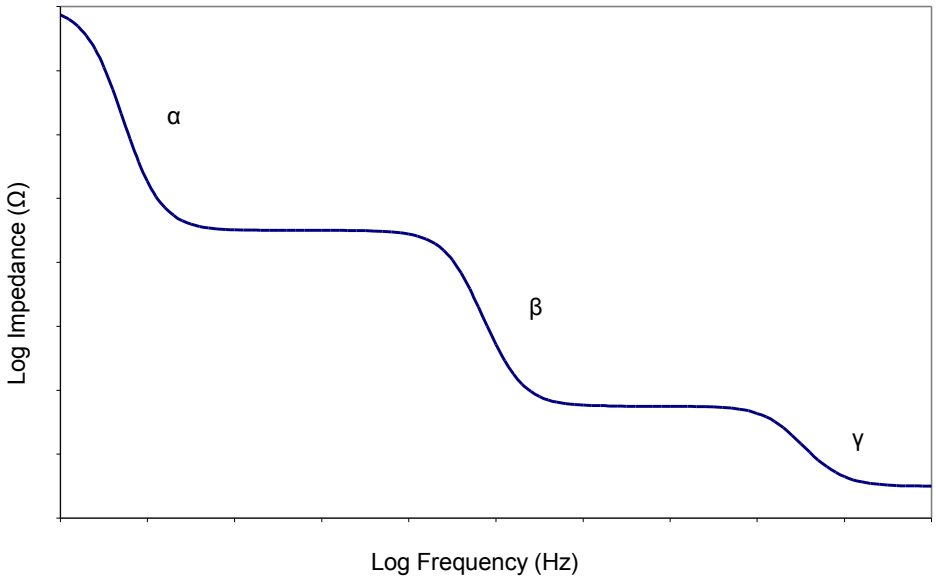

Figure 1-26. Typical dispersions produced by a biological material: α) Tangential flow of ions along cell surfaces; β) Build up of charge at the cell membranes; γ) Rotation of small molecules with dipoles.

Biological tissues can be modelled with a circuit containing resistors and capacitors as illustrated in Figure 1-27. The capacitor C_m represents the cell membrane where the inner and outer surfaces are the capacitor plates and the lipid bilayer and other structures are the dielectric material between the plates. The resistor R_m represents the ionic pathways through the cell membrane, for example, ion channels. The resistor R_c represents the cytoplasm solution and the resistor R_e the extracellular matrix.

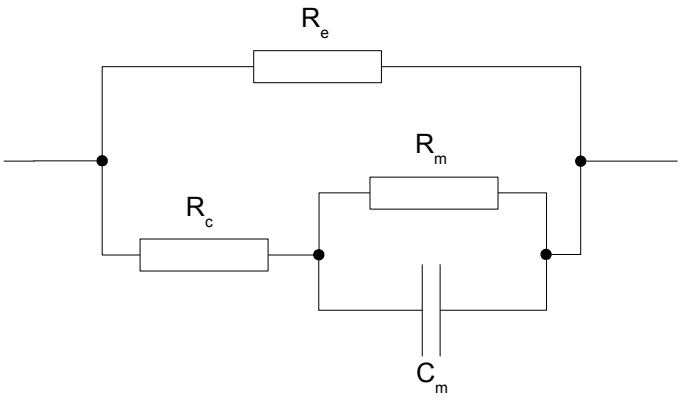

Figure 1-27. The equivalent circuit model for biological material containing cells.

In an ideal electrical circuit the centre of the complex semicircle always lies on the real axis. Cole discovered that in a biological system containing cells the centre of the complex semicircle lies below the real axis as illustrated in Figure 1-28 (Cole, 1932). The angle α formed between a vertical line passing through the centre of the complex semicircle and the radius is known as the membrane phase angle and is only found in biological tissues (Cole, 1932). The membrane phase angle is a measure of the current leakage through a cell membrane. At high frequencies the current passes through the cell membrane while at low frequencies the current flows around the cells. If the membrane was acting like an ideal capacitor then there would be no current leakage and the phase difference would be 90^{o}, however since there is leakage the phase difference is less than 90^{o}. This leakage produces the downward shift in the complex semicircle.

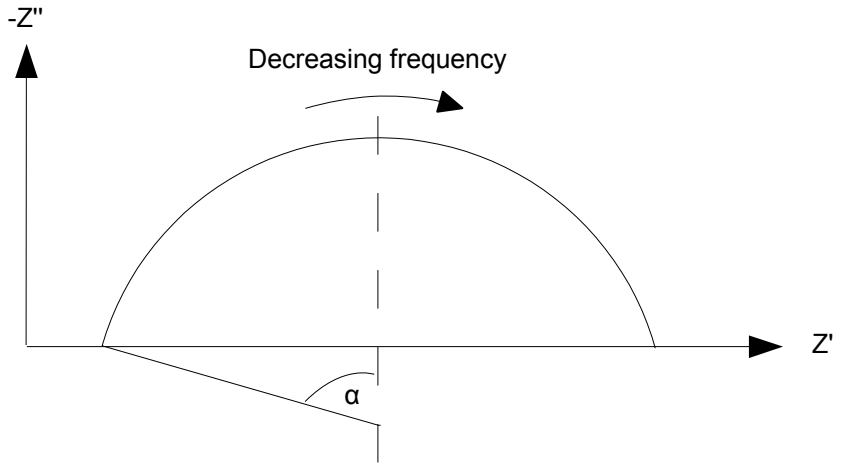

Figure 1-28. The membrane phase angle of biological materials.

To model imperfect capacitors in equivalent circuits, for example the leakage through a membrane, a constant phase element (CPE) has been created. The CPE is governed by Equation 1-32 where T is the value of $|Z|^{-1}$ at a frequency of 1 rad s^{-1} and P has a value between 0 and 1. Therefore the phase angle of the CPE is frequency independent and has a value of – 90*P degrees. The CPE can also be used to model diffusional processes at the electrode interface which were described previously in this section.

$$Z = \frac{1}{T(j\omega)^P} \tag{1-32}$$

In summary using a simple electrochemical circuit the electrical impedance characteristics of biological materials can be measured. These characteristics can be modelled with equivalent electrical circuits that represent physical properties. In turn this provides an understanding of the physical attributes or processes of the biological material. The use of electrical impedance may allow different materials to be identified or to detect processes that are occurring within the material.

1.6 Tissue impedance

Electrical impedance of tissues has been studied in a range of applications which include excised tissues, diagnosis of cancer, nutritional assessment, and muscle and lung functionality (Rigaud *et al.*, 1996), (Rutkove, 2009). Electrical impedance of excised tissues clearly show differences across different tissues as illustrated in Figure 1-29 for muscle, liver, lung, spleen and intestine (Rigaud *et al.*, 1995). This study also fitted the data to the Cole-Cole model and found electrical parameters for each of the circuit components.

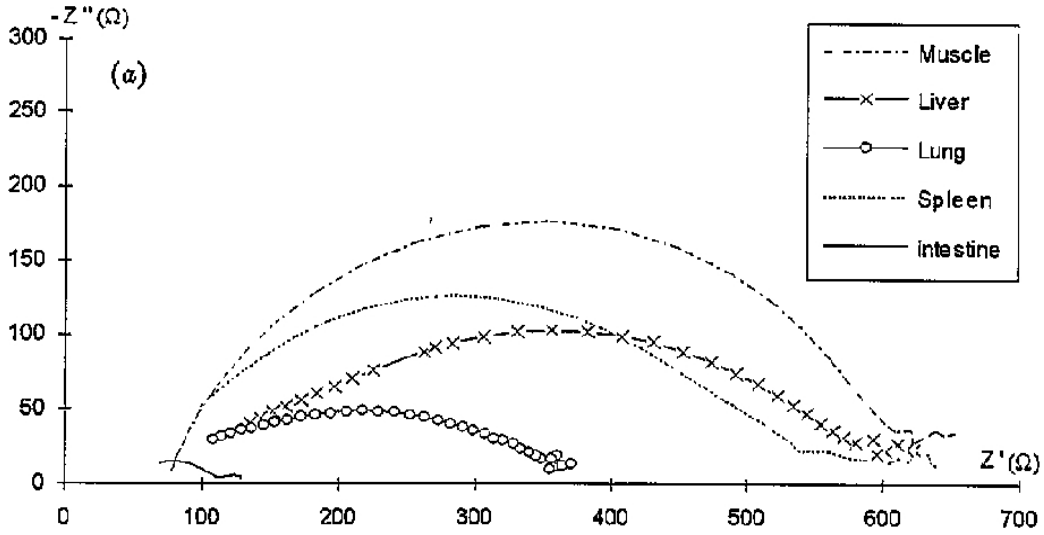

Figure 1-29. The complex plots of various excised tissues. Image taken from Rigaud *et al.*, 1995 and reproduced with the permission of IOP Publishing Ltd.

Electrical impedance myography is a non-invasive and painless procedure to measure muscle pathopysiologic changes (Rutkove, 2009). A high frequency, low-intensity electrical current is applied and the resulting impedance produces quantitative parameters that indicate the condition of the muscle. Electrical impedance tomography is an imaging technique used mainly for detecting physiologic and pathophysiologic changes in regional pulmonary ventilation (Bodenstein *et al.*, 2009). It has also been used to image the brain, breast cancer, the heart and the GI tract. To measure the lung function a circle of electrodes are placed around the body and impedance readings are performed between one electrode and each of the other electrodes. This is repeated for every electrode and from the resulting data an image of the lung is reconstructed.

Electrical impedance scanning has been most used to investigate breast cancer which produces a map of the tissue through an array of surface electrodes (Hope & Iles, 2004). The map indicates regions of high and low impedance. This technique may never replace standard mammography, however it could be used in conjunction to provide more information to allow clinicians to make the most informed diagnosis.

1.7 Impedance and bacteria.

Another area that the impedance technique has been used in is bacterial applications and includes Salmonella testing, food spoilage, monitoring of antibiotic resistance, biofilms, plant pathogens, damage to DNA and within enzyme assays, however there are still numerous areas that the technique could be used in (Silley & Forsythe, 1996). This section discusses the use of impedance in studying bacteria cell suspensions and bacteria biofilms.

1.7.1 Broth cultures

The first study of changes to the electrical properties of a medium by bacteria was performed by Stewart who discovered that over a period of 30 days the electrical conductivity of blood increased as the bacteria grew (Stewart, 1899). Several further studies were performed throughout the 20th century with an increased interest developing in the 1970s with the possibility of automation.

Ur and Brown measured the impedance changes of *Escherichia coli* in culture broth with gold alloy electrodes using a frequency of 10 kHz (Ur & Brown, 1975). It was shown that the impedance decreased with bacterial growth and that the impedance changes followed the standard bacteria growth curve. The impedance measured had a lag phase, a steady rise during the exponential phase, a continually rise during the stationary phase and a predicted constant level when the cells die. These impedance changes were likely to be due to the accumulation of charged metabolites which increased the conductivity and this method could be used to identify the presence of bacteria from a set of characteristic curves. This study led to the commercial instrument the Bactobridge.

Cady also discovered that the conductivity of the medium was increased due to uncharged molecules becoming charged molecules, and hence the number of ions and their mobility increased. (Cady, 1975). The capacitance also increased due to the molecules becoming smaller which decreased the distance of the double layer and increased the effective surface area. In addition and independently of Ur and Brown, Cady suggested that characteristic curves to identify species could be produced, and

that the time when the impedance started to change from the base level was related to the initial concentration and volume of solution. This study was also commercialised, into the Bactometer.

Noble *et al.* (1999) theorised a mathematical model to explain the changes in capacitance in a system measuring the growth of bacteria. The model was based on the Stern model of the electrode-electrolyte interface and an oxide layer on the electrodes. Bacteria impedance systems commonly use stainless steel electrodes with a passivation layer composed of chromium oxide and hydroxide which has an associated capacitance C_{ox}. Therefore combining the oxide layer capacitance with the Stern capacitance, C_{GC} produces the theorised total capacitance, C_N of the system, Equation 1-33. In a microbiology impedance system the capacitance should be effected by the thickness and structure of the passivation layer, the conductivity of the medium and the temperature.

$$C_N = \frac{1}{\frac{1}{C_S} + \frac{1}{C_{ox}}} \tag{1-33}$$

The model for capacitance was tested on *Pseudomonas aeruginosa*, *Escherichia coli*. *Staphylococcus aureus*, *Ataligenes faecalis* using the Bactometer at 1540Hz with stainless steel electrodes (Noble *et al.*, 1999). The model did not relate well to the results and therefore concluded that the media must be chosen carefully and that the capacitance may provide a better signal to measure growth and metabolism.

Richards *et al.* (1978) investigated the impedance methods by varying a number of parameters: pH, salt concentration and temperature, and suggested two possible instruments: An analogue system to measure a low number of samples, for example five; and a digital version that could handle up to 128 samples. These instruments measured the conductance since it was found to be more stable than the capacitance which had random fluctuations. From the graphs and data the lag phases, bacteria doubling times and initial concentrations could be determined. The digital instrument was commercialised into the Malthus Instrument and has been used with meat, dairy

products, brewing, water, cosmetics, pharmaceuticals and fabric conditioners (Hagan, 1990). Several authors have suggested methods to differentiate species, however no evidence was provided to support these statements for example, the spectral analysis of frequencies below 100 Hz may allow specific characteristics of species to be identified (Hause *et al.*, 1981).

Firstenberg-Eden and Eden (1984) extensively reviewed and experimented with the issues surrounding impedance measurements of bacteria and produced a mathematical model to calculate the initial numbers of bacteria based upon the detection time, the point at which the impedance begins to change steadily from the base level reading, and on various bacteria-medium parameters, for example generation times, lag times and metabolism rates .

The bacterial concentration, ion concentration and conductance with respect to time in the bacterial growth are illustrated in Figure 1-30. The bacterial concentration stays constant throughout the lag phase and then increases exponentially. The bacterial metabolism during these stages generates ions in the growth medium. The concentration of the ions generated by the bacteria increases over time. After a specified time, called the detection time the concentration of ions generated by the bacteria equals the initial ionic concentration of the solution. The conductance of the system is constant up to the detection point and then increases as the ions from the bacterial metabolism add to the total number of ions.

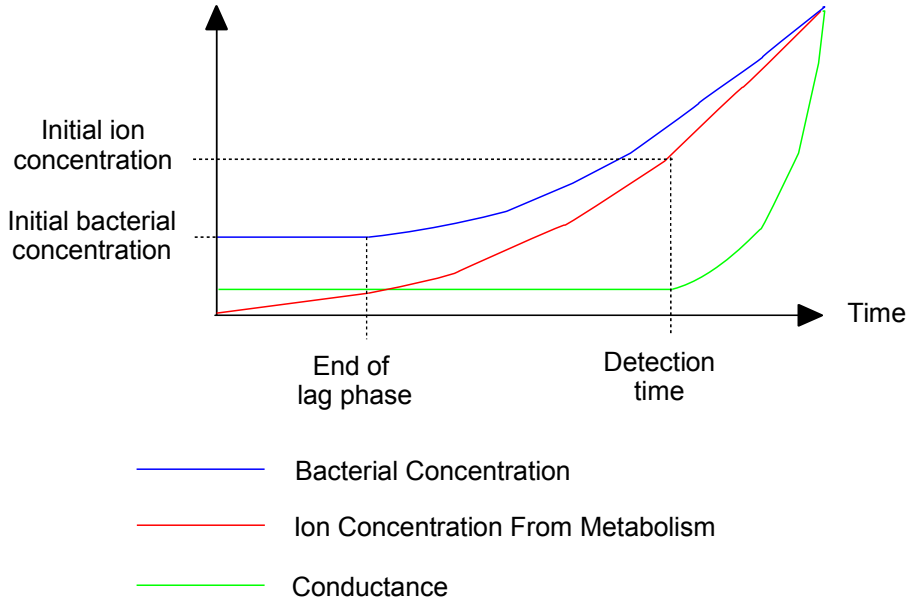

Figure 1-30. The parameters used in the mathematical model created by Firstenberg-Eden and Eden. Illustration based on figure from Firstenberg-Eden & Eden, 1984.

Using equations for the bacterial concentration and the concentration of ions produced from metabolism an equation for the detection time was derived (Eqn. 1-34) and is a function of the lag time t_L, the generation time t_g, the initial ion concentration C_{si}, the number of ions produced by each bacteria per unit time K_B and the initial bacterial concentration C_{BO}.

$$t_D = t_L + \frac{t_g}{\ln(2)} \ln\left(\frac{C_{si} \ln(2)}{K_B C_{BO} t_g}\right) \tag{1-34}$$

The initial bacteria concentration can be calculated, Equation 1-35, from the detection time and the medium-bacteria parameters.

$$\ln(C_{BO}) = \ln\left(\frac{C_{si} \ln(2)}{K_B t_g}\right) - \frac{\ln(2)}{t_g}(t_D - t_L) \tag{1-35}$$

The main conclusions that were drawn were: the concentration of the media effects growth rates and the extent to which the impedance changes from base levels; the detection time is dependent on temperature, media, electrode type, microbial concentrations and metabolism; after the detection point the change in impedance

may be proportional to the number of viable cells; and the specific application determines which media and electrode material to use and whether to measure impedance, conductance or capacitance.

Kell and colleagues have performed a number of experiments to investigate the electrical properties of bacteria in suspension. They found that the impedance changed on the type of bacteria, the bacteria population, the media, the frequency applied, the electrode type, the electrode surface to volume ratio, the temperature and the geometry of the test well (Harris & Kell, 1985). They concluded that the impedance method was useful as a control to indicate the presence of bacteria rather than being accurate in terms of viable cell numbers. This study led on to the development of the βugmeter to measure the biomass of concentrated cell suspensions using the principle that the radiofrequency dielectric properties of microbial cell suspensions are a function of the volume fraction (Harris *et al.*, 1987); (Kell & Davey, 1990). The probe measured the capacitance at 300 kHz and a change in biomass produced an instant result with negligible changes due to addition of other particles.

Felice and colleagues are one of the few groups that have looked at using the frequency response to calculate the different components that make up the total impedance as described by the model in Figure 1-23 (Felice *et al.*, 1992); (Felice & Valentinuzzi, 1999). The resistance of the media changed during bacterial growth and was frequency independent at a given point in time, and the reactance and resistance of the interface were frequency independent at low frequencies. The total resistance was governed more by the electrode type and geometry, and the total reactance was equal to the interface reactance until the frequency was greater than 1kHz where the dispersion of bacteria cells caused additional medium reactance.

1.7.2 Biofilms

Muñoz-Berbel and colleagues have performed a number of impedance studies of biofilms. Firstly the impedance changes at the electrode-electrolyte interface when biofilms formed on metal transducers was investigated (Muñoz-Berbel *et al.*, 2006). The system used a platinum counter electrode, a gold chip working electrode and a frequency sweep between 10 and 10kHz. They modelled their data with an equivalent circuit (Figure 1-31a) where R_s is the resistance of the solution and CPE_{dl} the constant phase element for the electrode-electrolyte double layer. The constant phase element parameter k was used to determine the properties of the biofilm.

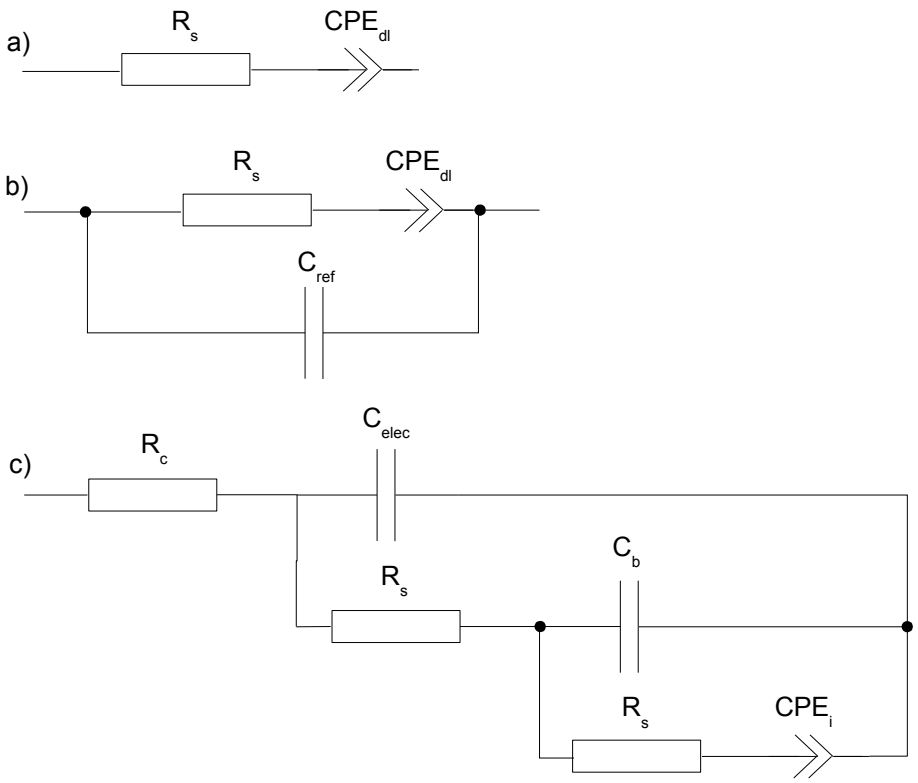

Figure 1-31. The equivalent circuit models used by Muñoz-Berbel and colleagues.

The main results were: the constant phase element parameter P, as described in Section 1.5.3 provided information about the biofilm; the parameter P increased on unused electrodes for the first 80 hours whereas it was constant for used electrodes; the biofilm did not form until the nutrients were limited which occurred after 80 hours; the parameter P decreased during the formation of the biofilm and stabilised once the biofilm was complete.

In a follow up study the attachment of *Escherichia coli* to platinum electrodes for quantification purposes was investigated (Muñoz-Berbel *et al.*, 2008). A three electrode system was used with a platinum working electrode, a platinum counter electrode and a silver-silver chloride reference electrode. The equivalent circuit to model the data is illustrated in Figure 1-31b where R_s is the resistance of the solution, CPE_i the constant phase element for the electrode-electrolyte interface and C_{ref} was an external reference capacitance.

The value of CPE_i and its parameter P changed with attachment time and concentration. In the pre-attachment stage the CPE_i increases as the double layer is affected by charged particles, bacteria and ions. In early attachment the change in CPE_i is given by the total capacitance C_i which is derived using Equation 1-36 where C_{pt} is the bare electrode capacitance and C_{bac} is the bacteria capacitance and θ is the coverage of bacteria. Therefore C_i decreases.

$$C_i = \theta \times C_{bac} + (1 - \theta) \times C_{pt} \tag{1-36}$$

In a companion study the electrical impedance was used to measure the bacteriophage infection of *Escherichia coli* biofilms (Garcia-Aljaro *et al.*, 2009). The data was fitted to an equivalent circuit model illustrated in Figure 1-31c. The components are: R_s is the solution resistance; R_p is the resistance of the biofilm pores; CPE_i is the electrode-electrolyte interface; C_b is the biofilm capacitance; and R_c and C_{elect} are related to the reference electrode. The results indicate that the biofilm capacitance, C_b and the CPE_i decreased upon bacteriphage infection, in contrast to an increase when there were no bacteriophages.

1.8 Electrodes and sensors for wounds

The type of electrode used in impedance studies must be chosen to suit the application, for example low impedance electrodes ensure the electrodes will not mask changes in the system and electrodes for tissue studies must be non-toxic to avoid damaging the cells. In relation to wounds there have not been a vast number of applications that use electrodes or sensors physically in the wounds. The main application is electrical stimulation to aid wound healing and a number of potential applications to monitor conditions within the wound to aid management and treatment. This section describes electrodes and their uses in wounds.

1.8.1 Electrodes

The material chosen for the electrodes to be used in biological measurements is very important. In testing different electrode types Woodward *et al.* (1996) found: electrodes must be very clean to avoid errors; gold electrodes fluctuate the least, platinum electrodes fluctuate more than gold however the polarisation effect is smaller; disposable silver-silver chloride electrodes had the second lowest fluctuations however drift affected repeatability; and the thickness of normal silver-silver chloride electrodes affected the results.

The toxicity of the electrode should also be considered as it is possible that prolonged contact may cause damage to the biological material. For example, silver and its ability to inhibit bacterial growth is well known. The main mechanism of bacterial growth inhibition by silver ions is generally agreed to be cell membrane damage and damage to associated proteins (Clement & Jarrett, 1994).

1.8.2 Electrical stimulation

Humans have a 'skin battery' where the stratum corneum with respect to the dermis has a negative potential in the tens of millivolt range which varies upon anatomical area (Foulds & Barker, 1983). These skin batteries drive a natural electric current during the wound healing process, for instance at the edge of epithelial wounds a large voltage gradient is produced and this electrical wound potential can be used as an indicator of wound healing rates (Cunliffe-barnes, 1945); (Illingworth & Barker, 1980).

Electrical stimulation devices are designed to mimic the natural current and enhance the healing rate of wounds. Electrical stimulation devices are classified as low intensity direct current, high voltage pulsed current, alternating current and percutaneously electrical nerve stimulation. A meta analysis of 15 studies that performed electrical stimulation on human chronic wounds concluded that it was effective alongside standard treatment, however the relative effectiveness of individual electrical stimulation devices remains unclear (Gardner *et al.*, 1999). Differences in the types of wounds studied by each of the devices makes comparisons of their relative merits difficult.

In reviewing the studies conducted on the antibacterial effect of electrical stimulation *in vitro*, it appears that the majority of techniques applied with direct current or high voltage pulsed current have an antibacterial effect (Kloth, 2005). Few studies have exclusively studied the bacterial effect *in vivo.* Rowley *et al.* (1974) studied the effect of direct current on *Pseudomonas aeruginosa in vivo* rabbits and discovered that there was a antibacterial effect.

1.8.3 Wound monitoring

Moisture content between a wound and a dressing is a critical factor in providing the optimum healing environment (Bishop *et al.*, 2003). A wound that is too dry delays healing as the epithelial cells are prevented from migrating across the wound and a

wound that is too wet can cause the surrounding skin to macerate. Real-time monitoring of hydration levels within leg ulcer dressings would be beneficial in terms of patient welfare and health costs.

The group at the University of Strathclyde that the work presented in this thesis has been performed within have previously developed a novel moisture monitoring system (McColl *et al.*, 2007). The system consists of a simulated wound bed and a sensor system as illustrated in Figure 1-32. The wound bed pumps fluids to mimic exudate flow and the sensor system uses pairs of silver-silver chloride electrodes to measure the electrical impedance of the fluid within the dressing. Wound exudate is an ionic solution and therefore the impedance produces an indication of the volume of fluid in the wound. The *in vitro* wound monitoring system was then further developed into a portable prototype that was clinically trialled on venous leg ulcers inside compression bandages where the device successful indicated the moisture levels within the dressings (McColl *et al.*, 2009). A spin-out company Ohmedics Ltd. (Glasgow, UK) has now been created to commercialise the wound monitoring system called WoundSense and is currently in pre-production.

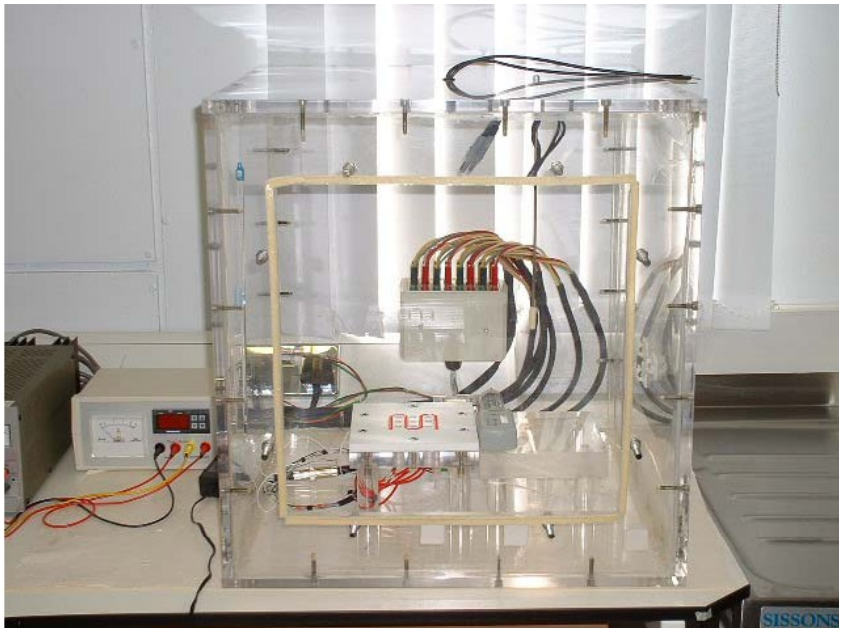

Figure 1-32. Wound monitoring system. It can investigate the fluid properties of dressings and comprises a wound bed simulator, fluid pump and environmental chamber. Image provided by personal correspondence, 2010.

Another method to manage wound healing is to record the size of the wound to evaluate how the wound healing is progressing. This is achieved by photographs or tracing the outline, both of which increase the risk of infection. A sensor aimed at monitoring the size of chronic wounds without removing the dressing has been developed (Weber *et al.*, 2010). ImpediMap is an array of electrodes in a sterile carrier dressing which measures the tissue impedance under each electrode and presents the data in terms of wound size or volume and wound severity. Intact skin has a large impedance and an open wound a very low impedance.

The wound mapping system was trialled alongside a clinical trial involving split thickness graft donor sites and was used to evaluate the principle of tissue characterisation and healing rates. The results indicate that the impedance was mainly resistive for days 2 and 3, compared with a resistive and capacitive impedance on days 8 and 9, indicating that the skin had regrown. There was also significant impedance differences between partially and fully regrown skin.

1.8.4 Impedance cell monitoring

The medical diagnostics group at the University of Stathclyde have also previously designed and manufactured a device which allows a monolayer of cells to grow on gold electrodes, whilst the electrical impedance is monitored (Personal correspondence, 2010). The device includes a series of working electrodes and a counter electrode, and a culture cube to contain cell growth on the appropriate regions of the electrodes. The use of a normalised impedance measurement, Z_n, to characterize cell impedance on macro and microelectrodes was pioneered by this group and is now widely accepted for use in practice.

The significant finding was that when such a normalised impedance was created at a time x and plotted across the frequency range (Z_{xnf} plot), different cell types demonstrated different characteristic responses from day to day in the growth cycle that were consistent from culture to culture. Such consistent characteristic responses meant that cells could be typed in culture according to their Z_{xnf} plot across the frequency spectrum. The frequency peaks in the Z_{xfn} plot that are part of this cell

characteristic signature tend to occur up to 1 MHz which indicates that ionic movement, ion channels and membrane characteristics of the individual cell types are contributing to this result.

Porcine coronary artery smooth muscle cells, porcine pulmonary artery endothelial cells and canine kidney epithelial cells have all been successfully characterised using this new approach. It was found that cell proliferation could be measured using the proposed method, but also that cell types could be differentiated from each other by their normalised, impedance-frequency profile. An example of the results obtained is illustrated in Figure 1-33, which shows the measured impedance, Z_{xnf}, in confluent monolayers of cells at day 7 normalised across a frequency range from 10Hz – 1MHz, $Z_{7nf.}$. It can be seen that each cell type produces a different impedance profile, in terms of magnitude, shape of curve and position in the frequency spectrum.

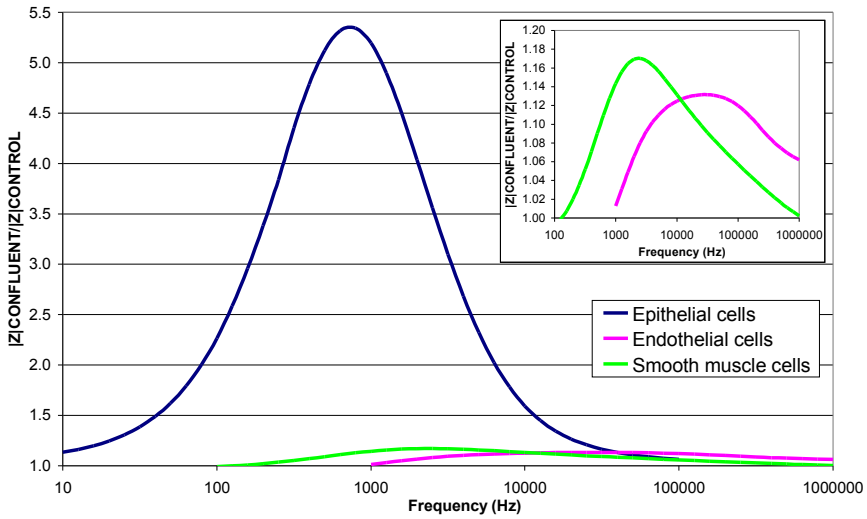

Figure 1-33. Three frequency signatures of different cell types using Z_{xnf}. Image provided by personal correspondence, 2010.

It was also observed that, using this technique, the effects of physical removal of cells and the addition of a drug could be tracked. The method and algorithm is now filed as a patent application by the University of Strathclyde (Shedden & Connolly, 2009) and the patent has been licensed by Ohmedics.

1.9 Conclusion and project objectives

1.9.1 Conclusions

Wounds occur in a significant number of the population and the risk of infection is high. Bacteria cause changes in the chemistry of wound healing and prolong healing times. In addition they grow in communities called biofilms which increases their defences and makes them much more difficult to be eliminated by current medical treatment, for example antibiotics. Infected wounds seriously affect patient welfare and produce enormous cost to the healthcare sector.

Current detection methods are slow and require sampling of the wound which can damage the healing skin and increases the risk of infection. There is an urgent need for the rapid detection of bacteria to increase patient welfare and reduce costs. Current research in addressing this problem are combining sensors, in particular biosensors, with microfluidic devices to allow rapid point of care diagnosis. Unfortunately many of these devices will still require a sample from the wound and hence have the problems associated with wound dressing removal.

Electrical impedance sensor technologies have an advantage that in its simplest form does not require additional substances, for example enzymes, to be added to provide a signal. Also by using a frequency sweep additional information can be gained about the system under test that other sensor techniques cannot provide. A number of studies are now combining impedance technology with sensors that can monitor wounds in real time by placing sensors underneath dressings. The advantages of this are that information can be received immediately without waiting for laboratory results and the dressing does not have to be removed. Therefore a sensor system that could monitor for infection underneath wound dressings would reduce a number of the current problems associated with wound care and infection.

1.9.2 Project objectives

The infection monitor for wounds project aims to create a sensor capable of monitoring infection underneath wound dressings. This would reduce the number of wound dressing changes required and improve the management of wound care. In doing this patient welfare may improve and the costs associated with wound care would reduce. The long term objective is to create a system that would consist of a sensor that could be placed on the wound surface underneath the dressing and measurements would be performed with a hand-held device that would indicate the level of infection and the species of bacteria present (Figure 1-34).

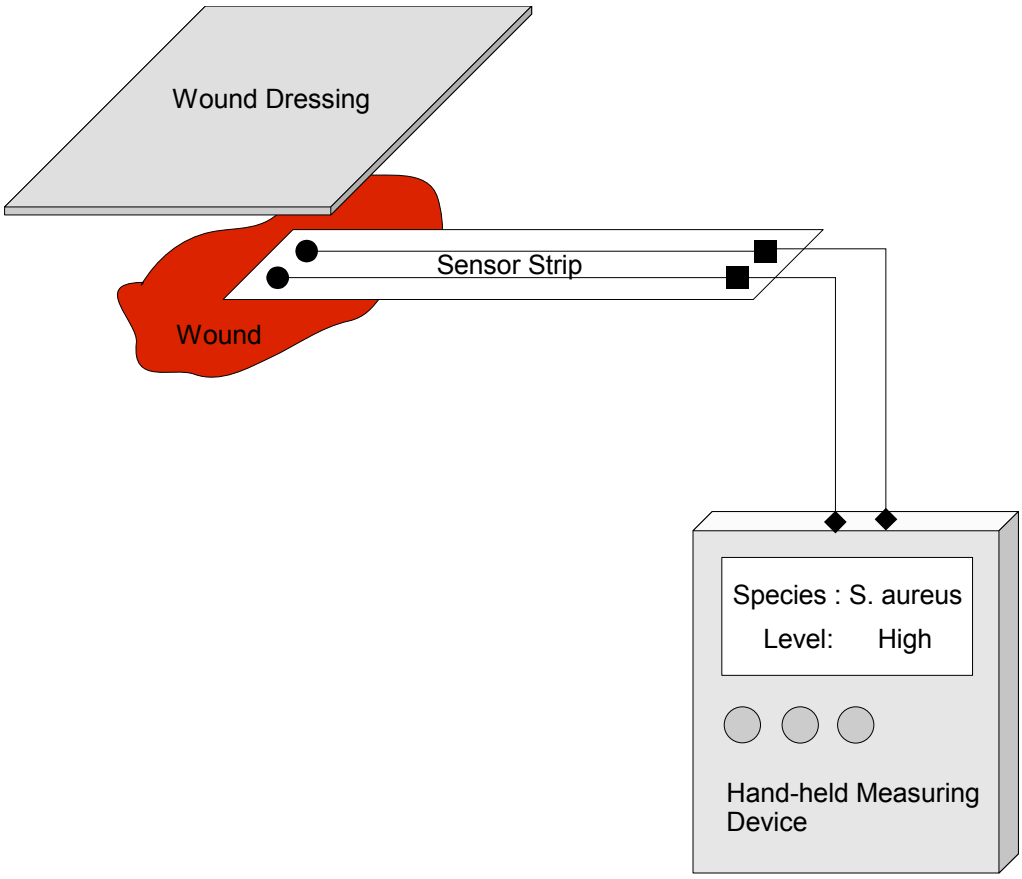

Figure 1-34. The key components of the infection monitor for wounds.

To achieve the objective a number of investigations were performed as a preliminary study of an infection monitor for wounds. The aims of these investigations were:

- **Investigation of electrodes**
  - Measure the electrical impedance of electrodes made of different conducting materials in different solutions.
  - Investigate the effect of different electrode types on bacterial growth.

- **Investigation of bacterial growth in suspension**
  - Measure the electrical impedance of *Staphylococcus aureus* growth from high cell densities with screen-printed Ag-AgCl and carbon sensors.
  - Investigate the effect of screen-printed Ag-AgCl sensors on the growth of *Staphylococcus aureus* from low cell densities.
  - Measure the electrical impedance of *Staphylococcus aureus* growth (multiple strains) from low cell densities with screen-printed Ag-AgCl sensors.
  - Analyse and circuit model the impedance of bacterial suspensions.

- **Investigation of biofilm growth on sensors.**
  - Grow biofilms of *Staphylococcus aureus* (multiple strains) and *Staphylococcus epidermidis* on screen-printed Ag-AgCl and carbon sensors.
  - Measure the electrical impedance of *Staphylococcus aureus* (multiple strains) and *Staphylococcus epidermidis* biofilm growth on screen-printed Ag-AgCl and carbon sensors.
  - Analyse and circuit model the impedance of biofilm growth.

The material and methods, the experimental findings and an analysis of the results from these investigations will now be presented.

2 Materials and methods

This chapter details the materials and methods used in the investigation into an infection monitor for wounds based on electrical impedance. The experiments were divided into two phases, suspension experiments and biofilm experiments. A summary of the experiments are illustrated in Figure 2-1. Briefly the suspension experiments involved examining different electrode materials for their impedance characteristics and their effect on the growth of bacteria, investigating the impedance characteristics of the growth of bacterial suspensions with carbon and silver-silver chloride (Ag-AgCl) electrodes, and finally further investigation of Ag-AgCl sensors with and without impedance measurements.

The biofilm experiments included improving the impedance characteristics of carbon sensors by electrochemical preconditioning, growing biofilms on sensors with and without impedance measurements, and the examination of the biofilms with an alamarBlue assay and with a microscopy staining technique. The impedance measurements from both the suspension and biofilm experiments were analysed for changes due to the presence of bacteria.

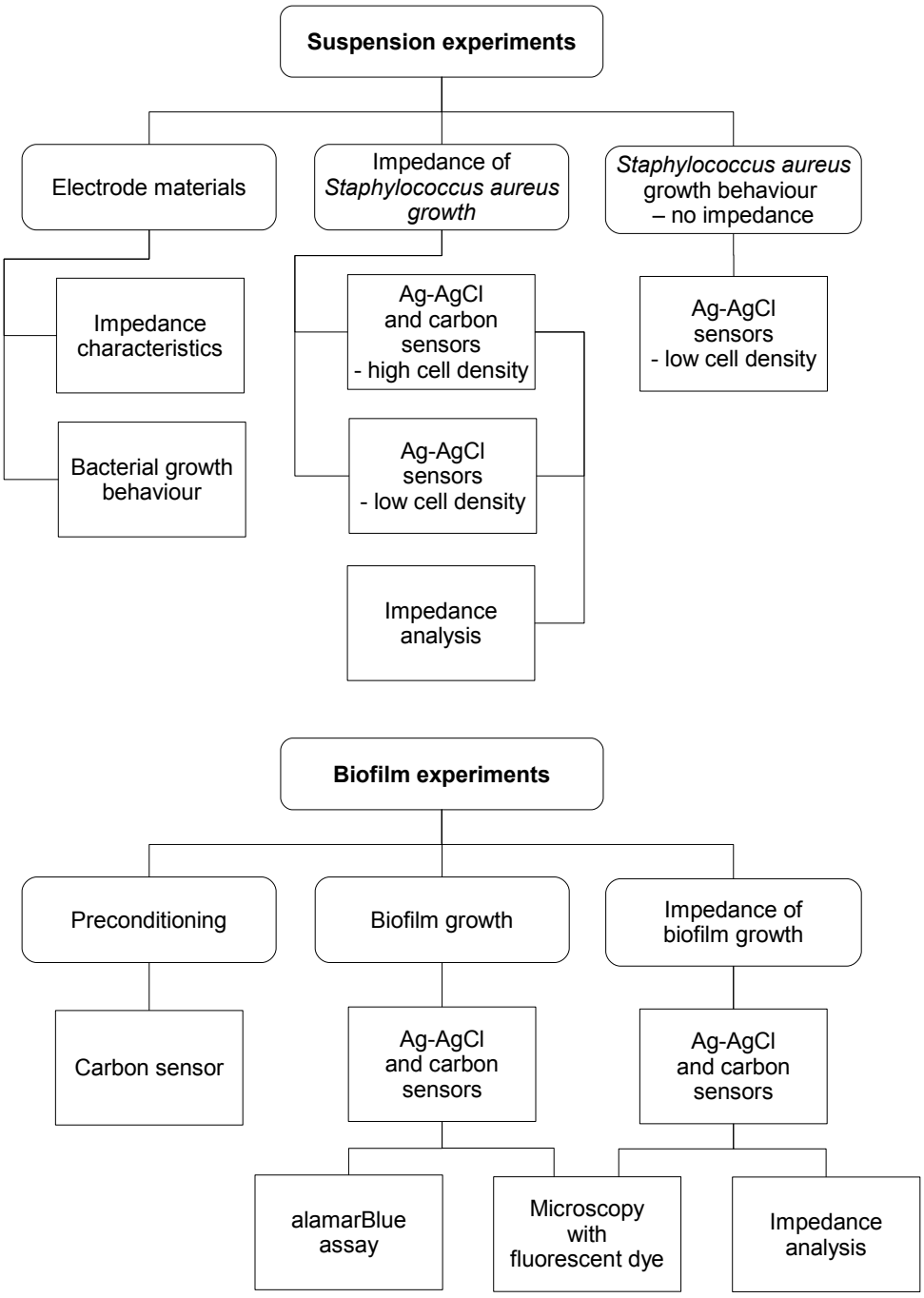

Figure 2-1. Summary of the experiments performed.

2.1 Media and bacteria

2.1.1 Media

A selection of media were used in the experiments. The initial impedance experiments were performed with:

- British Pharmacopoeia Solution A (142mM NaCl, 2.5mM $CaCl.2H_2O$ in 1L of distilled water).
- Mueller-Hinton Broth (Oxoid, Basingstoke, UK).
- A combination of Mueller-Hinton broth and Solution A at standard concentrations.

The remaining suspension experiments included:

- Mueller-Hinton Broth and Mueller-Hinton Agar (Oxoid, Basingstoke, UK).
- Lennox's Broth (1% Tryptone (w/v), 0.5% Yeast Extract (w/v), 1% NaCl (w/v), 0.1% Glucose (w/v) in distilled water).
- 10% Glucose (w/v).
- Lennox's Agar (1% Tryptone (w/v), 0.5% Yeast Extract (w/v), 1% NaCl (w/v), 0.1% Glucose (w/v), 2% Agar (w/v) in distilled water).

The biofilm experiments included:

- Mueller-Hinton broth And Mueller-Hinton agar.

2.1.2 Bacteria

The bacteria used in the experiments were *Staphylococcus aureus*: strains RN4220, SA081, and SA082; *Escherichia coli*: strain JM109; and *Staphylococcus epidermidis*: strain NCTC11964. Two of the *Staphylococcus aureus* strains SA081 and SA082 were isolated from the Glasgow Royal Infirmary on Baird-Parker media. All the staphylococcal strains were stored at -80^{o}C in a cryogenic tube with 375µL overnight culture of Mueller-Hinton broth and 625µL of 80% glycerol (v/v). The strains were streaked onto Mueller-Hinton agar and incubated for 24 hours before experiments. JM109 was also stored at -80^{o}C and streaked before experiments using Lennox's Broth and Lennox's Agar.

2.2 Electrodes

2.2.1 Electrode types

Three types of wire electrode were used: platinum (Pt-wire) with a diameter of 1mm and length 30mm (Goodfellow, Huntingdon, UK); silver (Ag-wire) with a diameter of 1mm and length 30mm (Goodfellow, Huntingdon, UK); and silver-silver chloride (Ag-AgCl-wire) electrodes were created from the silver wire electrodes using a chloriding procedure described in Section 2.2.2.

Screen-printed sensors based on the design of sensors created to monitor moisture levels within wound dressings were created (McColl *et al.*, 2007, 2009). Electrode material ink was screen-printed onto a substrate to form two electrodes, as illustrated in Figure 2-2. The electrodes were then cured in an oven and a polyethylene insulation layer was placed over the tracks leaving the tips and connection points exposed. The three types of sensors, Ag-AgCl, carbon and carbon tipped are illustrated in Figure 2-3. The carbon tipped sensors consisted of an electrode track and connection point made of silver and an electrode tip made of carbon.

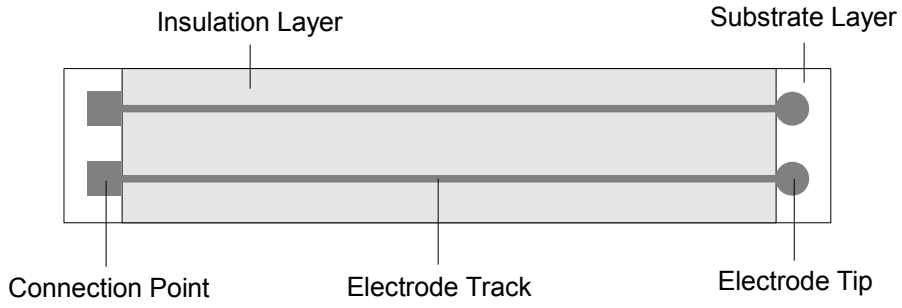

Figure 2-2. The basic design of the screen printed sensors. Note – this is not to scale.

The sensors were screen-printed onto various types of substrate throughout the experiments because of supply and manufacturing issues. The various electrode and substrate combinations used are summarised in Table 2-1. The original polyethylene substrate (-PE100) which was approved for medical usage was discontinued by the manufacturers and had to be substituted with two alternative polyethylene substrates (-PE200, -PE300). Acetate was used as the substrate in some experiments to conserve the polymer substrate for the bacterial experiments.

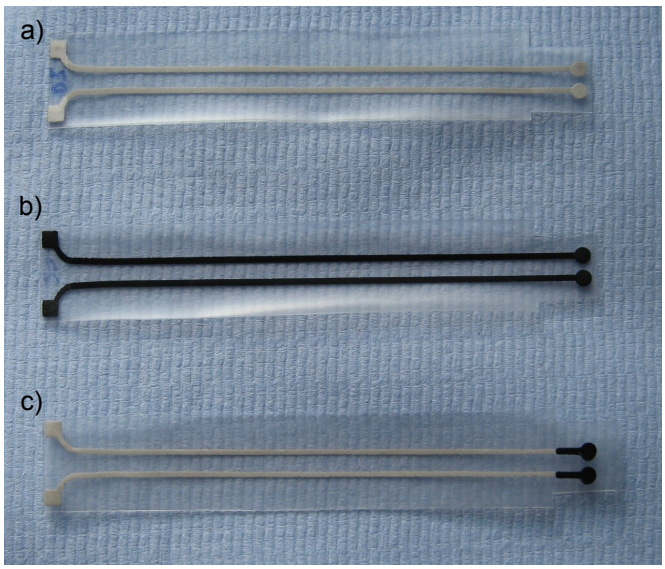

Figure 2-3. The screen-printed electrodes on polyethylene substrate: a) Ag-AgCl; b) Carbon; c) Carbon tipped with a silver track**.**

Table 2-1. Explanation of sensor combinations.

Substrate	Explanation	Sensors
-PE100	Original polymer substrate. Discontinued.	Ag-AgCl-PE100
-PE200	1st alternative polymer substrate. Ag-AgCl ink did not bond to substrate. Carbon electrodes were unstable.	C-PE200
-PE300	2nd alternative polymer substrate. Carbon ink bonded with thin layer which meant multiple prints were required to increase thickness.	Ag-AgCl-PE300 C-PE300 then C-PE300-v2 C-tip-PE300
-acetate	Used to conserve polyethylene material for bacterial experiments	Ag-AgCl-acetate C-acetate C-tip-acetate

2.2.2 Chloriding procedure

An electrochemical cell was created with 40ml of 0.1mM hydrochloric acid in a beaker, a Pt-wire electrode, an Ag-wire electrode and the circuit was completed with a Solartron 1287 electrochemical interface (Solartron, Hampshire, UK) (Figure 2-4). The chloride deposit was created by passing a fixed current across the electrodes for a specified time, with the silver wire positive with respect to the platinum electrode. The current density was found by dividing the current by the area of the deposit (Eqn. 2-1). The quantification of the chloride deposit was calculated by multiplying the current density with the time, t (Eqn. 2-2).

$$Current\ density = \frac{I}{A} \tag{2-1}$$

$$Chloride\ Deposit = Current\ density * t \tag{2-2}$$

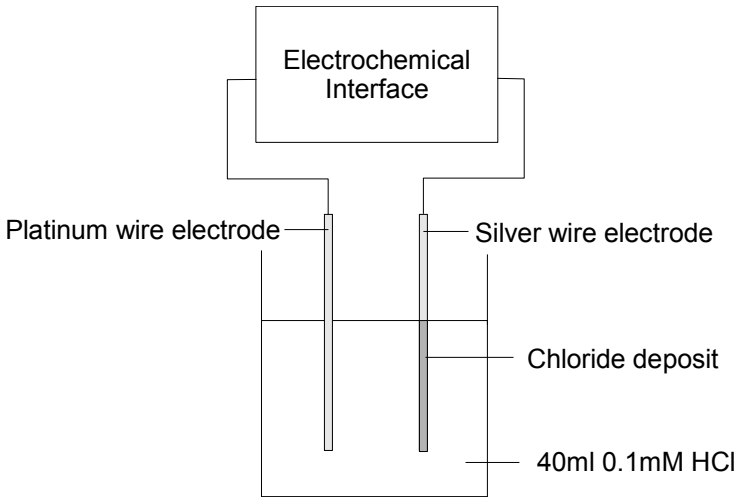

Figure 2-4. Electrochemical circuit to chloride electrodes. The circuit contains a platinum wire electrode, a silver wire electrode, hydrochloric acid and is completed by the electrochemical interface.

The standard procedure used in previous projects within this group was a current density of 400μA cm^{-2} for 30 minutes, which to chloride a 20mm length of Ag-wire gives an area of 0.636cm^2 and requires a current of 254.4μA. The procedure was duplicated to produce a pair of Ag-AgCl-wire electrodes.

2.2.3 Impedance of media with different electrode types procedure

To assess the impedance response of different media and different electrode types the following procedure was used. Two wire electrodes of the same material or a screen-printed sensor were placed in a beaker containing 40ml of media (Figure 2-5). The electrodes were connected up to a Solartron 1260 frequency response analyser (Solartron, Hampshire, UK). The Solartron 1260 was connected to a computer with the control software, ZPlot (Scribner Associates Inc., Southern Pines, USA). Five sequential impedance measurements were performed with a frequency sweep from 1MHz to 0.1Hz and a voltage of 200mV. The electrodes were rinsed in distilled water after each use.

To examine the different media the procedure was performed with Ag-AgCl-wire electrodes with Solution A, Mueller-Hinton broth (MHB), and the MHB/Solution A combination. For the comparison of different electrode types the procedure was performed with MHB, and these electrode materials: Ag-AgCl-wire; Pt-wire; Ag-wire; Ag-AgCl-PE100; and C-PE200.

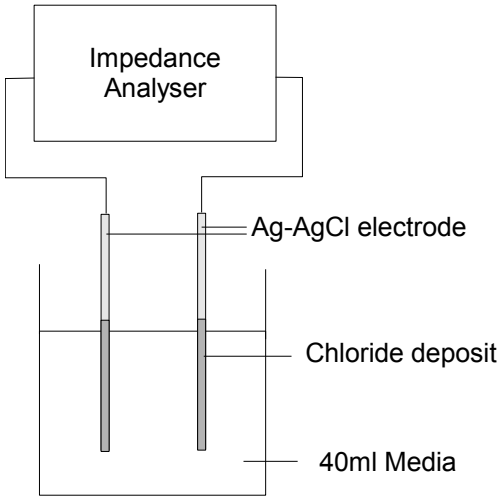

Figure 2-5. Impedance of media with different electrode types test rig. This test rig was used to investigate the impedance of various media types using various electrodes and consists of a pair of electrodes (Ag-AgCl-wire are shown) or a screen-printed sensor held in the media and connected to an impedance frequency analyser.

2.3 Bacterial growth with different electrode types procedure

The effect of different electrode materials on the growth of bacteria was investigated by the following procedure. Each electrode or sensor was sterilised for 10 minutes in 70% ethanol (v/v) (Sopwith *et al.*, 2002) and rinsed in sterile water before use. For each electrode type a 20ml glass bijoux vial was filled with 5ml of media and the electrode placed inside. A control vial was filled with only 5ml of media. Each vial was inoculated with a single colony of RN4220 and cultured overnight on an IKA KS130 orbital shaker, 160rpm (IKA, Staufen, Germany) in a LEEC GA2010 incubator, 37^{o}C (LEEC, Nottingham, UK). Final bacteria numbers were found by the plate counting method on Mueller-Hinton agar. Each experiment was performed in triplicate.

The parameters varied were the electrode type and the species of bacteria, as listed in Table 2-2. The *Staphylococcus aureus* strain, RN4220, was grown in MHB and the *Escherichia coli* strain, JM109, was grown in Lennox's broth. The electrodes grown with RN4220 were Ag-wire, Ag-AgCl-acetate, Ag-AgCl-wire, Ag-AgCl-PE100, and C-PE200. The strain JM109 was only grown with electrodes Ag-AgCl-PE100 and C-PE200.

Table 2-2. Parameters varied in the bacterial growth experiments.

Electrode type	Bacteria	Media
Ag-wire	RN4220	MHB
Ag-AgCl-acetate	RN4220	MHB
Ag-AgCl-wire	RN4220	MHB
Ag-AgCl-PE100	RN4220	MHB
C-PE200	RN4220	MHB
Ag-AgCl-PE100	JM109	Lennox's broth
C-PE200	JM109	Lennox's broth

2.4 Impedance measurements with bacterial suspensions – single

2.4.1 Test rig for bacterial suspensions with impedance – single

The test vial (RN4220-Z) consisted of a 20ml universal vial and a specially designed PTFE cap which held the screen-printed sensor down the centre of the vial (Figure 2-6). The tip of the sensor was shaped to allow the liquid to flow around the sensor substrate. The test vial was clamped in a clamp stand which was situated on the orbital shaker, 240rpm, inside the incubator (Figure 2-7). The sensor extension strip was connected via crocodile clips to connecting wires that exited the incubator and connected to the Solartron 1260 frequency response analyser. A second test vial, also clamped, was used as a media only control (MHB-Z). A third universal vial was used as a bacterial growth control and contained no sensor (RN4220-control).

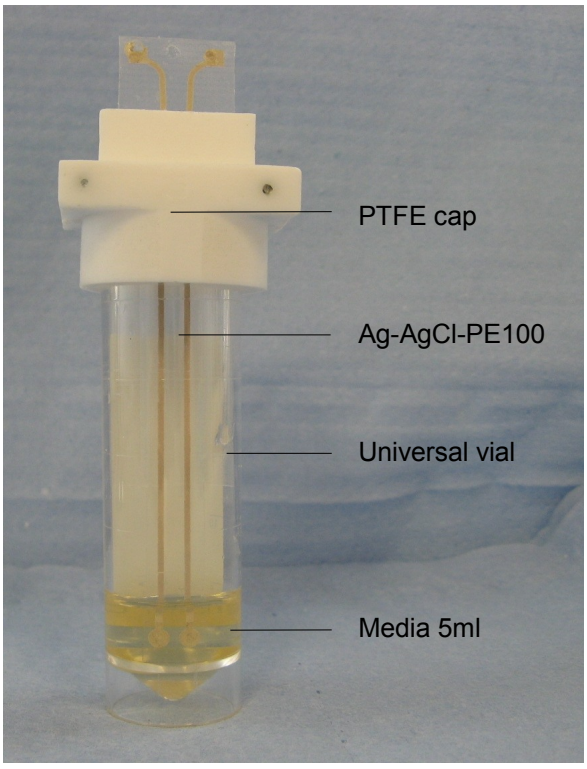

Figure 2-6. The single bacterial suspension test vial. The test vial comprised of a 30ml universal vial, 5ml of media, a specifically designed PTFE cap and a Ag-AgCl-PE100 sensor.

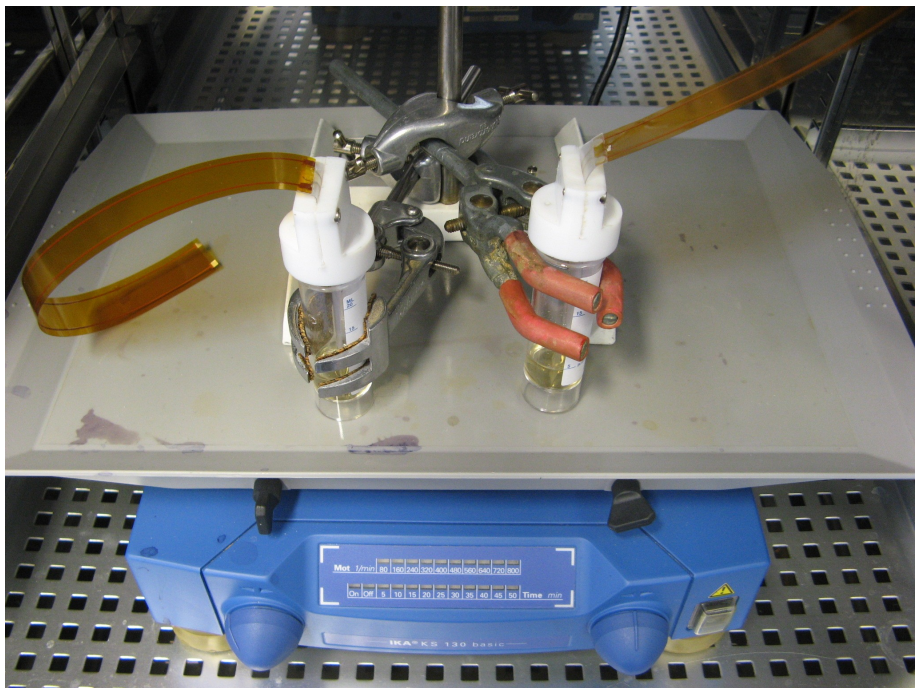

Figure 2-7. The single suspension test rig. The test rig showing the MHB-Z and RN4220-Z test vials.

2.4.2 Procedure for bacterial suspensions with impedance – single

The two test vials (RN4220-Z, MHB-Z) without their sensors and the bacteria control (RN4220-control) (as described in Section 2.4.1) were filled with 5ml of media. The sensors were tested for conductivity with an Ohm-meter and sterilised in 70% (v/v) ethanol for 10 minutes, rinsed in sterile water and placed in the test vials. The test vials were placed in the test rig and three impedance measurements with frequency sweeps from 1MHz to 0.1Hz at a voltage of 200mV were performed on each test vial. The first two measurements with the orbital shaker stationary and the third at 240rpm. The test vials were removed from the test rig and the sensors removed. The first two measurements were to ensure the system was functioning correctly and the third measurement was designated the start reading.

The RN4220-Z test vial and the RN4220-control vial were inoculated with a single colony of RN4220. Sensors were replaced in the test vials and all three vials replaced in the test rig. Impedance measurements with frequency sweeps from 1MHz to 0.1Hz at a voltage of 200mV were performed every hour for 17 hours on the RN4220-Z test

vial and performed on the MHB-Z test vial at 0, 16 and 17 hours. The final numbers of bacteria were found by the plate counting method from all three vials. The sample from the MHB-Z test vial was to check for contamination.

The complete procedure was reproduced five times for each of the parameter combinations and the experiments are summarised in Table 2-3. The first combination was Ag-AgCl-PE100 sensors with 5ml of Mueller-Hinton broth (MHB), the second was Ag-AgCl-PE100 with 4.9ml of MHB and 0.1ml of 10% glucose (w/v) to create a 0.2% glucose (v/v) concentration, and the final combination was C-PE200 sensors with 5ml of MHB. In addition the procedure was repeated with a single test vial containing media only to record the hourly measurements for 17 hours. This was performed five times for MHB only and MHB with 0.2% glucose only. The RN4220-Z test vial and RN4220-control vial were not used in this instance.

Table 2-3. Parameters varied in the single bacterial suspension experiments.

Media	Bacteria	Electrode Type
MHB	n/a	Ag-AgCl-PE100
MHB	RN4220	Ag-AgCl-PE100
MHB, Glucose	n/a	Ag-AgCl-PE100
MHB, Glucose	RN4220	Ag-AgCl-PE100
MHB	n/a	C-PE200
MHB	RN4220	C-PE200

2.5 Bacterial growth procedure – low inoculation densities

The growth of bacteria from a single colony which was approximately $1x10^6$ colony forming units per millilitre (CFU ml^{-1}) was deemed too high for clinical relevance in some situations and therefore was reduced to $1x10^3$ CFU ml^{-1}. However the growth of bacteria appeared to be partially inhibited from this density and therefore the reduction of bacterial growth levels in the presence of Ag-AgCl-PE300 sensors was investigated using different starting cell densities, pre-washed electrodes and with bacteria previously grown in the presence of the electrodes.

The general procedure for each of these experiments was a single colony of the bacterial strain was sub-cultured in 5ml of broth for 24 hours. Two universal vials were filled with 4.9ml of Mueller-Hinton broth (MHB) to create test and control vials. The Ag-AgCl-PE300 sensors were sterilised in 70% ethanol (v/v) for 10 minutes, rinsed in sterile water and placed in the test vial. The 24 hour culture was serially diluted and 100µL of culture was added to the test vial and the control to achieve the required starting density, approximately $1x10^3$ CFU ml^{-1}. Cultures were grown for 24 hours at 240rpm and 37°C. The final numbers of bacteria were found using the plate counting method. For each of the parameters varied the procedure was repeated three times for each strain of RN4220, SA081 and SA082.

The general procedure was adapted for each of the parameters varied and a summary of the experiments conducted are shown in Figure 2-8. **Starting cell densities:** Four sets of test and control vials were filled with 4.9ml of MHB. Each set of test and control vials were inoculated with a different starting density, approximately $1x10^5$, $1x10^4$, $1x10^3$ and $1x10^2$ CFU ml^{-1}. **Pre-washed electrodes:** The electrodes were sterilised as described in the general procedure and then placed in 5ml of MHB for 24 hours at 240rpm and room temperature prior to inoculation. The liquid was refreshed after 21 hours and 23 hours by removing the electrode, rinsing in sterile water and placing into a new universal vial with 5ml of fresh MHB. At 24 hours the liquid was refreshed once more and the vials inoculated. **Pre-grown bacteria:** The

general procedure was sequentially performed twice for each strain. The first culture was inoculated from the 24 hour culture and the second group of cultures were inoculated from one of the first cultures that had grown to expected levels.

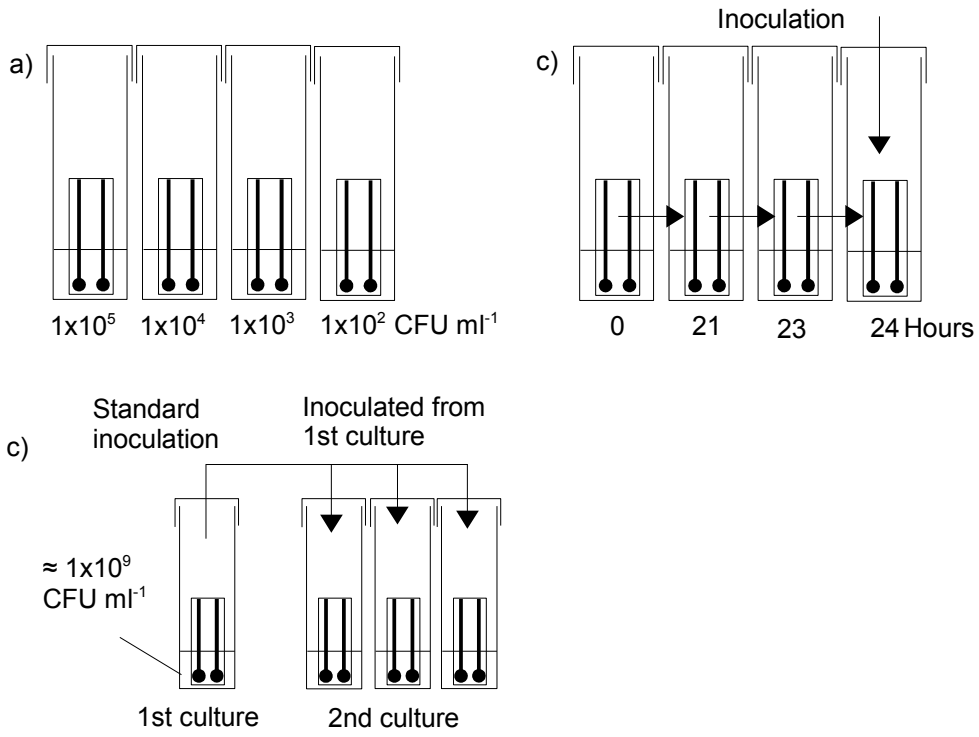

Figure 2-8. Parameters varied for investigating bacterial growth in the presence of Ag-AgCl-PE300 sensors: The three parameters varied were: a) starting cell densities; b) preparation of electrodes; and c) pre-grown bacteria.

2.6 Impedance measurements with bacterial suspensions – parallel

2.6.1 Test rig for bacterial suspensions with impedance – parallel

This test rig was designed for performing impedance measurements on eight bacterial suspensions in parallel. The test vial was modified from the single suspension test vial (Section 2.4.1) to include a syringe needle and rubber tubing for inoculation and sample collection without requiring to remove the sensor (Figure 2-9). In addition the shape of the PTFE cap was changed to make manufacturing of them easier. After some initial experiments the syringe needle and tubing were removed as a precaution against them having an effect on the growth or the impedance measurements. The test vials were then inoculated and sampled with a syringe needle which was withdrawn during experiments. The eight test vials were held in a specially designed PTFE test rack (Figure 2-10) which was situated on the orbital shaker, 240rpm, inside the incubator, 37^{o}C.

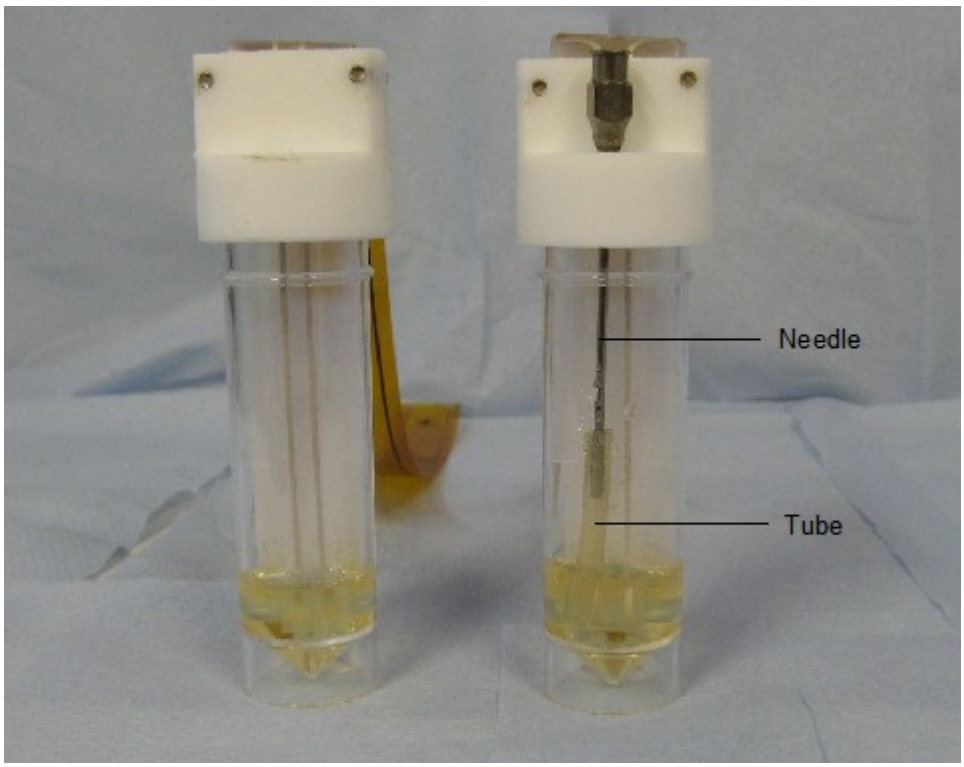

Figure 2-9. The modified test vial. The test vial comprising of a 30ml universal vial, 5ml of media, a specially designed PTFE cap and Ag-AgCl-PE300 electrodes. The needle and tube are shown in the right hand test vial.

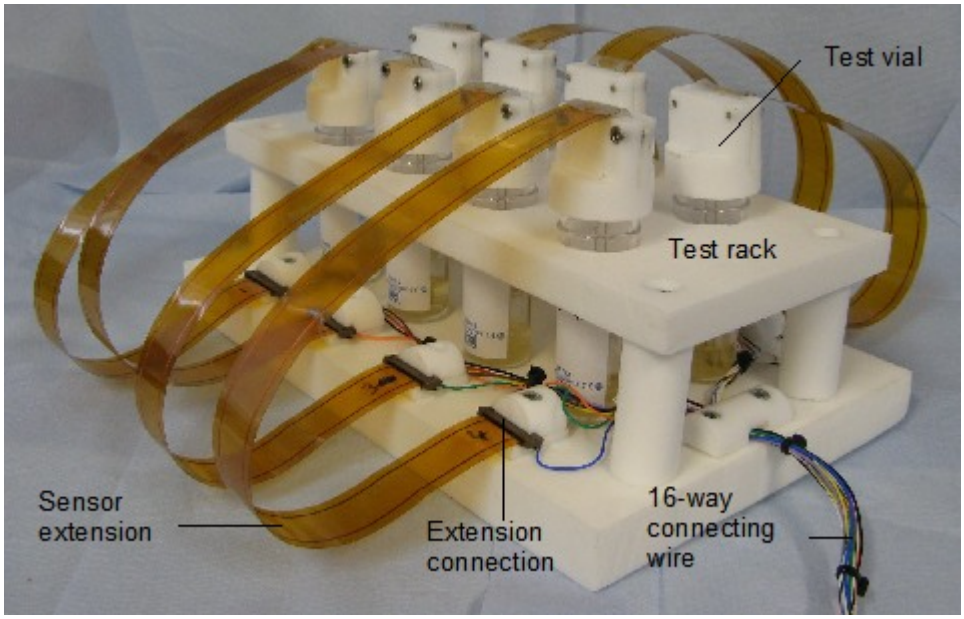

Figure 2-10. The test rack for impedance measurements of bacterial suspensions in parallel.

The electrical and impedance equipment configuration consisted of the Ag-AgCl sensors and their extensions connected to a 16-way cable on the test rack as illustrated in Figure 2-11. The 16-way cable passed out of the incubator to a specially designed junction box which converted the two electrode system to the standard four connections required by the impedance equipment. The junction box was connected to the Solartron 1281 multiplexor (Solartron, Hampshire, UK) via eight 4 way cables and this was connected to the Solartron 1260 impedance analyser via BNC cables. The Solartron 1260 was connected to a computer with the control software, ZPlot.

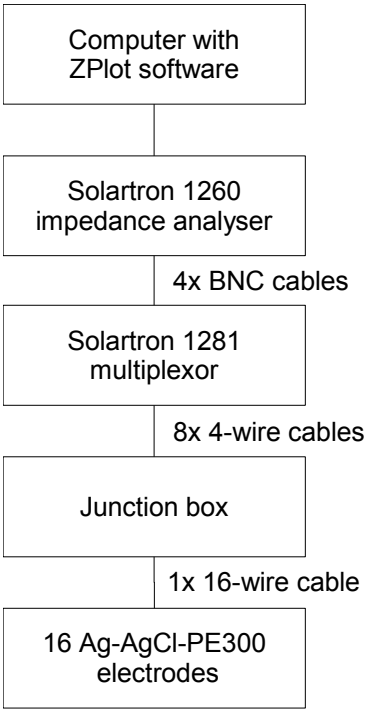

Figure 2-11. The electrical and impedance equipment configuration for the parallel bacterial suspension measurements. The equipment consisted of a computer with Zplot software, Solartron 1260 impedance analyser, Solartron 1281 multiplexor, and the Ag-AgCl-PE300 sensors.

2.6.2 Procedure for bacterial suspensions with impedance – parallel

The general procedure for the parallel bacterial suspensions was the required number of test vials were each filled with 4.9ml of media. The electrode resistances were measured with an ohm-meter, the sensor was sterilised in 70% ethanol (v/v) for 10 minutes (Sopwith *et al.*, 2002) and rinsed in sterile water before being placed into the test vials, secured by the test vial caps. The test vials were placed into the test rack and the sensor extensions connected to the cables. The test rack was placed into the test rig and two impedance sweeps from 1MHz to 0.1Hz at a voltage of 200mV were performed.

The test vials designated for bacterial growth were inoculated, via a syringe needle, with 100µL of MHB containing approximately $1x10^3$ CFU ml^{-1}, diluted from a 24 hour broth culture. Impedance measurements with frequency sweeps from 1MHz to 0.1Hz at a voltage of 200mV were performed every hour for 16 or 24 hours on the bacteria culture. The start and final numbers of bacteria were found using the plate counting method.

The first parallel suspension experiment varied the media and preparation of the sensors (Table 2-4). The Mueller-Hinton broth (MHB) with glucose was prepared by adding concentrated glucose to MHB, for example MHB with 0.2% glucose was prepared with 4.9ml MHB and 0.1ml of 10% glucose (w/v). The pre-washed sensors were used as described in the general procedure except between sterilisation and placement in the test vial they were washed for 24 hours in MHB with rinses in sterile water and placement into fresh media at 21 and 23 hours as in the experiments without impedance measurements (Figure 2-8). At 24 hours the sensor was rinsed in sterile water and placed into the test vials with fresh media.

Table 2-4. The test vial configuration for the first parallel bacterial suspension experiments.

Test vial	Media	Bacteria	Pre-washed sensor
1	MHB	n/a	No
2	MHB, 0.2% glucose	n/a	No
3	MHB	RN4220	No
4	MHB, 0.1% glucose	RN4220	No
5	MHB, 0.2% glucose	RN4220	No
6	MHB, 0.4% glucose	RN4220	No
7	MHB	n/a	Yes
8	MHB	RN4220	Yes

The second parallel bacterial suspension experiment investigated the influence of the impedance measurements on the bacterial growth. The general procedure for parallel bacterial suspensions was performed with the eight test vials containing 4.9ml of MHB. The eight vials were paired, 1 and 5, 2 and 6, 3 and 7, and 4 and 8. Each pair were inoculated with 100µL of MHB containing approximately $1x10^3$ CFU ml^{-1} diluted from separate 24 hour cultures. Impedance measurements were performed only on vials 1 to 4 (Table 2-5). This was repeated for each strain of *Staphylococcus aureus,* RN4220, SA081 and SA082. In addition to compare the impedance of the bacterial cultures the general procedure for parallel bacterial suspensions was performed with four vials containing only MHB and no bacteria.

Table 2-5. The test vial configuration to investigate the influence of impedance measurements on bacterial growth. This was performed with all three strains of *Staphylococcus aureus*.

Test Vial	Impedance Measurements	Bacteria
1	Yes	Culture 1
2	Yes	Culture 2
3	Yes	Culture 3
4	Yes	Culture 4
5	No	Culture 1
6	No	Culture 2
7	No	Culture 3
8	No	Culture 4

2.7 Preconditioning of carbon sensors

The bacterial growth with Ag-AgCl sensors was variable and to design a sensor that did not affect bacterial growth, carbon sensors were investigated further. Preconditioning of the electrodes with electrochemical methods was investigated to lower their electrical impedance.

2.7.1 Preconditioning with cyclic voltammetry

To investigate how the preconditioning altered the impedance of the sensors one frequency sweep was performed before and after the preconditioning procedure. The impedance was measured with the procedure described in Section 2.2.3 with the wire electrodes replaced with a carbon sensor, the media used was Mueller-Hinton broth and the frequency sweep was performed from 10MHz to 0.1Hz.

The preconditioning was performed in an electrochemical cell with a three electrode system as illustrated in Figure 2-12. The electrolyte was 40ml of potassium chloride. The reference electrode was a silver-silver chloride electrode, the working electrode was a platinum wire and the counter electrode was the experimental carbon or carbon tipped electrodes connected in parallel. The circuit was completed with a Solartron 1281 electrochemical interface and controlled through the computer software Corrware (Scribner Associates Inc., Southern Pines, USA).

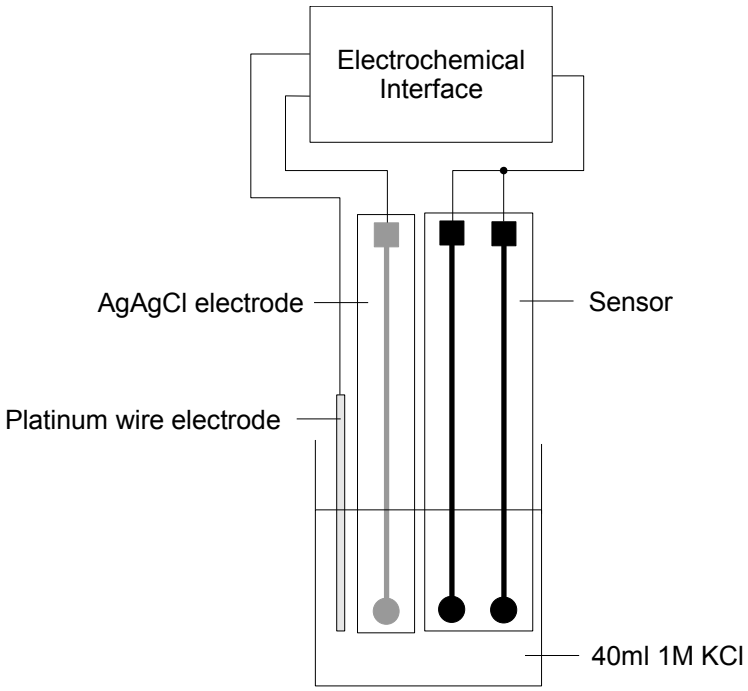

Figure 2-12. First electrochemical circuit to precondition the carbon electrodes. The circuit comprises of a platinum working electrode, a Ag-AgCl reference electrode, the carbon sensor as counter electrodes, potassium chloride solution and an electrochemical interface.

Cyclic voltammetry with a voltage, V, and a scan rate, r, was applied for a time, t. The parameters V and t were varied to find a suitable preconditioning method and the different parameter variations are listed in Table 2-6. For the parameter t, the same electrode was repeatedly preconditioned for 10 minutes between impedance measurements. The remaining parameters had new electrodes for each variation. Each parameter selection was performed on three C-acetate sensors and three C-tip-acetate sensors. Sensors on acetate were used in order to reserve the sensors on polyethylene substrate for the bacteria and impedance experiments.

Table 2-6. Parameter selections for investigating preconditioning of the electrodes with cyclic voltammetry.

Voltage (V)	Scan rate (mV s^{-1})	Time (minutes)
2.5	100	10, 20, 30
5.0	200	20
7.5	300	20

The preconditioning of the carbon tipped sensors resulted in a greater improvement in the impedance behaviour when compared with the preconditioned carbon sensors. However there was concern that the silver track of the C-tip-acetate sensors may be exposed to the media and therefore the C-tip-PE300 sensors were created with a shorter silver track, safely underneath the insulation layer. This increased the length of the carbon track and hence the resistance of the electrode increased, which had a detrimental effect on the preconditioning. In addition the current manufacturing method was unable to accurately reproduce carbon tipped sensors with similar electrical impedance behaviour. Therefore further preconditioning experiments were performed to simplify the procedure and improve the preconditioning of the pure carbon sensors.

2.7.2 Preconditioning with a square waveform

Impedance measurements were performed as described in Section 2.7.1. The preconditioning was performed in an electrochemical cell with a two electrode system as illustrated in Figure 2-13. The conditioning media was either 5ml of one mole of potassium chloride or Mueller-Hinton broth. The working electrode and the counter electrode were one of the electrodes in the experimental carbon sensor. The circuit was completed with a Solartron 1281 electrochemical interface and controlled by the Corrware software.

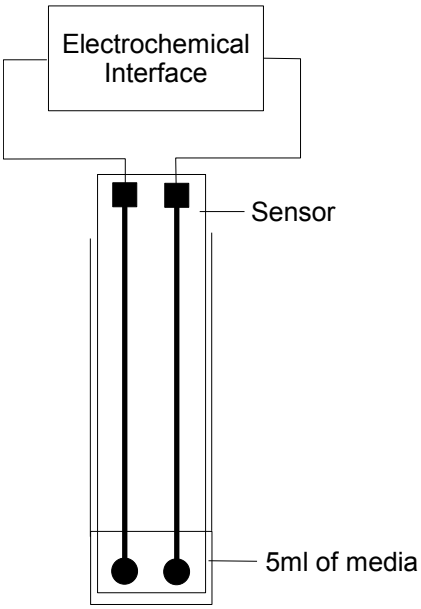

Figure 2-13. Second electrochemical circuit to precondition the carbon electrodes. The circuit comprises the carbon sensor acting as both the working and counter electrodes, 5ml of conditioning media and an electrochemical interface.

A square waveform with a voltage, V, and a period, P, was applied for a time t. The parameters V, P and t were varied to find a suitable preconditioning method and the different parameter variations are listed in Table 2-7. For the parameter t, the same electrode was repeatedly preconditioned for 10 minutes between impedance measurements. The remaining parameters had new electrodes for each variation. Each parameter selection was performed on three C-acetate sensors.

Table 2-7. Initial parameter variation for investigating preconditioning carbon sensors.

Sensor	Voltage (V)	Period (s)	Time (minutes)	Media
C-acetate	10	120	10, 20, 30, 40, 50	KCl
C-acetate	10	10, 40, 120, 300	20	KCl
C-acetate	5, 10, 12.5	120	20	KCl

The most suitable pre-conditioning parameters were a voltage of 10V, a period of 120s and a time of 20 minutes on the C-acetate sensors. More difficulties were discovered upon the creation of carbon sensors on the polyethylene substrate. The thickness of the carbon was significantly less than that on the acetate, which meant

that the electrode's resistance was greater by approximately a factor of 10 compared to the carbon electrodes on acetate. The higher starting impedance meant that after preconditioning the impedance of the C-PE300 sensors was still higher than the impedance of the C-acetate sensors. To solve the issue of the increased resistance, carbon sensors with thicker tracks were created, C-PE300-v2.

The final preconditioning experiment investigated the effect of the media on the impedance after preconditioning. The optimum preconditioning procedure was performed with KCl and MHB, each on three C-acetate and three C-PE300-v2 sensors (Table 2-8). Based on the overall impedance magnitude and phase the MHB produced a superior conditioning of the carbon electrodes on the polyethylene substrate compared with KCl. Therefore the carbon sensors (C-PE300-v2) for the biofilm experiments were preconditioned with a square-wave with a voltage of 10V, a period of 120s and for a time of 20 minutes in Mueller-Hinton broth.

Table 2-8. Further parameter variation for investigating preconditioning of carbon sensors.

Sensor	Voltage (V)	Period (s)	Time (minutes)	Media
C-acetate	10	120	20	KCl
C-acetate	10	120	20	MHB
C-PE300-v2	10	120	20	KCl
C-PE300-v2	10	120	20	MHB

2.8 Biofilm growth procedures

2.8.1 Procedure for biofilm growth without impedance measurements

To investigate the biofilm growth on the sensors without impedance measurements square surfaces, measuring 13mm by 13mm were created as illustrated in Figure 2-14. The sensor surface was created by cutting the tip off the full length sensors on polyethylene. The control surface was created by cutting a square from the polyethylene substrate (-PE300). Additional insulation was added to the sensor surfaces over the edge where the electrode tracks had been cut. This extra piece of insulator was also added to the control squares to mimic the sensors. Surfaces were sterilised with 70% ethanol for 10 minutes and then rinsed in sterile water before use.

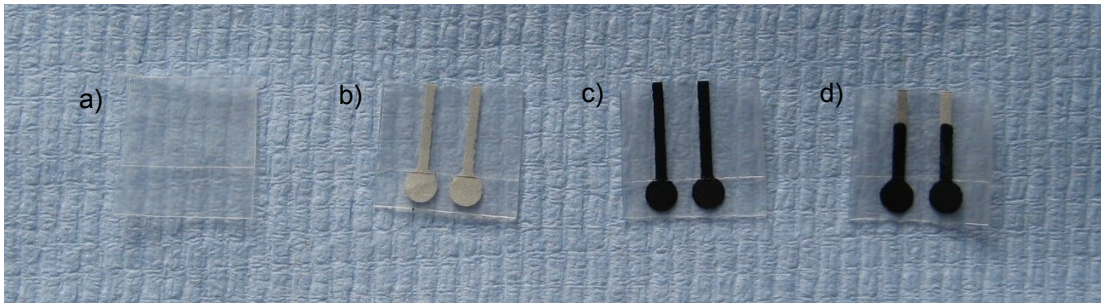

Figure 2-14. The surfaces for biofilm growth without impedance measurements: a) PE300 control surface; b) Ag-AgCl-PE300 sensor surface; c) C-PE300 sensor surface; d) C-tip-PE300 sensor surface (not used in biofilm experiments).

For biofilm growth, two 90mm petri dishes with three Ag-AgCl sensor surfaces inside the first dish and three control surfaces inside the second dish, as illustrated in Figure 2-15. A volume of 19.7ml of Mueller-Hinton broth (MHB) was added to each dish and then each dish was inoculated with 3 x 100µL of 24 hour culture at approximately $1x10^3$ CFU ml^{-1}. The dishes were then incubated at 37ºC for either 24 hours or 48 hours. Upon completion of the incubation period surfaces from the petri dishes were sequentially washed in 3 x 2ml of phosphate buffer saline (PBS) to remove loose bacteria. All surfaces were then either analysed with an alamarBlue assay, Section 2.8.4, or stained with a fluorescent dye and imaged with a microscope, Section 2.8.5.

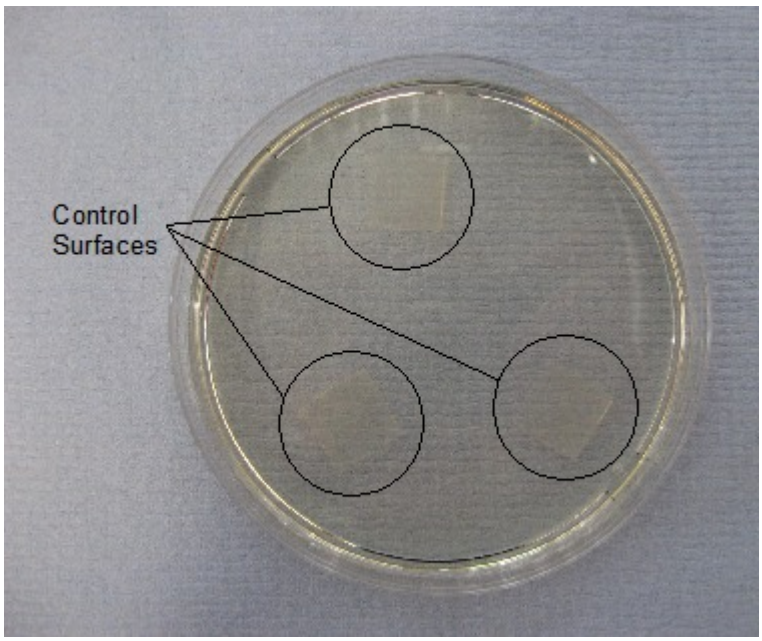

Figure 2-15. Petri dish configuration for biofilm growth with no impedance measurement. Three control surfaces are shown.

To grow biofilms on the carbon sensors the procedure with the petri dishes was modified due to the risk of leakage from the petri dishes as found during the experiments with impedance, as described in Section 2.8.2. Three carbon sensor surfaces and three control surfaces were placed into six wells within a 24-well plate, as illustrated in Figure 2-16. Each well had a volume of 1.9ml of MHB added and were inoculated with 100µL of 24 hour culture at approximately $1x10^3$ CFU ml^{-1}. The 24-well plate was incubated for 48 hours at 37°C and then the surfaces washed sequentially in 6 x 2ml of PBS. The washing in PBS of the surfaces from the 24-well plates was increased to 6 x 2ml to ensure all the loose bacteria were removed. All surfaces were then either analysed with an alamarBlue assay, Section 2.8.4, or stained with a fluorescent dye and imaged with a microscope, Section 2.8.5.

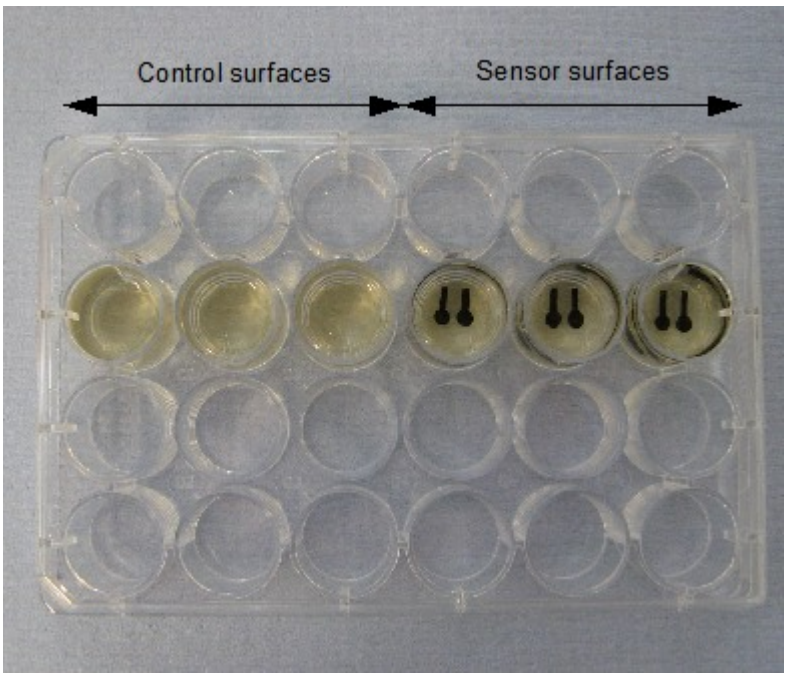

Figure 2-16. The 24-well plate configuration for biofilm growth without impedance measurements. Three control surfaces and three carbon sensor surfaces are shown.

2.8.2 Procedure for biofilm growth with impedance measurements

To examine the impedance measurements of biofilm growth on the sensors, a test rig was created. A Ag-AgCl-PE300 sensor was placed in a 60mm petri dish with the electrode tips centred and taped in place with a strip of the polyethylene insulation layer (Figure 2-17). This was repeated for six sensors, five for biofilm growth and one as a media only control. In addition one control surface (as described in Section 2.8.1) was placed in a 60mm petri dish. The test dishes were sterilised with 70% ethanol for 10 minutes and then rinsed out with sterile water three times.

A volume of 9.9ml of Mueller-Hinton broth (MHB) was added to each petri dish. In turn each of the sensors were connected to the Solartron 1260 frequency analyzer and two initial frequency sweeps were performed from 10MHz to 0.1Hz with a voltage of 200mV. The five bacterial test dishes and control surface were then inoculated with 100µL of 24 hour culture at approximately $1x10^3$ CFU ml^{-1}. The test dishes were then placed back in the test rig and incubated for 48 hours. A final impedance sweep on each dish was performed at 48 hours.

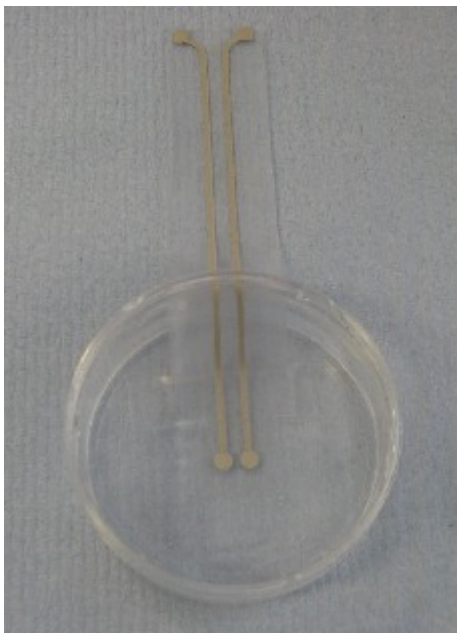

Figure 2-17. The petri dish with a Ag-AgCl-PE300 sensor.

The test rig for the carbon sensors was modified due to the possibility of leakage from the petri dish as found during the Ag-AgCl biofilm experiments. This was caused by the sensor substrate pressing the liquid up and over the side wall of the petri dish particularly when the dishes were nudged while connecting to the Solartron 1260. The second test rig was created by placing three sensors into a 24-well plate and adding 1.9ml of MHB to each sensor well. A second 24-well plate with three sensors was also created. Five of the sensors were for bacterial growth and one as a control system containing only 2ml of MHB. A square control surface (Section 2.8.1) was added to another well with 1.9ml of MHB.

All six sensors were then electrically connected to the connection points on the test rack used for the bacterial suspension experiments. One 24-well plate connected to the test rack is illustrated in Figure 2-18. The 16-way cable was connected to the multiplexor impedance equipment (Figure 2-11). Two initial frequency sweeps were performed. The five bacterial test dishes and control surface were then inoculated with 100µL of 24 hour culture at approximately $1x10^3$ CFU ml^{-1}. Impedance measurements were performed on each of the sensors every hour for 48 hours. No measurement was performed at zero hours, immediately after inoculation.

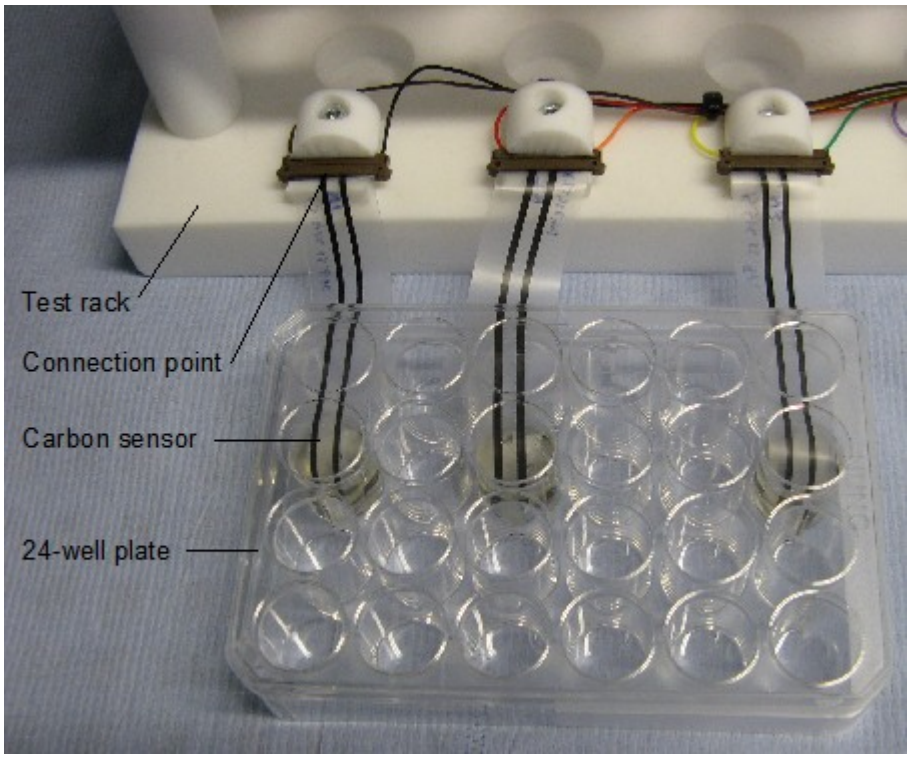

Figure 2-18. Test rig for carbon sensors. This illustrates one 24 well plate with three electrodes connected to the test rack. Another set of three electrodes would be connected to the other side of the test rack.

After the final impedance measurements the sensor tips from the test rigs were cut off and the Ag-AgCl tips were washed sequentially in 3 x 2ml of Phosphate Buffer Saline (PBS) while the carbon tips were washed in 6 x 2ml of PBS. The control surfaces were also washed. A 100µL sample from the control system, MHB-only was plated on to a MHB agar plate to test for contamination. Surfaces were then prepared for imaging (Section 2.8.5).

2.8.3 AlamarBlue assay optimisation

This procedure was performed with strains SA081, SA082 and NCTC11964. The biofilm growth without impedance measurements procedure was performed with twelve control surfaces in petri dishes for 48 hours. After the washing stage each surface was placed into a well within a 24-well plate. A volume of 300µL of MHB

and 30µL of alamarBlue was added to each well containing a surface. Each group of three surfaces had two controls: a well with 300µL of MHB; and a well with 300µL plus 30µL of alamarBlue. The 24-well plate was incubated at 37°C.

After 30 minutes the total volume from one group of three surfaces and their corresponding controls were transferred to a 96-well plate. The alamarBlue absorbance was measured with an Ascent Multiskan (Labsystems, Thermo Scientific, USA) at 540nm and 620nm. The alamarBlue absorbance measurements were repeated at 60, 90 and 120 minutes for each remaining group of three surfaces and their controls.

To calculate the percentage reduction of alamarBlue, firstly the absorbance controls at the lower and higher wavelengths (AC_{lw} and AC_{hw}) were calculated by subtracting the absorbance of the media only control from the media and alamarBlue control at the lower and higher wavelengths (Eqn. 2-3).

$$\begin{aligned} AC_{lw} &= Absorbance\ of\ media\ plus\ AB - Absorbance\ of\ media\ only \\ AC_{hw} &= Absorbance\ of\ media\ plus\ AB - Absorbance\ of\ media\ only \end{aligned} \quad (2\text{-}3)$$

The correction factor (C_F) was calculated for the use of unspecified filters (Eqn. 2-4).

$$C_F = \frac{AC_{lw}}{AC_{hw}} \quad (2\text{-}4)$$

The absorbance at the lower wavelength (A_{lw}) and at the higher wavelength (A_{hw}) was calculated by subtracting the absorbance of media only from the measured absorbance (Eqn. 2-5).

$$\begin{aligned} A_{lw} &= Measured\ absorbance - Absorbance\ of\ media\ only \\ A_{hw} &= Measured'\ absorbance - Absorbance\ of\ media\ only \end{aligned} \quad (2\text{-}5)$$

The percentage reduction was then calculated by subtracting the absorbance at the higher wavelength (A_{hw}) multiplied by the correction factor (C_F) from the absorbance at the lower wavelength (Al_w) (Eqn. 2-6).

$$Percentage\ reduction = (\ A_{lw} - A_{hw} C_F\ )\ x\ 100 \quad (2\text{-}6)$$

2.8.4 AlamarBlue assay experiments

The alamarBlue assay experiments were performed to provide a semi-quantitative comparison of biofilm growth on Ag-AgCl and carbon sensors compared with the polyethylene control surface. The experiments performed are summarised in Table 2-9, which includes an investigation into whether there was a difference between the petri dish and the 24-well plate procedures described in Section 2.8.1. To investigate Ag-AgCl sensors the biofilm growth without impedance measurements procedure was performed with 3 control surfaces and 3 Ag-AgCl-PE300 sensor surfaces in petri dishes. This was repeated for two strains of *Staphylococcus aureus*, SA081 and SA082.

Table 2-9. The investigations of biofilm growth on sensor surfaces with alamarBlue assay.

Sensor	Test dish	Bacteria
AgAgCl-PE300	Petri Dish	SA081, SA082
C-PE300	Petri Dish, 24 Well Plate	SA081, SA082
C-PE300-v2	24 Well Plate	SA081, SA082, NCTC11964

To investigate whether their was a different between biofilm growth in petri dishes or 24-well plates the biofilm growth without impedance measurements procedure was performed with 3 control surfaces and 3 C-PE300 sensor surfaces in both petri dishes and 24-well plates. This was performed with strains SA081 and SA082. Finally the carbon sensors with the lower track resistances were investigated with three control surfaces and three C-PE300-v2 sensor surfaces with the 24-well plate procedure. This was performed with the *Staphylococcus aureus* strains SA081 and SA082, plus the *Staphylococcus epidermidis* strain NCTC111964. The carbon sensors had been pre-conditioned with a square-wave of amplitude 10V, period 120s, for a time of 20 minutes in Mueller-Hinton broth (Section 2.7.2).

On completion of the washing in PBS each surface was placed into a single well within a 24-well plate. A volume of 300µL of MHB and 30µL of alamarBlue was added to each well containing a surface. Controls were added which consisted of 3 wells with 300µL of MHB and 3 wells containing 300µL of MHB and 30µL of

alamarBlue. The 24 well plate was incubated for 60 minutes. The total volume from each of the wells were transferred to a 96-well plate and the absorbance measured as described in Section 2.8.3.

2.8.5 Confocal laser scanning microscopy of biofilms

A summary of the biofilm experiments with confocal laser scanning microscopy (CLSM) is listed in Table 2-10. To investigate bacterial growth on Ag-AgCl sensors the biofilm growth without impedance measurements procedure was performed with 3 control surfaces and 3 Ag-AgCl-PE300 sensor surfaces using petri dishes. This was performed with strains SA081 and SA082. To investigate carbon sensors the biofilm growth without impedance measurements procedure was performed with 3 control surfaces and 3 C-PE300-v2 sensor surfaces using the 24-well plate procedure and repeated for strains SA081, SA082 and NCTC11964.

To investigate the impedance measurements of biofilms the biofilm growth with impedance measurements procedure was performed. Firstly Ag-AgCl-PE300 sensors were used with strains SA081 and SA082 in the petri dish test rig. The impedance procedure was performed with an additional three sensors with only MHB to increase the number of control samples to five. Secondly the biofilm growth of SA081, SA082 and NCTC11964 on C-PE300-v2 was investigated in the 24-well test rig. Again the procedure was repeated with an additional three sensors with only MHB.

The LIVE/DEAD *Bac*Light Bacterial Viability Kit (L7007, Molecular Probes, Invitrogen, Paisley, UK) was used to stain the biofilms. This kit uses a mixture of two nucleic acid stains, the green-fluorescent nucleic acid stain SYTO 9 and the red-fluorescent nucleic acid stain propidium iodide. The propidium iodide can only penetrate bacteria with damaged membranes. Therefore, cells with intact membranes will stain green and cells with damaged membranes will stain red. The excitation and emission maxima for these dyes are in the region 480/500nm for SYTO 9 and 490/635nm for propidium iodine.

Table 2-10. The investigations of biofilm growth on sensor surfaces with CLSM.

Sensor	Test dish	Impedance Measurements	Bacteria	Growth Time (Hours)
AgAgCl-PE300	Petri Dish	None	SA082	24
AgAgCl-PE300	Petri Dish	None	SA081, SA082	48
AgAgCl-PE300	Petri Dish	Before inoculation and at 48 hours	SA081, SA082	48
C-PE300-v2	24 Well Plate	None	SA081, SA082, NCTC11964	48
C-PE300-v2	24 Well Plate	Before inoculation and every hour for 48 hours	SA081, SA082, NCTC11964	48

After washing in PBS the surfaces were transferred to a 24-well plate. The staining mixture of the *Bac*Light kit consisted of 1.5µL of component A and 1.5µL of component B in 897µL of sterile water. A volume of 300µL of the staining mixture was added to each of the surfaces. The surfaces were incubated at room temperature in the dark for 15 minutes. Surfaces were then mounted onto a glass microscope slide and covered with a glass coverslip (22 x 22 mm). A Nikon Eclispe TE2000-S inverted confocal microscope (Nikon UK Ltd., Kingston upon Thames, UK) was used to view the surfaces. Images were captured with an integrated Hamamatsu digital camera (C4742-95) of three to five areas for each biofilm surface. Images were analysed with the IPLab Analytical Imaging 4.0 software (BD Biosciences, Rockville, USA).

2.9 Analysis of impedance measurements

The impedance measurements of both the bacterial suspension experiments and the biofilm experiments were analysed by comparing the impedance profiles for discernible differences caused by the presence of bacteria. To examine the relative changes over time the impedance measurements can be normalised, for example the normalised impedance modulus, $|Z|_n$, at each frequency point is calculated by dividing the hourly reading, $|Z|_{hour}$, by the reading at zero hours, $|Z|_{time = 0}$, as shown in Equation 2-7.

$$|Z|_n = \frac{|Z|_{hour}}{|Z|_{time = 0}} \tag{2-7}$$

Thus $|Z|_n$ equals one for all frequencies at time zero and deviations from this with time can be seen clearly on a graphical plot of $|Z|_n$ against frequency. Similarly the normalised phase angle, resistance and reactance can be calculated. The normalised impedance data is analysed by comparing the impedance profile plots against frequency to look for discernible differences caused by the presence of cells that were not present on the control plots. Of particular interest is the frequency band or location of any peaks in such graphs that occurred in the normalised impedance profiles over frequency. These had the potential to provide unique signature traces to indicate the presence of bacteria and differentiate species of bacteria. This technique was described in Section 1.8.4.

Equivalent circuit modelling was performed on the bacterial suspension, the preconditioning and the biofilm impedance data to provide further information on the physical processes occurring within the system. The ZView software (Scribner Associates Inc., Southern Pines, USA) was used to select a circuit model and fit the actual data to a the circuit model. The circuit model selected for each of the experiments was based on the best fit, the lowest component errors and one where all the components have a physical explanation. The changes over time in component values of the circuit were used to suggest the possible physical changes occurring in the system.

3 Results – Suspensions

To investigate the feasibility of an infection monitor for wounds a number of experiments were performed in vitro to discover the impedance response of bacterial growth. Bacterial suspensions and biofilms were chosen to represent two possible scenarios in wounds: free floating planktonic bacteria in the wound fluid and the formation of biofilms on the wound surface. Firstly the impedance measurements of bacterial suspensions were investigated and secondly the impedance measurements of biofilms on the sensors. This chapter details the results from the impedance experiments with suspensions of bacteria, while the results from the biofilm experiments are described in Chapter 4.

There were three phases in the suspension experiments. The first experimental phase investigated suitable electrode materials for measuring the impedance of bacterial cultures. The second phase was to investigate the growth of bacteria in suspension with impedance measurements. The final phase was further experiments with bacterial suspensions that had lower starting cell densities.

3.1 Selection of electrode material

Electrode materials were investigated in several stages. Firstly the bacterial growth media, Mueller-Hinton broth (MHB) was checked that it was suitable for impedance measurements. Secondly different electrode materials were investigated by examining their impedance behaviour in MHB. This was followed by testing the different electrode materials for their bacterial growth behaviour. Electrodes were selected for the impedance measurement of bacterial growth based on their impedance profile and their effect on bacterial growth.

3.1.1 Impedance of media

To investigate the suitability of bacterial broth for performing impedance measurements Ag-AgCl wire electrodes (prepared as described in Section 2.2) were tested in three different media: Solution A, Mueller-Hinton broth (MHB) and a combination of Solution A and MHB (prepared as described in Section 2.1). A

frequency sweep approach as described in 2.2.3 was used to characterise the basic impedance of the Ag-AgCl wire electrodes in the three media. The electrodes were suspended in the media and connected to the impedance analyser, Solarton 1260 as illustrated in Figure 2.5.

The mean impedance magnitude plots of four sequential frequency sweeps from 1MHz to 0.1Hz with a voltage of 200mV using Ag-AgCl-wire electrodes in different media are illustrated in Figure 3-1. The surface of the electrodes always undergoes a conditioning process when in contact with liquid and this is seen by the first frequency sweep having a higher impedance. Therefore the initial frequency sweep was excluded from the mean calculation of the four sequential frequency sweeps.

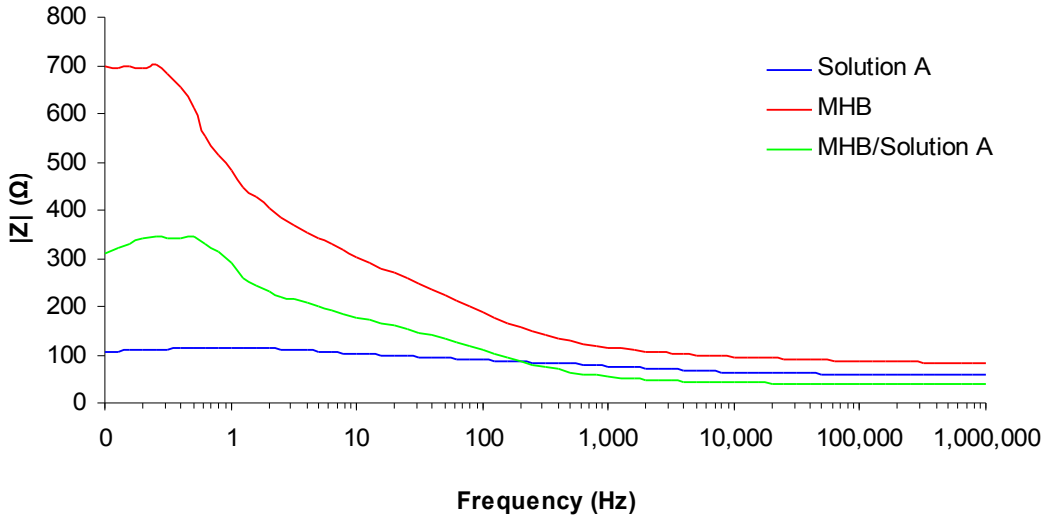

Figure 3-1. The impedance magnitude plots of Ag-AgCl-wire electrodes in different media: Solution A, MHB and a combination of Solution A and MHB.

The impedance for the basic circuit model illustrated in Figure 1-23 can be given as Equation 3-1.

$$Z = R_s + \frac{R_{dl} - j\omega R_{dl}^{2} C_{dl}}{1 + (\omega R_{dl} C_{dl})^2} \qquad (3\text{-}1)$$

From the theory discussed in Section 1.5.3, the total impedance is made from the solution resistance plus the interface impedance. At high frequencies the interface impedance becomes a short circuit and therefore the impedance represents the solution resistance. As the frequency decreases a dispersion or series of dispersions occur which represent the interface impedance. This consists of charge transfer resistances and double layer capacitances. A suitable media should have a low solution resistance and a low interface impedance to ensure changes in the impedance, for example the presence of bacterial cells, are not masked by the solution and interface impedances.

The solution resistance, with standard deviations, for Solution A was 60 ± 2.1Ω, for Mueller-Hinton broth was 85 ± 0.7Ω and for the MHB/Solution A combination was 39 ± 0.4Ω . Below 1kHz a dispersion or series of dispersions occurred with Solution A having the smallest dispersion(s) and MHB the largest. The interface impedances were 55 ± 7Ω for Solution A, 648 ± 102Ω for MHB, and 309 ± 3Ω for the MHB/Solution A combination. The MHB was selected for the proceeding experiments despite its larger overall impedance compared to the other two media. Solution A cannot be used due to lack of nutrients for bacterial growth and it was decided not to complicate the medium by adding Solution A to the MHB. The impedance of MHB was still relatively low anyway, for instance, the maximum impedance was under 1000Ω.

3.1.2 Impedance of electrode material

Once the bacterial broth, Mueller-Hinton broth (MHB) was shown to be suitable for impedance measurements five electrode materials were tested to find a material that had a suitable impedance profile. The electrode materials were silver wire, platinum wire, Ag-AgCl wire, screen-printed Ag-AgCl and screen-printed carbon prepared as described in Section 2.2.1. As described in Section 3.1.1 the electrodes were suspended in MHB and connected to the impedance analyser, Solartron 1260, and were examined with a frequency sweep from from 1MHz to 0.1Hz with a voltage of 200mV. The mean Bode plots, showing the magnitude of impedance and the phase angle as discussed in Section 1.5.3, of four sequential frequency sweeps for the five

electrode materials are illustrated in Figure 3-2. An initial frequency sweep that conditioned the electrodes was not included. The solution resistance, interface impedance and minimum phase of the five electrode types are listed in Table 3-1.

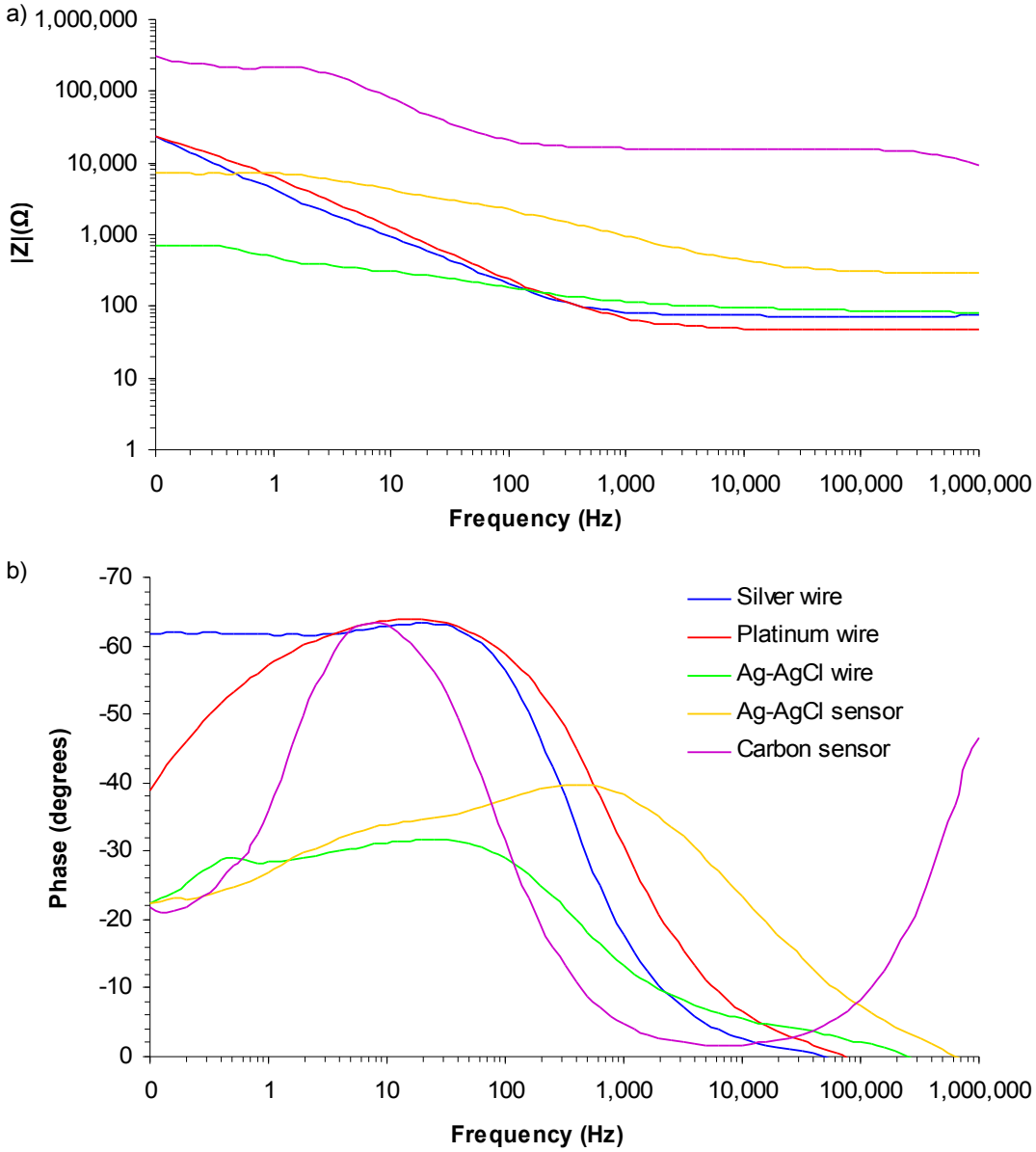

Figure 3-2. The Bode plots of different electrode materials in Mueller-Hinton broth: a) Magnitude plot; b) Phase angle plot.

Table 3-1. The average solution resistance, interface impedance and minimum phase of different electrode types in MHB. The * indicates the interface impedance value includes the impedance caused by diffusional processes. Standard deviations for the 4 frequency sweeps are shown.

Electrode material	Solution resistance (Ω)	Interface impedance (Ω)	Minimum phase (degrees)
Ag-AgCl wire	85 ± 0.7	648 ± 102	-31.6 ± 1.7
Silver wire	73 ± 1.4	$2.4x10^4 \pm 1.7x10^3$ *	-63.2 ± 1.9
Platinum wire	47 ± 0.01	$2.4x10^4 \pm 1x10^3$ *	-63.9 ± 0.4
Ag-AgCl screen-printed	289 ± 16	7121 ± 1624	-39.7 ± 6.3
Carbon screen-printed	unavailable	$3.1x10^5 \pm 2.7x10^4$ *	-63.5 ± 2.4

The silver wire and platinum wire have a similar solution resistance to the Ag-AgCl wire, whereas their interface impedance is over 10 times higher. This is caused by diffusional processes as discussed in Section 1.5.3. The differences between the Ag-AgCl wire electrode and the Ag-AgCl screen-printed sensor are related to the surface area, the size of the electrodes and the chemical composition of the screen-printed sensor. This does mean it has an interface impedance in the thousands compared with the hundreds. The screen-printed carbon sensors have the highest overall impedance profile produced by a very high electrode resistance and diffusional processes. The diffusional processes with the silver wire electrodes, the platinum wire electrodes and the carbon screen-printed sensors create minimum phase angles 20 to 30^o higher than the Ag-AgCl electrodes.

3.1.3 Growth of bacteria with electrode materials

Having checked the impedance behaviour of electrodes in broth only, the next step was to look at the growth behaviour with these electrodes in the presence of bacteria without impedance measurements. The experimental procedure was described in Section 2.3. As a common pathogen of wounds a strain of *Staphylococcus aureus*, RN4220, was selected for this investigation. The RN4220 was grown in suspension with the presence of five electrode materials for 17 hours against controls that contained no electrodes. The final numbers of the bacteria are illustrated in Figure 3-3. The broths were each inoculated with a single colony of bacteria which provided a

starting density of approximately $1x10^6$ colony forming units per ml (CFU ml^{-1}). The control levels of bacteria always reached approximately $1x10^9$ CFU ml^{-1} when counted with the plate counting method. This was deemed to be the expected level of growth that should be achieved if growth was not inhibited given that the stationary phase of growth had been reached.

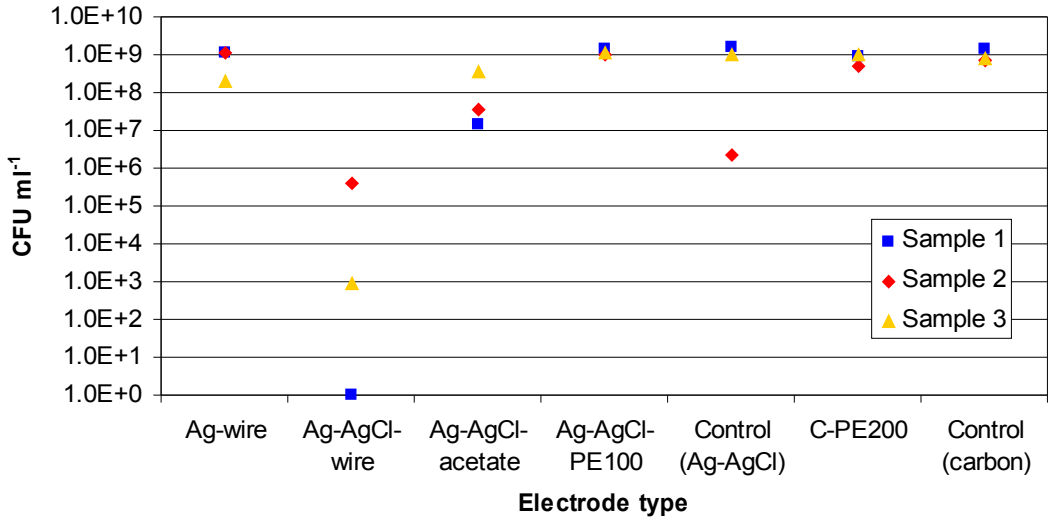

Figure 3-3. The final numbers of RN4220 with different electrode types sampled after culturing for 17 hours in Mueller-Hinton broth.

The levels of bacteria reached $1x10^9$ CFU ml^{-1} with Ag-wire electrodes, screen-printed Ag-AgCl (Ag-AgCl-PE100) sensors and screen-printed carbon (C-PE200) sensors. The bacteria did not reach $1x10^9$ CFU ml^{-1} with Ag-AgCl wire electrodes, down by a mean factor of 10^4, or with Ag-AgCl-acetate sensors, down by a mean factor of 10. These results indicate that a number of materials had a detrimental effect on the growth of these bacteria, probably due to the release into the media of silver ions which are known to damage bacteria.

An alternative bacterial species, *Escherichia coli*, was chosen to compare the growth behaviour of the screen-printed sensors. The strain JM109 was selected and grown in the presence of the Ag-AgCl and carbon screen-printed sensors. The final numbers of bacteria in a 17 hours culture of JM109 in the presence of these electrode materials are illustrated in Figure 3-4. The bacteria, JM109, did not reach expected levels of

growth with Ag-AgCl-PE100 sensors and was 3 factors below $1x10^9$ CFU ml^{-1}. The non-inhibited levels of growth with C-PE200 sensors was reached. These results indicate that the Ag-AgCl sensors may have a varying growth behaviour depending on the species of bacteria.

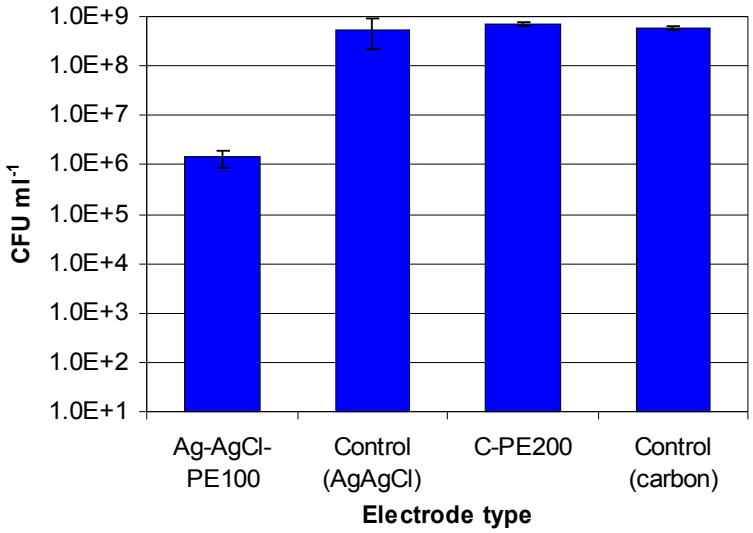

Figure 3-4. The final numbers of JM109 with different electrode types after an overnight culture in Lennox's Broth.

The characteristics of the ideal electrode material would be a low interface impedance and no effect on the growth of bacteria. These results indicate that a compromise may have to made. The wire electrodes were discounted due to their poor growth behaviour and because the long term aim would be to use screen-printed sensors on a flat substrate that could be placed underneath a wound dressing without causing pressure points. The screen-printed Ag-AgCl sensors had a lower interface impedance than carbon, however inhibited the growth of some species of bacteria. On the other hand the screen-printed carbon sensors appear not to inhibit growth and unfortunately have a very high impedance. Both the screen-printed Ag-AgCl and carbon sensors were chosen for the impedance investigations given their opposite characteristics in impedance and growth behaviour.

3.2 Impedance – Bacteria in single suspensions and Ag-AgCl sensors

To investigate the impedance of bacterial growth the single suspension procedure as described in Section 2.4 was performed. To recap briefly this procedure was designed to observe the impedance changes over time due to the growth of bacteria in suspension and show whether there were discernible differences that would indicate the presence of bacteria. The *Staphylococcus aureus* strain, RN4220 was selected as a species commonly isolated from wounds. Impedance measurements were performed every hour for 17 hours and the parameters varied were the sensor type and the media type. The three configurations were: AgAgCl-PE100 sensors and Mueller-Hinton broth (MHB); Ag-AgCl-PE100 sensors and MHB with 0.2% glucose; and C-PE200 sensors with MHB.

All the vials for bacteria were inoculated with a single colony from an MHB agar plate which made the starting cell density approximately $1x10^6$ CFU ml^{-1}. All the vials reached approximately $1x10^9$ CFU ml^{-1} at the end of the experiment, approximately 17 hours from inoculation which matched the control vials of bacteria.

3.2.1 Impedance – Single suspensions and Ag-AgCl sensors

An example of the z-plots over time for MHB-only, the control system without bacteria, and the RN4220 culture with Ag-AgCl-PE100 sensors are illustrated in Figure 3-5. The control impedance was steady over time except at low frequencies where there was a decrease. In contrast the RN4220 culture impedance curves decreased over time and became more convoluted. The control data shown in Figure 3-5 had a starting solution resistance of 275Ω which decreased to 210Ω at 17 hours, the maximum resistance decreased from 5593 to 1469Ω, and the maximum reactance increased from -2578 to -1202Ω. In comparison the data shown for RN4220 culture had a solution resistance of 256Ω at the start which decreased to 226Ω at 17 hours, the maximum resistance decreased from 3720 to 1322Ω, and the maximum reactance increased from -1650 to -841Ω. This was the first sign that the growth of bacteria was producing a different impedance profile.

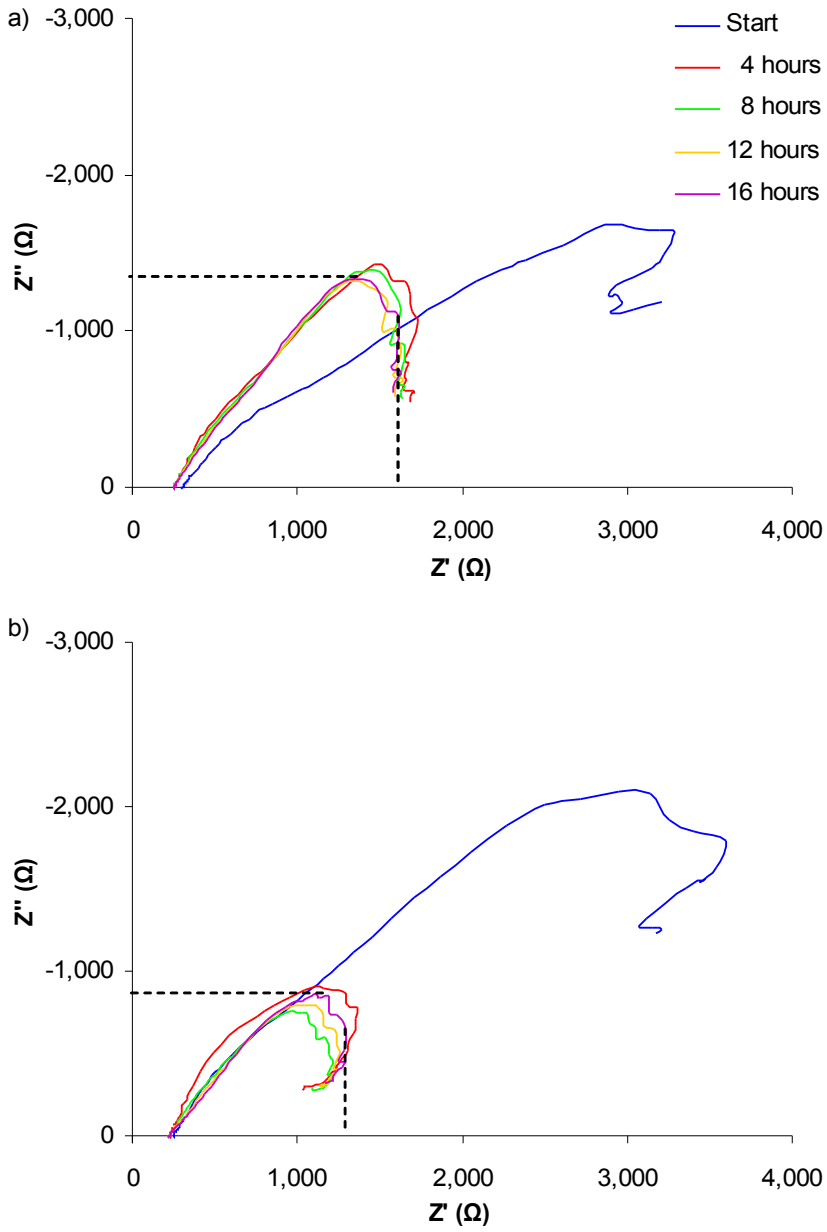

Figure 3-5. An example of a z-plot with Ag-AgCl-PE100 sensors for bacteria in suspensions: a) Mueller-Hinton broth only; b) RN4220 culture. Impedance sweep from 1MHz to 0.1Hz.

Electrical impedance is represented as a complex quantity as described in the theory within Section 1.5.2. To recap, impedance is defined by Equations 1-10 to 1-12.

$$Z = R + jX = Z' + Z'' \tag{1-10}$$

$$|Z| = \sqrt{(Z')^2 + (Z'')^2} \tag{1-11}$$

$$\theta = \arctan\left(\frac{Z''}{Z'}\right) \tag{1-12}$$

From the impedance data gathered the frequency profiles of the impedance magnitude, phase angle, resistance and reactance can be obtained. Each of these profiles were examined for differences in the occurrence of peaks between the media only and the RN4220 culture that could be used as a means to identify the presence of the bacteria. The focus was on differences between the frequencies that peaks occurred at. A peak formed in the impedance magnitude, phase and reactance profiles in all the Ag-AgCl sensor experiments.

The peaks in the phase angle profile over frequency were of most interest and are illustrated in Figure 3-6 for the control culture, MHB-only, and the RN4220 culture. The MHB-only data shows a phase peak and a subsidiary peak which are not entirely resolved due to the overlapping frequencies of the two peaks. The peak itself occurred at a lower frequency and then the subsidiary peak was noted in the hundreds of hertz. Over time the subsidiary peak phase angle decreased which made the original peak appear more pronounced. The phase peaks of the MHB-only descended below 10Hz between 5 and 11 hours and below 6Hz between 7 and 13 hours across all five samples.

In contrast in the RN4220 cultures the first phase peak remained at a higher frequency and the subsidiary phase angle decreased. This appears to make the RN4220 culture phase peak a single peak with no subsidiary peak. The first phase peak never decreased below 10Hz after 4 hours except in one experiment where it falls to 6.31Hz at 17 hours, however before this time it does not descend below 19.95Hz. This was repeatable over 5 separate culture runs. Therefore it appears that

the two cultures do have separate signature traces in the phase angle over frequency and is the first indication that peaks in signature traces could distinguish between the absence and/or growth of bacteria.

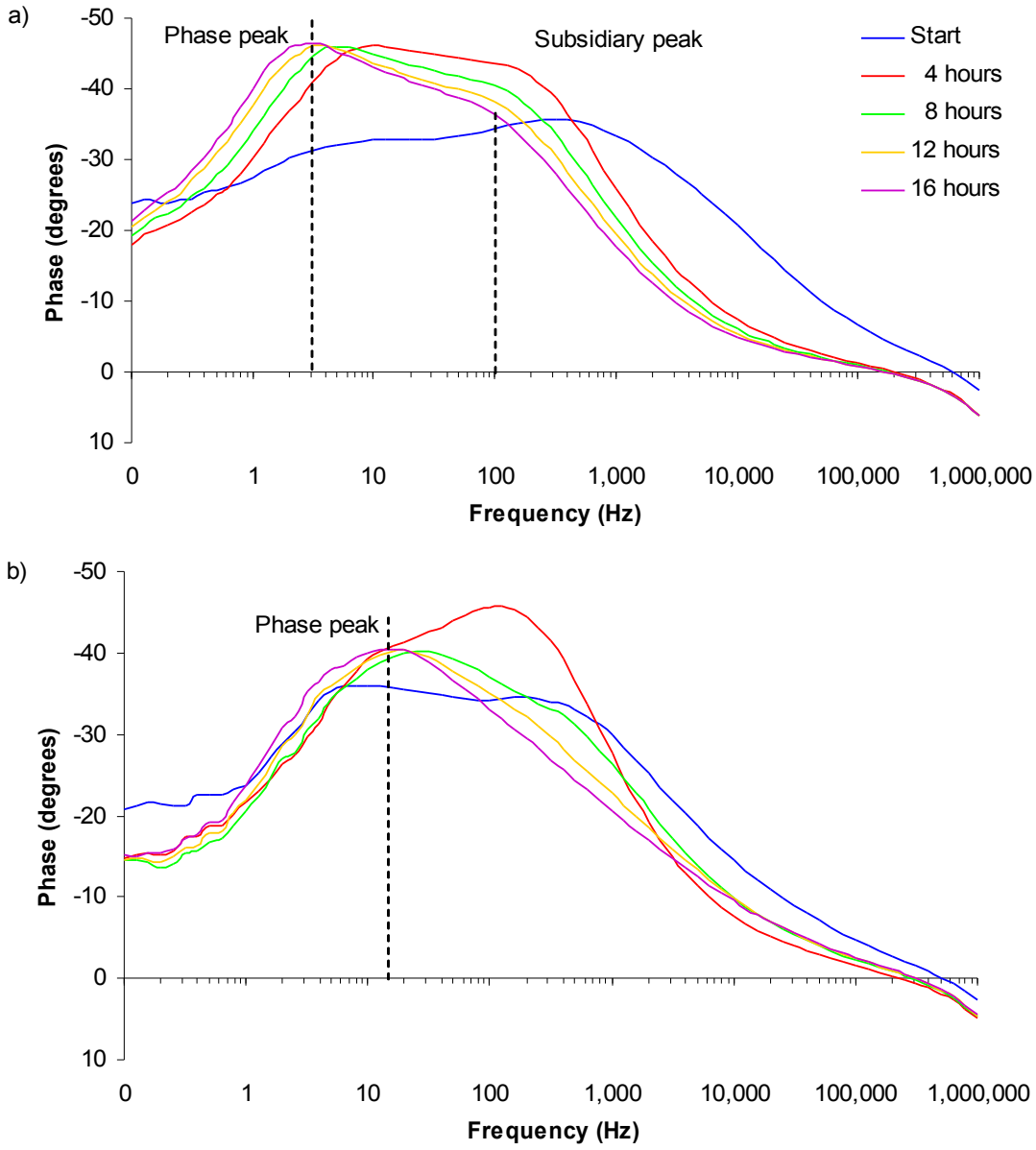

Figure 3-6. An example of the phase plots with Ag-AgCl-PE100 sensors for bacteria in suspensions: a) Mueller-Hinton broth only; b) RN4220 culture. Impedance sweep from 1MHz to 0.1Hz.

In the experiments with glucose added to the media the phase peak also remains at a higher frequency of 20 to 30Hz in the RN4220 cultures compared with 5 to 10Hz in the controls. This was also repeatable over 5 separate cultures runs and again there appears to be discernible behaviour in the phase angle peak that distinguishes between the absence and/or growth of bacteria.

The peaks that occurred in the impedance profiles over frequency are summarised in Table 3-2 with the mean and range of frequencies at the start and 17 hour impedance readings in the five experimental runs for each of the Ag-AgCl sensor experiments. There was less distinction between the media-only controls and bacterial cultures of the magnitude peak and the reactance peak. The magnitude peak occurred at less than 5Hz and the reactance peak occurred below 8Hz.

Table 3-2. The mean frequencies of the impedance peaks for Ag-AgCl-PE100 sensors with bacterial suspensions.

Media	Bacteria	Start frequency (Hz)		17 hour frequency (Hz)		Mann-Whitney test ($p < 0.05$)
		Mean	Range	Mean	Range	
|Z| peak						
MHB	Control	0.92	0.10 - 2.00	1.10	1.00 - 1.26	-
MHB	RN4220	0.74	0.10 - 2.00	1.17	1.00 - 1.58	No ($p = 0.92$)
MHB-glucose	Control	0.68	0.10 - 1.00	1.05	1.00 - 1.26	-
MHB-glucose	RN4220	1.31	0.10 - 3.16	2.95	1.26 - 3.98	Yes ($p = 0.02$)
Phase peak						
MHB	Control	70.03	5.01 - 316.23	2.86	2.00 - 3.98	-
MHB	RN4220	8.09	2.00 - 12.59	11.47	6.31 - 15.85	Yes ($p = 0.01$)
MHB-glucose	Control	47.05	12.59 - 158.49	6.01	5.01 - 10.00	-
MHB-glucose	RN4220	72.25	12.59 - 158.49	20.99	19.95 - 25.12	Yes ($p = 0.01$)
Z'' peak						
MHB	Control	2.64	1.26 - 3.98	1.45	1.00- 2.00	-
MHB	RN4220	2.82	1.00 - 5.01	3.42	2.00 - 3.98	Yes($p = 0.02$)
MHB-glucose	Control	3.85	1.26 - 5.01	2.70	2.00 - 3.16	-
MHB-glucose	RN4220	3.20	0.10 - 3.98	6.70	5.01 - 7.94	Yes ($p = 0.01$)

A Mann-Whitney test was performed to show whether the frequency peaks of the bacterial cultures were significantly different from the media only at 17 hours. The data was deemed not suitable for parametric tests due to the narrow range of frequencies that the samples occurred at and hence could not be shown to be a

normal distribution. Therefore the Mann-Whitney test was selected as the non-parametric equivalent to the parametric student's t-test. The results of this statistical test are listed in Table 3-2. This confirms that for the phase peaks there is a significant difference between the media-only and bacterial cultures that could be used to distinguish between the absence and/or growth of bacteria. The Mann-Whitney test also shows that for the magnitude peak of the experiments with glucose, and the reactance peaks for both media types that there was a significant difference between the media-only and bacterial cultures. However it can be seen from the individual frequency ranges of the peaks that there is an overlap between the media-only and the bacterial cultures which would make these peaks less reliable for distinguishing the absence and/or growth of bacteria.

3.2.2 Normalised impedance – Single suspensions and Ag-AgCl sensors

The medical diagnostics group at the University of Strathclyde has previous found that normalising the impedance produces distinct frequency peaks and profiles dependent on the type of cell layer that formed on gold electrodes, as described in Section 1.8.4. The normalised readings were created by dividing the hourly readings by the starting reading which was the final impedance measurement performed before inoculation as described in Section 2.9. Thus at any frequency the impedance value is normalised against its starting value of impedance on the electrode and relative changes from the starting condition can be viewed at different frequency values. This is expected to be important to show different behaviours because the relative change from the starting condition due to the growth of bacteria should not be the same as the media without bacteria.

An example of the normalised impedance magnitude plot over time for Mueller-Hinton broth (MHB)-only and RN4220 culture with Ag-AgCl sensors are illustrated in Figure 3-7. In the five control cultures with MHB-only the peak occurred between 2 and 100Hz and decreased over time to between 0.78 and 0.34. Similarly in the five RN4220 cultures the peak occurred between 6 and 32Hz and decreased over time to between 0.76 and 0.41. Therefore there was no discernible differences between the normalised impedance magnitude peaks that would distinguish the absence and/or

growth of bacteria. The difference seen in the normalised magnitude profile is that the value below 1Hz was always lower relative to the peak in the five RN4220 cultures compared with the MHB-only controls.

The normalised impedance profiles for the experiments with glucose added to the media show some clear trends and differences. An example of the normalised impedance magnitude plot for the control of MHB with glucose (0.2%) and the RN4220 culture in MHB with glucose (0.2%) are illustrated in Figure 3-8. In the MHB-glucose-only by 17 hours a first peak occurred between 1 and 3Hz and a second one between 200 and 1.3kHz. In contrast in the RN4220-glucose experiments the first and second peaks were not present at the end of the experiment, however a third peak between 2.5k and 6.3kHz was present. The change of the peaks in the RN4220 cultures occurred between 4 and 8 hours. This was repeatable over five separate cultures and is the first indication that discernible differences in the normalised profiles occur due to the presence of bacteria depending on the media contents.

There was also a discernible difference in the normalised phase peak between the MHB with glucose and the RN4220 culture in MHB with glucose, as illustrated in Figure 3-8. The normalised phase peak at 17 hours was between 1 and 2 Hz in all five media-only cultures and between 10 and 32Hz for the RN4220-glucose cultures. The change in frequency peak occurred between 4 and 8 hours and this provides more evidence that under the correct conditions the normalised signature traces over frequency contain discernible differences that will indicate the absence and/or growth of bacteria.

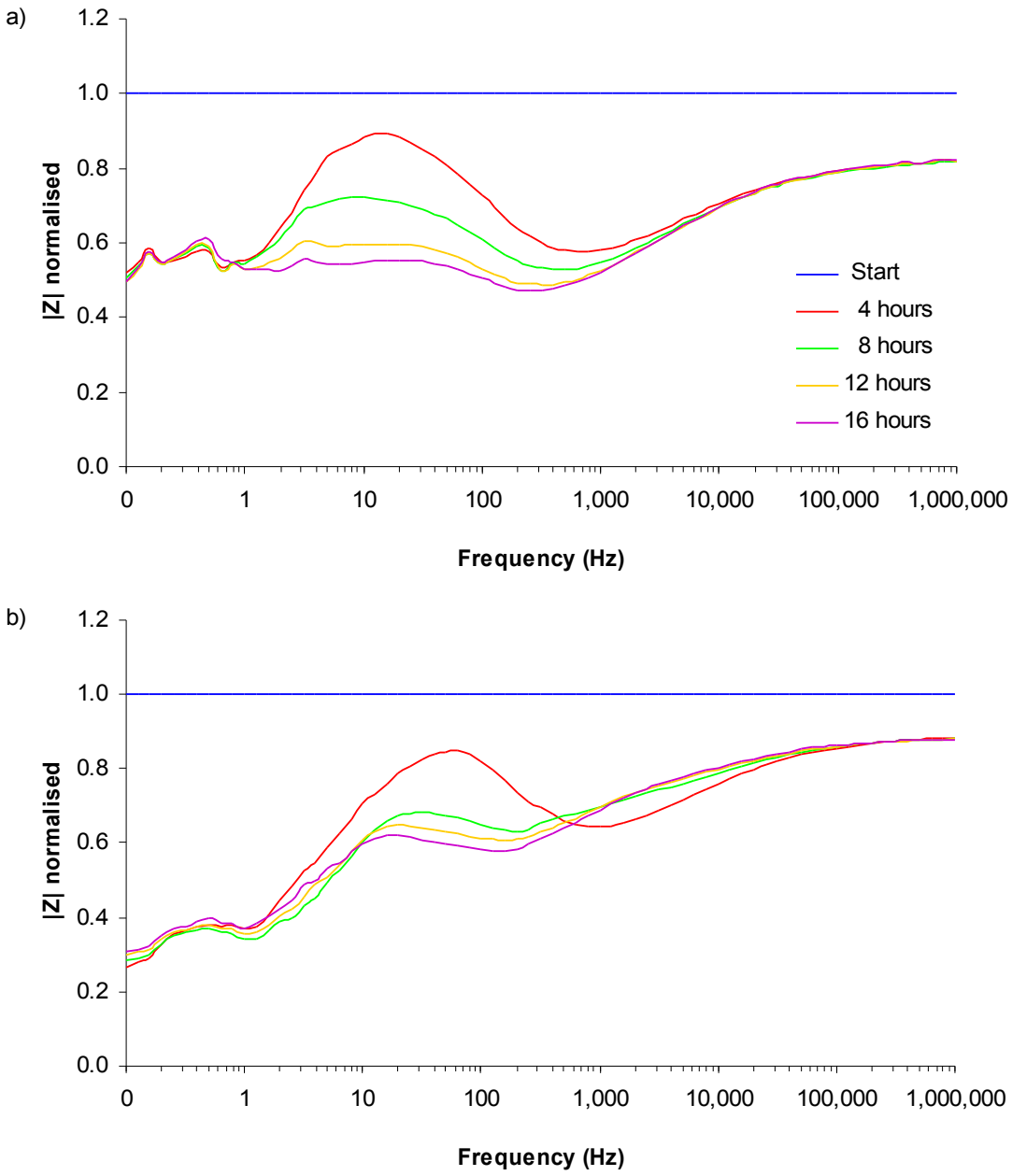

Figure 3-7. An example of the normalised magnitude plots over time with Ag-AgCl-PE100 sensors for bacterial suspensions: a) Mueller-Hinton broth only; b) RN4220 culture.

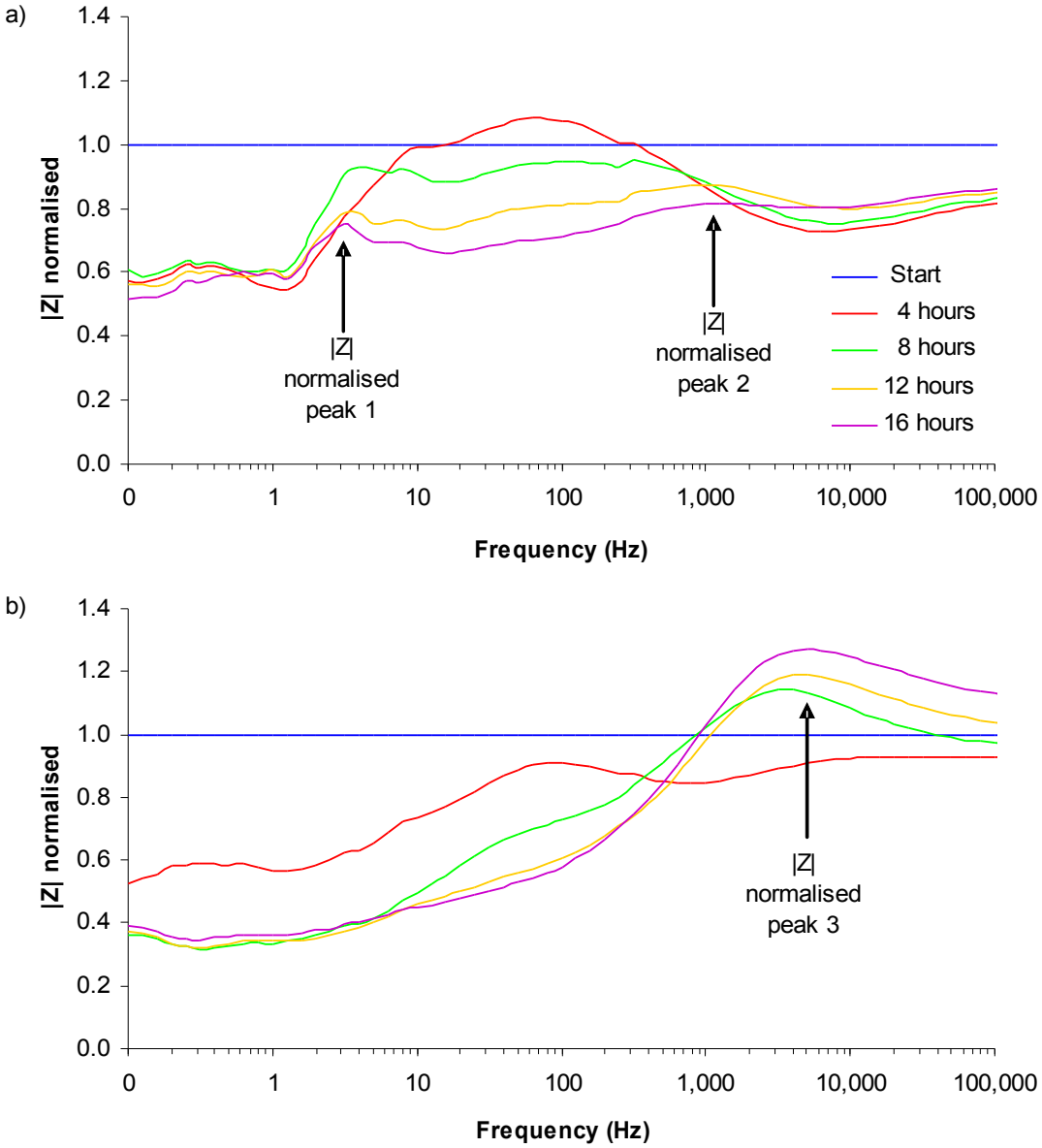

Figure 3-8. An example of the normalised magnitude plots over time with Ag-AgCl-PE100 sensors for bacterial suspensions: a) MHB with glucose only; b) RN4220 culture in MHB with glucose.

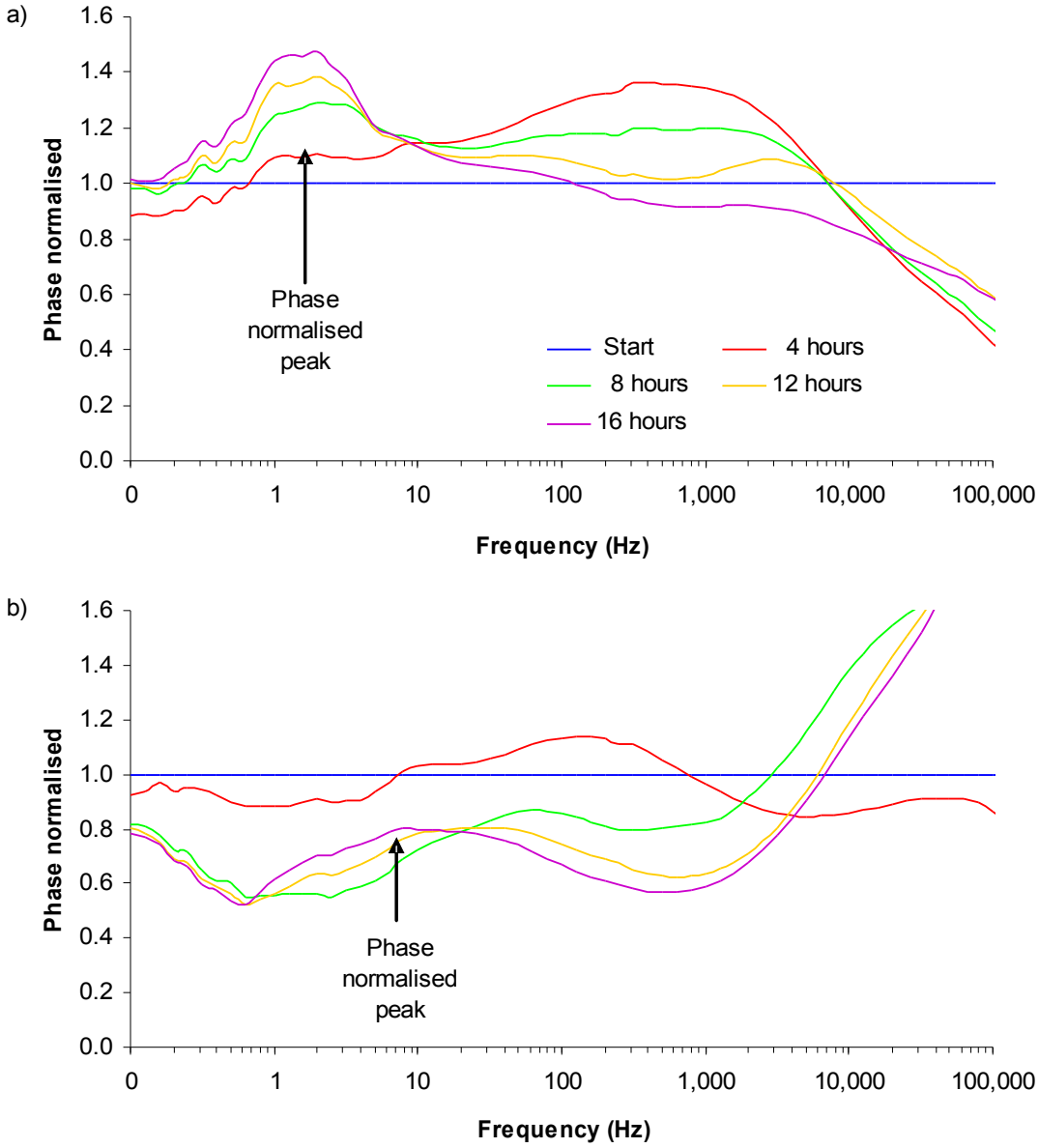

Figure 3-9. An example of the normalised phase plots over time with Ag-AgCl-PE100 sensors for bacterial suspensions: a) MHB with glucose only; b) RN4220 culture in MHB with glucose.

The peaks that occurred in the normalised impedance profiles over frequency are summarised in Table 3-3 with the mean and range of frequencies for the 17 hour impedance readings in the five experimental runs for each of the Ag-AgCl sensor experiments. A Mann-Whitney test, as described in Section 3.2.1, was performed to find whether the frequency peaks of the bacterial cultures were significantly different from the media-only at 17 hours. This confirms that for the MHB-only and RN4220 cultures there is no significant difference in the normalised magnitude and phase. In the experiments with glucose in the media there were significant differences confirming that the normalised profiles can be used to distinguish between the absence and/or growth of bacteria.

Table 3-3. The mean frequencies of the normalised impedance peaks for Ag-AgCl-PE100 sensors with bacterial suspensions.

Media	Bacteria	17 hour frequency (Hz)		Mann-Whitney test ($p < 0.05$)
		Mean	Range	
|Z| normalised peak 1				
MHB	Control	33.13	2.00 -100.00	
MHB	RN4220	21.07	6.31 - 31.62	No (p = 1.00)
MHB-glucose	Control	2.78	1.26 – 3.16	
MHB-glucose	RN4220	-	-	Peak not present
|Z| normalised peak 2				
MHB	Control	-	-	
MHB	RN4220	-	-	-
MHB-glucose	Control	729.23	199.53 - 1258.93	
MHB-glucose	RN4220	-	-	Peak not present
|Z| normalised peak 3				
MHB	Control	-	-	
MHB	RN4220	-	-	-
MHB-glucose	Control	-	-	
MHB-glucose	RN4220	4565	2512 - 6310	No peak for comparison
Phase normalised peak				
MHB	Control	1.33	0.79 - 2.00	
MHB	RN4220	6.87	0.79 -1 9.95	No (p = 0.25)
MHB-glucose	Control	1.62	1.62 – 2.00	
MHB-glucose	RN4220	23.66	10.00-31.62	Yes (p = 0.01)

3.2.3 Equivalent circuits – Single suspensions and Ag-AgCl sensors

Equivalent circuit modelling involves representing the biological impedance system by electrical components. Each element is defined an equivalent physical process and by fitting the actual impedance data to the circuit the component values can be found. The analysis of these component values provides further information on the physical process occurring within the biological system over time plus in a detection system differences between the component values could be used to distinguish the presence of bacteria.

The equivalent circuit model method, as described in Section 2.9, starts by selecting a circuit based on examining the z-plots for features that can be represented by components. Once a circuit has been chosen the actual data is fitted to the equivalent circuit with computer software (ZView) which generates values for each of the components and uses these values to create a simulated impedance measurement. Two parameters are provided to indicate how well the circuit represents the actual measurements. The fit parameter is a measure of how closely the simulated data matches the actual data, the lower the value the better the fit is. The component error is a measure of how much a component value can shift up or down while keeping the fit value constant and large errors tend to indicate that the model contains too many components. The circuit model is adjusted until the measures of fit are satisfactory.

The data from the Ag-AgCl sensors was fitted to the equivalent circuit illustrated in Figure 3-10 where R_s is the resistance of the solution, R_{dl1} and R_{dl2} are the double layer resistance and C_{dl1} and C_{dl2} are the double layer capacitance as discussed in Section 1.5.3. This circuit was chosen based on the approximate semi-circle of the z-plot (Figure 3-5) which is represented by the standard model, as shown in Figure 1-23 a parallel resistor and capacitor in series with a resistor. The parallel resistor and capacitor produce a peak in the phase angle and given that the Ag-AgCl sensor phase angle contains a peak and a subsidiary peak (Figure 3-6) a second resistor and capacitor in parallel were added to the circuit model. This also led to an improvement in the measures of fit.

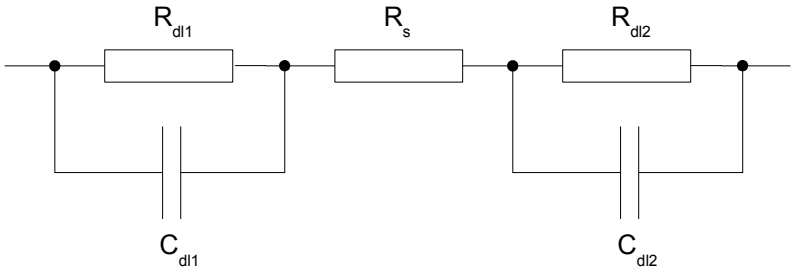

Figure 3-10. The equivalent circuit model for the Ag-AgCl sensors.

An example of the actual readings and simulated readings for the start and 17 hour measurements from the RN4220 culture with Ag-AgCl sensors equivalent circuit are illustrated in Figure 3-11. The simulated impedance magnitude has a close match above 10Hz and becomes less close at low frequencies. The simulated data also does not form a smooth line. The simulated impedance phase has two peaks which match the actual data, however there are much more distinct. The actual phase peaks are merged, particularly with the 17 hour reading. Also at low frequencies the actual phase does not move to zero as the simulated data implies. Therefore the equivalent circuit model simulates the actual data adequately and examination of the components should provide information on the physical processes occurring in the system.

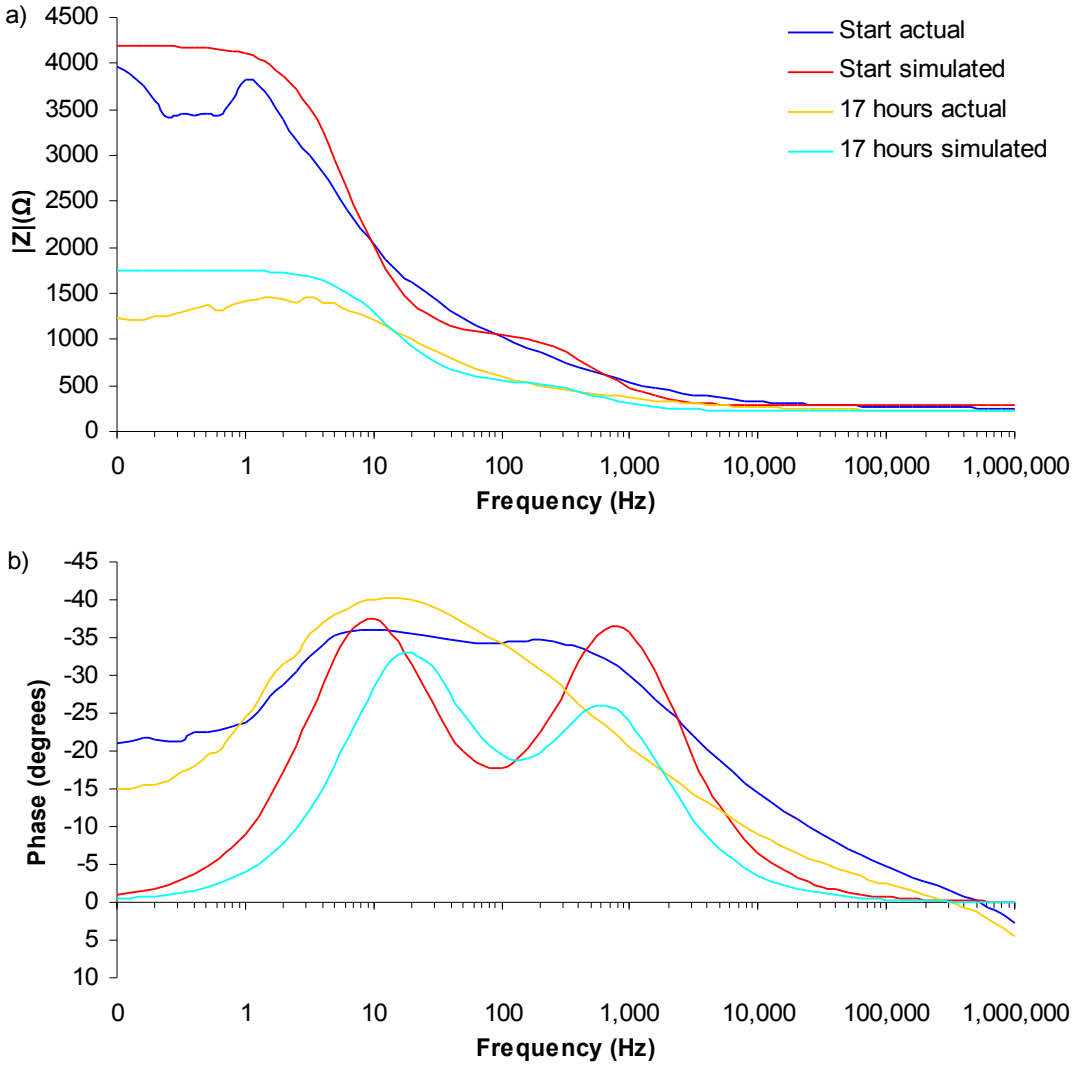

Figure 3-11. Bode plot of actual and simulated data with Ag-AgCl-sensors for a bacterial suspension: a) Impedance magnitude; b) Impedance phase. Impedance sweep from 1MHz to 0.1Hz. The starting value and 17 hour values are shown.

The generated component values from the ZView software for the start and 17 hour readings with Ag-AgCl sensors in MHB only and RN4220 culture are listed in Table 3-4. The measures of fit are also listed. Both the MHB only and RN4220 cultures start with fits in the low forties and progress to a fit in the seventies and eighties. The model is consistent across all experiments with the standard deviation of the fit values between 3.4 and 6.9. The component errors are all less than 15% with all standard deviations less than 1.3%.

Table 3-4. The mean circuit model component values from the suspension experiment with Ag-AgCl sensors for the start and 17 hour readings. Data from MHB only and RN4220 experiments. The numbers in brackets indicate standard deviation.

Experiment	Component value		Component error (%)	
	Start	17 hour	Start	17 hour
Fit-Weighted sum of squares				
MHB-only	43.8 (± 5.7)	76.5 (± 3.4)		
RN4220	42.3 (± 3.6)	80.7 (± 6.9)		
R_s (Ω)				
MHB-only	287 (± 49)	211 (± 25)	3.8 (± 0.6)	3.5 (± 0.3)
RN4220	306 (± 20)	238 (± 27)	3.5 (± 0.4)	3.4 (± 0.2)
R_{dl1} (Ω)				
MHB-only	807 (± 269)	452 (± 49)	7.6 (± 1.1)	9.8 (± 0.2)
RN4220	799 (± 121)	314 (± 25)	7.4 (± 0.5)	13.0 (± 1.3)
R_{dl2} (Ω)				
MHB-only	3203 (± 1294)	1937 (± 98)	6.3 (± 0.3)	7.5 (± 0.3)
RN4220	3197 (± 629)	1424 (± 179)	6.0 (± 0.3)	6.7 (± 0.1)
C_{dl1} (F)				
MHB-only	$5.6x10^{-7}$ (± $3.5x10^{-7}$)	$3.0x10^{-6}$ (± $9.0x10^{-7}$)	9.9 (± 0.8)	11.7(± 0.5)
RN4220	$6.7x10^{-7}$ (± $5.8x10^{-7}$)	$2.9x10^{-6}$ (± $1.5x10^{-6}$)	9.7 (± 0.4)	15.1 (± 0.7)
C_{dl2} (F)				
MHB-only	$1.1x10^{-5}$ (± $6.4x10^{-6}$)	$3.2x10^{-5}$ (± $8.5x10^{-6}$)	10.7 (± 0.3)	11.9 (± 0.9)
RN4220	$1.4x10^{-5}$ (± 1.4x10-^{5})	$1.8x10^{-5}$ (± $6.9x10^{-6}$)	10.2 (± 0.5)	12.8 (± 0.8)

Once a suitable circuit model has been selected the main reason for performing equivalent circuit modelling can be undertaken, which is examining the changes in the component values over time. The mean component values for MHB-only and RN4220 culture with Ag-AgCl sensors over time are illustrated in Figure 3-12. For MHB only all three resistor values decrease for the first 3 hours, R_s is then stable for the remaining hours at an average of 207Ω, R_{dl1} is also stable at a mean of 478Ω, whereas R_{dl2} increases over time from 1782 to 1937Ω. C_{dl1} and Cd_{l12} both rise over the 17 hours with increases of $2.4x10^{-6}$ and $2.1x10^{-5}$ F respectively. The R_s value for RN4220 culture is constant at approximately 230Ω, and in contrast R_{dl1} decreases for the first 12 hours from 799 to 303Ω and then fluctuates with a mean of 307Ω, and R_{dl2} decreases for the first 7 hours from 3197 to 1113Ω and then rises to 1424Ω in the remaining 10 hours. The C_{dl1} and C_{dl2} of the RN4220 cultures both rise over the 17 hours with increases of $2.3x10^{-6}$ and $4.0x10^{-6}$ F respectively.

The differences of the interface resistances, R_{dl1} and R_{dl2} between the media only and RN4220 cultures clearly show that the presence of the bacteria are causing changes in the impedance profile within a short time frame, 4 to 5 hours. The physical processes producing these changes are discussed fully in Section 5.2.3. The changes in the resistor values provide evidence that the growth of bacteria could be detected by performing equivalent circuit modelling of the impedance measurements. The original vision for the infection monitor for wounds was for a hand-held device to be connected to the sensors, for example once a day, to perform a measurement. These results suggest that the growth could be detected more rapidly if the infection monitor system was capable of performing measurements once an hour by an electronic module that was permanently attached. Alternatively the equivalent circuit modelling has potential for use in a laboratory system where it may be more feasible to perform measurements once an hour.

The component values from modelling the impedance data from the experiments with glucose in the media produced very similar changes to the experiments without glucose. The average component values for MHB-glucose-only and RN4220-glucose culture with Ag-AgCl sensors over time are illustrated in Figure 3-13. The differences between the RN4220-glucose and RN4220 experiments are that the R_{dl1} and R_{dl2} values decrease to lower resistances with glucose. The R_{dl1} value decreases to 725Ω with glucose compared to 1424Ω and the R_{dl2} value decreases to 232Ω compared with 314Ω. The C_{dl2} component of RN4220-glucose differs from the control while in RN4220 it was the C_{dl1} component. These changes are likely to be related to the different products produced by the metabolism of glucose by the bacteria and changing the charge carriers at the electrode interface. In turn this changes the impedance characteristics of the interface and hence the values of the components modelling it. These results also further validate the circuit model chosen and the potential to use circuit modelling as a method to distinguish the absence and/or the growth of bacteria.

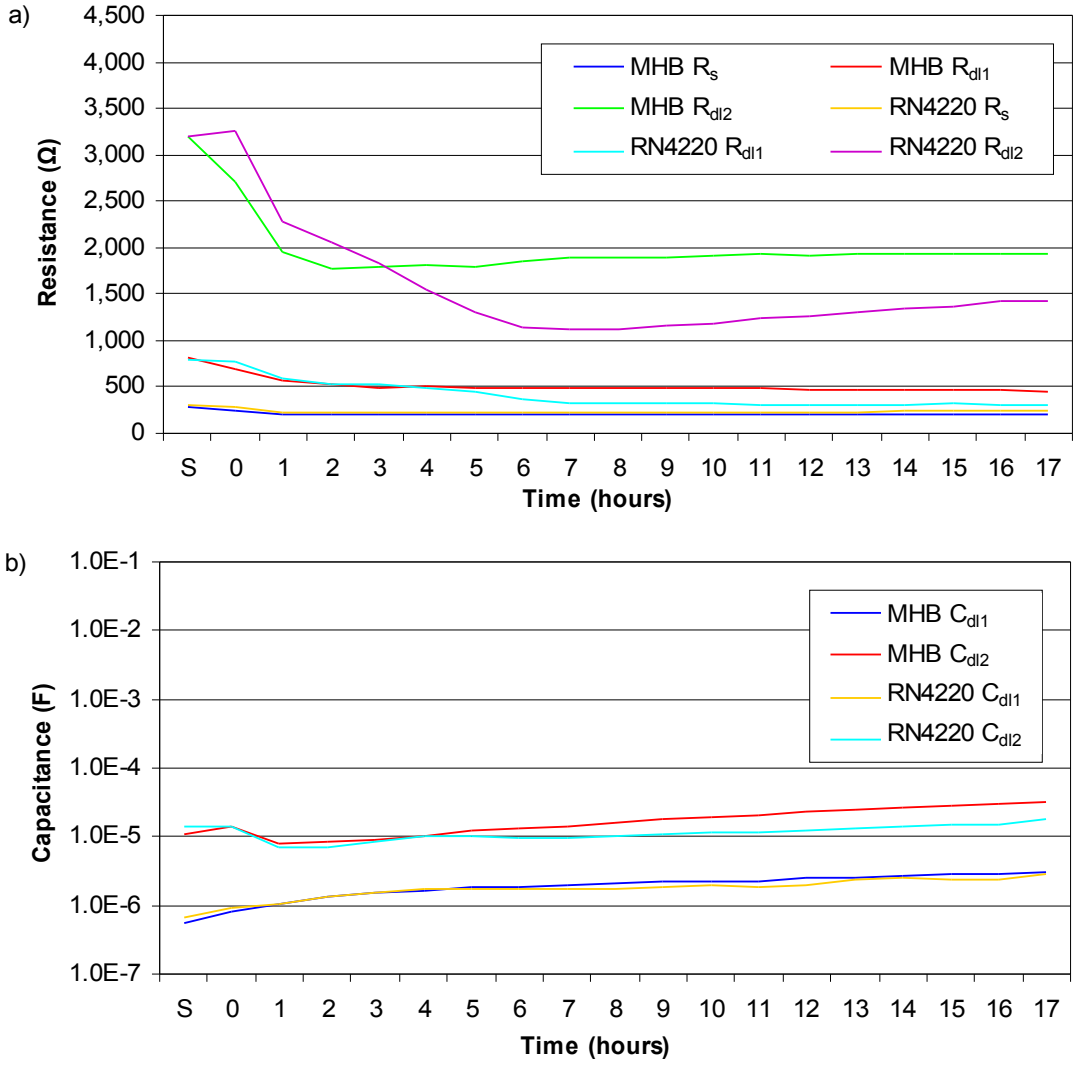

Figure 3-12. Circuit model component values over time for AgAgCl-PE300 sensors with and without RN4220 culture in MHB. S indicates Start measurement. a) Resistor values; b) Capacitor values.

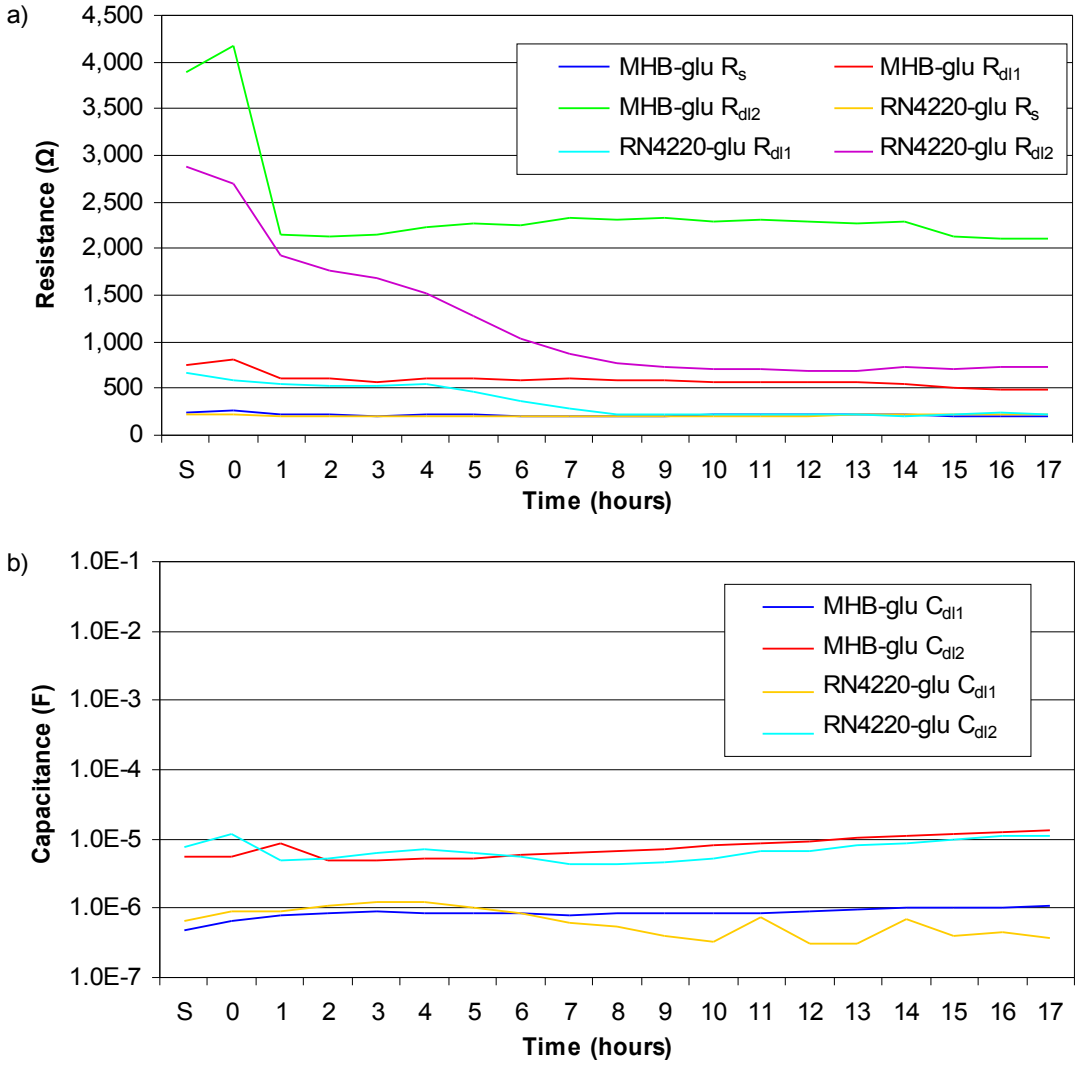

Figure 3-13. Circuit model component values over time for AgAgCl-PE300 sensors with and without RN4220 culture in MHB with glucose. S indicates Start measurement. a) Resistor values; b) Capacitor values.

3.3 Impedance – Bacteria in single suspensions and carbon sensors

The growth of RN4220 with impedance measurements was repeated with the screen-printed carbon sensors (C-PE200) for MHB-only (control) and RN4220 culture. These sensors appeared not to inhibit both species of bacteria tested in the growth experiments and therefore if they could detect the presence of bacteria they might be a better choice for detecting a number of different species. The carbon sensors had a higher impedance profile compared with the Ag-AgCl sensors (Figure 3-2) and therefore it was anticipated that a difference due to the presence of bacteria might not be observed by the carbon sensors due to their high impedance profile masking any changes.

3.3.1 Impedance – Single suspensions and carbon sensors

An example of the Bode plots from the carbon sensors for the start and 17 hour measurements of the MHB-only and RN4220 cultures are illustrated in Figure 3-14. It is immediately clear that there was considerable variation between individual carbon sensors. In the data shown between 100 and 100kHz the impedance magnitude was approximately 28.5kΩ for the MHB-only compared with 12.1kΩ for the RN4220 culture. Similarly the phase angle peak of -55.7^{o} occurred at 2.5Hz for the MHB-only compared with -65.4^{o} at 8Hz for the RN4220 cultures. These large variations between individual carbon sensors occurred across all the sensors used for this experiment and makes it difficult to compare the controls with the bacterial cultures for discernible differences.

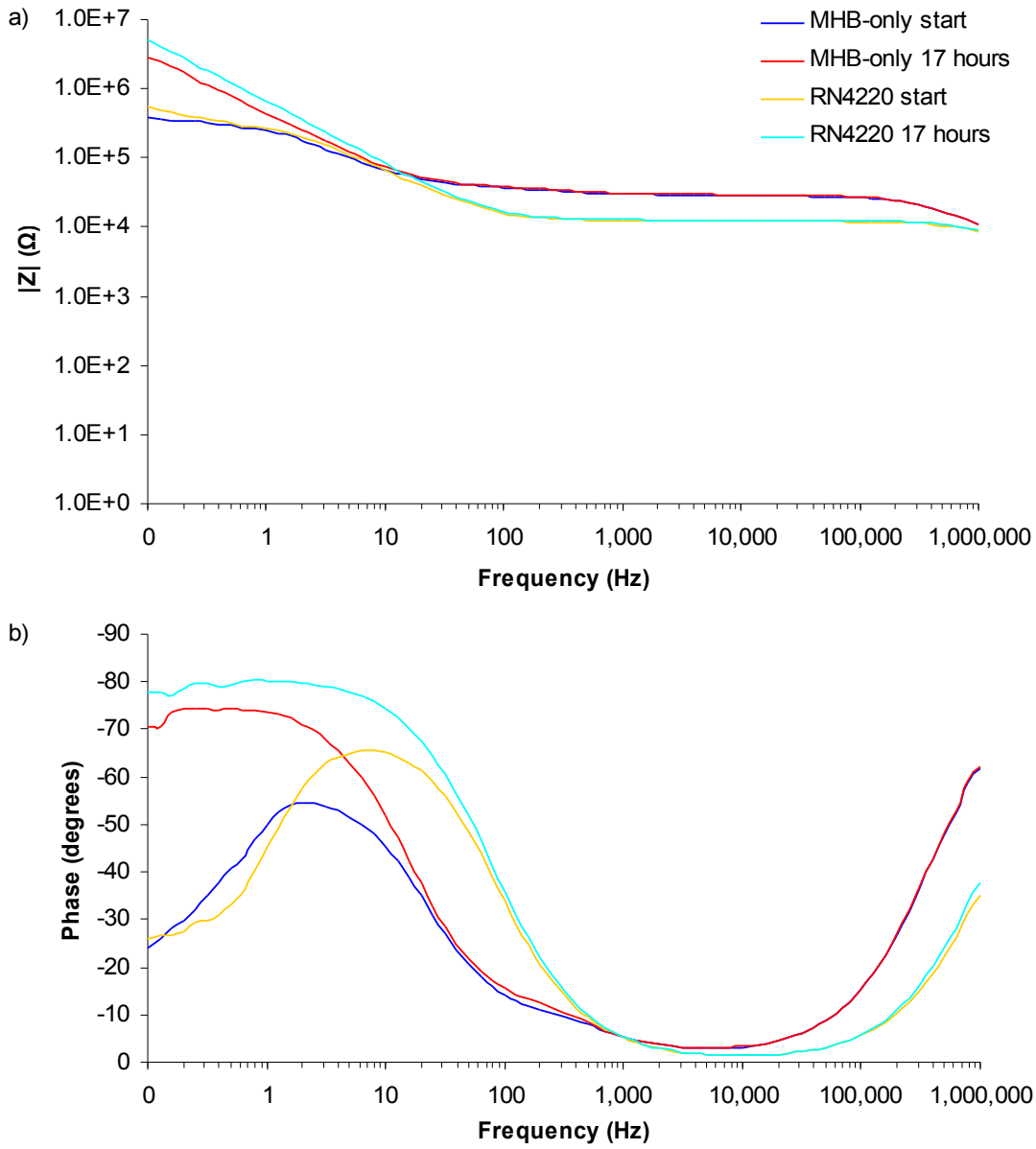

Figure 3-14. An example of the Bode plots with carbon sensors for single bacterial suspensions: a) Magnitude plot; b) Phase angle plot.

3.3.2 Normalised impedance – Single suspensions and carbon sensors

The impedance from the carbon sensors were normalised as previously described in Section 3.3.2. An example of the normalised Bode plots for MHB-only and RN4220 culture are illustrated in Figure 3-15. There were no peaks in either the normalised magnitude or phase profiles. The differences below 10Hz in the magnitude plot between the MHB-only and RN4220 are caused by the variation between individual carbon sensors, as discussed in Section 3.3.1. This confirms that these carbon sensors are unsuitable for detecting the absence and/or growth of bacteria. In the biofilm experiments, detailed in Chapter 4, carbon sensors were manufactured on the polyethylene substrate PE300 (Section 2.2.1) and individual sensors had closely matched impedance profiles and were more stable over time. The carbon sensors for the single suspension experiments were manufactured on the polyethylene substrate, PE200 and therefore these impedance profiles suggest that the carbon ink was not bonded correctly to the PE200 substrate compared with the PE300. The carbon ink over time immersed in the liquid could have gradually detached from the substrate and caused the changes in the impedance profiles.

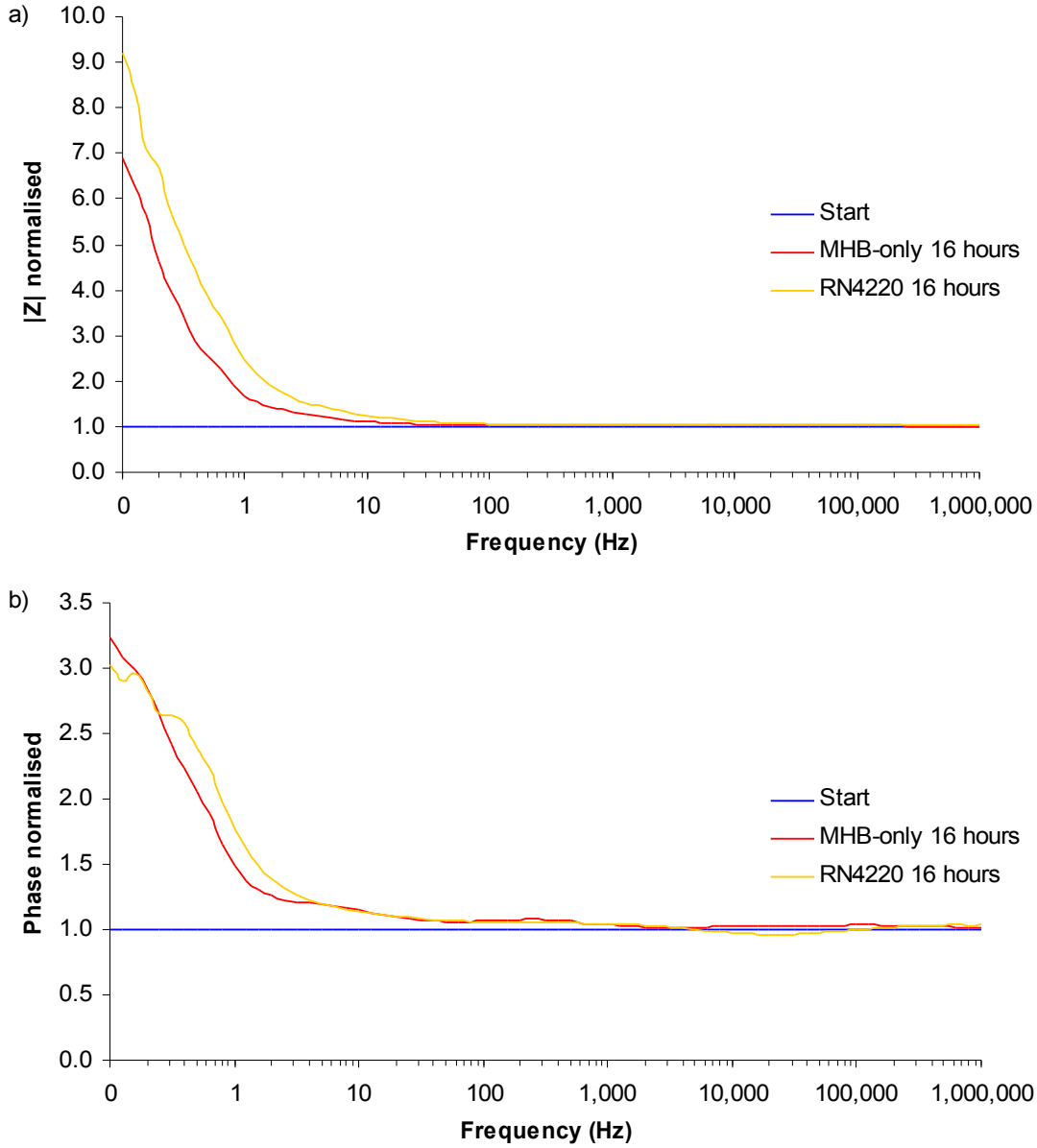

Figure 3-15. An example of the normalised Bode plots for the single bacterial suspensions: a) Normalised magnitude plot; b) Normalised phase plot.

3.3.3 Equivalent circuits – Single suspensions and carbon sensors

Equivalent circuit modelling of the carbon sensors was performed to investigate whether the bacteria were producing any changes to the impedance profiles despite the lack of evidence in the analysis of the impedance data (Sections 3.3.1 and 3.3.2). An example of the z-plots over time for MHB-only control and RN4220 culture with carbon sensors are illustrated in Figure 3-17. The z-plots at high frequencies contain an arc of a semicircle and at low frequencies the reactance tends towards infinity. To recap the discussion in Section 1.5.3 the semicircle is produced by the interface impedance which in circuit models is represented by a parallel resistor and capacitor. The high reactance is produced by diffusion processes between the bulk solution and the electrode. Therefore a different equivalent circuit was chosen to model the carbon sensors because of the differences in the impedance characteristics when compared to the Ag-AgCl sensors (Figure 3-5).

The circuit model selected is illustrated in Figure 3-16. The semicircle at high frequencies caused by the electrode-solution interface is represented by a parallel resistor R_{dl1} and capacitor C_{dl1}. Extrapolating the semicircle until it crosses the resistance axis shows that it will not cross at the origin and therefore there must be a resistor R_s to represent the solution in series with the interface impedance. The reactance at low frequencies is tending towards infinity implies that there is diffusion processes at work which can be represented by the constant phase element CPE_d, as discussed in Section 1.5.3.

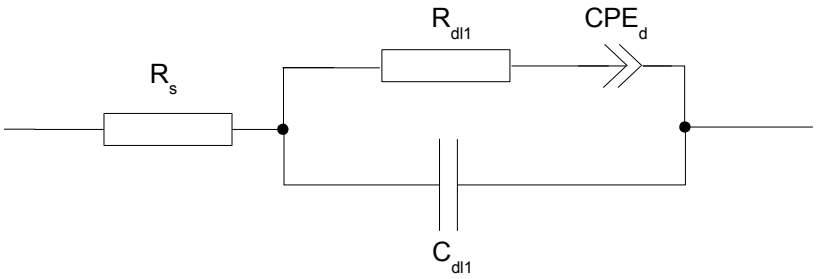

Figure 3-16. The equivalent circuit model for the carbon sensors.

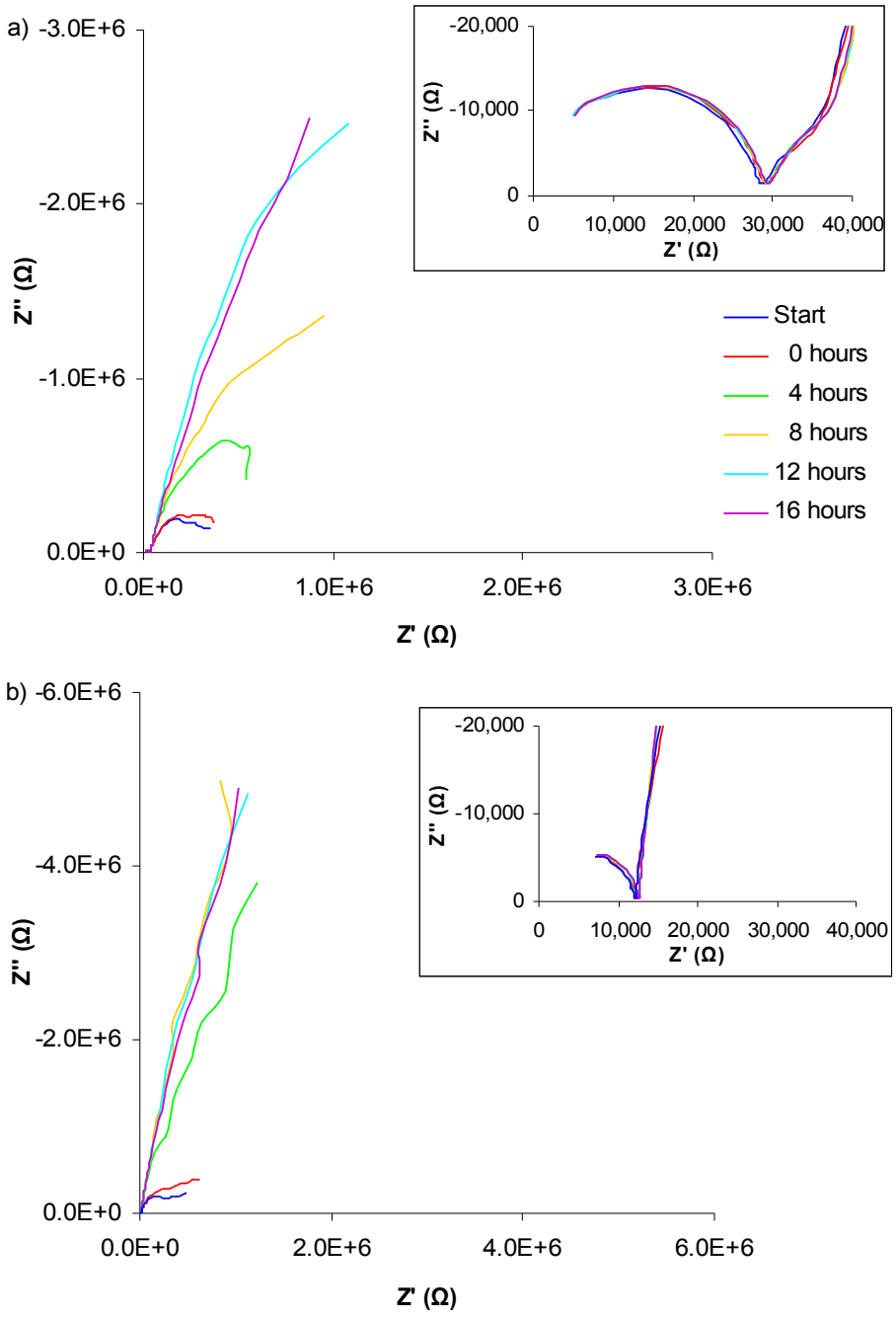

Figure 3-17. An example of a z-plot with carbon sensors for single suspensions: a) Mueller-Hinton broth only; b) RN4220 culture. Impedance sweep from 1MHz to 0.1Hz. The inserts show the high frequency semicircles caused by the impedance of the interface.

The higher accuracy of the equivalent circuit for carbon sensors compared with Ag-AgCl sensors are illustrated in Figure 3-18 with the actual readings and simulated readings from the RN4220 equivalent circuit shown. The simulated impedance magnitude matches closest at all frequencies while the simulated impedance phase match changes over time, with the best fit at 17 hours.

The generated component values for the start and 17 hour measurement from the carbon sensors with MHB only and RN4220 culture are listed in Table 3-5. The fit parameter is a measure of how closely the simulated data matches the actual data, the lower the value the better the fit is. The component error is a measure of how much a component value can shift up or down while keeping the fit value constant and large errors tend to indicate that the model contains too many components. The fit starts for both the MHB only and RN4220 cultures at less than twenty and decreased to less than ten. There was more variability in the MHB fit than the RN4220 culture with standard deviations around 7 compared with 0.1 to 3.5. The component errors are all less than 15% with all standard deviations less than 4.6%.

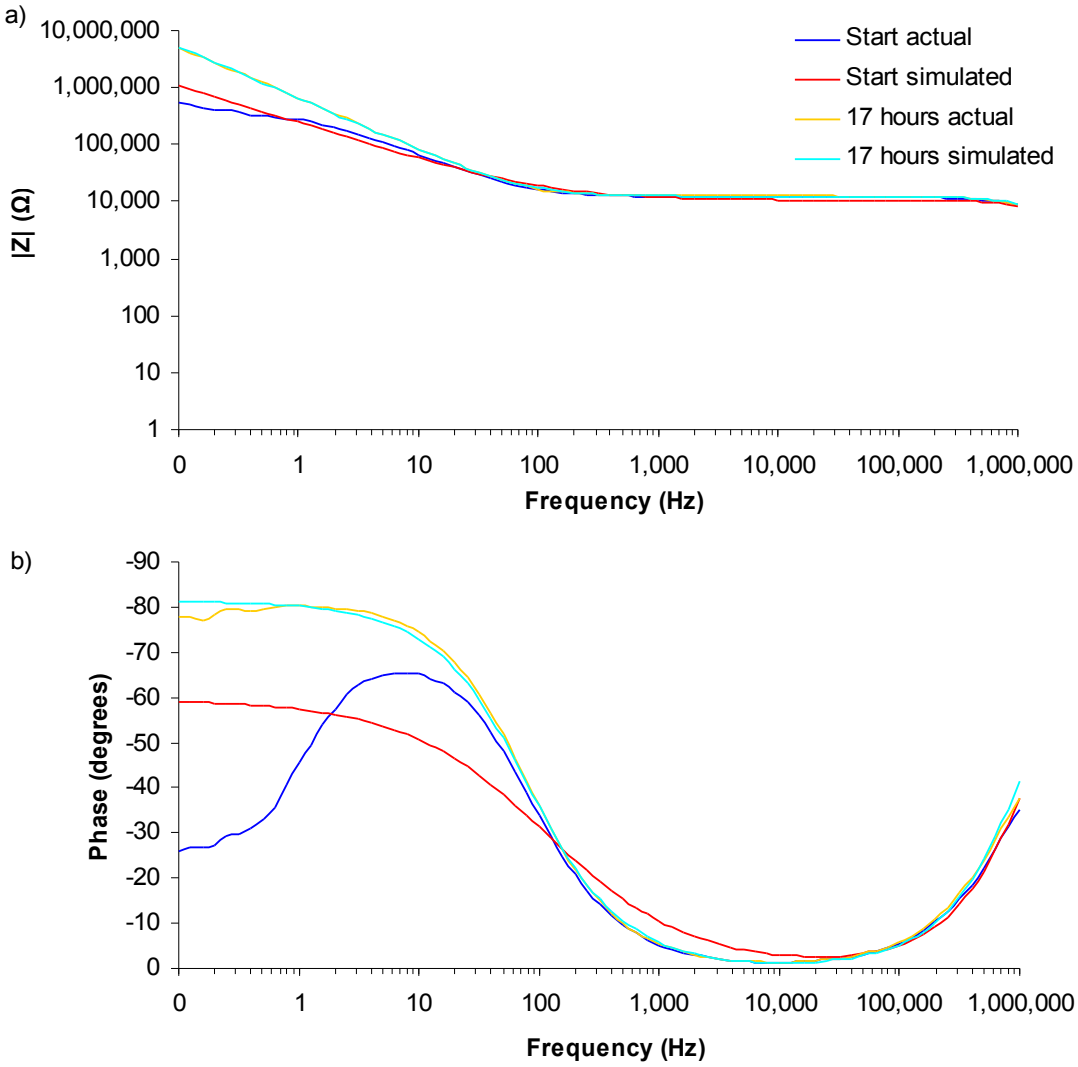

Figure 3-18. Bode plot of actual and simulated data with carbon sensors for a bacterial suspension: a) Impedance magnitude; b) Impedance phase. Impedance sweep from 1MHz to 0.1Hz. The starting value and 17 hour values are shown.

Table 3-5. The mean circuit model component values from the suspension experiment with Ag-AgCl sensors for the start and 48 hour readings. Data from MHB only and RN4220 experiments. The numbers in brackets indicate standard deviation.

Experiment	Component value		Component error (%)	
	Start	17 hour	Start	17 hour
Fit-Weighted sum of squares				
MHB	18.6 (7.0)	4.5 (6.8)		
RN4220	16.9 (± 3.5)	7.8 (± 0.1)		
R_s (Ω)				
MHB	Fixed at 220	Fixed at 220		
RN4220	Fixed at 220	Fixed at 220		
R_{dl1} (Ω)				
MHB	16.7k (± 5.6k)	19.1k (± 6.6k)	3.6 (± 0.8)	1.3 (± 1.1)
RN4220	12.5k (± 4.8k)	14.3k (± 5.3k)	3.3 (± 0.4)	1.7 (± 0.07)
C_{dl1} (F)				
MHB	$1.1x10^{-11}$ ($\pm 5.7x10^{-12}$)	$1.1x10^{-11}$ ($\pm 5.4x10^{-12}$)	11.2 (± 4.6)	4.1(± 2.9)
RN4220	$1.1x10^{-11}$ ($\pm 5.6x10^{-12}$)	$1.0x10^{-11}$ ($\pm 5.8x10^{-12}$)	12.7 (± 3.7)	6.7 (± 0.4)
CPE_d -T				
MHB	$1.4x10^{-6}$ ($\pm 6.0x10^{-7}$)	$4.6x10^{-7}$ ($\pm 1.5x10^{-7}$)	7.5 (± 2.0)	2.5(± 2.4)
RN4220	$7.6x10^{-7}$ ($\pm 2.9x10^{-7}$)	$2.4x10^{-7}$ ($\pm 4.2x10^{-8}$)	6.8 (± 1.0)	3.4 (± 0.1)
CPE_d-P				
MHB	0.62 (± 0.03)	0.8 (± 0.8)	3.3 (± 0.8)	0.8 (± 1.4)
RN4220	0.72 (± 0.07)	0.4 (± 0.9)	2.4 (± 0.3)	1.1 (± 0.03)

The solution resistance R_s in the circuit model was fixed at 220Ω because the actual data does not cover the frequency at which the solution resistance would be shown. The R_{dl1} component increases on average by 2kΩ for both MHB-only and RN4220 cultures, and could be caused either by molecules adhering to the electrode surface and decreasing the ease of transferring charge or by the electrode surface disintegrating. The C_{dl1} component is constant over time and there are changes in the CPE_d components, however due to the variability between individual sensors it is difficult to draw any firm conclusions.

3.4 Growth of bacteria – Lower inoculation densities

The bacterial growth with different electrode materials (Section 3.1.3) and the impedance with suspensions experiments (Section 3.2 and 3.3) were inoculated with approximately $1x10^6$ CFU ml^{-1}. This density of cells was considered to be too high for clinical usefulness given the increased likelihood of an infection occurring above $1x10^5$ CFU ml^{-1} and infections can also occur at less than $1x10^5$ CFU ml^{-1}, as described in Section 1.2.5. This led to the starting cell densities being reduced to approximately $1x10^3$ CFU ml^{-1}. However, it quickly became apparent that the growth of *Staphylococcus aureus* with screen-printed Ag-AgCl sensors from this inoculation density were not reaching the same final cell densities as the controls within 24 hours.

This was the first indication that all Ag-AgCl electrodes, whether wire or screen-printed, may inhibit bacterial growth depending on initial cell densities and volume of inhibiting material released from the electrodes. A further group of growth experiments with *Staphylococcus aureus* strains in the presence of Ag-AgCl sensors were performed to confirm that the electrodes were causing the growth inhibition. All the experiments from this point with Ag-AgCl sensors were performed with screen-printed sensors on the alternative polyethylene substrate, denoted Ag-AgCl-PE300. This was due to the original polyethylene substrate (-PE100) no longer being available, as detailed in Section 2.2.1.

3.4.1 Investigation of reduced bacterial growth rates

The investigation into the reduced bacterial growth rates in the presence of Ag-AgCl sensors involved three experiments. The first looked at the effect of different starting cell densities on the final cell densities to confirm the dependency of the initial cell numbers on the final cell numbers. The second experiment involved pre-washing the sensors to discover whether the inhibiting substance could be removed before inoculation. The final experiment investigated the possibility of bacteria previously grown in the presence of the Ag-AgCl sensors developing a resistance to the inhibiting substance. The complete methods for these experiments are detailed in Section 2.5.

To investigate the effect of different starting cells densities on the final cell densities bacteria were grown from approximately $1x10^2$, $1x10^3$, $1x10^4$ and $1x10^5$ CFU ml^{-1} in the presence of the Ag-AgCl-PE300 sensors. Two clinical strains of *Staphylococcus aureus*, SA081 and SA082, were selected for testing as well as the RN4220 lab strain used in previous experiments. The clinical strains were included as they were expected to be more robust than the lab strain and therefore have better growth abilities with the Ag-AgCl sensors. There were three replicates for each strain of *Staphylococcus aureus* (RN4220, SA081 and SA082) for each of the cell densities. The number of replicates was kept at three to minimise the number of screen-printed sensors used given the potential difficulty that might occur in obtaining more polyethylene substrate if it was to run out again.

The numbers of bacteria after culturing for 24 hours in the presence of Ag-AgCl-PE300 sensors from this experiment are illustrated in Figure 3-19. The results confirm that below a critical starting cell density it was not guaranteed that the final cell densities would reach $1x10^9$ CFU ml^{-1}. The control cultures that contained no sensors always reached $1x10^9$ CFU ml^{-1} within 16 to 24 hours which is expected given that the generation time under optimum conditions is approximately 30 minutes for *Staphylococcus aureus*. For RN4220 the critical density was approximately 1000 CFU ml^{-1} while for SA081 and SA082 the density was approximately $1x10^5$ CFU ml^{-1}. Given that it was expected that the clinical strains would be more robust their critical density was conversely lower than that of RN4220. The wide variation in the final cell densities of SA081 and SA082, between $1x10^5$ and $1x10^9$ CFU ml^{-1} suggest the amount of inhibiting substance has more influence than the starting cell density.

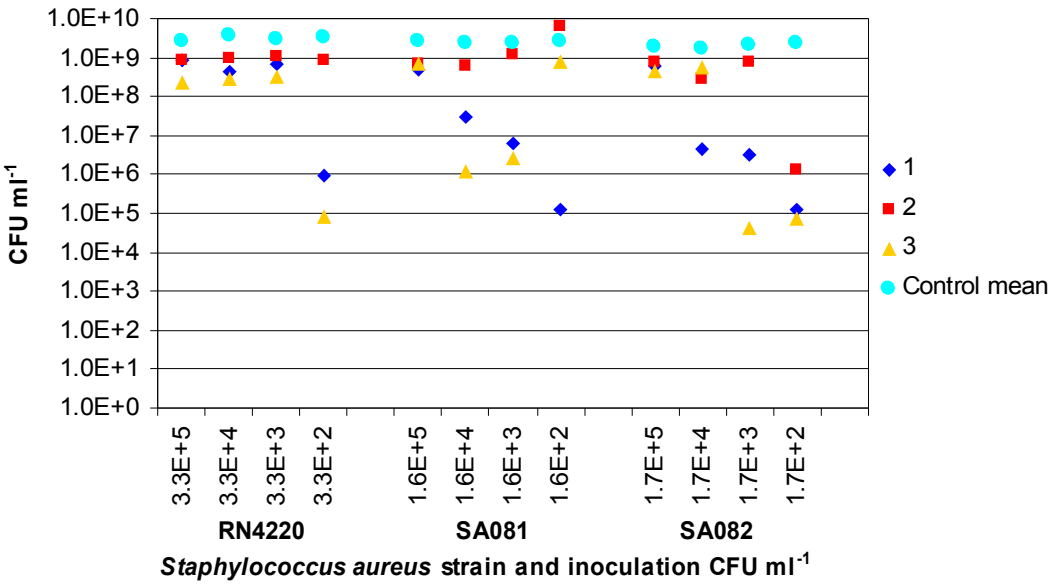

Figure 3-19. The final numbers of RN4220, SA081 and SA082 with Ag-AgCl-PE300 after 24 hours culturing from different starting densities. Three replicate cultures are shown for each of the three strains of *Staphylococcus aureus* at each starting density.

The second experiment investigated whether normal growth could be achieved by washing a significant quantity of the potential inhibiting substance off the electrodes. Screen-printed Ag-AgCl-PE300 sensors were soaked for 24 hours in Mueller-Hinton broth with two changes of media before the sensors were placed in fresh MHB and the liquid inoculated with approximately $1x10^3$ CFU ml^{-1}. The numbers of bacteria grown after culturing for 24 hours with the pre-washed Ag-AgCl-PE300 sensors is illustrated in Figure 3-3. All the *Staphylococcus aureus* strains reached expected growth levels in all experiments, indicating that it may be possible to wash the inhibiting substance off the electrodes. This washing process may provide a possible way forward for the infection monitor in terms of not inhibiting the bacteria. On the other hand inhibiting the bacteria in a wound would not do any harm.

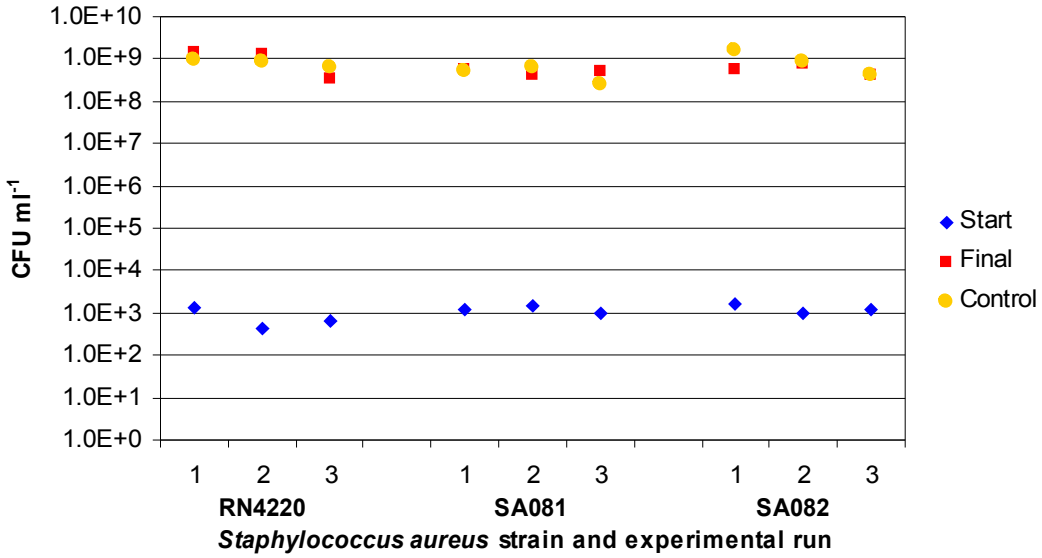

Figure 3-20. The starting and final numbers of RN4220, SA081 and SA082 with pre-washed Ag-AgCl-PE300 sensors for a 24 hour culture. Three replicate cultures are shown for each of the three strains of *Staphylococcus aureus*.

The final experiment investigated whether bacteria previously grown in the presence of Ag-AgCl sensors developed any resistance and would grow to $1x10^9$ CFU ml^{-1} in a secondary culture with fresh Ag-AgCl sensors. The numbers of bacteria grown after culturing for 24 hours and then regrown for a further 24 hours in the presence of Ag-AgCl-PE300 sensors are illustrated in Figure 3-21. All three RN4220 cultures grew to control levels. None of the clinical strains reached the control growth levels with SA081 ranging from $1x10^5$ to $1x10^7$ CFU ml^{-1} and SA082 ranging from 0 to $1x10^7$ CFU ml^{-1}. These results imply that the bacteria are unlikely to be developing any form of resistance to the sensors. To really test this a very large number of samples would be required since possible mutations may only be occurring in a very small percentage of cells and a sample of 3 would not show this. The clinical strains again appear to be less robust than the lab strain which was not expected.

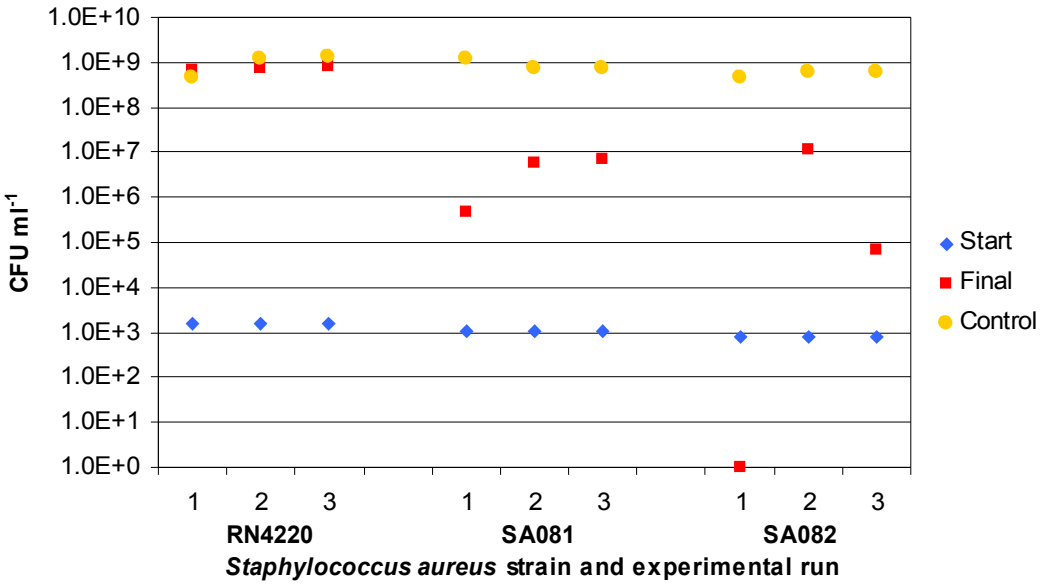

Figure 3-21. The numbers of bacteria grown with Ag-AgCl-PE300 sensors inoculated from a pre-grown culture with AgAgCl-PE300 sensors. Three replicate cultures are shown for each of the three strains of *Staphylococcus aureus*.

3.5 Impedance – Bacteria in parallel suspensions

The Ag-AgCl sensors were clearly inhibiting the growth of *Staphylococcus aureus* from low starting cell densities, especially the clinical strains. An impedance experiment was performed to discover whether a difference in impedance profiles occurred when the bacteria were grown from low cell densities. To increase the throughput of experiments a parallel test rig, described in Section 2.6.1, was designed and built. This allowed up to 8 test vials containing controls or bacterial cultures to be measured in parallel.

This experiment was performed to investigate whether the differences in the impedance signature traces observed when the bacteria grew from high cell densities were still evident from low cell densities. The effect of glucose and pre-washed sensors was also further investigated. The normalised impedance profile of the bacterial culture had contained some interesting peaks when glucose was added to the media (Section 3.2.2) and this experiment would investigate the effect of the glucose concentration on these peaks. The bacteria appeared not to be inhibited by the pre-washed sensor experiments (Section 3.4.1) and thus if this was still the case when impedance measurements were employed then a potential solution to the inhibition would be found.

The experiment (as described in Section 2.6.2) was performed with 3 control vials containing: Mueller-Hinton broth (MHB); MHB plus 0.2% glucose; and MHB with a pre-washed Ag-AgCl-PE300 sensor. The five bacterial vials contained RN4220 with: MHB plus 0.1% glucose; MHB plus 0.2% glucose; MHB plus 0.4% glucose; or MHB with a pre-washed Ag-AgCl-PE300 sensor. The experiment was replicated three times creating a total of 24 vials. The experiments were analysed as were the single suspension experiments by finding the final cell densities, examining the impedance and normalised impedance profiles, and performing equivalent circuit analysis.

3.5.1 Growth – Parallel suspensions

The growth levels of RN4220 after 16 hours with Ag-AgCl-PE300 sensors in different media and with pre-washed sensors are illustrated in Figure 3-22. The growth levels indicate that there was wide variation in growth rates across different media and between experiments. In the first experimental run only the RN4220 in MHB-glucose (0.2%) culture grew to a density in excess of $5x10^7$ colony forming units per ml (CFU ml^{-1}), in experiment 2 all the vials with RN4220 grew to to more than $5x10^7$ CFU ml^{-1} and in the final experimental run RN4220 in MHB-glucose (0.2%) culture and the RN4220 culture with pre-washed sensors reached densities above $5x10^7$ CFU ml^{-1}.

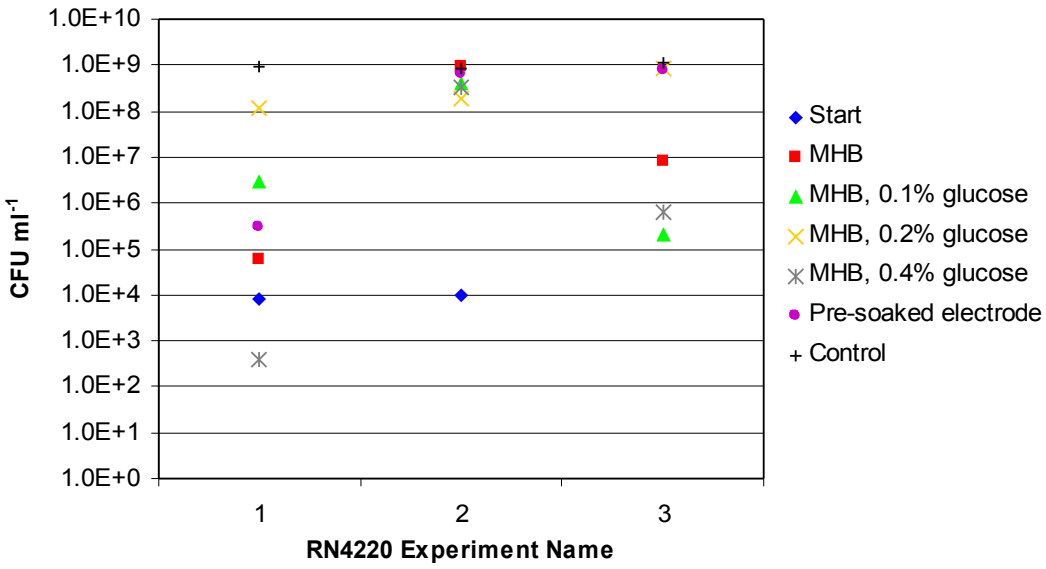

Figure 3-22. The growth levels of RN4220 after 16 hours with various types of media or pre-washed sensors from low starting cell densities.

These results clearly show that the Ag-AgCl sensors have an inconsistent effect on the growth of bacteria possibly due to differing amounts of inhibiting substances released. One of the three pre-washed sensors did not achieve the expected density of $1x10^7$ CFU ml^{-1} which suggests either it was not soaked for long enough or that the impedance measurements may be causing more of the inhibiting substance to be released into the media. The range of cell densities will provide data on the detection

limits of the impedance measuring system used in this experiment. It was expected that below a critical cell density there would be insufficient cells to produce a change in the impedance profile.

3.5.2 Impedance – Parallel suspensions

The impedance measurements were performed every hour for 16 hours on all eight vials. An example of the z-plots between a media only and a bacterial vial that grew to cell densities matching the control levels are illustrated in Figure 3-23. The z-plots of the controls without bacteria were similar to the single suspension experiments (Section 3.2). There were two distinct impedance profiles for the bacterial vials irrespectively of the media contents or sensor preparation. The z-plots of those where the final levels of bacteria were below approximately $5x10^7$ colony forming units per ml (CFU ml^{-1}) appeared to be the same as the controls. In contrast the z-plots of the vials where the levels of bacteria grew in excess of $5x10^7$ CFU ml^{-1} became more convoluted, as in all the z-plots with bacteria in the single suspension experiments did. Therefore it appears that the impedance procedure used in these experiments has a sensitivity of approximately $5x10^7$ CFU ml^{-1}.

The frequency of the phase peak was where differences were seen due to the presence of bacteria in the single suspension experiments (Section 3.2.1). Therefore the impedance data from the parallel suspension experiments were examined with particular attention to the phase. In the phase plots from the parallel experiments there was a peak and a subsidiary peak as seen in the single suspension experiments (Figure 3-6a). However, the first noticeable issue was that in the starting readings there were two types of phase profiles as illustrated in Figure 3-24, one where the peak was higher than the subsidiary peak and one where the peak was lower than the subsidiary peak. This change raised concerns that there was a greater range of behaviour between individual sensors than desirable. In turn this might effect the ability of each sensor to detect bacteria.

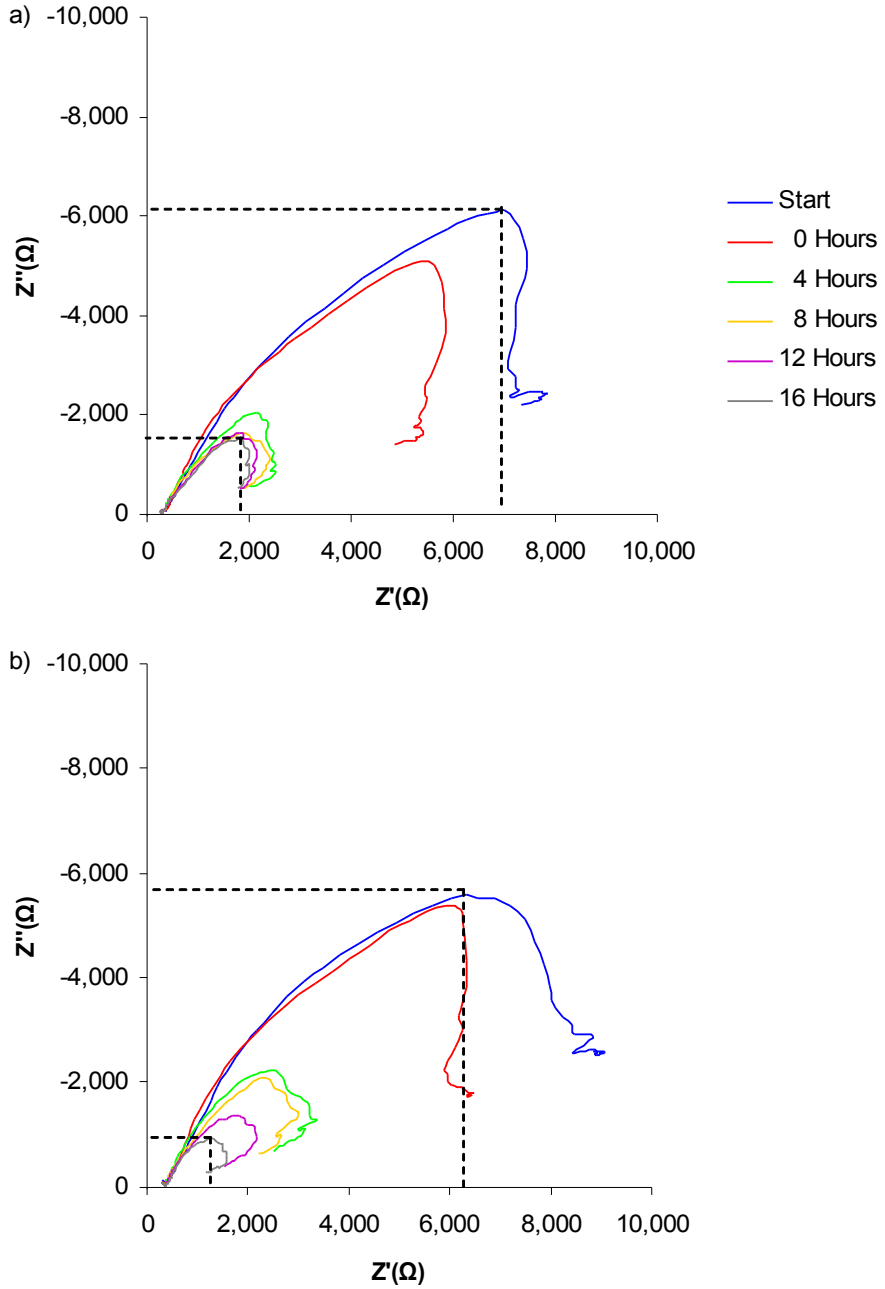

Figure 3-23. An example of the z-plots with Ag-AgCl-PE300 sensors in the parallel suspension experiments: a) MHB-glucose 0.2%; b) RN4220-glucose 0.2%, final growth level of approximately $1x10^9$ CFU ml^{-1}.

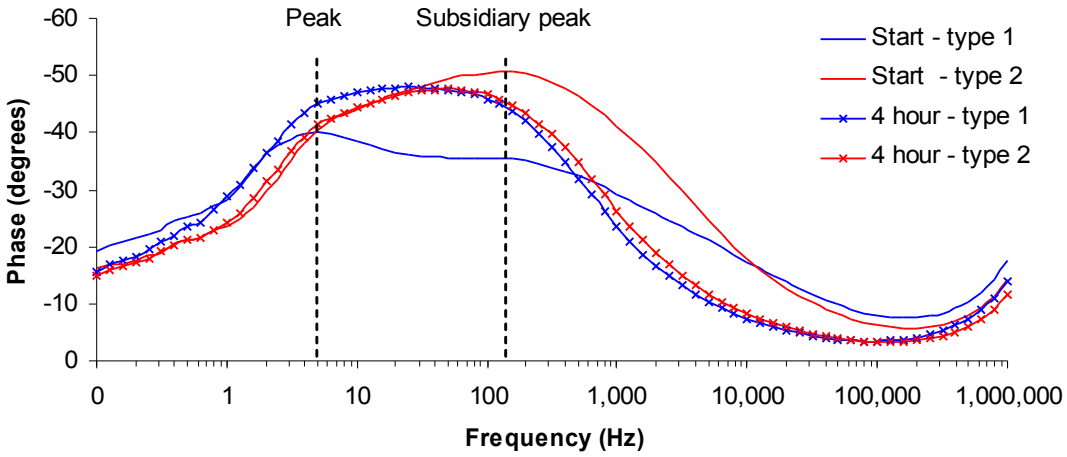

Figure 3-24. An example of the two types of phase starting measurements.

On further examination the different phase profiles appear to stabilise after 3 hours in the controls (Figure 3-24) and therefore should not cause any significant differences in the phase profiles over time. It was expected that the different starting measurements may cause a difference in the normalised measurements because it shows relative changes from the starting condition. The normalised data is discussed in Section 3.5.3. The type 1 phase profiles occurred in 10 of the 24 vials and these sensors were from a previous batch of Ag-AgCl-PE300 sensors and the remaining 14 from a newer batch. This indicates that the manufacturing process may not always be consistent.

In all 24 vials irrespectively of the media type or preparation of the sensor there were three types of phase plots as illustrated in Figure 3-25. The examples shown all have type 2 starting measurements and those with type 1 were similar except for the first 3 hours as discussed previously.

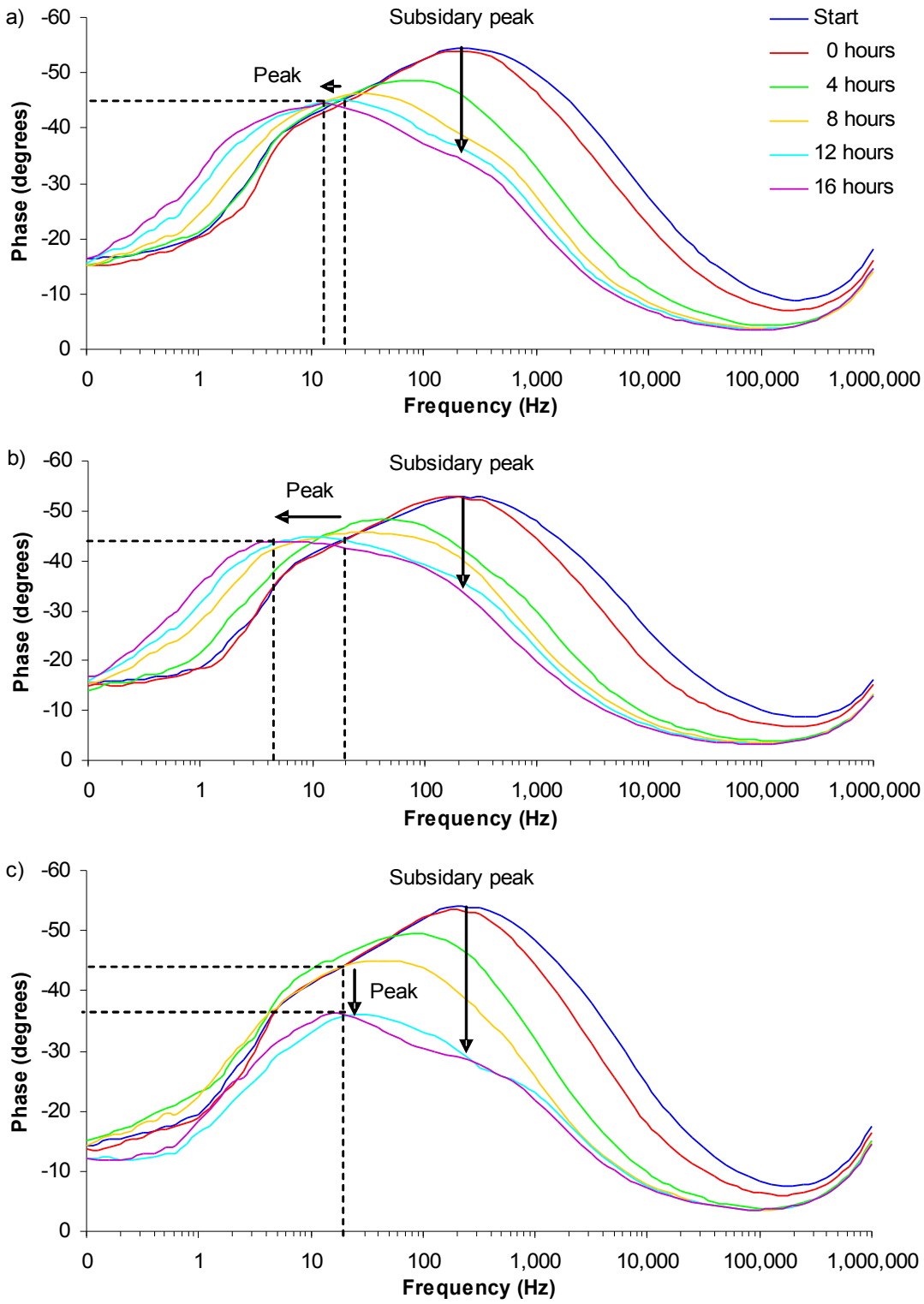

Figure 3-25. An example of the phase plots with Ag-AgCl-PE300 sensors in parallel suspensions: a) MHB with 0.2% glucose; b) MHB with 0.1% glucose and low density RN4220; c) MHB with 0.1% glucose and high density RN4220. Black arrows indicate changes in the phase peak over time.

For the examples shown, in the media only (Figure 3-25a) the subsidiary peak starts at 251Hz and over time decreases in phase angle while possibly keeping the frequency reasonable steady. In contrast the peak starts at approximately 20Hz and shifts down in frequency to 12.6Hz and probably keeps its phase angle steady. The movement of the peak and subsidiary peak are similar for all the media only controls: Mueller-Hinton broth (MHB); MHB with 0.2% glucose; and MHB with pre-washed sensors. The exact changes in the frequency of the peaks cannot be determined solely by examination as the peaks are unresolved. The effect of the changes in the two peaks is that the phase angle maximum shifts down in frequency and increases in the phase angle. The importance of defining the peak and subsidiary peak rather then the maximum phase angle becomes apparent when comparing the defined peak with and without bacteria.

There were two contrasting phase plots for the vials inoculated with RN4220. The first (Figure 3-25b) was very similar to the media only profiles and a difference could not be distinguished. These profiles occurred in all the inoculated vials where the final cell numbers were less than $5x10^7$ CFU ml^{-1}. The second phase profile (Figure 3-25c) occurred in vials with RN4220 where the final cell densities were in excess of $5x10^7$ CFU ml^{-1}. The subsidiary peak movement was similar to the media only and the low density bacteria vials. The difference was observed in the peak which decreased in phase angle and had very little movement in its frequency. These three signature phase profiles were repeatable in the 24 separate culture vials with 9 media only, 7 below $5x10^7$ CFU ml^{-1} and 8 above $5x10^7$ CFU ml^{-1}. Therefore it appears that once bacterial cultures reach a sufficient cell density a separate signature trace in the phase angle over frequency occurs and indicates that comparing signature traces could discern between the absence and or/growth of bacteria, only if the potential growth inhibition could be removed.

Based on the observed changes in the phase plot profile it was expected that the media only and the low cell density bacterial vials should have a different frequency of phase peak compared with the high cell density bacterial vials at 16 hours. The frequencies at which the impedance phase peak occurred at for the parallel bacterial

suspension experiments at 16 hours are listed in Table 3-6. For each bacterial vial the frequency of the phase angle was compared with the frequencies of the controls to find whether a difference occurred. Statistical tests were not performed due to the low number of samples caused by not being able to group all the similar bacterial samples. For example with the pre-washed sensors there was only one low density sample and two high density samples.

Table 3-6. The impedance phase peak frequencies for the parallel suspension experiments. Blue lettering indicates phase peak corresponds with cell density greater than $8.5x10^6$ CFU ml^{-1} while red lettering indicates a false negative.

Media	Control or bacteria	Sensor pre-washed	Number	16 hour phase peak frequency	>$8.5x10^6$ CFU ml^{-1}	Frequency > 13Hz
MHB	Control	No	1	6.31	-	-
			2	10.00	-	-
			3	7.94	-	-
MHB	RN4220	No	1	5.01	No	No
			2	**19.95**	**Yes**	**Yes**
			3	**15.85**	**Yes**	**Yes**
MHB - glucose 0.2%	Control	No	1	3.16	-	-
			2	12.59	-	-
			3	10.00	-	-
MHB - glucose 0.1%	RN4220	No	1	6.31	No	No
			2	**15.85**	**Yes**	**Yes**
			3	3.98	No	No
MHB - glucose 0.2%	RN4220	No	1	**6.31**	**Yes**	**No**
			2		Yes	-
			3	**39.81**	**Yes**	**Yes**
MHB - glucose 0.4%	RN4220	No	1	3.98	No	No
			2	**15.85**	**Yes**	**Yes**
			3	5.01	No	No
MHB	Control	Yes	1	5.01	-	-
			2	7.94	-	-
			3	5.01	-	-
MHB	RN4220	Yes	1	3.16	No	No
			2	**7.94**	**Yes**	**No**
			3	**31.62**	**Yes**	**Yes**

The phase peak frequency at 16 hours appeared in most cases to show a difference when the cell densities were above $8.5x10^6$ CFU ml^{-1}. Table 3-6 lists when the final cell numbers were above $8.5x10^6$ CFU ml^{-1} and when a difference occurs between the bacterial cultures and the media only controls. The frequency at 16 hours were below 13Hz for all the media only vials and the bacterial vials with less than this cell density. In contrast the bacterial vials with more than $8.5x10^6$ CFU ml^{-1} had a phase peak at frequencies more than 13Hz except in two cases, one RN4220 in MHB-glucose (0.2%) and one RN4220 with a pre-washed sensor experiment. Also the RN4220 in MHB vial in the 3rd replicate experiment has a final cell density of $8.5x10^6$ CFU ml^{-1} and a phase peak frequency indicating high cell density. However the phase profile matches that of the low cell densities vials (Figure 3-25b) indicating a possible false positive.

The phase profiles of the two cases in which the phase peak frequency was not above 13Hz despite final cell numbers greater than $8.5x10^6$ CFU ml^{-1} matched the high cell density profile (Figure 3-25c) until the final measurement at 16 hours. The phase profiles for the final 5 hours for these two cases are illustrated in Figure 3-26. The 16 hour measurement of both the RN4220 in MHB with glucose (0.2%) (Figure 3-26c) and the RN4220 with a pre-washed sensor (Figure 3-26b) differ from their 15 hour readings. If the phase peak of the 15 hour readings are used to compare with the control then the RN4220 with a pre-washed sensor is no longer a false negative, however the RN4220 in MHB with glucose (0.2%) has a higher frequency which is similar to the controls. There is no obvious explanation for the change in the 16 hour reading and discounting these readings does not remove all the false negatives anyway. Therefore comparing the signature phase traces always indicates cell densities in excess of $5x10^7$ CFU ml^{-1} whereas the frequency of the phase peak would detect cell densities in excess of $8.5x10^6$ with a greater risk of false results.

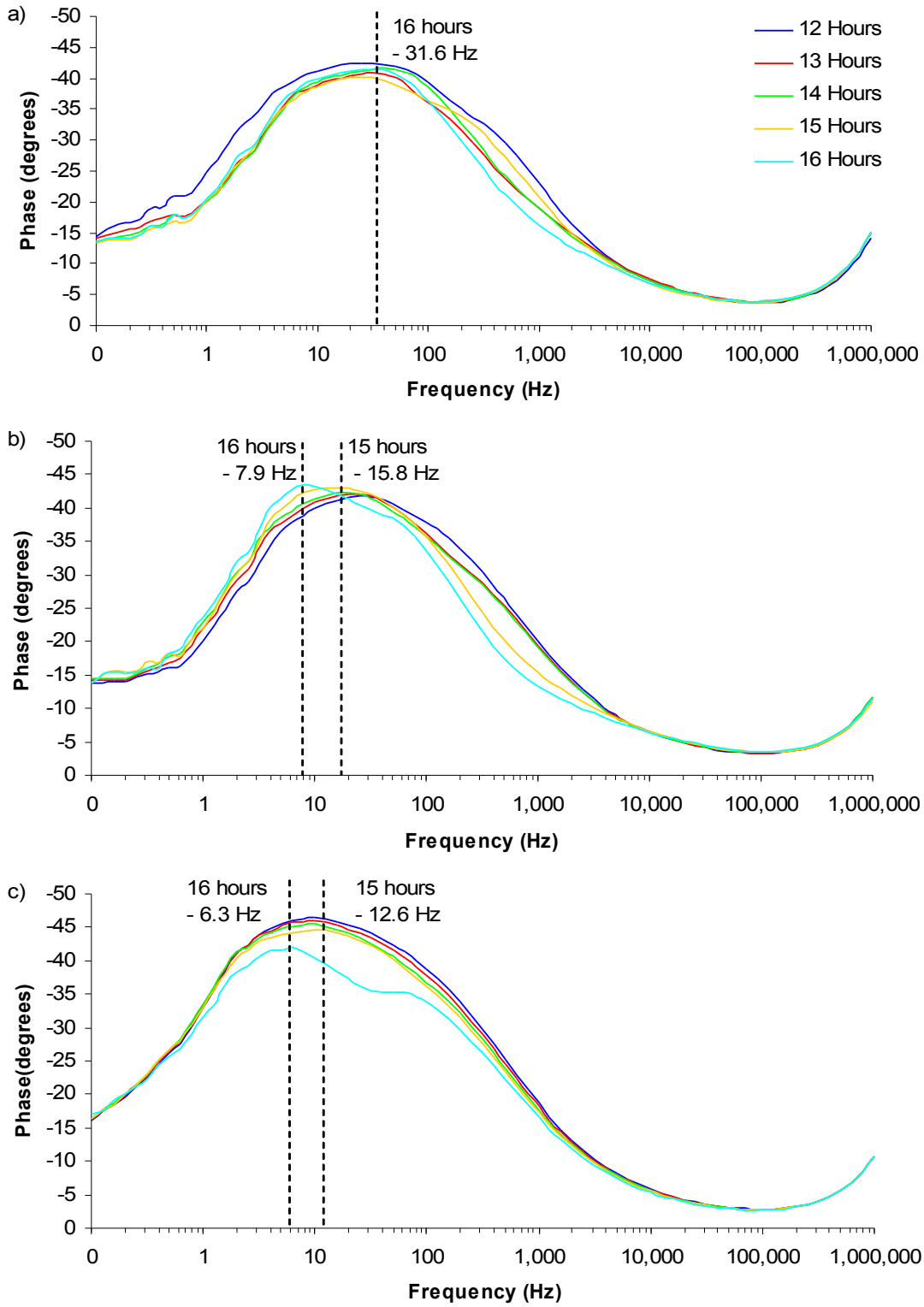

Figure 3-26. Phase plots for the false negatives in the parallel suspension experiments: a) RN4220 with pre-washed sensor, sample 3; b) RN4220 with pre-washed sensor, sample 2, false negative,;c) RN4220 in MHB with 0.2% glucose, sample 1, false negative.

3.5.3 Normalised impedance – Parallel suspensions

To briefly recap, normalisation of the impedance data was performed by dividing each hourly reading by the starting reading to show relative changes from the starting condition, as described in Section 2.9. The normalised data was examined for the differences in the frequencies that the peaks occurred at that could be used for detection purposes. As expected there were differences between the normalised plots depending on whether the starting readings was type 1 or type 2 as discussed in Section 3.5.2. The normalised impedance magnitude profiles for type 1 are illustrated in Figure 3-27 and for type 2 in Figure 3-28. For each of the three scenarios, media only, low cell density and high cell density there were corresponding profiles irrespectively of the media contents or whether the sensor had been pre-washed.

For type 1 the normalised magnitude peak occurred between 10 to 40 Hz for all 10 vials and for type 2 the peak occurred at less than 5 Hz. There was no discernible difference in the range of frequencies that the peaks occurred at between the media only and the bacterial cultures, even at high densities. There were changes in the magnitude of the normalised peak for type 2 and a similar change at low frequencies for type 1. As expected the profiles for media only and low densities of bacteria are the same with the normalised magnitude of the peak stabilising after 3 hours. In the examples in Figure 3-28 this is at approximately 0.3 for the media only and 0.4 for the low cell densities. In comparison the normalised magnitude peak decreases over time as the cell density increases, from 0.4 to less than 0.2 over the last 12 hours of the experiment time. Therefore it appears that the difference in starting conditions are not effecting the changes due to high cell densities in a significant way and indicates that the differences between individual sensors may be acceptable.

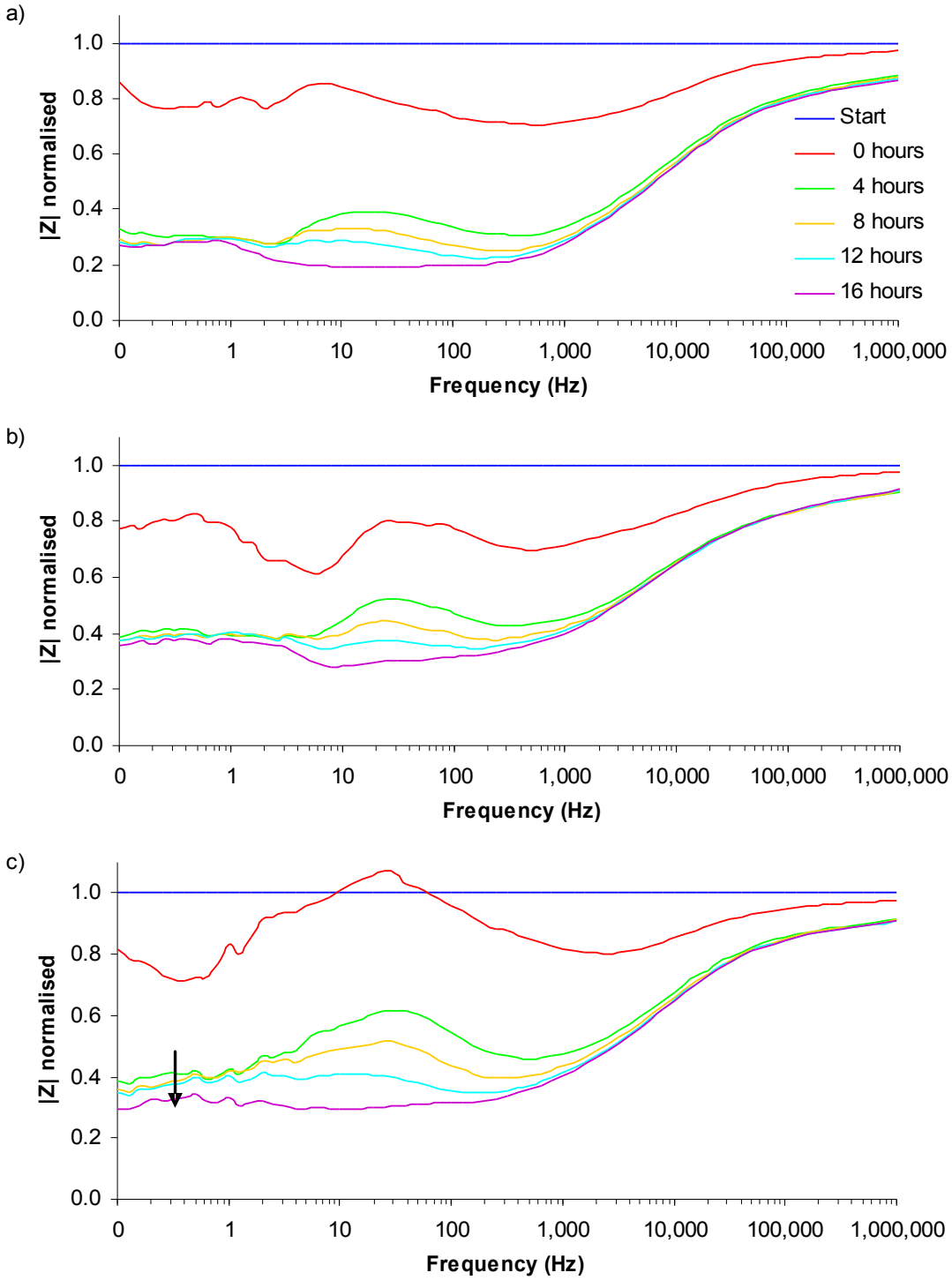

Figure 3-27. Examples of the normalised magnitude plots in the parallel suspension experiments, 1st replica: a) MHB with 0.2% glucose; b) MHB with 0.1% glucose and low density RN4220; c) MHB with 0.2% glucose and high density RN4220. Black arrow indicates change in normalised magnitude over time at low frequencies due to high density bacteria.

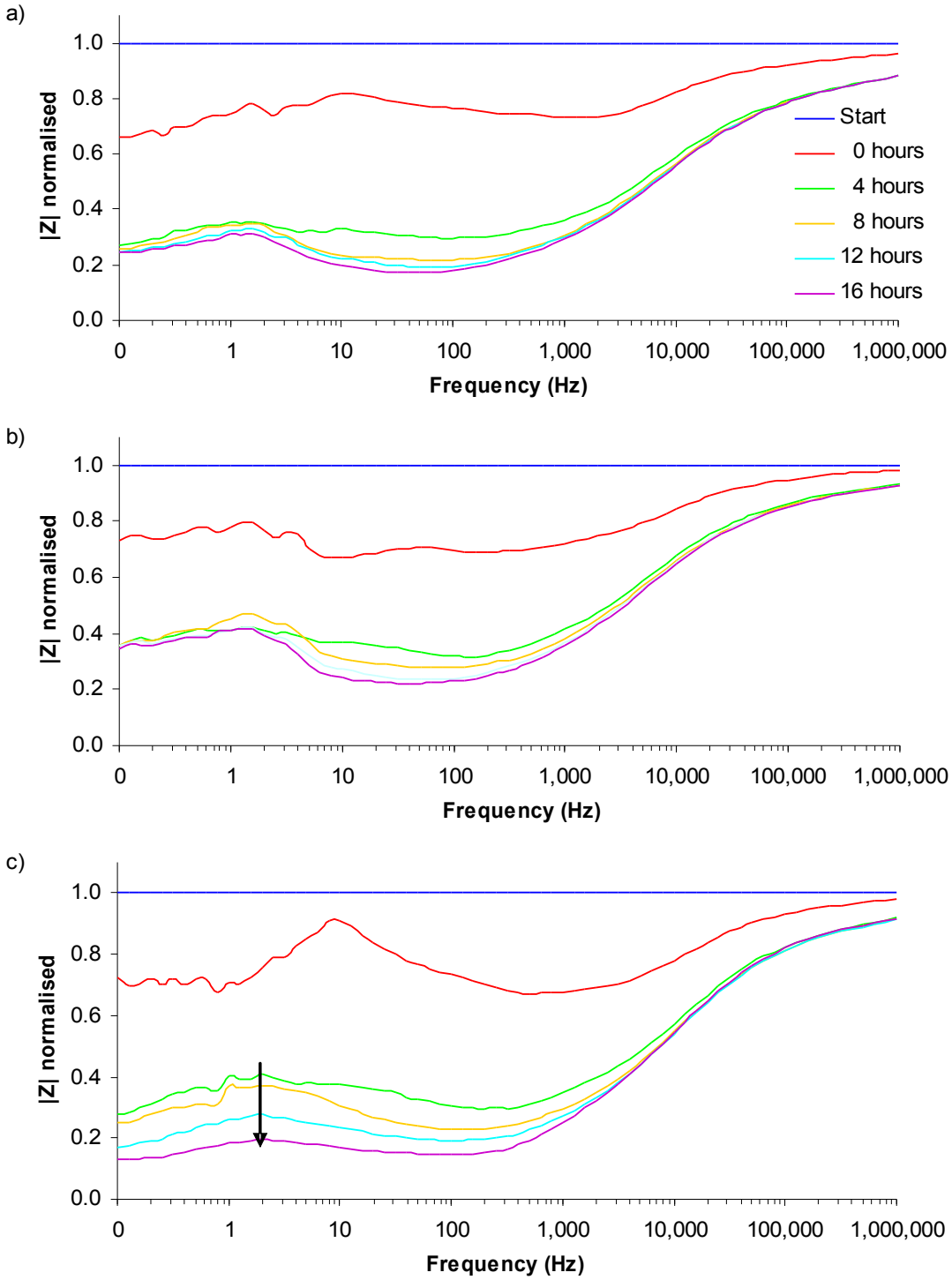

Figure 3-28. Examples of the normalised magnitude plots in the parallel suspension experiments, 3rd replica: a) MHB with 0.2% glucose; b) MHB with 0.1% glucose and low density RN4220; c) MHB with 0.2% glucose and high density RN4220. Black arrow indicates change in normalised magnitude peak over time due to high density bacteria.

The profiles chosen for Figures 3-27 and 3-28 were those where glucose had been added to the media to show that compared with the single suspension experiments (Figure 3-8) the same secondary magnitude peak between 1.5k and 5Hz did not appear. A possible explanation for this was that the glucose-bacteria process that produced the peaks did not occur as the increased number of generations in the growth due to the lower starting cell numbers used more of the glucose in building the cells. Therefore it was not possible to discover the effect of different glucose concentrations on the formation of this secondary peak. In terms of the infection monitor for wounds the volume of glucose available would be limited due to the competition with the host cells and therefore the secondary peak may not be observed in vivo.

In the normalised phase plots the three different profiles were again evident as illustrated in Figure 3-29 with the media only and low cell density being similar and a contrasting profile for the high cell densities. No difference was observed in the range of frequencies that the peak occurred at with and without bacteria. The peak always occurred at less than 5Hz and no differences were seen in the six vials that contained the 10 to 30Hz magnitude peak. The media only and the low cell density profiles have a normalised phase peak that increases over time and when there is a high level of growth the peak fluctuates. In the examples shown the media only has a normalised phase peak that increased over the 16 hours by 1.557 and for the low density bacteria by 1.894. In the high density bacterial vial the normalised phase peak increased for the first 5 hours to 1.26, followed by a decrease to 0.84 at 11 hours and then an increase to 0.96 in the remaining hours. These results provide further evidence that comparison of signature traces between high cell densities and controls will show discernible differences, whereas the outcome based on the position of frequency peaks in the normalised data would not.

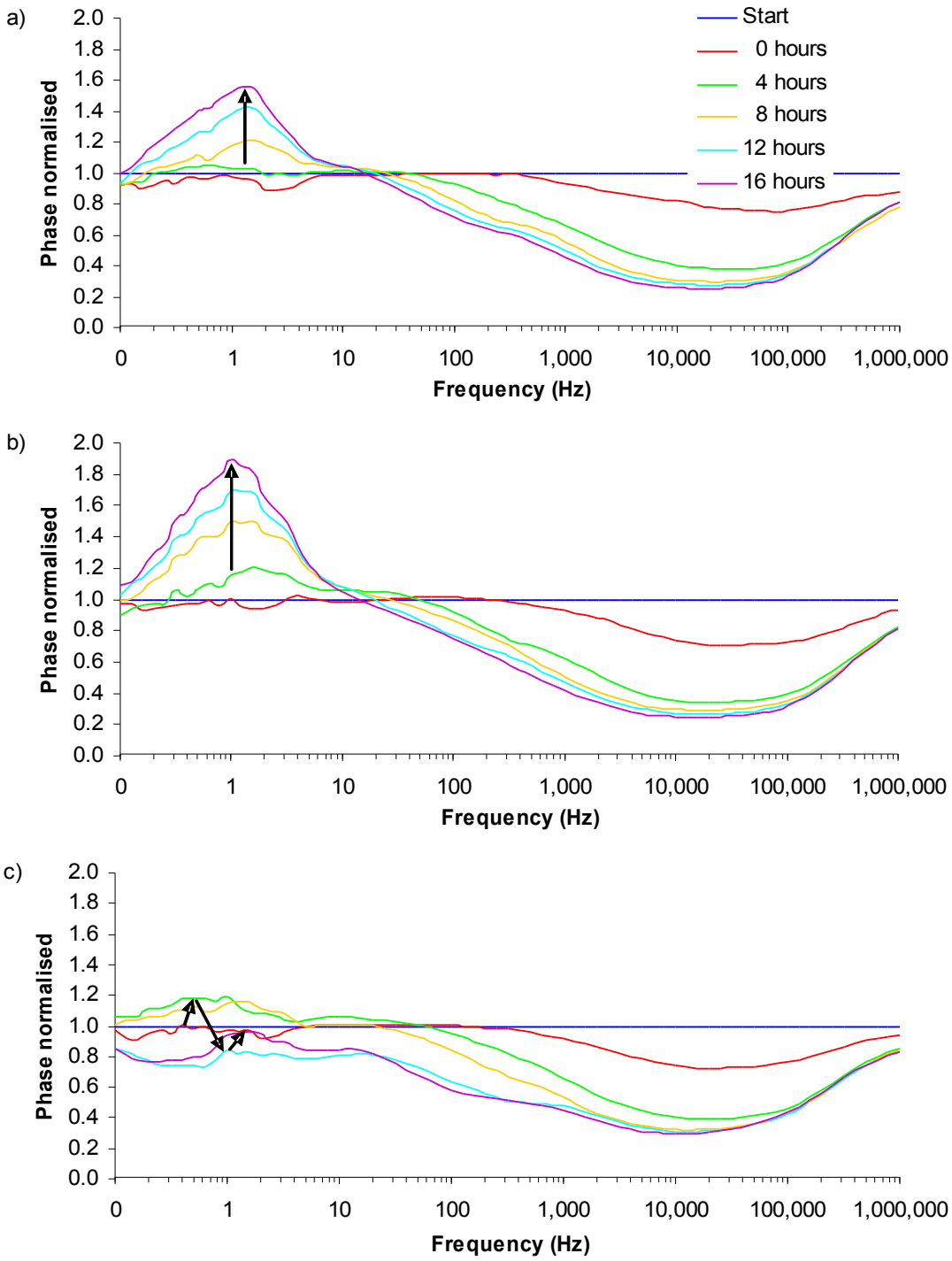

Figure 3-29. Examples of the normalised phase plots in the parallel suspension experiments: a) MHB with 0.2% glucose; b) MHB with 0.1% glucose and low density RN4220; c) MHB with 0.1% glucose and high density RN4220. Black arrows indicate changes in normalised phase peak over time.

3.5.4 Equivalent Circuits – Parallel suspensions

Equivalent circuit modelling of the parallel suspension experiments was performed to find whether there were similar changes when compared to the single suspension experiments. The impedance measurements were fitted to the same equivalent circuit that the single suspensions with Ag-AgCl sensors were fitted to, as illustrated in Figure 3-10a.

The changes expected in the circuit component values are best seen in the phase profiles described in Section 3.5.2. From the theory in Section 1.5.3 and as for the single suspension experiments described in Section 3.2.1 the phase peak influences the electrode interface components R_{dl1} and C_{dl1} and the subsidiary peak influences the components R_{dl2} and C_{dl2}. The greater the phase angle of the peak the larger the corresponding resistor is and the higher the frequency of the phase peak the smaller the corresponding capacitor is. Therefore in the high cell density vials the R_{dl1} and R_{dl2} components should decrease further and the C_{dl1} component should increase less when compared to the media only and low cell density vials.

The R_{dl1} and C_{dl1} component values over time for the 3rd replicate of the parallel suspension experiment are illustrated in Figure 3-30. All the resistor values stabilise in the first three hours and then the media only and low density vials remain stable with a very gradual decrease. In comparison the two vials, MHB with 0.2% glucose and MHB with pre-washed sensors, that reached cell densities in excess of $5x10^7$ CFU ml^{-1}, start decreasing from their stable values between 8 and 9 hours. They decrease below the R_{dl1} values of the controls and low cell densities and stabilise again between 13 and 15 hours. A similar change occurred in the R_{dl2} values of these experiments.

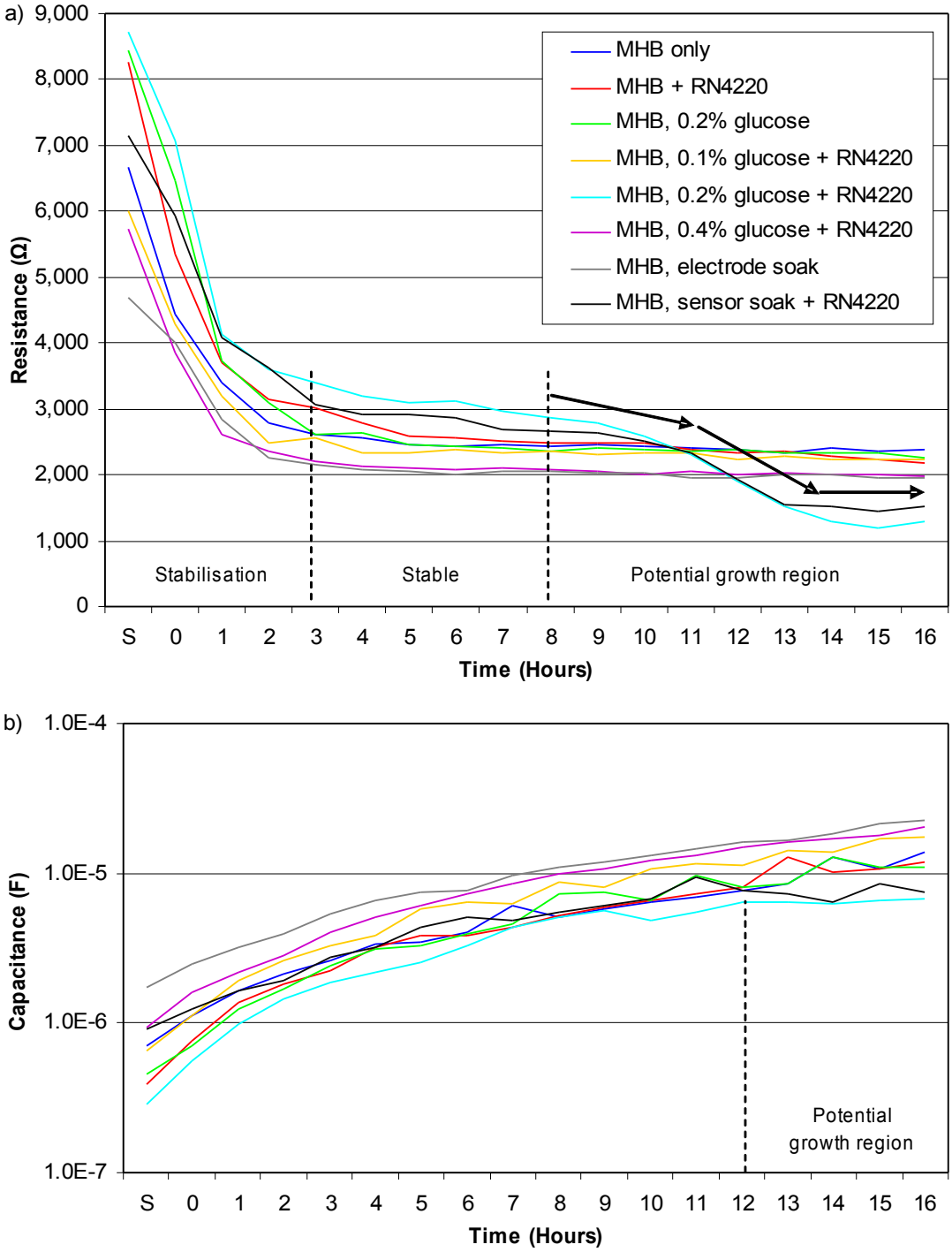

Figure 3-30. Examples of the equivalent circuit components over time for the parallel suspension experiements. a) R_{dl1} component, b) C_{dl1} component. Black arrows indicate the changes due to high levels of growth.

In the 8 vials when the final bacterial numbers were greater than $5x10^7$ CFU ml^{-1} the value of R_{dl1} and R_{dl2} decreased below 1,800Ω and 400Ω respectively when the final bacterial numbers were greater than $1x10^7$ CFU ml^{-1}. The start and 16 hour component values for R_{dl1} and R_{dl2} of the parallel suspensions experiments are listed in Table 3-7. The decrease in the resistor values from that of the low density and media only vials occurred between 8 and 10 hours.

Table 3-7. The component values of R_{dl1} and R_{dl2} for the multiple suspension experiments. Blue lettering indicates a decrease in resistance for final cell densities greater than $1x10^7$ CFU ml^{-1}. The sensor failed in the 2nd experiment of RN4220-glucose 0.2%.

Media	RN4220 present	Sensor pre-washed	Number	R_{dl1} component value		R_{dl2} component value		>$5x10^7$ CFU ml^{-1}
				Start	16 hour	Start	16 hour	
MHB	No	No	1	5801	2278	1562	532	-
			2	7493	2363	1107	541	-
			3	6655	2386	1036	593	-
MHB	Yes	No	1	3376	1906	910	501	No
			2	6795	**1656**	1124	**276**	**Yes**
			3	8266	2176	1188	504	No
MHB - glucose 0.2%	No	No	1	6688	2087	2074	515	-
			2	9391	2473	1329	553	-
			3	8452	2268	1127	507	-
MHB - glucose 0.1%	Yes	No	1	5182	2025	1273	501	No
			2	6697	**1050**	1061	**338**	**Yes**
			3	5999	2224	917	610	No
MHB - glucose 0.2%	Yes	No	1	4474	**1496**	1130	**396**	**Yes**
			2	Not available		Not available		Yes
			3	8718	**1292**	1173	**247**	**Yes**
MHB - glucose 0.4%	Yes	No	1	5310	2418	1436	589	No
			2	6978	**780**	1176	**270**	**Yes**
			3	5725	1979	1121	556	No
MHB	No	Yes	1	4044	2208	1045	582	-
			2	6131	1936	990	415	-
			3	4698	1947	861	454	-
MHB	Yes	Yes	1	4252	1835	1054	461	No
			2	6067	**1425**	965	**286**	**Yes**
			3	7139	**1523**	1210	**313**	**Yes**

The R_s components in all the parallel suspension experiments decreased in the first three hours and then stabilised at a mean of 285Ω. No change was noticeable in all the vials with final high cell densities indicating that the cells do not change the conductivity of the media sufficiently for a noticeable change. The C_{dl1} component over time increases steadily with a mean change of $1.4x10^{-5}$ F. A small difference occurs in the vials with high cell densities where the C_{dl1} component reduces its rate of increase. In the example in Figure 3-30b this change occurs at approximately 12 hours and the difference at 16 hours is $5.3x10^{-6}$ F. No noticeable differences were observed in C_{dl2} component between the media only and high cell densities. The mean increase of the C_{dl2} component in all the parallel suspension experiments was $5.6x10^{-6}$ F.

The results of the equivalent circuit modelling of the parallel suspension experiments further validates the circuit model chosen with similar changes in all components to the single suspension experiments. The changes occur later in time indicating the difference in the time that it takes for the lower starting cell densities to reach the level required to produce observable changes. The differences in the components between the media only and high cell densities also matched the predictions based on the changes in the phase profiles. The physical processes producing the component changes over time are discussed in Section 5.2.3.

3.6 Influence of impedance measurements on bacterial growth

The comparison of the final cell densities between the bacterial growth experiments without impedance and the parallel suspension experiments with experiments indicated there was a small possibility that the application of the electrical probe signal to the electrodes in cultures was having an effect on the cultures. An example is that there was no inhibition of RN4220 with the sensors that had been pre-washed and no impedance measurements performed (Section 3.4.1), whereas there was when impedance measurements were performed (Section 3.5.1). Therefore the effect of impedance measurements on the growth of bacteria was investigated.

Two clinical strains of *Staphylococcus aureus*, SA081 and SA082, isolated from the Glasgow Royal Infirmary, Scotland were selected in addition to RN4220. It was expected that the clinical strains would be more robust than the lab strain RN4220. The three strains were grown with Ag-AgCl sensors from approximately $1x10^3$ CFU ml^{-1} with and without applied voltage and frequency signals for impedance measurements as described in Section 2.6. To recap the parallel suspensions test rig with the parallel suspensions procedures was used. In total for each strain 8 vials were cultured with Mueller-Hinton broth (MHB), 4 had no impedance measurements and 4 had impedance measurements performed every hour for 24 hours. Hourly impedance measurements were also performed on control vials containing MHB only and a total of 4 controls were measured.

The experiments were analysed as were the parallel suspension experiments by finding the final cell densities, examining the impedance and normalised impedance, and performing equivalent circuit analysis. The phase and normalised phase were focused on as these parameters were where the most significant changes were seen in the single and parallel suspension experiments.

3.6.1 Growth – Influence of impedance measurements on bacterial growth

The growth of bacteria with and without impedance measurements in the presence of Ag-AgCl-PE300 sensors are illustrated in Figure 3-31. The strain RN4220 reaches control levels without impedance measurements, however it does not with impedance measurements. In the vials without impedance measurements the strain SA081 reaches the control levels in 3 out of the 4 cultures and the strain SA082 in 2 out of the 4 cultures. With impedance measurements SA081 reaches control levels in none of the 4 cultures and SA082 in 2 out of the 4 cultures.

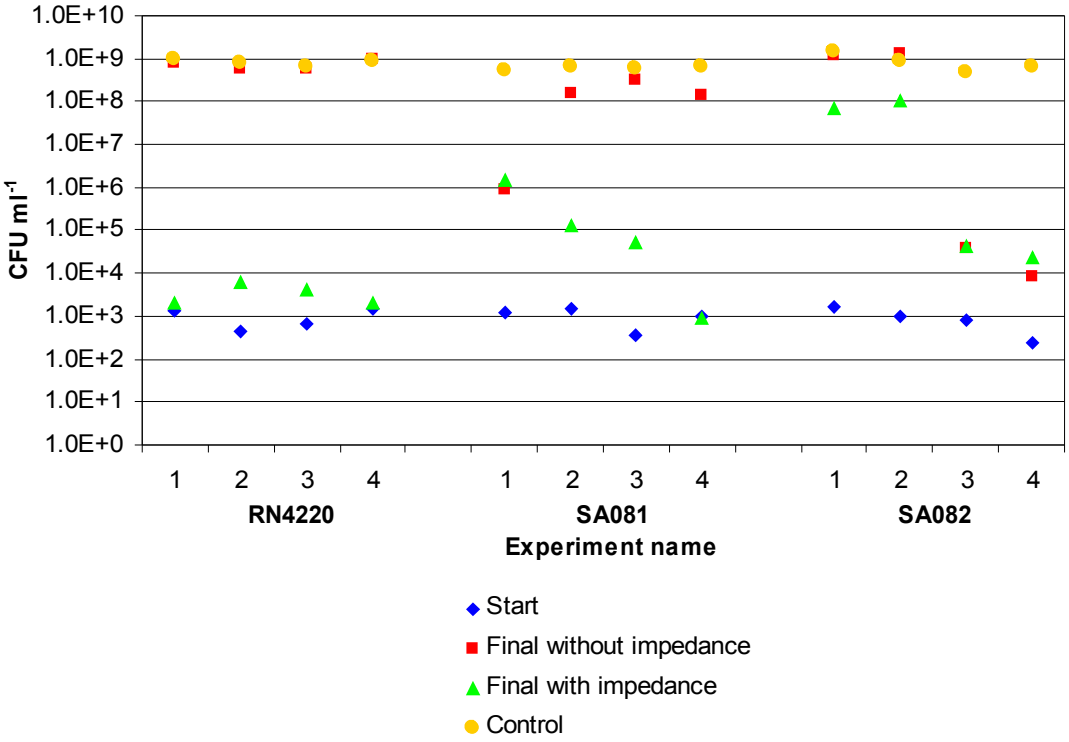

Figure 3-31. The growth levels after 24 hours with and without impedance measurements for three strains of *Staphylococcus aureus.*

The final cell densities of RN4220 in this experiment clearly suggest that the impedance measurements are inhibiting their growth. The cell densities from SA081 vial 1 and SA082 vials 3 and 4 indicate similar levels of growth with and without impedance measurements. The other 3 vials of SA081 indicate that the impedance measurements are effecting the growth, whereas the other 2 vials of SA082 indicate

no inhibition. Therefore it appears that impedance measurements may increase inhibition and this is most likely by increasing the volume of silver ions released into the media.

3.6.2 Phase – Influence of impedance measurements on bacterial growth

The phase profiles were examined based on the results of the parallel suspension experiments with data from low cell densities expected to be similar to the media only and data from high cell densities to be different. This was the case and the examples of the three profiles are illustrated in Figure 3-32. There was a peak and subsidiary peak as described in 3.5.2. In the media only and low density vials the peak shifts downwards in frequency and decreases in phase angle. The shift down in frequency of the high density vials is less than either the low density vials or media only, and there is an increase in phase angle. This occurred in both the SA082 vials that grew to more than $5x10^7$ CFU ml^{-1}. Therefore it appears that the examination of phase profiles of multiple strains of *Staphylococcus aureus* show a difference in the signature trace when growth is in excess of $5x10^7$ CFU ml^{-1} compared with low density or media only. This is the first evidence that the phase signature traces over frequency can be used to discern high growth levels in multiple strains of *Staphylococcus aureus*.

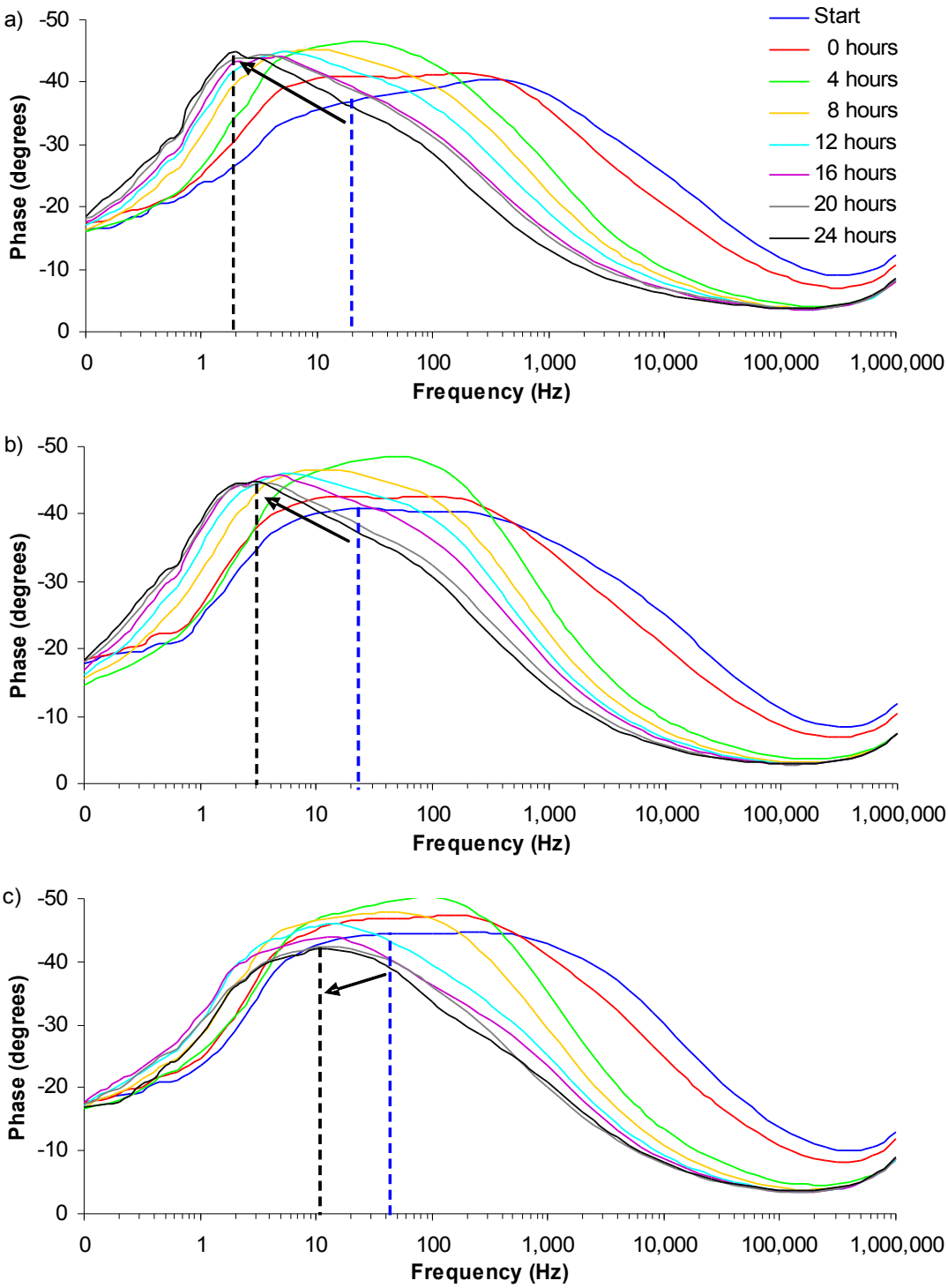

Figure 3-32. Examples of the phase angle plots from the experiment on the influence of impedance measurements: a) MHB; b) MHB and low density SA082; c) MHB and high density SA082. Black arrows indicate changes in the phase peak over time.

The parallel suspension experiments show that the frequency of the phase peak was not as reliable to indicate bacteria as it was in single suspension experiments. The frequencies of the phase peak at 24 hours in the experiment on the influence of impedance measurements are listed in Table 3-8. All the media only vials had a phase peak of 2.0 or 3.2Hz. All the bacterial vials with low densities at 24 hours had phase peaks at frequencies of 6.3Hz or less except in two of the RN4220 vials. The two SA082 vials that had final cell densities in excess of $1x10^7$ CFU ml^{-1} had frequencies larger than 6.3Hz. These results again indicate that the impedance technique is successful on multiple stains of *Staphylococcus aureus,* however there are two false positives within the RN4220 vials. This provides further evidence that the the use of signature frequencies to indicate the absence and/or growth of bacteria is less reliable than comparing the signature traces over frequency with the controls.

Table 3-8. The phase angle peak frequencies for the experiment on the influence of impedance measurements.

Experiment	Number	Phase peak frequency (Hz)	> $1x10^7$ CFU ml^{-1}	Frequency > 6.3Hz
MHB	1	3.2	No	-
	2	3.2	No	-
	3	3.2	No	-
	4	2.0	No	-
RN4220	1	6.3	No	No
	2	6.3	No	No
	3	**10.0**	**No**	**Yes**
	4	**12.6**	**No**	**Yes**
SA081	1	4.0	No	No
	2	3.2	No	No
	3	2.5	No	No
	4	4.0	No	No
SA082	1	**7.9**	**Yes**	**Yes**
	2	**12.6**	**Yes**	**Yes**
	3	3.2	No	No
	4	5.0	No	No

3.6.3 Normalised phase – Influence of impedance measurements

The normalised phase peak occurred in all 4 control and 12 bacterial cultures at less than 5 Hz with no discernible differences between the controls and bacterial cultures. The differences in magnitude changes of the peaks as seen in the parallel suspension experiments (Figure 3-29) were observed. Examples of the changes over time of the normalised phase in these experiments are illustrated in Figure 3-33. The 4 media only and 10 low densities vials of RN4220, SA081 and SA081 started at approximately 8 hours and increased over time while 2 high density SA082 vials increased until 13 to 14 hours where it decreased. The change in normalised phase peak must be related to the changes in the phase profile. Despite the low number of high cell densities this appears to show that the signature traces are valid for multiple strains of *Staphylococcus aureus* which is important for a detection system which should be capable of detecting growth of all strains of a species.

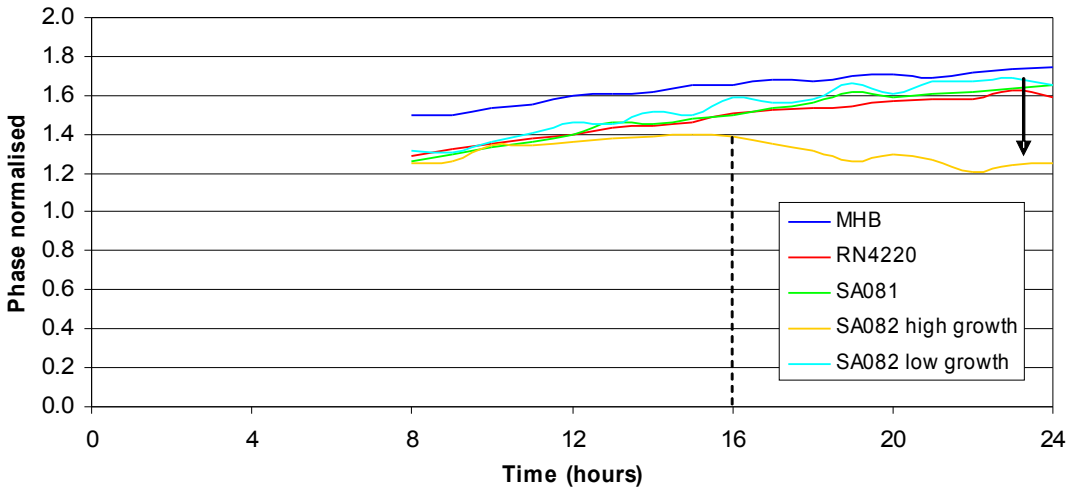

Figure 3-33. Examples of the normalised phase peak over time from the experiment on the influence of impedance measurements. Dotted black line indicates point of change and black arrow indicates the difference between high and low cell densities.

3.6.4 Equivalent circuits – Influence of impedance measurements

The equivalent circuit modelling on the data from the experiments on the influence of impedance measurements was performed as for the parallel suspension experiments (Section 3.5.4). The changes with a high level of growth in the resistor and capacitor representing the interface were observed again as illustrated in Figure 3-34. The R_{dl1} component decreases rapidly in the first 3 hours (average of 3,700Ω) as it stabilises to the conditions and then is stable for the remaining hours in the media only or the vials with low growth levels. When high levels of growth occur the resistance decreases further and in the example shown occurs after 12 hours. This decrease is related to the decrease in the phase peak seen in the phase profiles.

The C_{dl1} component increases over time for media only and vials with low final cell densities. The average is $3.1x10^{-5}$ F. In the vials with high levels of growth the capacitance reduces the rate of increase and then decreases towards the end of the experiment. The capacitance changes are related to the smaller shift in frequency of the phase peaks seen in the phase profiles of high cell densities. This appears to validate the circuit model for multiple strains of *Staphylococcus aureus* which like the signature traces is important in that it is independent of the strain. This confirms that the comparison of circuit model components over time could be used to discern between the absence and/or growth of bacteria.

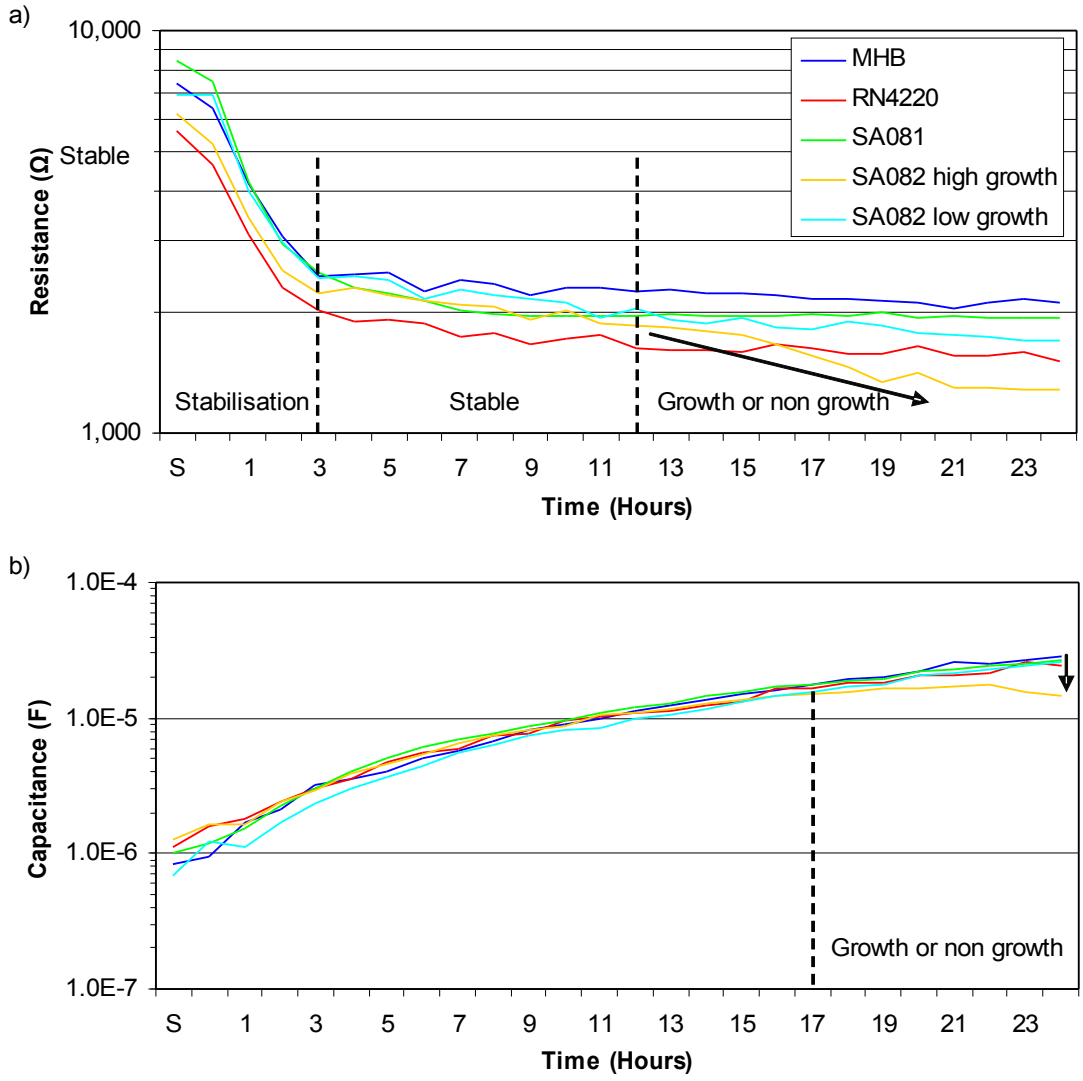

Figure 3-34. Examples of the equivalent circuit components over time for the experiment on the influence of impedance measurements: a) R_{dl1} component; b) C_{dl1} component. Black arrows indicate the changes due to high levels of growth.

3.7 Summary of results – Suspensions

Two screen printable electrode materials, Ag-AgCl and carbon were chosen for the impedance studies of bacterial growth based on their impedance behaviour and effect on normal bacterial growth. The Ag-AgCl sensors had discernible differences in their impedance profiles over frequency to distinguish the absence and/or presence of bacteria when grown from a high starting cell density, particularly in the phase angle. Additional differences occurred in the impedance magnitude over frequency profile with the bacterial cultures grown in the presence of glucose in the media. The carbon sensors appeared to have little effect on the growth behaviour of bacteria and the electrodes used in the suspension experiments were unstable over time and therefore it was difficult to determine whether growth of bacteria caused distinguishable differences.

When the starting cell density were lowered, the Ag-AgCl sensors had a variable inhibiting effect on the normal growth rate of the *Staphylococcus aureus* strain, most likely due to the release of silver ions into the media. This effect can be reduced by washing the sensors for 24 hours prior to inoculation and unfortunately appears to worsen when impedance measurements are performed once an hour. Despite the normal growth rate being disrupted once the cell densities had reached cell densities in excess of $5x10^7$ CFU ml^{-1} the discernible differences indicating the presence of bacteria appeared in all three *Staphylococcus aureus* strains. The equivalent circuit modelling of the cultures with Ag-AgCl sensors showed that discernible differences in the component values over time occur once the cell densities reach approximately $5x10^7$ CFU ml^{-1} and also provide additional information on the physical processes occurring within the cultures. The implications of these results are discussed in Chapter 5.

4 Results – Biofilms

In the environment bacteria grow in biofilms and there is increasing evidence that biofilms also occur in wounds. If the bacteria in the wounds were to grow a biofilm on the electrodes at the surface of the wound then the impedance profile should change because there would be an electrode-biofilm interface instead of an electrode-fluid interface. Therefore the final experimental phase investigated the growth of biofilms on screen-printed sensors and their corresponding impedance measurements.

Two materials for the sensor electrodes were selected for the biofilm experiments, Ag-AgCl and carbon. The Ag-AgCl sensors were chosen for their low impedance profiles and their impedance change in response to high cell densities of bacteria in suspension, as presented in Chapter 3. It was hypothesised, based on the variable growth of bacteria with Ag-AgCl in the suspension experiments, that the bacteria would detect the inhibiting substances and prefer to grow elsewhere from the Ag-AgCl electrode surfaces. Therefore carbon was chosen as an alternative electrode material since it had less inhibition of the bacteria in the suspension experiments of Chapter 3. One aspect of carbon as an electrode material is that it displays higher impedance than Ag-AgCl in conducting solutions and this in turn can reduce the sensitivity of impedance measurements to bacterial effects. Thus electrochemical preconditioning of the carbon sensors was investigated to discover whether their relative high impedance could be reduced.

Firstly this chapter details the results from the preconditioning of the carbon sensors and secondly the growth of biofilms on screen-printed sensors with and without impedance measurements. The biofilms were analysed with an alamarBlue® assay to provide a semi-quantitative result and by confocal laser scanning microscopy with a LIVE/DEAD® *Bac*Light™ florescence dye to image the actual biofilms. The impedance data was examined for discernible differences between the control system and the bacterial cultures.

4.1 Carbon electrode preconditioning

The carbon sensors had a relative high impedance profile in the suspension experiments of Chapter 3. Several electrochemical preconditioning procedures were investigated that modified the surface of the electrodes. The intention was that such a preconditioning would facilitate better electron transfer at the surface of the carbon and hence a lower impedance. In turn this should increase the sensitivity of the impedance measurements to bacterial effects.

The polyethylene substrate, PE300, that the electrodes were normally printed on was reserved for the experiments with bacteria because it was in short supply and had better growth behaviour in the suspension experiments (Section 3.1.3). Thus the carbon sensors were initially screen printed on to acetate. Two types of carbon sensors, pure carbon and carbon tipped (formed by printing carbon on to the tips of silver electrode tracks) as shown in Figure 4-1 were printed and prepared as described in Section 2.2.1.

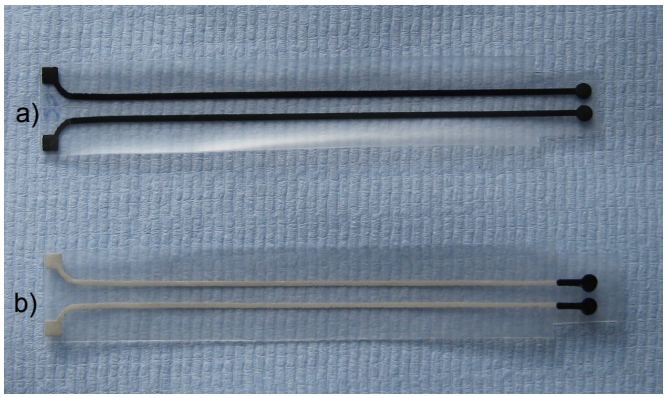

Figure 4-1. The screen-printed sensors used in the carbon preconditioning experiments:
a) Carbon on PE300 (C-PE300); b) Carbon tipped on PE300 (C-tip-PE300).

4.1.1 Preconditioning with cyclic voltammetry

The carbon sensors on acetate, C-acetate and C-tip-acetate, were investigated with an electrochemical preconditioning procedure based on cyclic voltammetry as described in Section 2.7.1. To recap a typical cyclic voltammetry cycle of potential against time was applied to the sensors in a solution of 1M of potassium chloride (KCl) and Figure 2-12 shows the circuit arrangement for this voltage conditioning phase. The parameters varied in the preconditioning procedure were the time the cyclic voltammetry was applied for (10, 20 and 30 minutes) and the voltage range (2.5, 5.0 and 7.5 volts).

The Bode plots for the preconditioning of C-acetate and C-tip-acetate sensors with the time parameter varied are illustrated in Figures 4-2 and 4-3. The greater improvement in the interface impedance of the C-tip-acetate over the C-acetate sensors can be seen clearly. Also of interest, with the preconditioning of C-tip-acetate sensors was the observed increase in impedance magnitude, where at 100kHz the average increase was 1083Ω with an applied voltage cycle of ±2.5V for 20 minutes. The most likely cause was that the preconditioning procedure was decreasing the depth of the carbon layer and increasing its track resistance. This increased track resistance actually causes the interface impedance to increase in the high frequency region and is therefore detrimental to the objective of lowering the impedance of the electrodes.

The average values of the maximum impedance magnitude and phase before and after preconditioning for each type of sensor are listed in Tables 4-1 and 4-2. For the C-acetate sensors the largest decrease in impedance magnitude observed, $1.3 \times 10^7\ \Omega$, and in phase, 22.1^o, occurs with an applied voltage cycle of ±7.5V for 20 minutes. Whereas the actual lowest impedance magnitude occurs with an applied voltage cycle of ±5V cycle for 20 minutes. For the C-tip-acetate sensors, based on carbon over silver, the largest decrease in magnitude, $1.2 \times 10^7\ \Omega$, and phase, 42.3^o, occurs with a voltage cycle of ±5V for 20 minutes. The C-tipped sensor's phase angle

reduction was nearly twice that of the pure carbon sensors. Increasing the conditioning times beyond 20 minutes for both sensor types had an adverse effect on the impedance.

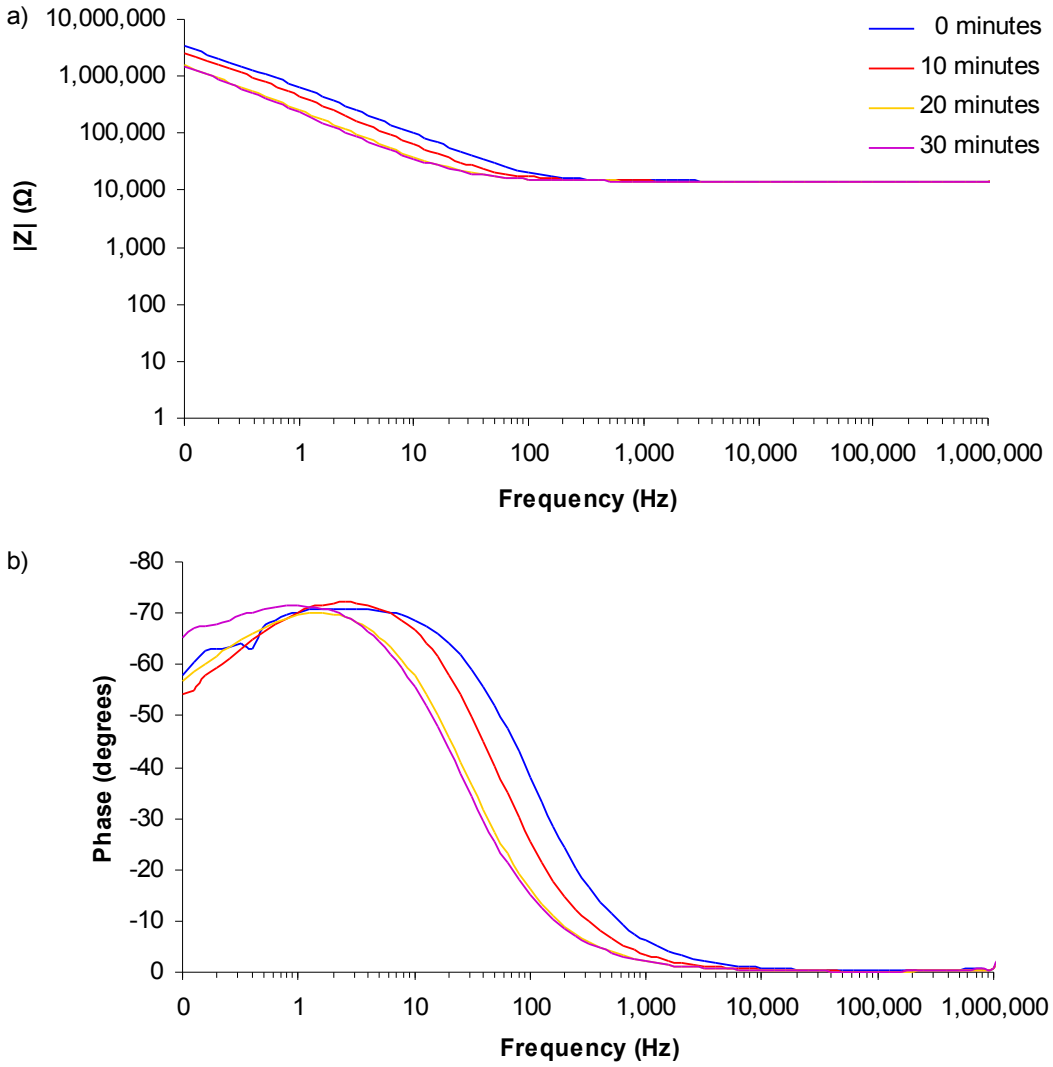

Figure 4-2. The Bode plots for preconditioning of C-acetate sensors with the time parameter varied: a) Magnitude plot; b) Phase angle plot.

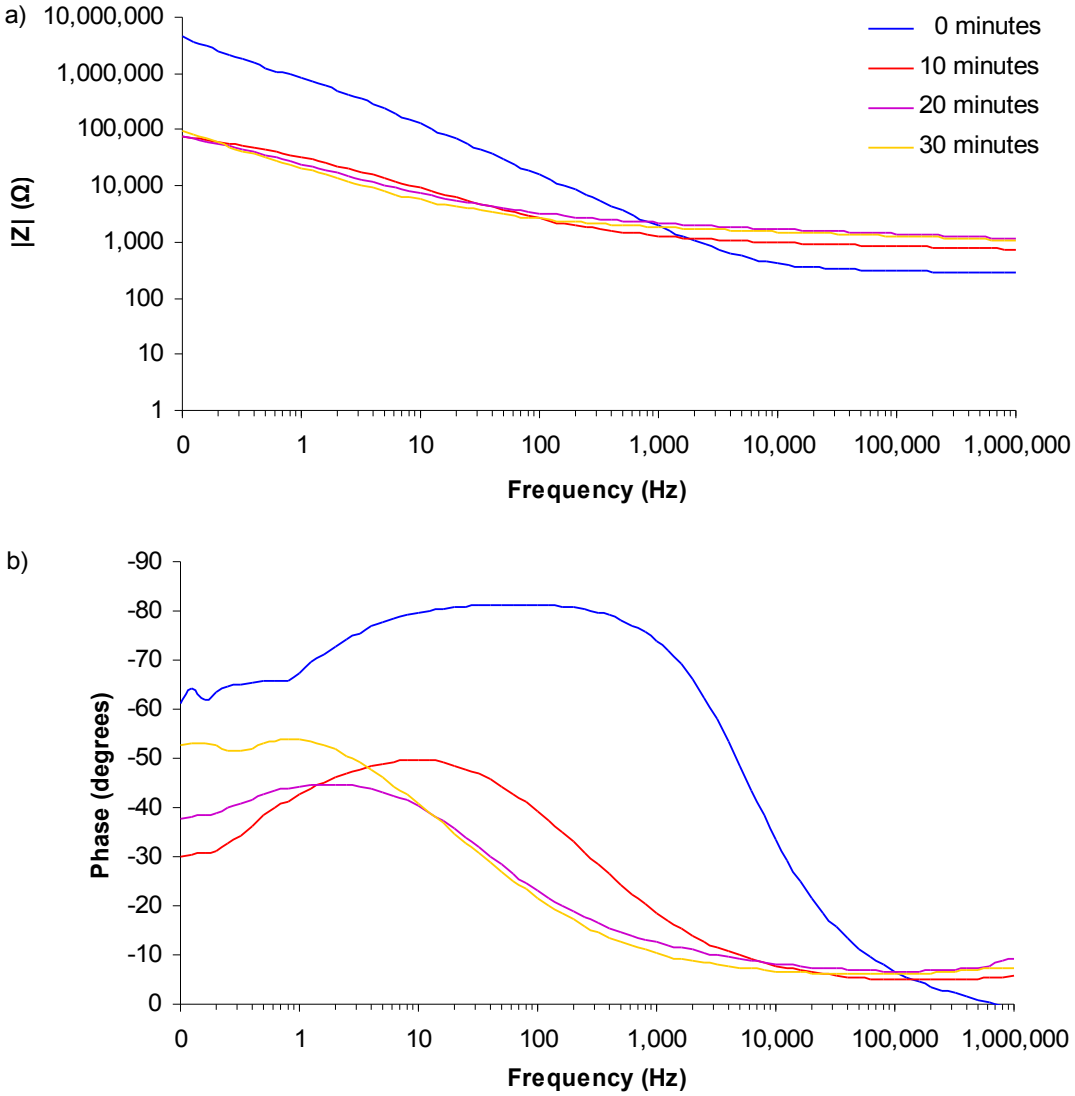

Figure 4-3. The Bode plots for preconditioning of C-tip-acetate sensors with the time parameter varied: a) Magnitude plot; b) Phase angle plot.

Table 4-1. The average maximum impedance magnitude and minimum phase angle before and after preconditioning of C-acetate sensors. Standard deviations are shown in brackets.

Voltage (V)	Time (minutes)			
	0	10	20	30
Average maximum impedance magnitude (Ω) at 0.1Hz				
2.5	$3.4x10^6$ (± $1.6x10^6$)	$2.6x10^6$ (± $3.8x10^5$)	$1.6x10^6$ (± $1.2x10^5$)	$1.5x10^6$ (± $6.3x10^5$)
5	$1.2x10^7$ (± $8.3x10^5$)		$8.4x10^5$ (± $4.0x10^4$)	
7.5	$1.5x10^7$ (± $3.2x10^6$)		$1.2x10^6$ (± $1.3x10^6$)	
Average minimum phase angle (degrees)				
2.5	-74.8 (± 2.5)	-73.5 (± 1.8)	-70.2 (± 1.5)	-71.8 (± 3.8)
5	-81.8 (± 0.4)		-63.4 (± 0.5)	
7.5	-84.8 (± 1.9)		-62.7 (± 7.3)	
Average frequency of minimum phase angle (Hz)				
2.5	2.0	2.5	1.6	1.0
5	1.6		0.6	
7.5	1.6		1.3	

Table 4-2. The average maximum impedance magnitude and minimum phase angle before and after preconditioning of C-tip-acetate sensors. Standard deviations are shown in brackets.

Voltage (V)	Time (minutes)			
	0	10	20	30
Average maximum impedance magnitude (Ω) at 0.1Hz				
2.5	$4.6x10^6$ (± $2.1x10^6$)	$8.5x10^4$ (± $4.8x10^4$)	$7.7x10^4$ (± $3.6x10^4$)	$9.8x10^4$ (± $2.2x10^4$)
5	$1.2x10^7$ (± $9.6x10^6$)		$4.1x10^4$ (± $1.8x10^3$)	
7.5	$8.7x10^6$ (± $6.9x10^5$)		$1.9x10^5$ (± $1.9x10^5$)	
Average minimum phase angle (degrees)				
2.5	-81.6 (± 0.9)	-56.3 (± 6.5)	-46.8 (± 9.1)	-60.4 (± 0.8)
5	-80.4 (± 1.8)		-38.1 (± 5.9)	
7.5	-79.3 (± 0.8)		-62.7 (± 8.4)	
Average frequency of minimum phase angle (Hz)				
2.5	63.1	10.0	1.6	1.0
5	251.0		0.1	
7.5	251.0		1.26	

Based on the results of the preconditioning with cyclic voltammetry the carbon tipped sensors were initially selected for the biofilm growth experiments due to their lower impedance post conditioning. The C-tip-acetate sensors were manufactured with the silver track underneath the exposed carbon tip. To reduce the risk of the silver contacting the liquid it was decided to decrease the length of the silver track to ensure it was underneath the insulator layer of the sensors. The carbon tipped sensors on the polyethylene substrate (C-tip-PE300) were manufactured with this small modification which meant that the length of the carbon track between the carbon tip and the silver track was increased. The carbon track resistance defines the impedance magnitude at approximately 100kHz and hence a longer carbon track produces a higher impedance before conditioning. In turn this means the post conditioning impedance was also higher.

In addition to the small modification to the silver track length, the current manufacturing method for screen-printing the carbon tipped electrode on the polyethylene material, PE300 was unable to accurately reproduce the sensors. Multiple pairs of silver tracks are screen-printed on to a single PE300 sheet and then oven cured which causes the PE300 sheet to shrink across its width. Thus the silver tracks are closer together and each pair had to be lined up by hand to print the carbon tips. This caused variations in the length of the carbon track and therefore variations in the impedance before and after the preconditioning procedure. The variations between six C-tip-PE300 sensors after preconditioning are illustrated in Figure 4-4. The impedance at 0.1Hz varies between 67.2kΩ and 1.4MΩ, and the phase angle peak occurs between 0.1 and 79Hz with values between -10.4 and -35.5^{o}. This was deemed to be an unacceptable variation and investigations with carbon tipped sensors was discontinued.

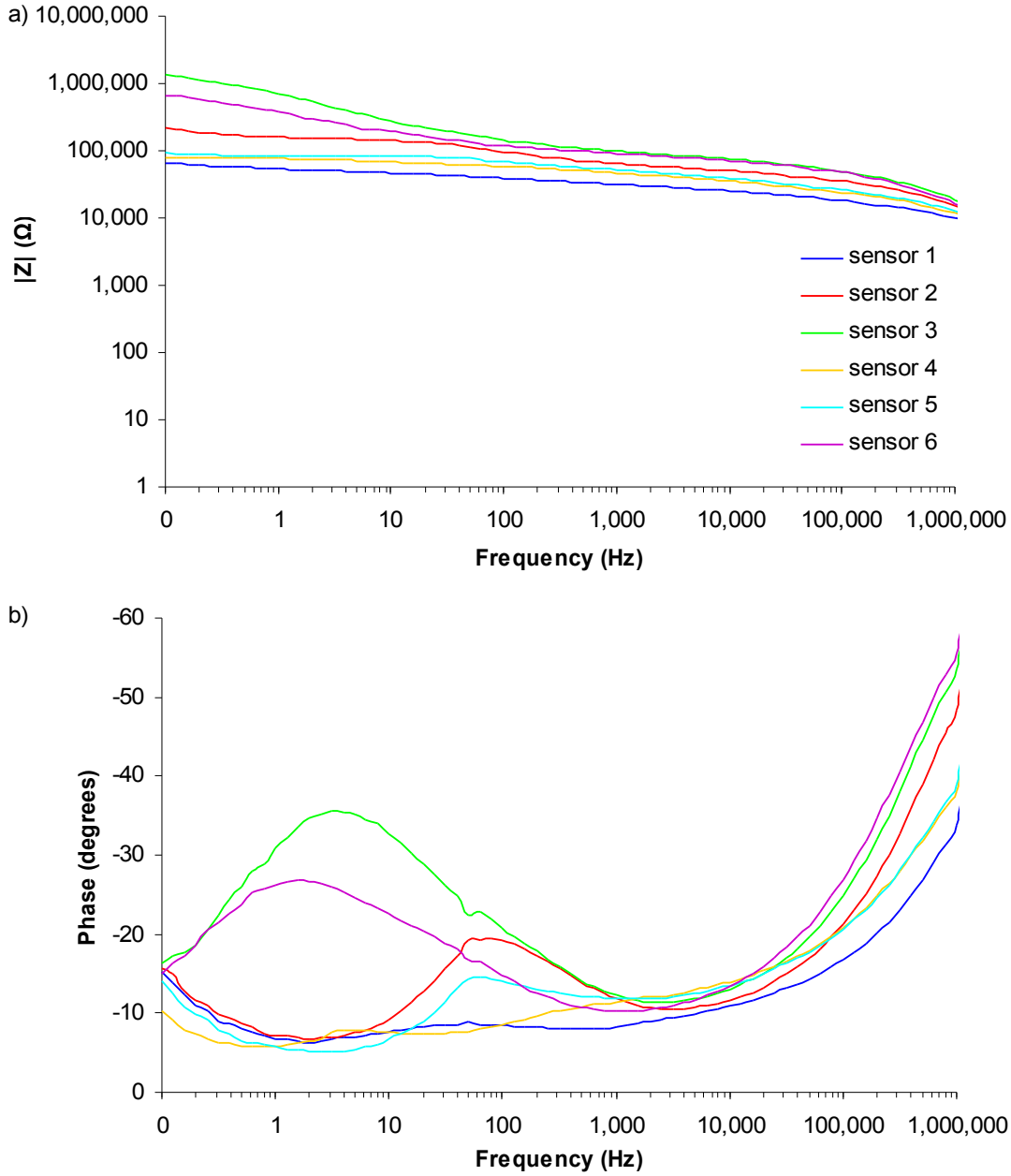

Figure 4-4. The Bode plots for the six C-tip-PE300 sensors post conditioning: a) Magnitude plot; b) Phase angle plot.

4.1.2 Preconditioning with a square-wave

To create reproducible sensors that would have more repeatable impedance characteristics, preconditioning of pure carbon printed sensors was further investigated. A simpler preconditioning procedure was selected for trial to ease any future manufacturing protocols. Only the two electrodes of the sensor itself were required, whereas before a three electrode conditioning system was employed (Figure 2.12) and this new method would also allow multiple sensors to be preconditioned in parallel. The highest voltage value of the cyclic voltammetry appeared to be the significant element in preconditioning the carbon sensors. Therefore a square-wave conditioning pattern was selected for application to the sensors in solution since the voltage during conditioning would always be near its maximum, unlike the cyclic voltammetry.

A square-wave that alternates between plus and minus the amplitude, has a period, P was applied for a time, t, to the C-acetate sensors in potassium chloride (KCl) as shown in Figure 2.13. The time was varied between 10 and 50 minutes at an amplitude of 10 volts and period 120 seconds. The period was varied between 5 and 300 seconds at an amplitude of 10 volts for 20 minutes. Finally the amplitude was varied between 5 and 12.5 volts with s period 120 seconds for 20 minutes. Each combination was performed on three sensors.

The Bode plots for the carbon preconditioning in KCl with a voltage of 10V, period 120s and the time parameter varied are illustrated in Figure 4-5. The length of time the preconditioning is applied for increases the magnitude and decreases the phase angle and stabilises after 40 to 50 minutes. At frequencies below 1Hz the phase angle was lowest between 10 to 20 minutes.

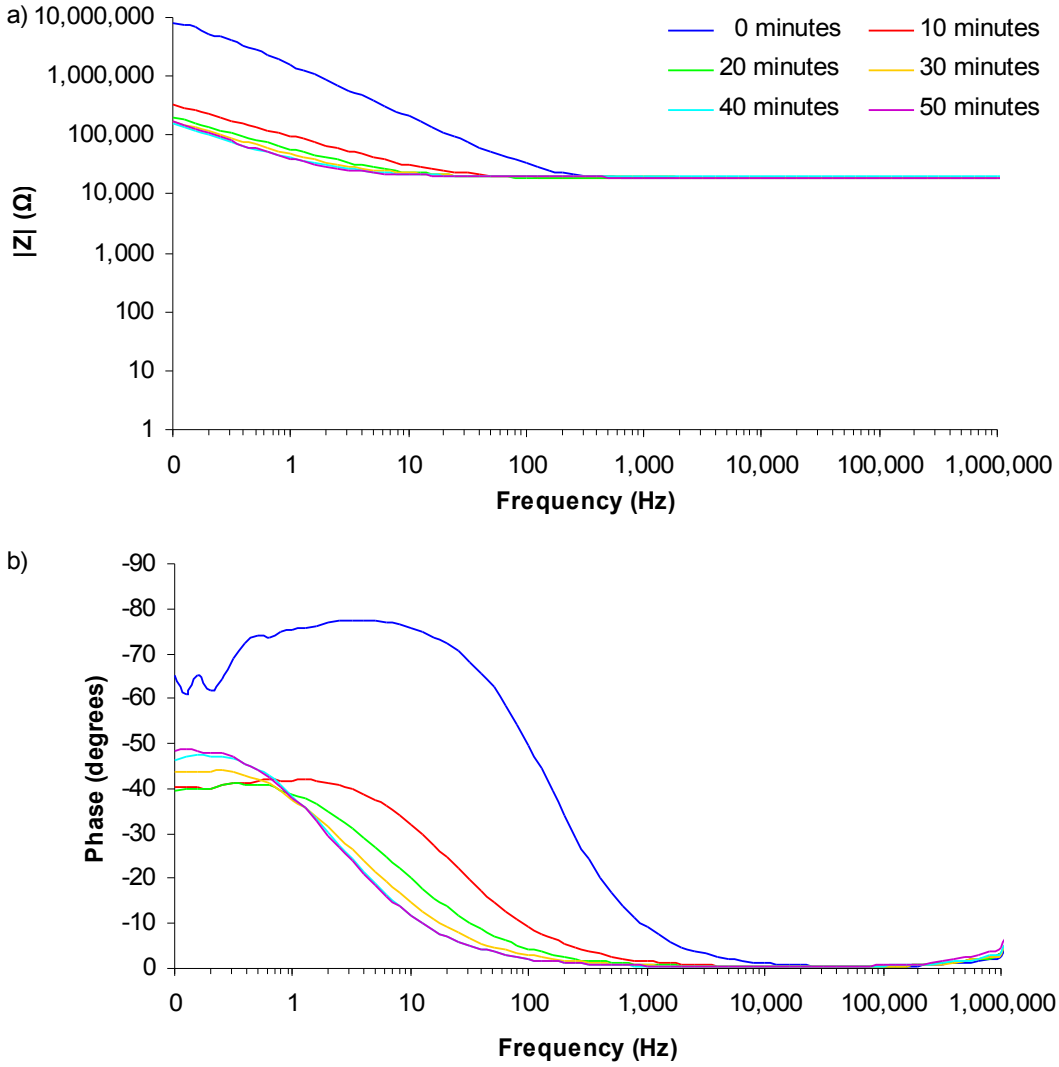

Figure 4-5. The Bode plots for preconditioning of C-acetate sensors with the time parameter varied: a) Magnitude plot; b) Phase angle plot.

The average values of the maximum impedance magnitude and minimum phase angle before and after preconditioning are listed in Table 4-3. Observations of the data are that the optimum amplitude to apply was 10V as this reduced the impedance magnitude into the 10^4 Ω range while the other voltages only reached the 10^5 Ω range. The 10V wave also produced the lowest phase angle, 19.9° or 6.8° lower than the 5V and 12.5V waves respectively. The optimum period was 120s for the impedance magnitude or 300s for the phase angle. The standard deviation for the phase at 300s is 6.8° compared with 1.9° for 120s, therefore 120s appeared to produce a tighter range of impedance changes. The time of application of the wave which produced the lowest magnitude was 30 minutes compared with 10 to 20 minutes for the phase angle.

The optimum preconditioning parameters were a square-wave with an amplitude of 10V, a period of 120 seconds and either a time of 20 or 30 minutes. It was decided to select the shortest time to ease preparation of the electrodes because it was unknown whether the impedance magnitude or phase angle should be prioritised. Therefore the preconditioning parameters chosen was a square wave with a period of 120s, an amplitude of 10V and applied for 20 minutes producing sensors with impedance magnitudes in the range of 2.0×10^4 Ω and phase angles in the region of -43°.

The conversion of the carbon sensors from the acetate on to the polyethylene substrate (C-PE300) presented another issue with the screen-printed electrodes. The track resistance of the electrodes on the polyethylene was ten time larger than on the acetate. The C-acetate electrodes track resistances were in the region of 10kΩ while those of C-PE300 were in the region of 100kΩ. This meant that due to the higher starting impedance, the impedance characteristic after preconditioning was poor, even when compared with the C-acetate sensors before preconditioning. This led to the development of carbon sensors with a thicker track depth (C-PE300-v2) by performing multiple screen-prints. These carbon sensors had resistances similar to the carbon on acetate sensors.

Table 4-3. The average maximum impedance magnitude and minimum phase before and after preconditioning of C-acetate sensors in KCl. Standard deviations are shown in brackets.

Period(s)	Voltage (V)	Time (minutes) 0	10	20	30	40	40
Average maximum impedance magnitude (Ω) at 0.1Hz							
120	5	$1.0x10^{7}$ ($\pm 1.3x10^{6}$)		$6.4x10^{5}$ ($\pm 4.1x10^{4}$)			
120	10	$8.3x10^{6}$ ($\pm 2.1x10^{6}$)	$3.4x10^{4}$ ($\pm 4.8x10^{4}$)	$2.0x10^{4}$ ($\pm 3.6x10^{4}$)	$1.8x10^{4}$ ($\pm 2.2x10^{4}$)	$1.5x10^{5}$ ($\pm 3.6x10^{4}$)	$1.7x10^{5}$ ($\pm 1.3x10^{5}$)
120	12.5	$7.8x10^{6}$ ($\pm 2.6x10^{6}$)		$3.3x10^{5}$ ($\pm 1.5x10^{5}$)			
10	10	$1.0x10^{7}$ (σ,$3.8x10^{6}$)		$2.8x10^{5}$ (σ,$2.1x10^{5}$)			
40	10	$9.0x10^{6}$ (σ,$8.2x10^{5}$)		$2.8x10^{5}$ (σ,$6.6x10^{3}$)			
300	10	$8.9x10^{6}$ (σ,$5.3x10^{6}$)		$3.2x10^{5}$ (σ,$1.3x10^{5}$)			
Average minimum phase angle (degrees)							
120	5	-76.7 (± 2.8)		-63.1 (± 5.9)			
120	10	-78.6 (± 2.3)	-43.2 (± 6.3)	-43.2 (± 1.9)	-45.1 (± 5.6)	-47.7 (± 3.0)	-48.7 (± 13.8)
120	12.5	-74.7 (± 2.2)		-50.0 (± 13.9)			
10	10	-79.0 (± 3.1)		-59.2 (± 1.2)			
40	10	-74.8 (± 2.80		-60.1 (± 4.8)			
300	10	-75.6 (± 2.6)		-41.5 (± 6.8)			
Average frequency of minimum phase angle (Hz)							
120	5	3.2		0.6			
120	10	3.2	0.6	0.3	0.1	0.1	0.1
120	12.5	1.6		0.3			
10	10	1.3		0.1			
40	10	1.0		0.1			
300	10	3.2		0.8			

4.1.3 Preconditioning of the final carbon sensors

A final preconditioning experiment was performed with the C-acetate sensors and the C-PE300-v2 sensors to investigate whether conditioning in the bacterial growth medium, Mueller-Hinton broth (MHB) would increase the effectiveness of the preconditioning over the KCl. The intention was that if molecules within the MHB adhered to the surface of the carbon electrodes during the preconditioning then these molecules would facilitate a better electron transfer when in the MHB of the impedance experiments. The average values of the maximum impedance and minimum phase angle are listed in Table 4-4 and the Bode plots are illustrated in Figure 4-6. Comparing the C-acetate and C-PE300-v2 sensors in KCl indicates a comparable magnitude decrease, $9.8x10^6$ Ω and $1.2x10^7$ Ω, however the phase angle decreased 32.8° compared with 14.5°. The C-PE300-v2 sensors in MHB had a more improved impedance after conditioning with a decrease in magnitude of $2.5x10^6$ Ω and in phase angle of 27.5° which suggests that the media does enhance the effectiveness of the preconditioning as expected. Therefore all the pure carbon sensors for the biofilm experiments were conditioned in MHB.

Table 4-4. The average maximum impedance magnitude and minimum phase angle before and after preconditioning of carbon sensors with different media. Standard deviations are shown in brackets.

Electrode	Media	Before	After
Average impedance magnitude at 0.1Hz (Ω)			
C-acetate	KCl	$1.00x10^7$ (± $1.6x10^6$)	$2.3x10^5$ (± $5.9x10^4$)
C-acetate	MHB	$1.2x10^7$ (± $8.7x10^5$)	$1.2x10^5$ (± $9.1x10^3$)
C-PE300-v2	KCl	$1.3x10^7$ (± $1.6x10^6$)	$8.0x10^5$ (± $7.9x10^4$)
C-PE300-v2	MHB	$2.6x10^7$ (± $2.8x10^6$)	$1.6x10^5$ (± $1.5x10^4$)
Average minimum phase angle (degrees)			
C-acetate	KCl	-80.4 (± 1.5)	-47.6 (± 4.0)
C-acetate	MHB	-81.1 (± 1.2)	-55.6 (± 0.8)
C-PE300-v2	KCl	-77.2 (± 1.2)	-62.7 (± 0.5)
C-PE300-v2	MHB	-78.9 (± 1.1)	-51.4 (± 2.5)
Frequency of minimum phase angle (Hz)			
C-acetate	KCl	1.6	0.13
C-acetate	MHB	2.0	0.1
C-PE300-v2	KCl	2.5	0.50
C-PE300-v2	MHB	7.9	0.1

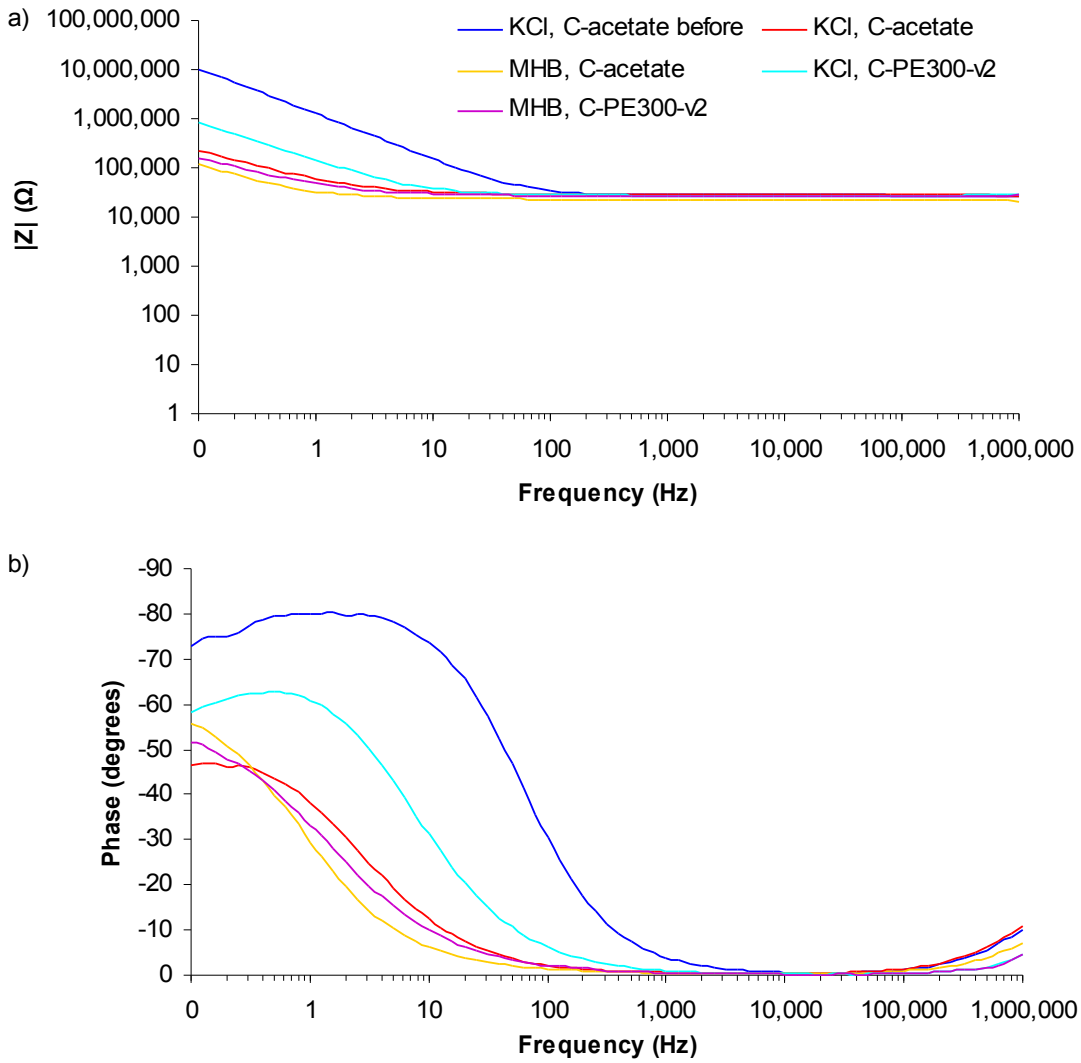

Figure 4-6. The Bode plots for preconditioning of C-acetate and C-PE300-v2 sensors with the media varied: a) Magnitude plot; b) Phase angle plot.

To examine the effects of preconditioning on the carbon surface the electrodes were imaged with a scanning electron microscope (SEM). An example of the surface of the carbon electrode tips before and after preconditioning are illustrated in Figure 4-7. The micrographs before preconditioning show a honeycomb pattern whereas the preconditioning procedure removes this structure to leave a more uniform surface with a smaller scale roughness. The honeycomb pattern is most likely to be an imprint of the mesh within the mask of the electrode outlines used in the screen-printing procedure.

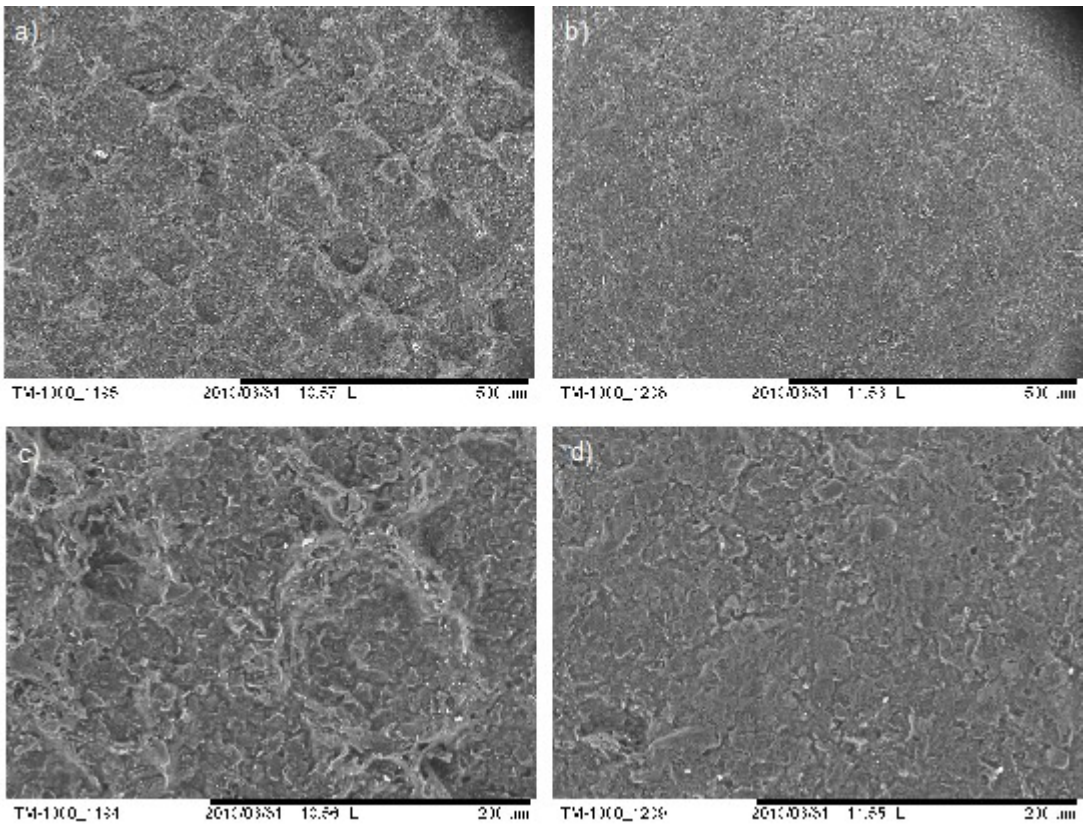

Figure 4-7. SEM micrograph examples of preconditioning on the carbon surface of C-PE300-v2 sensors: a) Before preconditioning, x180**;** b) After preconditioning, x180; c) Before preconditioning, x500; d) After preconditioning, x500. The scale bar for x180 indicates 500µm and for x500 indicates 200µm. The preconditioning procedure was a square-wave with an amplitude 10V, a period of 120s and a time of 20 minutes in MHB.

To analyse the impedance changes due to the preconditioning the data from the C-PE300-v2 sensors in MHB was modelled with an equivalent circuit, illustrated in Figure 4-8. The component R_s represents the resistance of the solution, the R_{dl1} and C_{dl1} represents the double layer at the electrode interface and the CPE_d component represents the diffusional processes between the bulk solution and the electrode interface. The CPE_d has two values, CPE_d-T is a measure of the pseudocapacitance magnitude and the CPE_d-P is a measure of how close to an ideal capacitor the diffusional processes are. The component values before and after preconditioning are listed in Table 4-5. The fit is a measure of how accurate the simulated impedance data from the equivalent circuit is to the actual data.

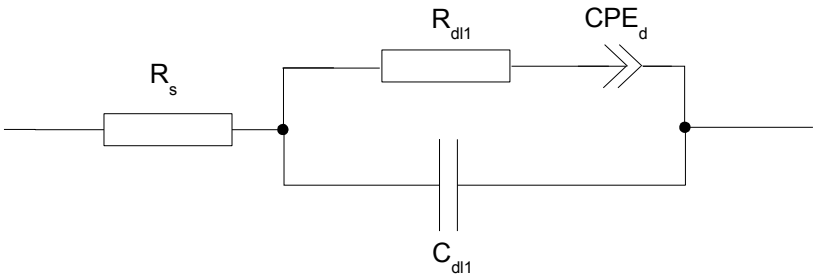

Figure 4-8. The equivalent circuit model for the carbon sensors.

Table 4-5. The mean component values for the equivalent circuit of preconditioned carbon sensors. The numbers in brackets indicate the standard deviation.

Component	Average component value		Average error in component value (%)	
	Before	After	Before	After
Fit	8.07 (± 2.47)	0.39 (± 0.04)		
R_{dl1} (Ω)	$2.4x10^{4}$ (± 473)	$2.7x10^{4}$ (± 310)	1.63 (± 0.29)	0.17 (± 0.01)
C_{dl1} (F)	$3.26x10^{-13}$ ($\pm 3.63x10^{-15}$)	$4.17x10^{-13}$ ($\pm 1.57x10^{-14}$)	85.65 (± 14.90)	7.38 (± 0.37)
CPE_T	$5.07x10^{-8}$ ($\pm 7.14x10^{-9}$)	$9.64x10^{-6}$ ($\pm 8.44x10^{-7}$)	2.60 (± 0.45)	0.39 (± 0.03)
CPE_P	0.88 (± 0.01)	0.69 (± 0.02)	0.61 (± 0.10)	0.28 (± 0.03)

The actual impedance data had stray impedance at high frequencies which masked the true impedance. Therefore in the circuit model the solution resistance was fixed at 220Ω otherwise the generation of the remaining component values was inaccurate because the correct solution resistance could not be determined from the actual impedance data. The preconditioning caused the R_{dl1} value to rise by 3kΩ, the C_{dl1} value to decrease by $9.1x10^{-14}$ F, the CPE_d-T value to increase by $9.6x10^{-6}$ and the CPE_d-P value to fall by 0.19. These changes in component values indicate the preconditioning is increasing the double layer interface represented by R_{dl1} and C_{dl1} while reducing the impedance of the diffusional processes represented by CPE_d. The preconditioning procedure reduces the impedance at low frequencies, however it does not reduce the charge transfer resistance, R_{dl1} and is therefore not facilitating better electron transfer at the surface of the carbon electrode as expected.

4.2 Biofilms

The next aspect of the investigation of the Ag-AgCl and carbon electrodes as impedance sensors for bacterial growth meant exposing the electrode to bacteria in culture and growing for a sufficient time until a biofilm was formed. Three experiments were performed with the first analysing the biofilms with an alamarBlue assay which provides a comparison of relative cell numbers between individual biofilms. The second was to analyse the biofilms on the electrodes with confocal laser scanning microscopy (CLSM). The final stage was to culture the sensors with bacteria growth and perform impedance measurements. The growth of bacteria was confirmed by CLSM and the impedance data analysed to see the influence of biofilms on the impedance characteristics.

A number of surfaces for the growth of biofilm experiments were created, as described in Section 2.8.1. A 13 by 13mm square of the polyethylene substrate, PE300, was created for use as a control surface and contained no electrode materials. For the alamarBlue assay and CLSM without impedance measurements a sensor surface consisting of the exposed tip of the screen printed electrodes on the polyethylene surface, PE300, was cut from the full length electrodes. For the experiments involving impedance experiments the full length sensors were used and then the exposed tip cut off for the CLSM analysis.

The surfaces were cultured with bacteria in petri dishes or 24-well plates for 48 hours as described in Sections 2.8.1 and 2.8.2 and shown in Figure 4-9. For the Ag-AgCl sensor experiments without impedance measurements and analysed with the alamarBlue assay or CLSM three Ag-AgCl-PE300 sensor surfaces and three PE300 control surfaces were grown in 90mm petri dishes with 20ml of MHB. For the impedance experiments each sensor was cultured in a separate 60mm petri dish with 10ml of MHB. The two clinical strains of *Staphylococcus aureus*, SA081 and SA082, were selected as a species commonly isolated from wounds for the Ag-AgCl experiments.

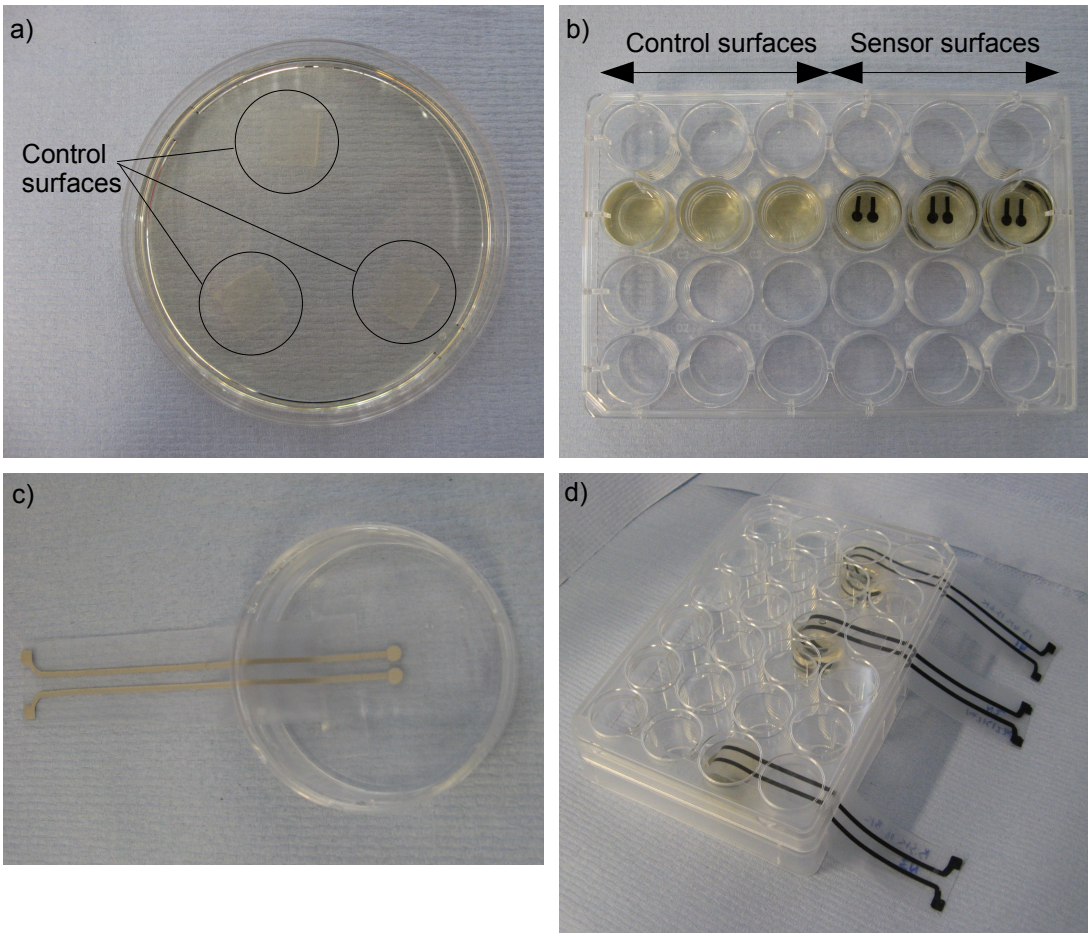

Figure 4-9. The culture dishes for the biofilm experiments: a) Ag-AgCl-PE300 sensor surfaces in petri dishes; b) C-PE300-v2 sensor surfaces in 24-well plate; c) Ag-AgCl-PE300 full length sensors in petri dishes; d) C-PE300-v2 full length sensors in 24-well plate.

For the carbon sensor experiments each C-PE300-v2 sensor surface and PE300 control surface were grown in individual wells with 2ml of MHB within a 24-well plate. The full length carbon sensors with impedance measurements were also grown in 24-well plates. The reason for the change was the risk of liquid tracking along the full length sensors and out of the petri dishes as occurred in Ag-AgCl sensors experiments. In addition to the fluid leakage the intention was that the wells of the 24-well plate would facilitate better growth of bacteria on the sensors by concentrating the cells on the surface and hence produce a more mature biofilm. For the carbon sensor experiments the two *Staphylococcus aureus* strains, SA081 and SA082 plus a third strain of a different species were selected. This was to investigate whether species could be differentiated if the biofilms were detected and the strain was NCTC11964 representative of *Staphylococcus epidermidis*, another species commonly isolated from wounds.

4.3 Biofilms – AlamarBlue assay

It was essential to introduce some control experiments to ensure that bacteria were live and in their normal growth cycle. The formation of biofilms on the sensor surfaces were analysed with an alamarBlue assay to provide additional information to the LIVE/DEAD *Bac*Light staining. The alamarBlue is an indicator dye which incorporates an oxidation-reduction indicator that fluoresces and changes colour in response to the chemical reduction of growth medium, resulting from cell growth (alamarBlue datasheet, 2008). That is growing cells cause a chemical reduction of alamarBlue causing the colour to change from blue to red. Measuring the absorbance of the culture determines the absorbance values for the oxidized and reduced forms of the indicator. The percentage reduction of the alamarBlue indicator is the difference between the absorbance of the control without cell growth and the culture with cell growth and is calculated as described in Section 2.8.3. The higher the number of cells in the culture, the higher the percentage reduction of the alamarBlue. In this study it was used to quantify the relative cell numbers between biofilms formed on individual surfaces.

4.3.1 AlamarBlue assay optimisation

Firstly the alamarBlue assay was calibrated to determine the optimum incubation time for the reduction of the alamarBlue. Bacteria were grown on four control surfaces, that is the PE300 substrate, for 48 hours. The surfaces were washed to remove loose bacteria and then incubated with the alamarBlue solution, as described in Section 2.8.3. The four control surfaces were incubated either for 30, 60, 90 or 120 minutes before the alamarBlue absorbance was measured and the reduction calculated. The calibration was replicated three times for each of the strains of *Staphylococcus aureus*, SA081 and SA082, and *Staphylococcus epidermidis*, NCTC11964.

The alamar blue reduction for the biofilms grown on the square control surfaces for the three strains, SA081, SA082 and NCTC11964 is illustrated in Figure 4-10. The alamarBlue reduction is dependent on the number of cells and the incubation time.

For a fixed number of cells the reduction increases as the incubation time is increased as more indicator dye is reduced by the cells until the alamarBlue is fully reduced. Beyond this time the reduction value does not have a linear correlation with the number of cells. The optimum incubation time is shortly before the alamarBlue is fully reduced to provide the maximum range of reduction values for the range of cell numbers. For the strains SA081 and NCTC11964 the maximum reduction was approaching after 90 to 120 minutes with one or two samples with percentage reductions over 80%. An incubation time of 60 minutes for all strains was chosen to ensure that the samples would not reach the maximum reduction of alamarBlue.

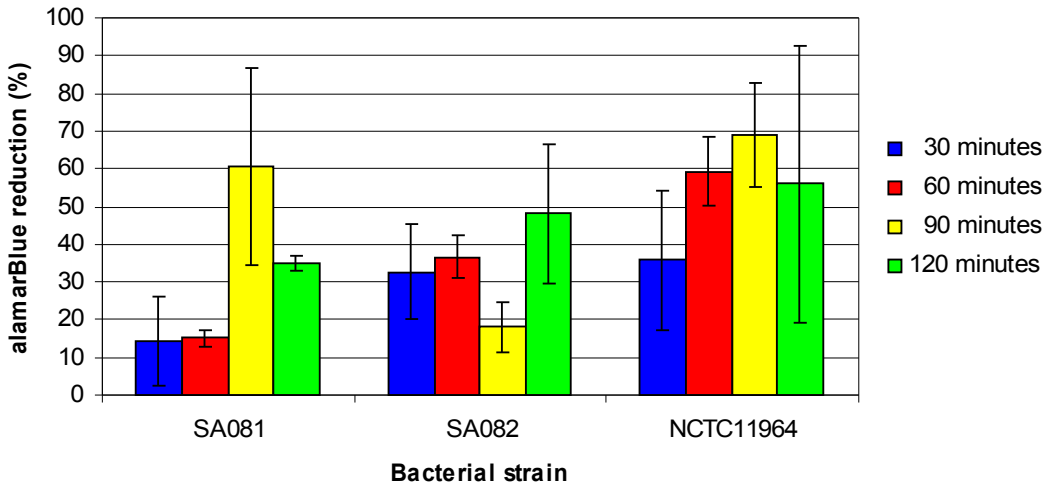

Figure 4-10. Calibration values for alamarBlue reduction of biofilms grown on control surfaces. Errors bars indicate the standard deviation for 3 replicate samples.

The calibration of the alamarBlue assay with these PE300 control surfaces was complicated by the fact that firstly the number of cells on individual surfaces were not fixed and secondly the surface samples for each incubation time were not related. Therefore at a given incubation time there was considerable variation in the three samples with standard deviations ranging between 1.9% and 36.6%. When comparing the incubation times of a single strain because the samples at a given time were not related to the other times, the linearity between incubation time and cell numbers was not always observed. For example, the three samples of SA082 with an incubation time of 90 minutes must all have had less cells, shown by the lower

percentage reduction of 18.1%, compared with the 60 and 120 minute samples with 36.6% and 48.2% reduction respectively. Therefore the alamarBlue assay should be used with caution when comparing the growth of bacteria between the control surfaces and the sensor surfaces due to the variation on cell numbers between individual surfaces.

4.3.2 AlamarBlue assay and Ag-AgCl sensors

The control surfaces and the Ag-AgCl sensor surfaces, as discussed in Section 4.2 were grown with the biofilm growth without impedance measurement procedure (Section 2.8.1). The percentage reduction values were normalised to the controls by dividing each individual surface reduction by the mean reduction value of the control surfaces. The normalisation shows how the bacterial growth on the electrode surfaces compares with the controls, and allows comparisons between strains where there may be differences in the ability to reduce the alamarBlue indicator dye.

The normalised alamarBlue reduction of biofilms grown on Ag-AgCl sensor surfaces are illustrated in Figure 4-11. The mean values of the normalised alamarBlue reduction indicates that there was a 35% and 39% decrease on the Ag-AgCl sensosr compared with the controls for the strains SA081 and SA082 respectively. The top surface area of the controls were 169mm^2 and the combined surface area of two electrode tips was 14.1mm^2. Therefore if the cells on the sensor surfaces were growing everywhere except on the electrode surface then the decrease in the numbers of cells should be 8.3%. However the alamarBlue reduction values implies that the number of cells on average has been reduced 4 to 5 times this amount which indicates that the Ag-AgCl electrodes are effecting growth on a larger area of the sensor surfaces than the electrode tips. The location of the cells on the surfaces cultured cannot be determined by the alamarBlue assay, where as the confocal laser scanning microscopy (CLSM) results presented in Section 4.4 confirm that there was virtually no cells on the electrode surfaces or in the immediate surrounding areas.

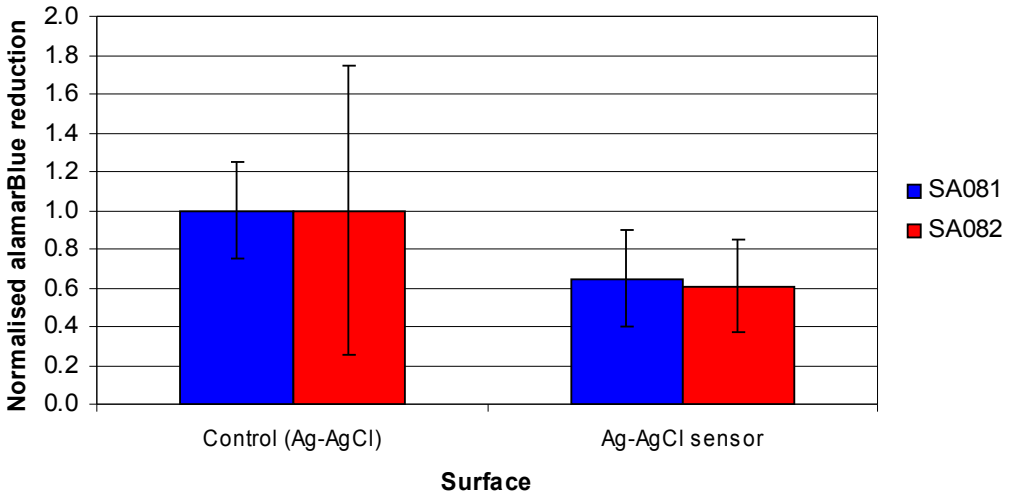

Figure 4-11. Normalised alamarBlue reduction of biofilms grown on Ag-AgCl-PE300 sensor surfaces. Errors bars indicate the standard deviation for 3 replicate samples.

A student's t-test ($\alpha = 0.05$) was performed to show whether there was a significant difference between the sensor surface and the control surfaces. The p-values were 0.08 for SA081 and 0.23 for SA082 which indicates there were no significant differences despite the lower mean normalised reduction values. One of the Ag-AgCl sensor surfaces with SA081 had a normalised reduction of 0.9 compared with 0.5 for the other 2 samples suggesting that either it was poorly washed and contained loose bacteria or there was some dense areas of cells around the edges of the surface. Similarly one of the PE300 control surfaces with SA082 was 0.2 compared with 1.3 and 1.5 for the other 2 samples which indicates a very poor growth on this particular surface. These two outliers in the normalised data cause there to be no significant differences when it was expected there should be given the results of the CLSM.

4.3.3 AlamarBlue assay and carbon sensors

The biofilm growth procedure was modified from petri dishes to 24-well plates for the carbon sensors, as described in Section 4.2. To ensure that this change in procedure did not have an adverse effect on the growth of bacteria the two *Staphylococcus aureus* strains, SA081 and SA082 were cultured in the presence of the PE300 control surface and the C-PE300 sensor with both the petri dish procedure and the 24-well plate procedure, as described in Section 2.8.1. The biofilm growth was then analysed with the alamarBlue assay, as described in Section 2.8.4. The normalised alamarBlue reduction of biofilms grown on carbon sensor surfaces are illustrated in Figure 4-12. The normalisation was against the PE300 controls in the petri dishes to compare the difference in the 24-well plates. It is clearly shown that the normalised reduction in the 24-well plates was higher than the petri dishes indicating either there was more cells or the 24-well plate culturing method led to cells that had the ability to reduce the alamarBlue assay at a faster rate compared with those cells grown in the petri dishes.

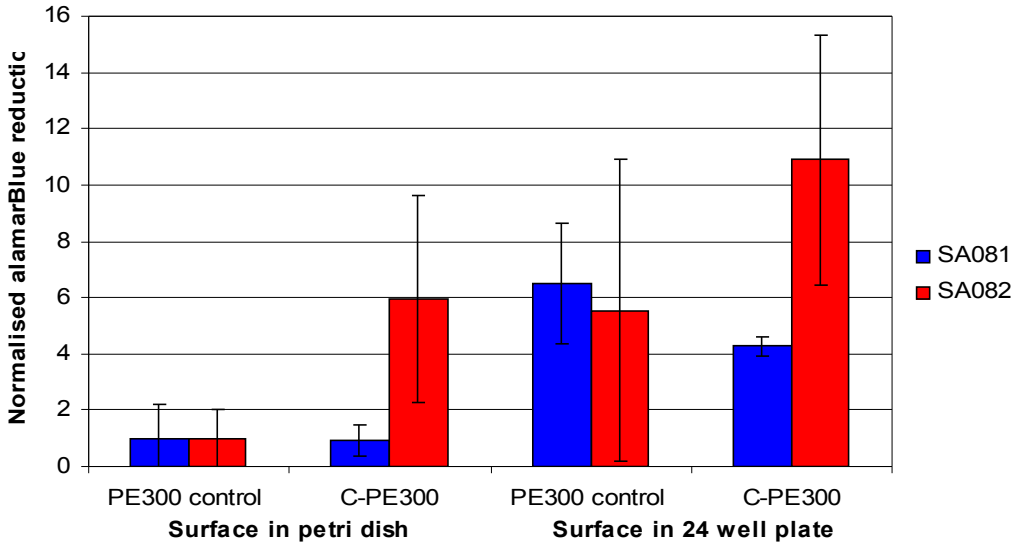

Figure 4-12. Normalised alamarBlue reduction of biofilms grown on carbon sensor surfaces. Errors bars indicate the standard deviation for 3 replicate samples.

The final alamarBlue experiment involved the lower resistance carbon sensors, C-PE300-v2 with all three strains, *Staphylococcus aureus* SA081 and SA082, and *Staphylococcus epidermidis* NCTC11964. The normalised alamarBlue reductions are illustrated in Figure 4-13 and shows that the carbon electrodes do not effect the number of adhered cells for the strain SA081, however the carbon electrodes do appear to reduce the cell numbers of SA082 and NCTC11964. To confirm this a student's t-test ($\alpha = 0.05$) was performed which indicated no significant differences for SA081 (p-value = 0.51) and SA082 (p-value = 0.23). There was a significant difference for NCTC11964 with a p-value of 0.03 suggesting that this strain prefers not to grow on the carbon electrode material.

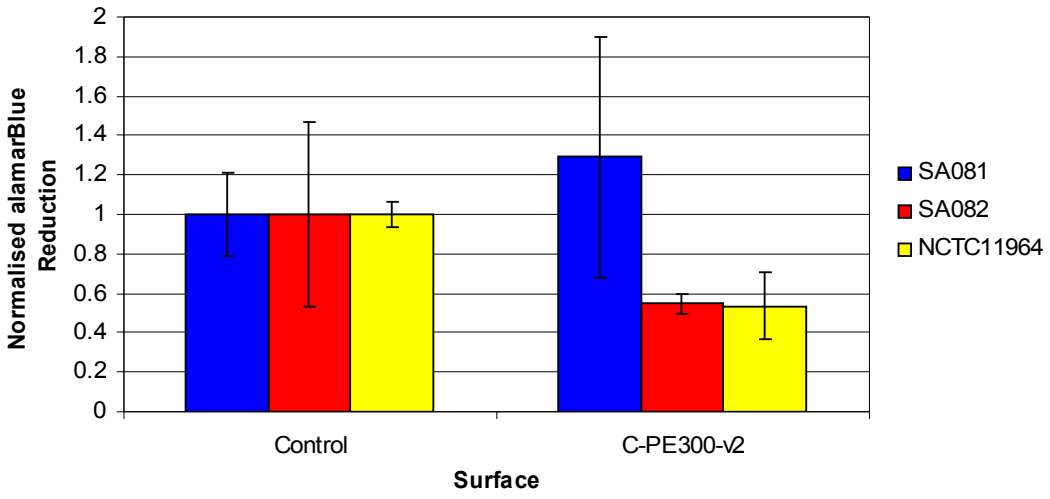

Figure 4-13. Normalised alamarBlue reduction of biofilms grown on the final carbon sensor surfaces. Error bars indicate the standard deviation for 3 replicate samples.

The results from the alamarBlue assay experiments show that the number of cells varies considerably between individual surfaces; the 24-well plate procedure appears to promote more cells to adhere to the surfaces; growth is better on the carbon electrode surfaces compared with the Ag-AgCl electrode surfaces; and the particular strain of *Staphylococcus epidermidis (*NCTC11964) selected appears to adhere less well to the carbon surfaces when compared to the *Staphylococcus aureus* strains.

4.4 Biofilms – Confocal laser scanning microscopy

The next step after the alamarBlue assay which provided a semi-quantitative analysis of the biofilms was to visualise the cells on the surfaces with confocal laser scanning microscopy. The biofilms were stained with a LIVE/DEAD *Bac*Light kit which is a mixture of green-fluorescent nucleic acid stain, SYTO® 9 and the red-fluorescent nucleic acid stain, propidium iodide. The two strains have different spectral characteristics and different abilities to penetrate bacterial cells. Therefore the bacteria with intact membranes stain fluorescent green and those with damaged membrane stain fluorescent red.

There is a great diversity of biofilm structures, as discussed in Section 1.1.3, with the staphylococcal strains expected to form three dimensional biofilms under the correct growth conditions. For example, in ten strains of *Staphylococcus aureus* half of them formed flat and compact structures while the other half had patchy coverage and confluent growth areas (Bridier *et al.*, 2010). The average thickness of these biofilms was 34µm. Some examples of biofilms stained with LIVE/DEAD *Bac*Light dyes are shown in Figure 4-14.

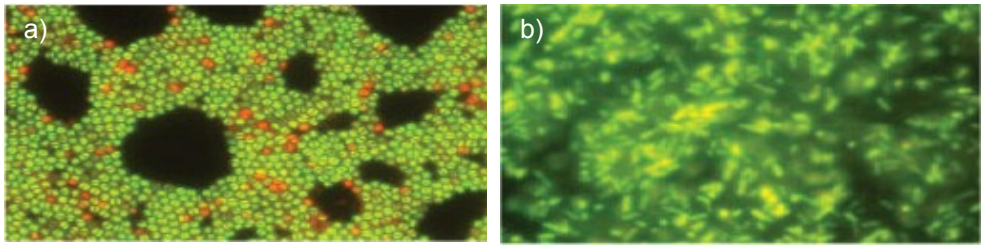

Figure 4-14. Micrograph examples of biofilm growth with LIVE/DEAD *Bac*Light stain. Staining performed after 24 hours of growth. a) A monolayer of *Staphylococcus aureus*; b) Three dimensional biofilm of *Pseudomonas aeruginosa*. (Personal correspondence, 2008).

For each strain, SA081 and SA082 biofilms were grown on three Ag-AgCl sensor surfaces and three control sensors. The number of images for each surface was between 3 and 5 to provide an overview of the biofilm.

4.4.1 Confocal laser scanning microscopy and Ag-AgCl sensors

The control surfaces and the Ag-AgCl sensor surfaces, as discussed in Section 4.2 were grown with the biofilm growth without impedance measurement procedure (Section 2.8.1). Before the surfaces were extracted from the petri dishes there was no visible signs of colonies on the electrode surfaces while there were many colonies equally spaced apart on the base of the petri dishes and on the control surfaces. These colonies were made from loose bacteria and were not adhered to each other or to the petri dish/control surfaces. After the washing stage to remove loose bacteria the surfaces were stained with the LIVE/DEAD *Bac*Light kit and 3 to 5 images of each surface were taken to provide an overview of the biofilm (Section 2.8.5).

The micrograph examples for SA081 grown on the control surface and the Ag-AgCl sensor surfaces without impedance measurements are illustrated in Figure 4-15. The controls of SA081 after 24 hours showed that some areas had a dense coverage while other areas had very few cells. On the surface of the Ag-AgCl electrodes there were very few cells plus there were more dead cells indicated by the red colouring. Between the electrodes tips there was better growth with small areas of closely packed cells.

The micrograph examples for SA082 grown on the control surface and the Ag-AgCl sensor surfaces without impedance measurements are illustrated in Figure 4-16. The growth of SA082 on the controls and Ag-AgCl sensor surfaces after 24 hours were very similar to the SA081 cultures with coverage ranging form dense to scarce on the control surfaces and very few cells on the electrode surfaces. The SA082 strain was then cultured for 48 hours to investigate whether a more mature biofilm could be formed. The controls of SA082 after 48 hours showed more groups of tightly packed cells plus a small number of three dimensional towers while the Ag-AgCl sensor surface still showed very few cells. However there were more very small clusters of cells on the surface of the electrodes.

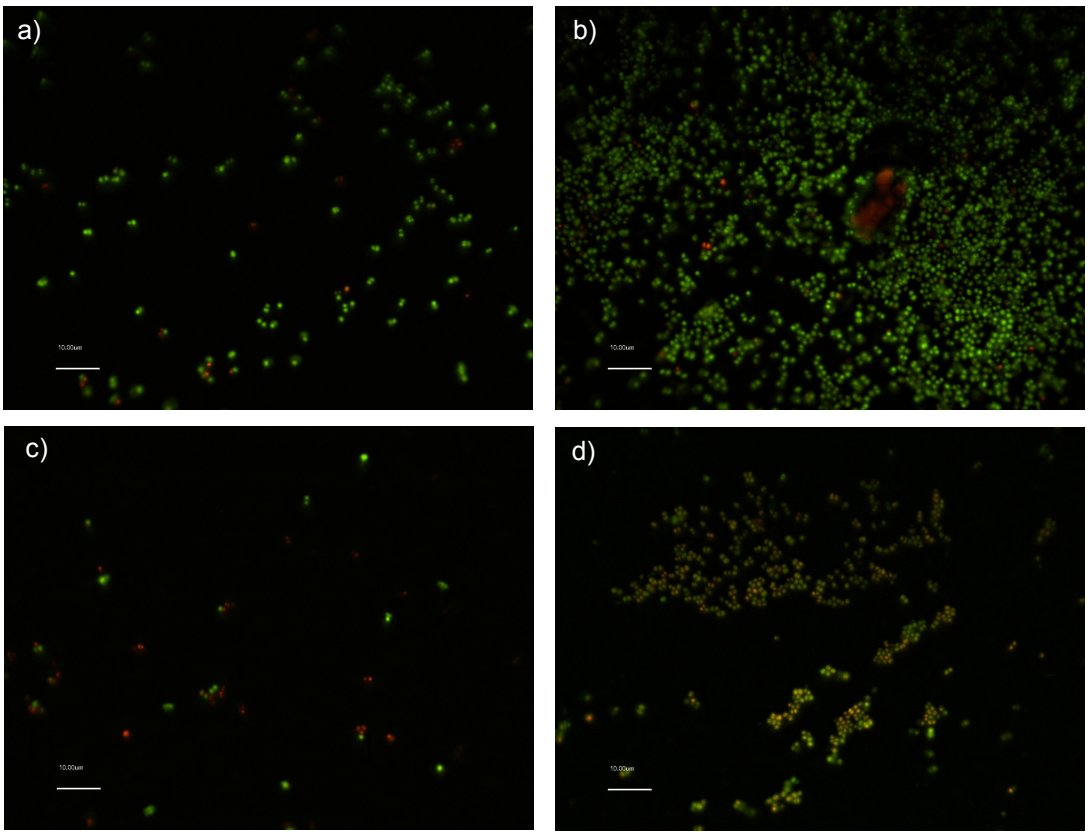

Figure 4-15. Micrograph examples of SA081 biofilm growth on Ag-AgCl-PE300 sensors without impedance measurements and imaged with LIVE/DEAD *Bac*Light stain. Staining performed after 24 hours of growth and scale bars indicate 10μm. a) SA081 control surface; b) SA081 control surface; c) SA081 sensor surface, on actual electrode surface; d) SA081 sensor surface, between electrode tips.

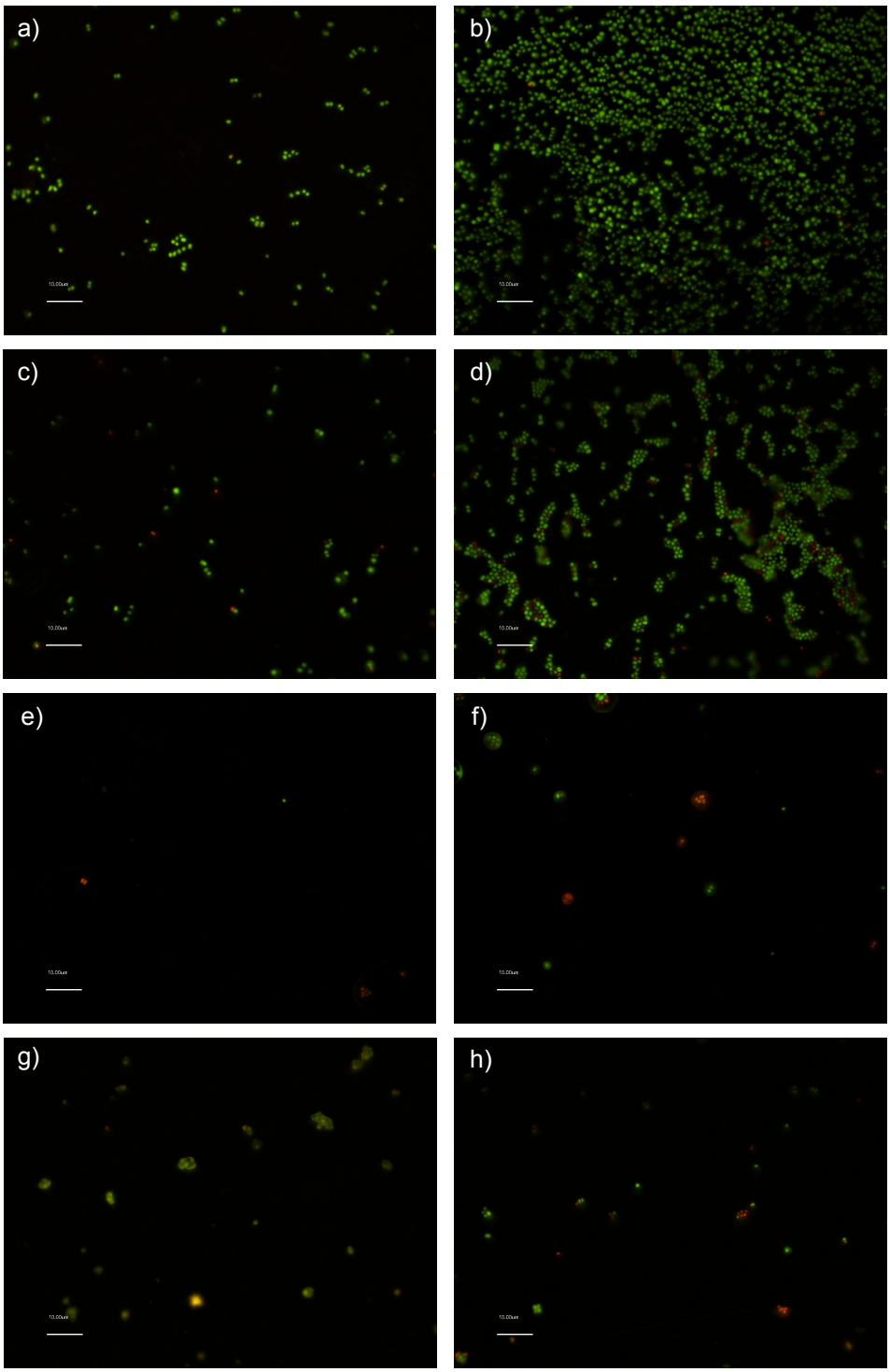

Figure 4-16. Micrograph examples of SA081 biofilm growth on Ag-AgCl-PE300 sensors without impedance measurements and imaged with LIVE/DEAD *Bac*Light stain. Staining performed after 24 or 48 hours and scale bars indicate 10µm. a) & b) SA082 control surface, 24 hours; c) & d) SA082 control surface, 48 hours; e) & f) SA082 sensor surface, on electrode surface, 24 hours; g) & h) SA082 sensor surface, on electrode surface, 48 hours.

The final experimental phase investigated the impedance characteristics of biofilm growth on the electrode surfaces and the impedance data is detailed in Section 4.5. One PE300 control surface and five Ag-AgCl-PE300 sensors were cultured using the biofilm growth with impedance measurement procedure (Section 2.8.2). The biofilms on the electrodes were again analysed with CLSM and the LIVE/DEAD *Bac*Light stain. After the final impedance measurement was performed the electrode tips were cut off to create square surfaces, then stained and imaged as were the surfaces without impedance measurements.

The SA081 micrograph examples of AgAgCl sensors with impedance measurements after 48 hours are illustrated in Figure 4-17. The control surfaces of SA081 showed that growth was very similar to that of the controls in the non-impedance measurement experiments. There were dense and sparse cell areas, small cell clusters and a number of three dimensional towers. The sensor surfaces were also similar to the experiments without impedance measurements with very sparse cell populations and small cell clusters. This indicates that performing a limited number of impedance measurements on Ag-AgCl sensors does not effect the biofilm growth and that the bacteria prefer to grow elsewhere and not in the vicinity of this electrode material.

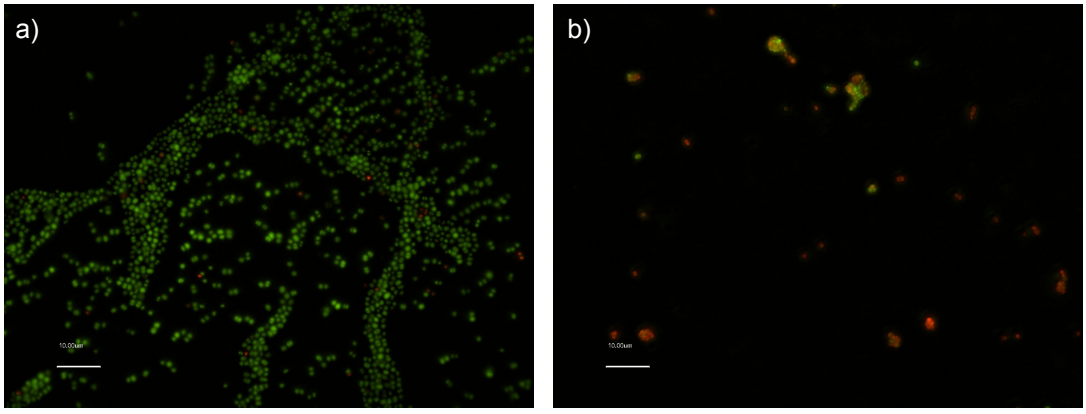

Figure 4-17. Micrograph examples of SA081 biofilm growth on Ag-AgCl-PE300 sensors with impedance measurements and imaged with LIVE/DEAD *Bac*Light stain. Staining performed after 24 hours of growth and scale bars indicate 10µm. a) SA081 control surface; b) SA081 sensor surface, on electrode surface.

The SA082 micrograph examples of AgAgCl sensors with impedance measurements after 48 hours are illustrated in Figure 4-18. The control surface in this experiment had small clusters of cells and no areas of high cell densities. As shown with the alamarBlue assay there were variations in the number of cells between individual surfaces and therefore the control here could be one with lower cell numbers. The Ag-AgCl sensor surfaces again contained very few cells and confirms that poor adhesion of cells and the proceeding poor growth of biofilms occurs with *Staphylococcus aureus* on this electrode material under these conditions.

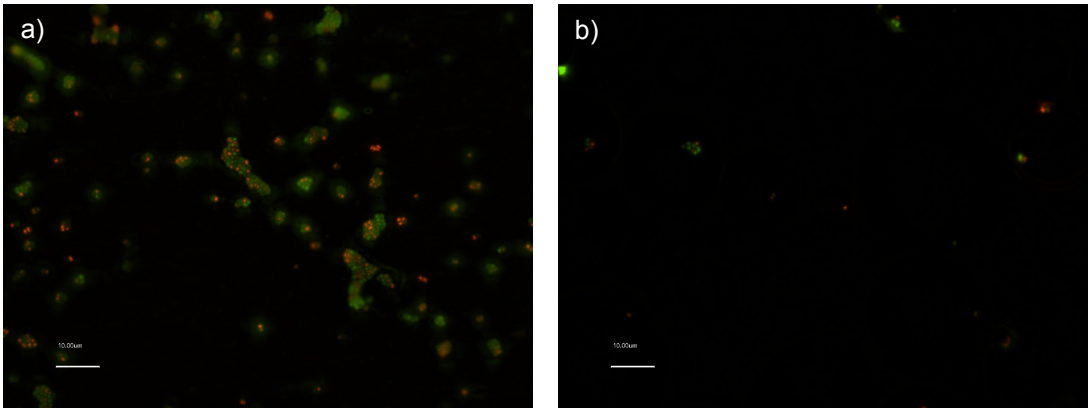

Figure 4-18. Micrograph examples of SA082 biofilm growth on Ag-AgCl-PE300 sensors with impedance measurements and imaged with LIVE/DEAD *Bac*Light stain. Staining performed after 48 hours of growth and scale bars indicate 10µm. a) SA082 control surface; b) SA082 sensor surface, on electrode surface.

4.4.2 Confocal laser scanning microscopy and carbon sensors

Having established that there was very little growth on the Ag-AgCl sensors, the biofilm experiments with confocal laser scanning microscopy were repeated with carbon sensors, C-PE300-v2. The 24-well plate procedures were used rather then the petri dishes as discussed in Section 4.2 and the *Staphylococcus epidermidis* strain, NCTC11964 was also included. Before the surfaces were extracted from the 24-well plates there were visible signs of equally spaced apart colonies on all the control surfaces and the carbon electrode surfaces with both *Staphylococcus aureus* strains. These colonies again contained loose bacteria that were not adhered together or to

the surfaces and were removed in the washing step. The *Staphylococcus epidermidis* strain appeared not to attach and remained suspended throughout the media which was not expected.

The micrograph examples for SA081 growth on carbon sensors without impedance measurements are illustrated in Figure 4-19. The controls of SA081 had densely populated areas of tightly packed cells, areas with a number of tightly packed groups of cells and sparsely populated areas. The sensor surfaces contain areas with large numbers of cell clusters or sparse populations.

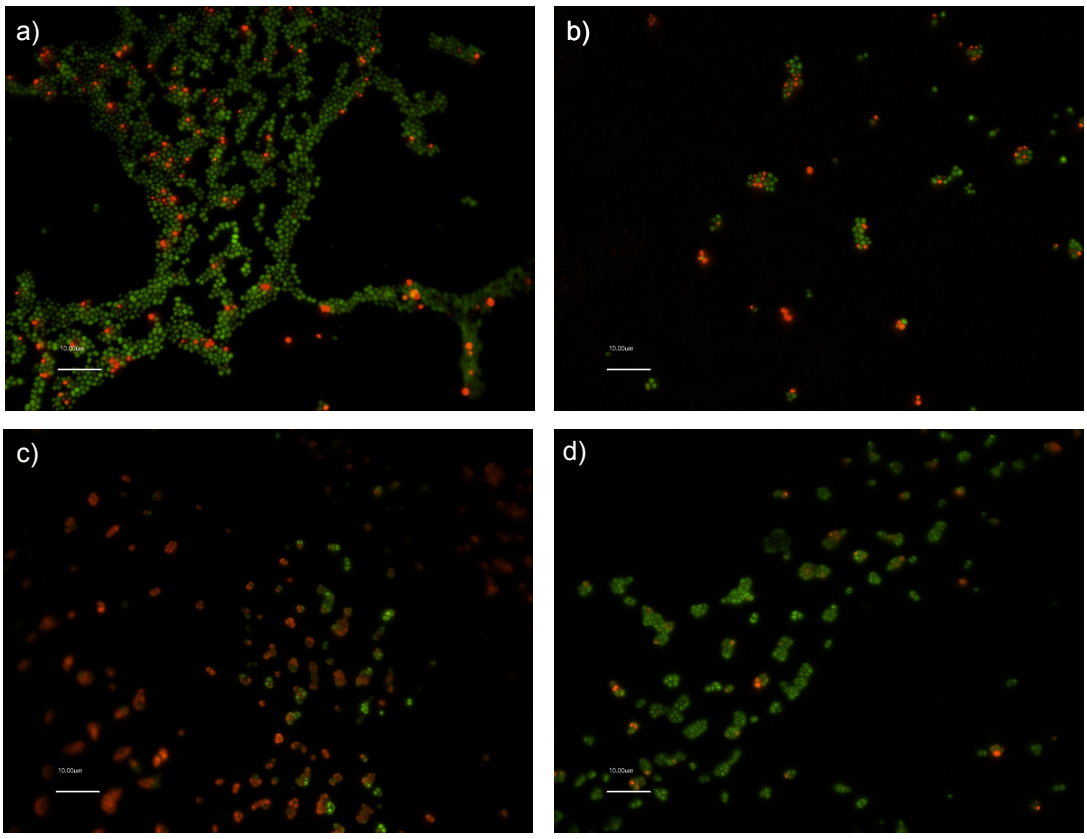

Figure 4-19. Micrograph examples of SA081 biofilm growth on C-PE300-v2 sensors without impedance measurements and imaged with LIVE/DEAD *Bac*Light stain. Staining performed after 48 hours of growth and scale bars indicate 10µm. a) & b) SA081 control surface; c) & d) SA081 sensor surface, on electrode surface.

The micrograph examples for SA081 on carbon sensors with impedance measurements are illustrated in Figure 4-20. The controls of SA081 showed low density areas with small cell clusters. The sensor surfaces showed sparsely populated areas, areas with large numbers of cell clusters, and densely populated areas. This suggests that the SA081 strain is not effected by the impedance measurements and may prefer to grow on the carbon surface rather than the polyethylene substrate PE300.

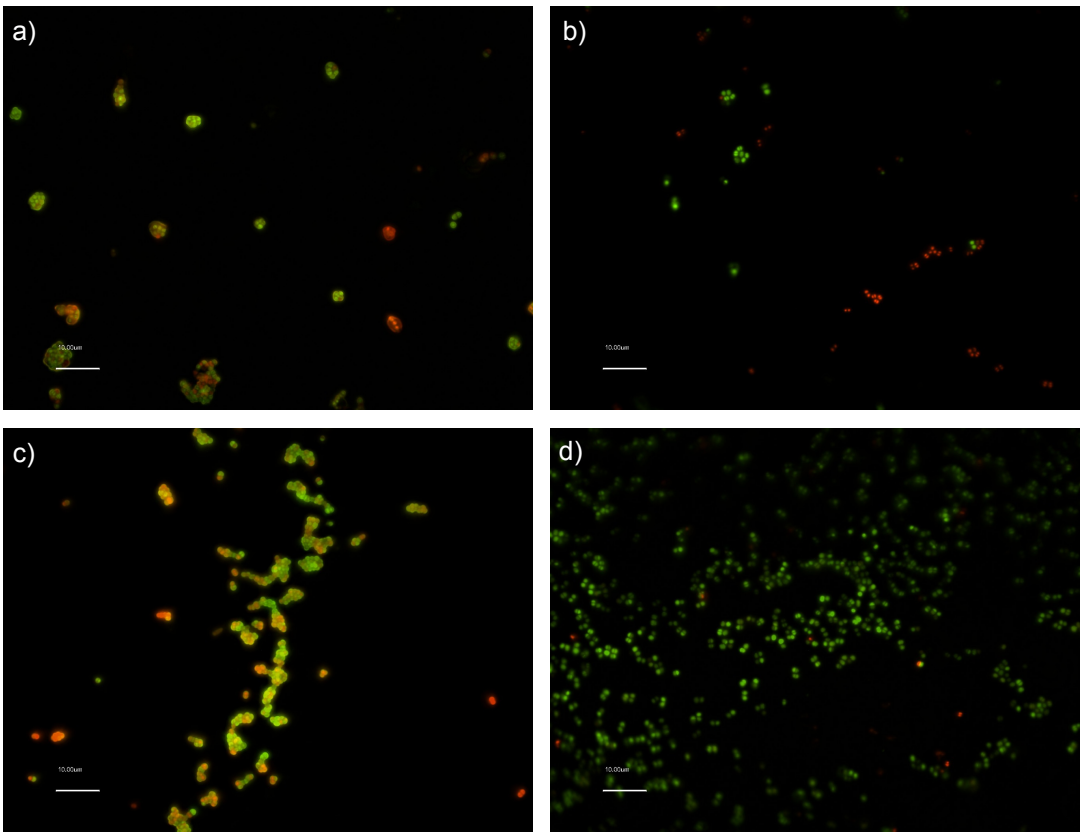

Figure 4-20. Micrograph examples of SA081 biofilm growth on C-PE300-v2 sensors with impedance measurements and imaged with BacLight live/dead stain. Staining performed after 48 hours of growth and scale bars indicate 10μm. a) SA081 control surface; b), c) & d) SA081 sensor surface, on electrode surface..

The micrograph examples for SA082 growth on carbon sensors without impedance measurements are illustrated in Figure 4-21. The controls of SA082 had areas with a large number of cell clusters in clumps or extensive lines, and sparsely populated areas. The carbon sensor surfaces were similar with areas containing large numbers of cell clusters and sparse populations. The larger scale micrograph (Figure 4-21d) illustrates more clearly the three dimensional nature of the cell clusters.

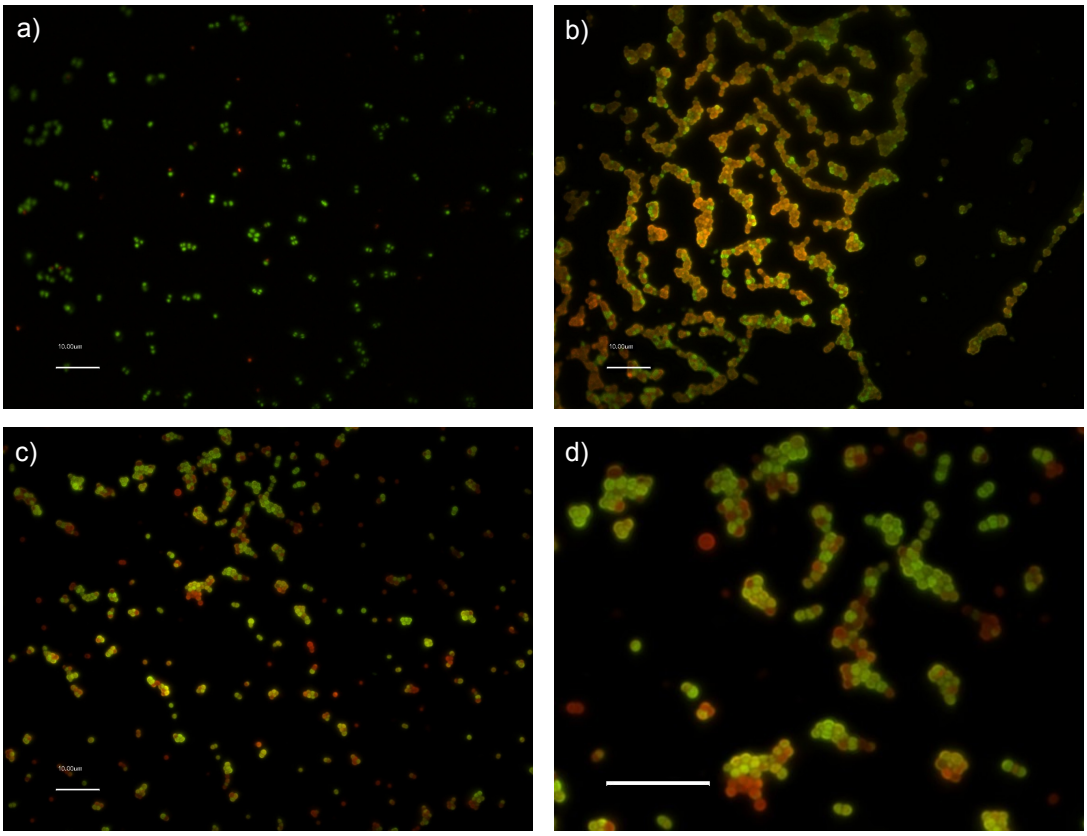

Figure 4-21. Micrograph examples of SA082 biofilm growth on C-PE300-v2 sensors without impedance measurements and imaged with LIVE/DEAD *Bac*Light stain. Staining performed after 48 hours of growth and scale bars indicate 10µm. a) & b) SA082 control surface; c) SA082 sensor surface, on electrode surface; d) Larger scale of image c).

The micrograph examples for SA082 on carbon sensors with impedance measurements are illustrated in Figure 4-22. The controls of SA082 showed low density areas indicating lower levels of growth when compared with the controls of the experiment without impedance measurements. This could indicate the considerable variation in cell growth on the polyethylene substrate. The sensor surfaces showed sparsely populated areas, areas with large numbers of cell clusters, and densely populated areas. On two of the sensor surfaces grown independently the densely populated areas contained cells stained red indicating damaged membranes. This possibly indicates that the influence of impedance measurements every hour was having some effect on the vitality of the SA082 cells.

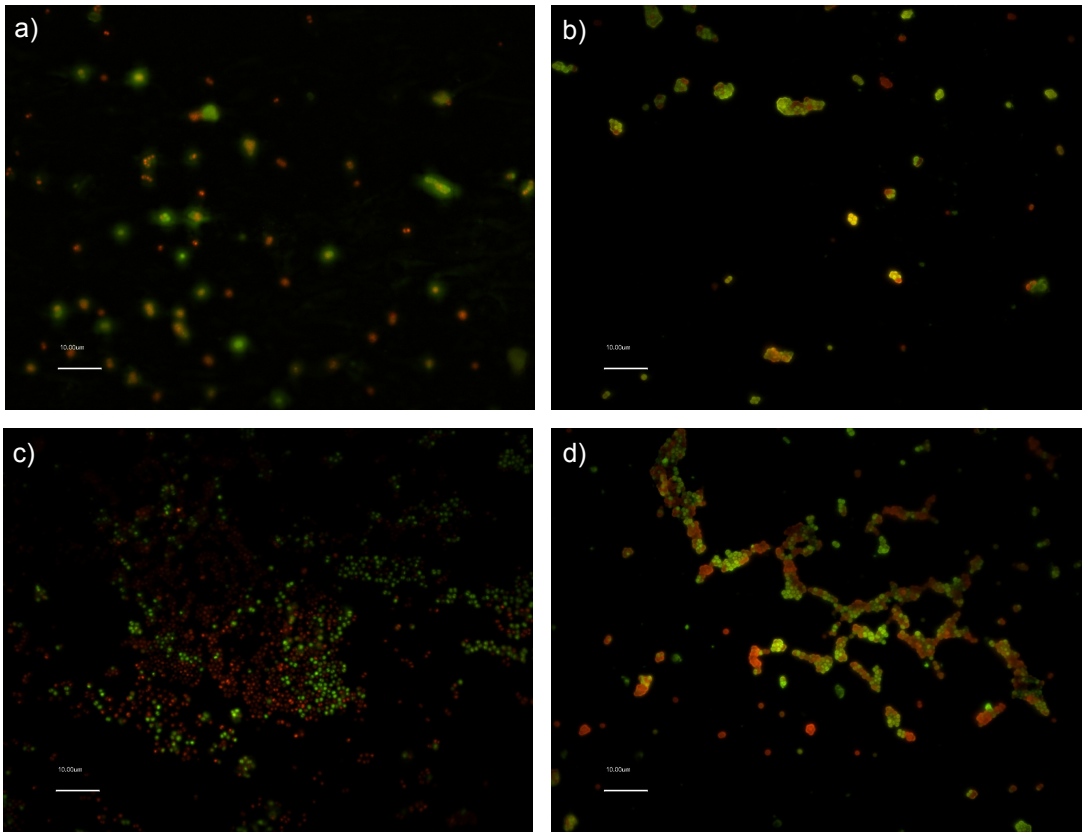

Figure 4-22. Micrograph examples of SA082 biofilm growth on C-PE300-v2 sensors with impedance measurements and imaged with LIVE/DEAD *Bac*Light stain. Staining performed after 48 hours of growth and scale bars indicate 10µm. a) SA082 control surface; b), c) & d) SA082 sensor surface, on electrode surface.

The micrograph examples of NCTC11964 on carbon sensors are illustrated in Figure 4-23 and showed that small cell clusters and slightly denser populated areas of single cells occurred on both the control and sensor surfaces. The lack of cells was most likely due to the bacteria remaining suspended in the liquid.

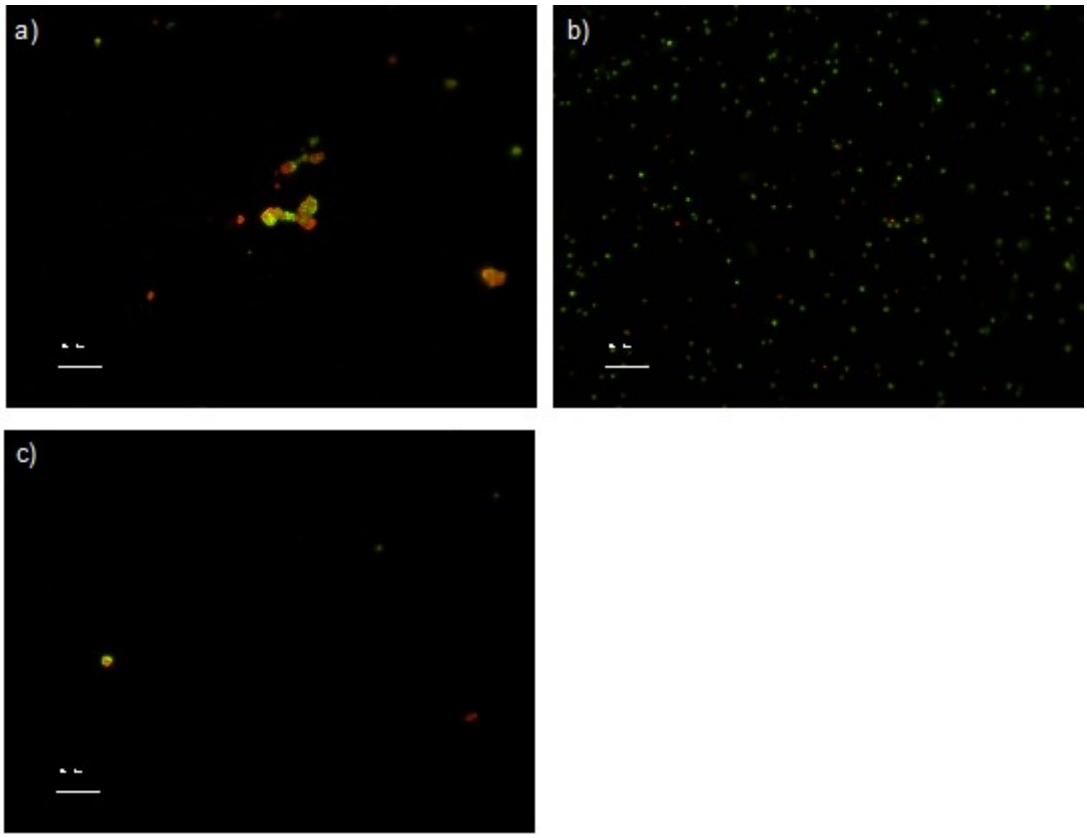

Figure 4-23. Micrograph examples of NCTC11964 biofilm growth on C-PE300-v2 sensors with impedance measurements and imaged with LIVE/DEAD *Bac*Light stain. Staining performed after 48 hours of growth and scale bars indicate 10µm. a) NCTC11964 control surface; b) & c) NCTC11964 sensor surface, on electrode surface.

The main results from the CLSM analysis are: three dimensional biofilms are not forming under the current culture conditions; the 24-well plates encourage the formation of extension cell clusters; the Ag-AgCl electrodes prevent the formation of biofilms within 48 hours; the *Staphylococcus aureus* strains were adhering to the carbon electrode surfaces; the impedance measurements had an insignificant effect on the bacterial growth; and the *Staphylococcus epidermidis* strain, NCTC11964 was most likely not attaching to the surfaces.

4.5 Biofilms – Impedance measurements

Having examined by microscopy the formation of biofilms on the carbon sensors the final step was to analyse the impedance data. It was hypothesised that if a good biofilm formed on the electrodes then the interface between the electrode and the media should change because the interface would effectively become the biofilm. This would then produce discernible differences in the impedance signature traces over frequency that could be used for the detection of bacteria. In addition to the detection, the identification of species by unique signature traces for each biofilm may be possible, similar to the profiles for specific cell layers described in Section 1.8.4.

The biofilm growth with impedance measurements procedure as described in Section 2.8.2 was performed with Ag-AgCl sensors and carbon sensors. The impedance measurements were analysed by comparing the impedance and normalised impedance profiles of the bacterial cultures against the controls to determine if discernible signature traces occurred. To gain a further understanding of the processes occurring in the biological system the impedance data was fitted to equivalent circuit models.

4.5.1 Impedance and Ag-AgCl sensors

The micrographs for the growth of SA081 and SA082 on the Ag-AgCl electrodes as discussed in Section 4.4.1 showed that very few cells attached to the surface. Therefore it was expected that the impedance profiles would not show a discernible difference between the media-only control and the bacterial cultures. As explained in the theory of Section 1.5.3 and in the suspensions results chapter (Section 3.2.1) electrical impedance can be shown as impedance magnitude, phase, resistance and reactance profiles over frequency. An example of these four profiles over frequency for MHB-only, SA081 culture and SA082 culture are illustrated in Figures 4-24 and 4-25. Peaks occurred in all four profiles of all five controls, five SA081 and SA082 cultures. There are no immediate indications that there are any differences between the bacterial cultures compared with the controls.

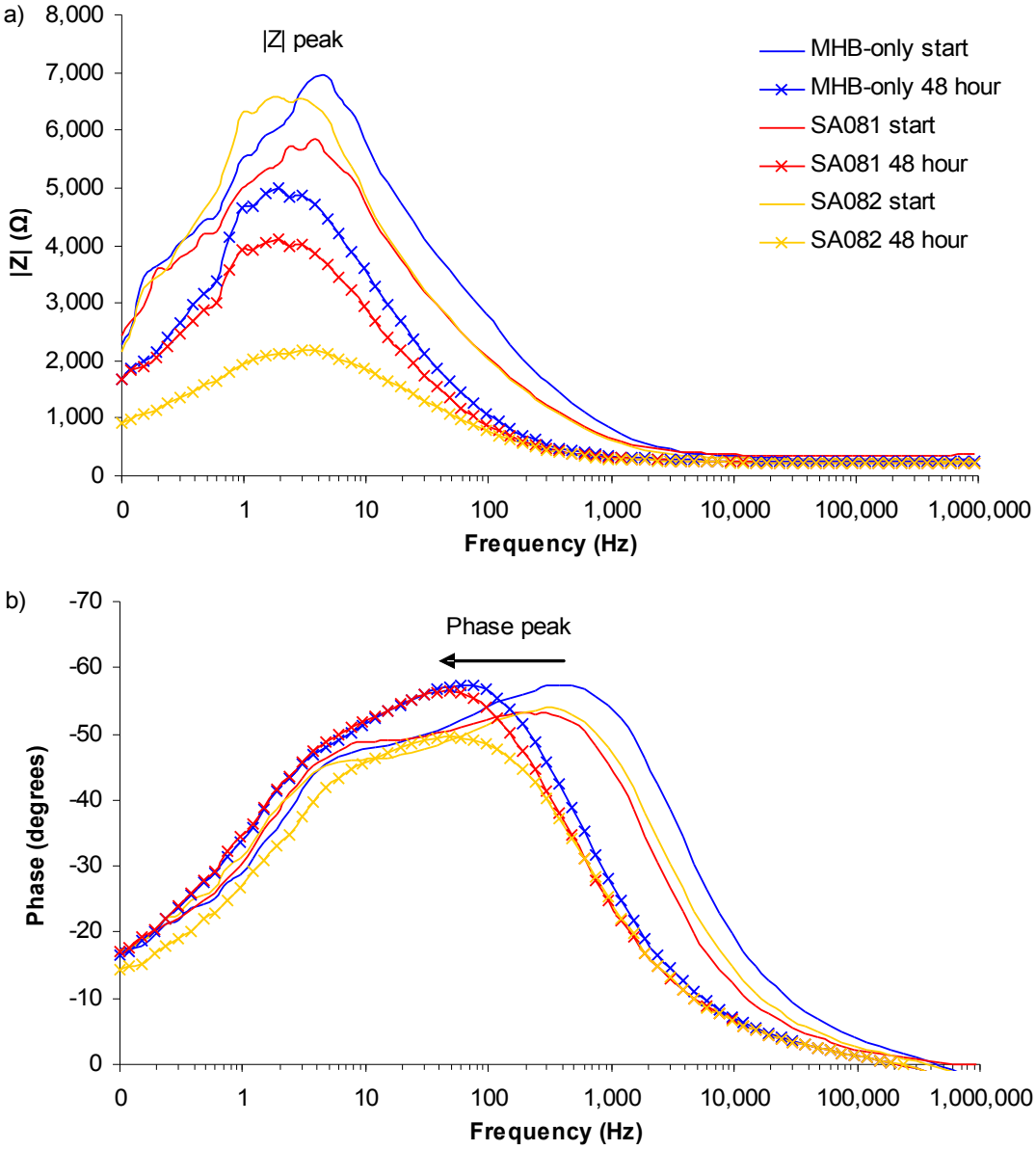

Figure 4-24. An example of Bode plots for biofilm growth with Ag-AgCl sensors: a) Magnitude; b) Phase.

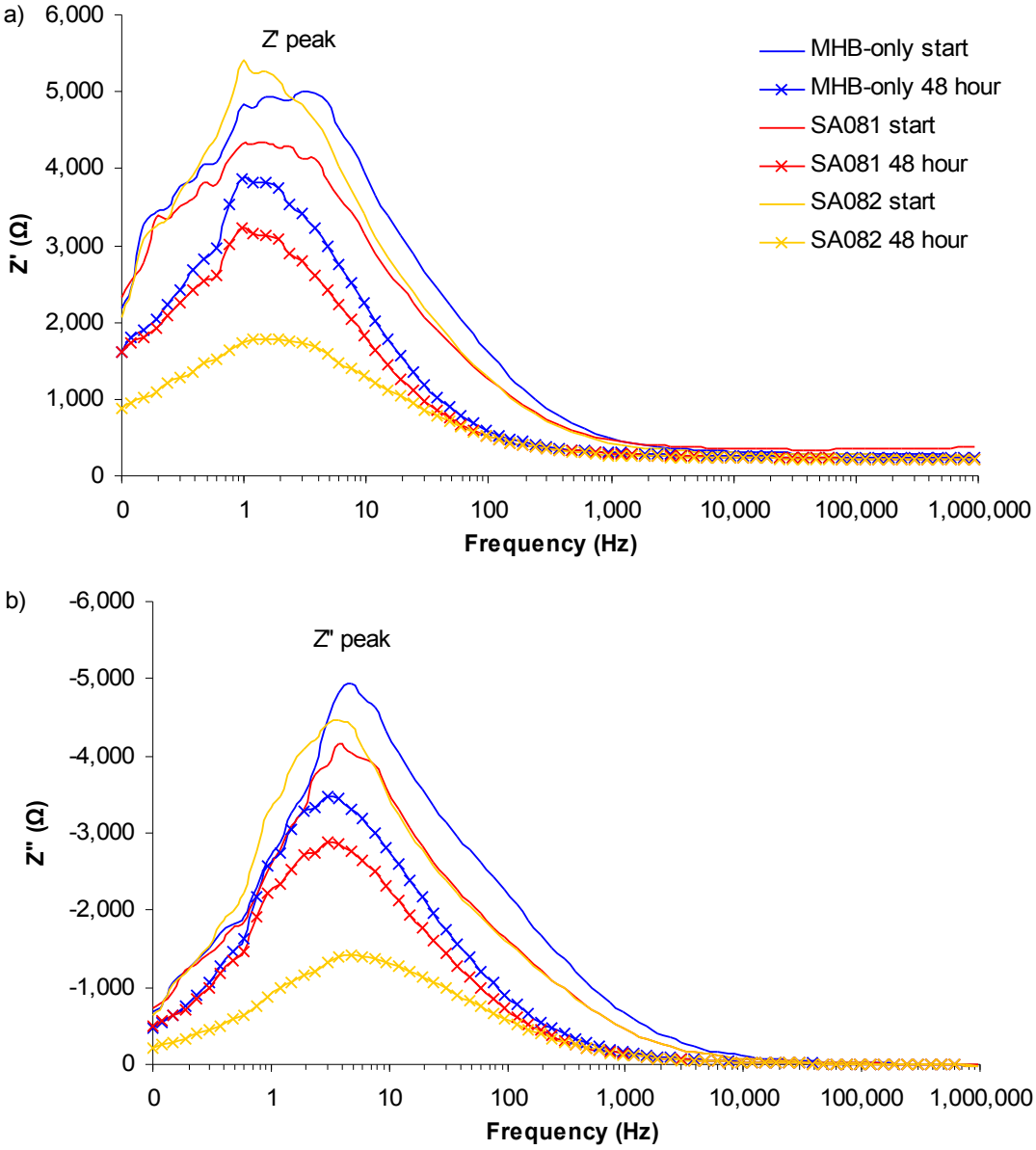

Figure 4-25. An example of Z' and Z'' plots for biofilm growth with Ag-AgCl sensors: a) Resistance; b) Reactance.

The frequencies that the peaks in the impedance data occur at for the biofilm growth experiments with Ag-AgCl sensors are listed in Table 4-6. A magnitude peak occurred between 1 to 8Hz in all the experiments at the start and the frequencies decreased to less than 3Hz by 48 hours. The phase peak occurred mostly in the hundreds of hertz with some lower outliers. This shifted down to between 2 to 25Hz by the end of the experiments. A Z' peak occurred below 7Hz at the start and shifted down to less than 2Hz at the final measurement. The Z" peak was between 3 to 10Hz and decreased to between 1 to 5Hz. As expected there appears to be no discernible differences to distinguish the presence of bacteria due to the lack of cell growth on the Ag-AgCl sensors.

A noticeable difference was observed in that the impedance magnitude peak of the five separate SA082 cultures consistently decreased between 2.5k and 4.5kΩ compared with SA081 where the change in impedance magnitude of the peak varied across the 5 samples between plus and minus 5kΩ. This was mirrored in both the resistance and reactance peaks. Comparing the BacLight images as previously shown in Figure 4-18 there was no difference between the growth of cells with SA081 and SA082. Therefore the most likely reason for this difference is either the production of chemicals that are alternating the media, or the presence of cells in close proximity to the electrodes was different between the SA081 and SA082 strains.

The data from the biofilm experiments, as in the single suspension experiments (Section 3.2.1), was deemed not suitable for parametric statistical tests due to the narrow range of frequencies that the samples occurred at and hence could not be shown to be a normal distribution. Therefore a Mann-Whitney test was performed to find whether the frequency peaks of the bacterial cultures were significantly different from the media only at 48 hours. The Mann-Whitney test was selected as the non-parametric equivalent to the parametric student's t-test. The results of this statistical test are listed in Table 4-6. There were no significance differences between the peaks of the bacterial cultures and the peaks of the MHB-only controls except with the SA082 magnitude and reactance peaks. However it can be seen from the individual

frequency ranges of the peaks that there is an overlap between the media-only and the bacterial cultures which would make these peaks less reliable for distinguishing the absence and/or growth of bacteria.

Table 4-6. The mean peaks and troughs from the biofilm experiments with Ag-AgCl sensors.

Experiment	Initial frequency (Hz)		48 hour frequency (Hz)		Mann-Whitney test ($p < 0.05$)
	Start	Range	Start	Range	
|Z| peak					
MHB	5.9	3.8 - 7.9	1.2	0.8 - 1.9	-
SA081	3.7	2.4 – 4.8	1.7	0.9 – 3.0	No ($p = 0.52$)
SA082	2.4	1.5 - 3.0	2.4	1.9 - 3.0	Yes ($p = 0.02$)
Phase peak					
MHB	165	8 - 378	18	2 - 60	-
SA081	226	150 - 300	46	15 - 75	No ($p = 0.12$)
SA082	300	All 300	46	38 - 48	No ($p = 0.13$)
Z' peak					
MHB	3.6	0.5 - 6.3	0.9	0.8 - 1.0	-
SA081	2.5	1.5 - 3.8	1.2	0.9 - 1.9	No ($p = 0.34$)
SA082	1.4	0.9 - 1.9	1.4	0.9 - 1.9	No ($p = 0.14$)
Z'' peak					
MHB	7.5	4.8 - 10.0	1.8	1.3 - 3.0	-
SA081	4.9	3.8 - 7.5	3.1	1.5 - 4.8	No ($p = 0.07$)
SA082	4.4	3.8 - 6.0	3.8	3.0 - 4.8	Yes ($p = 0.01$)

4.5.2 Normalised impedance and Ag-AgCl sensors

As previously described, normalisation of the impedance data was performed by dividing each hourly reading by the starting reading to show relative changes from the starting condition, as described in Section 2.9. The normalised data was examined for differences in the signature traces, and in particular the frequencies that the peaks occurred at, which could be used for detection purposes. The normalised profiles of MHB-only control and SA081 were similar with marked differences with the SA082 strain as there were in the impedance profiles (Section 4.5.1). The normalised magnitude and phase plots are illustrated in Figure 4-26.

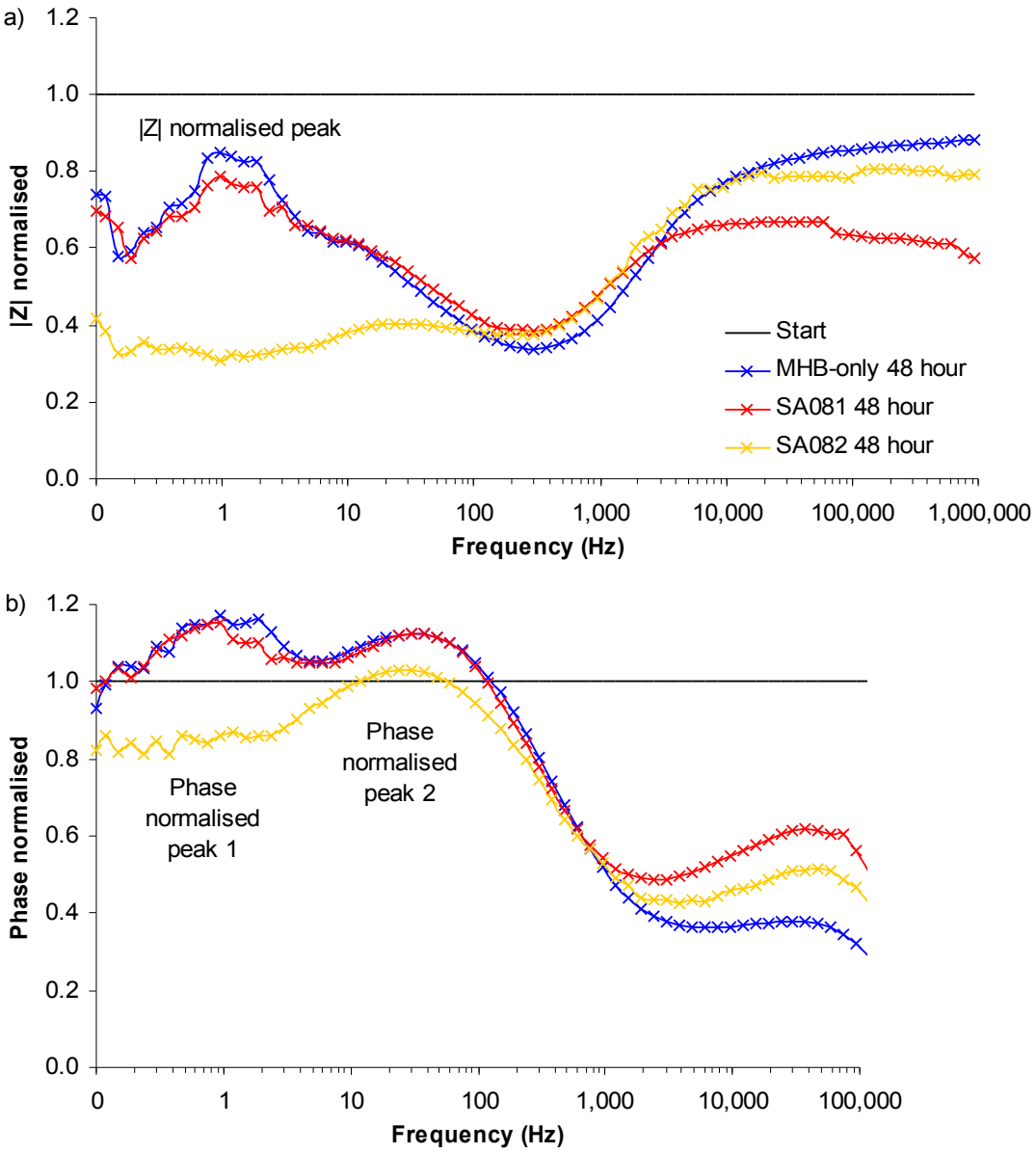

Figure 4-26. An example of the normalised Bode plots for biofilm growth with Ag-AgCl sensors.
a) Magnitude; b) Phase.

The frequencies that the normalised peaks in the impedance data occurred at for the biofilm growth experiments with Ag-AgCl sensors are summarised in Table 4-6. The normalised magnitude peak occurred at frequencies of less than 12Hz in the MHB-only and SA081 in all 5 samples. In the SA082 samples the normalised peak was smaller and occurred at less than 24Hz. The MHB-only and SA081 had two phase angle peaks, the first occurred at less than 2Hz and the second in the region of 20Hz. In contrast the SA082 samples only had the second normalised phase angle peak. The resistance and reactance peaks in all samples occurred at similar frequencies to the normalised magnitude. These results show that the normalised profiles over frequency show differences for the SA082 and the one possible cause is that the metabolised products differ for the SA082 strain compared with the SA081 strain.

A Mann-Whitney test was performed to find whether the frequency peaks of the bacterial cultures were significantly different from the media only at 48 hours. There were no significant differences between the peaks in the normalised profiles except that the first normalised phase peak was not present. The results from the biofilm experiments with Ag-AgCl sensors indicate that the current experimental procedure is not capable of distinguishing the absence and/or biofilm growth of multiple strains of bacteria due to the lack of cell adhesion to the electrodes.

Table 4-7. The mean normalised peaks and troughs from the biofilm experiments with Ag-AgCl sensors. The * indicates the peak was only present in 3 of 5 experiments.

Experiment	48 hour frequency (Hz)		Mann-Whitney test ($p < 0.05$)
	Mean	Range	
|Z| normal peak			
MHB	1.8	0.8 - 5.0	
SA081*	4.7	1.0 - 11.9	No ($p = 0.65$)
SA082	8.5	0.9 - 23.8	No ($p = 0.40$)
Phase normal peak 1			
MHB	0.7	0.2 - 0.9	
SA081	0.8	0.2 - 1.2	No ($p = 0.23$)
SA082	-	-	Peak not present
Phase normal peak 2			
MHB *	22.5	12.6 - 30.0	
SA081	26.8	9.5 - 37.8	No ($p = 0.65$)
SA082	22.1	15.0 - 23.8	No ($p = 0.53$)
Z' normal peak			
MHB	1.7	0.8 - 5.0	
SA081*	4.7	0.95 - 11.9	No ($p = 0.29$)
SA082	6.9	0.9 - 18.9	No ($p = 0.20$)
Z'' normal peak			
MHB	0.9	0.8 - 1.0	
SA081*	1.1	1.0 - 1.2	No ($p = 0.17$)
SA082	11.9	0.9 - 23.8	No ($p = 0.05$)

4.5.3 Impedance and carbon sensors

The biofilm experiments with carbon sensors was performed with the 24-well procedure as discussed in Section 2.8.2. The carbon sensors used were the C-PE300-v2 as described in Section 2.2.1 and prepared with an electrochemical preconditioning procedure as described in Section 2.7.2. The two clinical strains of *Staphylococcus aureus*, SA081 and SA082, were again selected as a species commonly isolated from wounds. A third strain of a different species was selected as a comparison to investigate whether species could be differentiated if the biofilms were detected. The strain was NCTC11964 representative of *Staphylococcus epidermidis*, another species commonly isolated from wounds. For each strain five carbon sensors in Mueller-Hinton broth (MHB) were inoculated at approximately

$1x10^3$ CFU ml^{-1} and a sixth sensor was used as a control containing only Mueller-Hinton broth (MHB). Two additional MHB only experiments were performed to increase the number of media-only samples to five.

It was noticed that the start readings for the SA082 experiments contained small inductive loops as illustrated in Figure 4-27. All the electrical connections were checked and re-secured which eliminated the inductive loops for the remaining measurements. The first hour measurements were designated a pseudo-start measurement for the SA082 experiment to avoid any misinterpretation of the data caused by the inductive loop altering the impedance profiles.

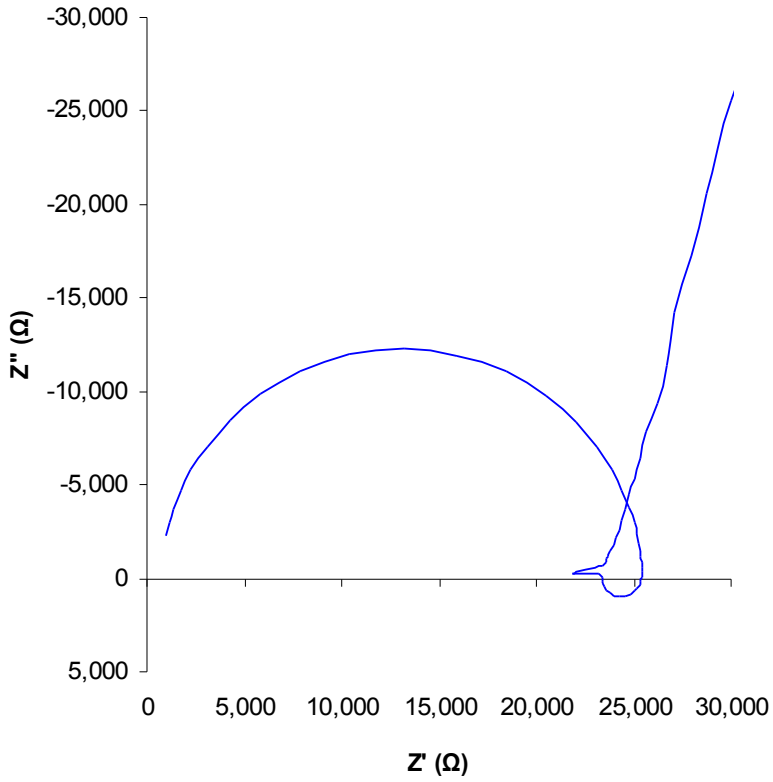

Figure 4-27. An example of the inductive loop in the start measurements of the biofilm experiment with SA082 and carbon sensors.

Examination of the impedance profiles showed that there were peaks in the phase and reactance profiles over frequency. Examples of the reactance peak are illustrated in Figures 4-28 and 4-29. At the start the reactance peak occurred in the range of

60kHz to 200kHz. The reactance peak of the control system, MHB-only decreased steadily over the 24 hours by 2kΩ and its frequency shifted down on average by 20kHz (Figure 4-28a). Similarly the NCTC11964 decreased by approximately 6kΩ and shifted down in frequency by 30kHz (Figure 4-28b). The NCTC11964 strain did not adhere to the electrodes like the other 2 strains as shown in Figure 4-23 and therefore it would be expected to be similar to the MHB-only.

The SA082 samples also decreased by 2kΩ and shifted down by 20kHz indicating no discernible difference from the media-only (Figure 4-29a). Given that there were cells attached to the electrodes as shown in Figure 4-16 there are two possible reasons for the cells not producing an apparent change. Firstly there could have been insufficient cells to produce a change because a large portion of the electrode is still in contact with the media. In at least two of the five samples there were considerable numbers of dead cells and these are less likely to be detectable because of their damaged membranes not causing a barrier to the flow of the current. Therefore creating conditions similar to the media-only. The second reason is the type of carbon sensors used in these experiments are unsuitable for detecting bacteria due to their relative high impedance profiles.

In contrast the SA081 reactance peak increased by 2kΩ and then decreased by 1.2kΩ with an upwards frequency shift of 5kHz and then downwards by 2kHz (Figure 4-29b). The timing of the frequency shift varies, however the upwards and then downward shifts occur across all 5 separate cultures. This is the first indication that the carbon sensors might produce noticeable differences that would enable the absence and/or presence of attached cells to be detected. The reason that this strain SA081 produced changes could be due to a better cell coverage across the electrodes compared with the SA082 strain. The main evidence against this is that the change occurs almost immediately when it would be expected that there would be insufficient cell coverage to produce any noticeable change. This is further discussed in Section 4.5.4 where the relative changes from the initial conditions can be seen.

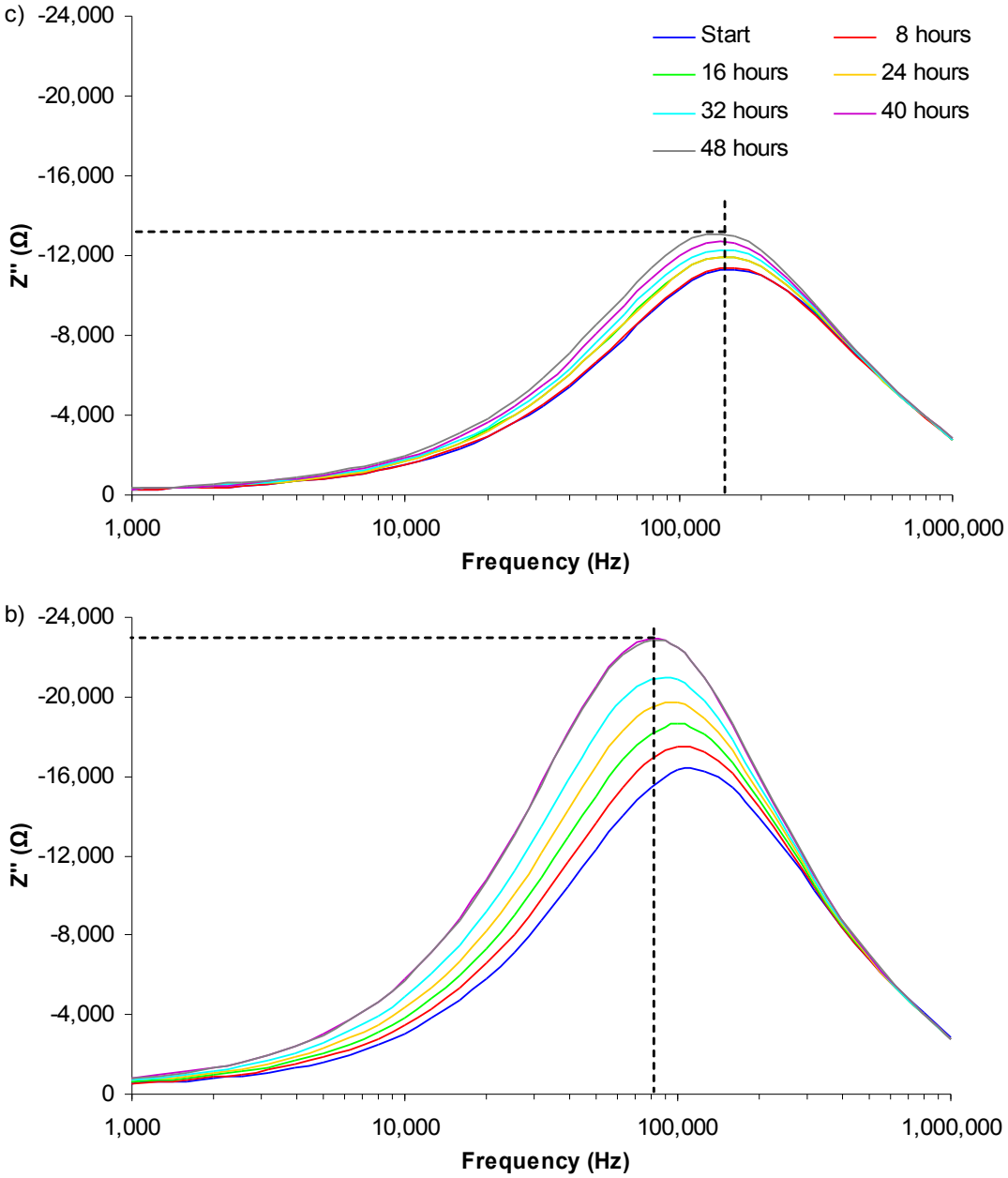

Figure 4-28. An example of the reactance peaks from the carbon sensors in the biofilm experiments: a) MHB-only control; b) NCTC11964.

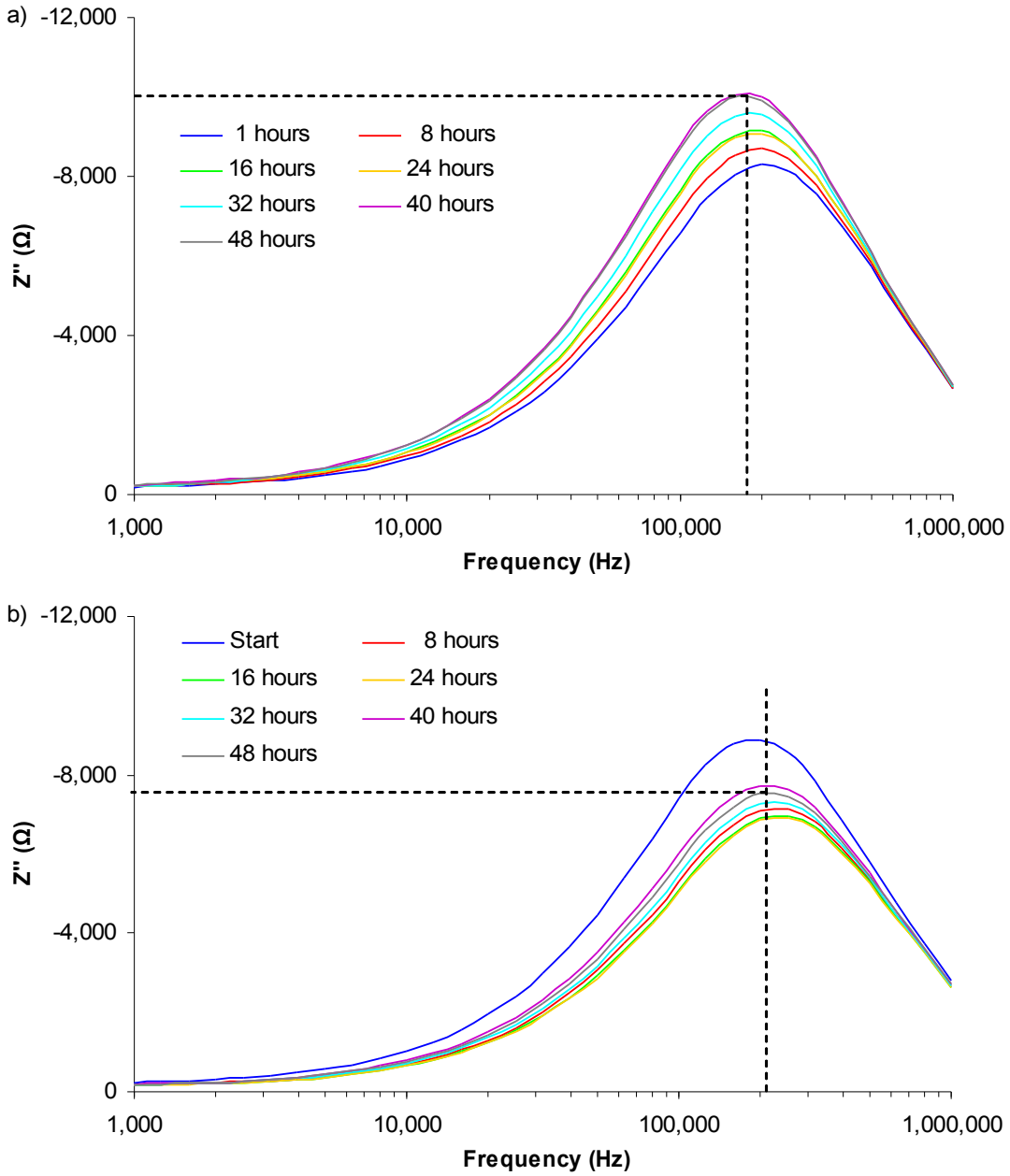

Figure 4-29. An example of the reactance peaks from the carbon sensors in the biofilm experiments: a) SA082; b) SA081.

The reactance peak magnitude and frequency at the start and 48 hour measurements are summarised in Table 4-8. A statistical test for significant differences between the frequency of the reactance peak in the bacterial cultures and the media only control was not performed because the 48 hour frequency is related to the start frequency. For example the 48 hour frequency range of the SA081 samples was higher than the MHB-only frequency range, however the start frequency range was also higher. Therefore any significant difference between the samples would not be valid.

Table 4-8. The reactance peak from the biofilm experiments with carbon sensors.

Experiment	Start		48 hour	
	Mean	Range	Mean	Range
Reactance peak frequency (Hz)				
MHB-only	$1.4x10^5$	$1.3x10^5$ to $1.6x10^5$	$1.2x10^5$	$1.0x10^5$ to $1.3x10^5$
SA081	$1.7x10^5$	$1.6x10^5$ to $2.0x10^5$	$1.9x10^5$	$1.6x10^5$ to $2.0x10^5$
SA082	$1.9x10^5$	$1.6x10^5$ to $2.0x10^5$	$1.5x10^5$	$1.3x10^5$ to $1.6x10^5$
NCTC11964	$1.2x10^5$	$0.8x10^5$ to $1.6x10^5$	$9.4x10^4$	$0.6x10^5$ to $1.3x10^5$
Reactance peak value (Ω)				
MHB-only	$-1.2x10^4$	$-1.1x10^4$ to $-1.4x10^4$	$-1.4x10^4$	$-1.3x10^4$ to $-1.7x10^4$
SA081	$-1.0x10^4$	$-1.0x10^4$ to $-1.1x10^4$	$-0.9x10^4$	$-0.8x10^4$ to $-7.0x10^4$
SA082	$-0.9x10^4$	$-0.8x10^4$ to $-1.0x10^4$	$-1.1x10^4$	$-1.0x10^4$ to $-1.3x10^4$
NCTC11964	$-1.6x10^4$	$-1.2x10^4$ to $-2.2x10^4$	$-2.2x10^4$	$-1.6x10^4$ to $-3.0x10^4$

The reactance peak occurs at frequencies where the double layer at the electrode interface primarily defines the impedance. The interface is modelled by a resistor and capacitor in parallel and from the theory in Section 1.5.3 the equation for the imaginary part of the impedance , Z'', is given in Equation 4-1 where ω is the angular frequency, R_{dl} is the double layer resistance and C_{dl} is the double layer capacitance.

$$Z'' = \frac{-j\omega R_{dl}^2 C_{dl}}{1 + (\omega R_{dl} C_{dl})^2} \qquad (4\text{-}1)$$

The reactance peak of MHB-only, NCTC11964 and SA082 shifts down in frequency and up in magnitude. Therefore the angular frequency decreases and it would be expected that the capacitor, C_{dl} decreases given capacitors are frequency dependent. The resistance R_{dl} would increase to increase the magnitude of the reactance peak. Assuming that the bacterial cultures of SA082 and NCTC11964 are behaving as the

MHB-only these changes could be the adhesion of molecules to the electrode surface over time and altering the properties of the double layer at the interface. In the SA081 samples initially the opposite occurs and the resistor should decrease and the capacitor increase. This indicates that this strain could be producing molecules that are smaller and with greater charge and therefore reducing the charge transfer resistance of the electrode interface. Alternatively the adhesion of the cells are producing changes at the electrode interface, however the question remains why these changes were not seen with the SA082 strain. The changes in the component values are discussed further with the equivalent circuit modelling in Section 4.5.5.

The phase peak changes in magnitude also showed that the SA082 and NCTC11964 were most similar to the MHB-only while the SA081 samples were different. The phase peaks are summarised in Table 4-9. The phase peak occurred in the region of 60kHz and is stable in all the experiments. The MHB-only control phase peak decreased steadily over the 48 hours by approximately 2°. Similarly the NCTC11964 decreased on average by 3° and the SA082 strain decreased on average by 2°. The SA081 phase peak had contrasting changes with a increase on average of 2° in the first 16 to 17 hours and then a decrease of 1° in the remaining hours of the experiment. This was repeatable in all the five separate cultures of each strain and confirms that the SA081 strain has a different behaviour.

Table 4-9. The phase peak from the biofilm experiments with carbon sensors.

Experiment	Start		48 hour	
	Mean	Range	Mean	Range
Phase peak frequency (Hz)				
MHB-only	$6.0x10^5$	$5.0x10^5$ to $6.3x10^5$	$6.0x10^5$	$5.0x10^5$ to $6.3x10^5$
SA081	$6.3x10^5$	$6.3x10^5$ to $6.3x10^5$	$7.0x10^5$	$6.3x10^5$ to $7.9x10^5$
SA082	$6.6x10^5$	$6.3x10^5$ to $7.9x10^5$	$6.3x10^5$	$6.3x10^5$ to $6.3x10^5$
NCTC11964	$5.8x10^5$	$5.0x10^5$ to $6.3x10^5$	$5.1x10^5$	$4.0x10^5$ to $6.3x10^5$
Phase angle of peak (degrees)				
MHB-only	-64.7	-63.2 to -66.6	-66.5	-65.5 to -69.1
SA081	-61.5	-60.3 to -62.1	-59.3	-57.7 to -61.3
SA082	-60.8	-59.4 to -62.3	-63.4	-61.9 to -64.8
NCTC11964	-66.6	-63.8 to -70.8	-70.0	-66.6 to -73.6

4.5.4 Normalised impedance and carbon sensors

As previously described, normalisation of the impedance data from the carbon sensors was performed by dividing each hourly reading by the starting reading to show relative changes from the starting condition, as described in Section 2.9. The SA082 experiments were normalised to the first hour measurement due to the inductive loops in the actual start measurement as discussed in Section 4.5.3.The normalised data was examined for differences in the signature traces, and in particular the frequencies that the peaks occurred at, which could be used for detection purposes. Peaks in the normalised profiles occurred in the phase and the resistance.

The impedance profiles discussed in Section 4.5.3 showed that the NCTC11964 profile was similar to the MHB-only control profile because of the lack of adhesion of the bacteria to the sensor. The SA082 profile was also similar to the MHB-only control possibly due to less bacteria adhered to the electrodes when compared to the the SA081 strain. The SA081 had marked differences in its phase and reactance profiles indicating that the cells or cell clusters may be causing a difference. It was expected that the normalised data would indicate the same four scenarios.

Examples of the normalised phase profiles are illustrated in Figures 4-30 and 4-31. The peak at 50Hz was caused by the electricity mains frequency and should be ignored. The peak in the MHB-only controls occurred at a mean frequency of $3.8x10^5$ Hz and increased steadily over the 48 hours by approximately 1.17. Similarly for NCTC11964 the peak occurred at a mean frequency of $3.2x10^5$ Hz and rose on average by 1.42, and for SA082 the peak occurred at a mean frequency of $3.2x10^5$ Hz and rose on average by 1.25. In contrast all the SA081 samples decreased for the first 16 to 17 hours on average by 0.19 and then increased on average by 0.06 in the remaining hours. This confirms that the normalised data have the same four scenarios as seen in the impedance data.

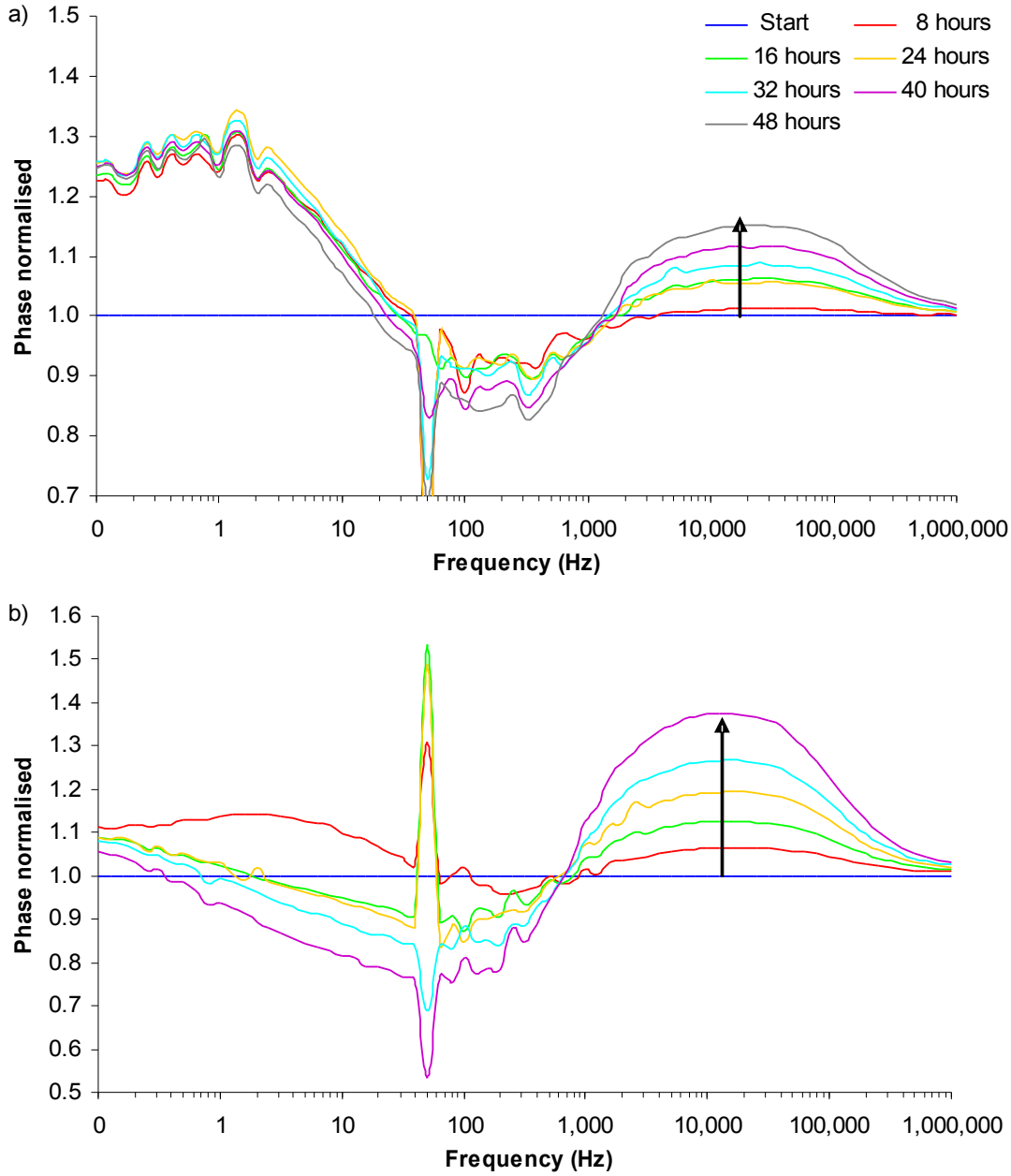

Figure 4-30. The normalised phase profiles for carbon sensors: a) MHB-only control; b) NCTC11964. Black arrows indicate change in magnitude of the phase angle peak.

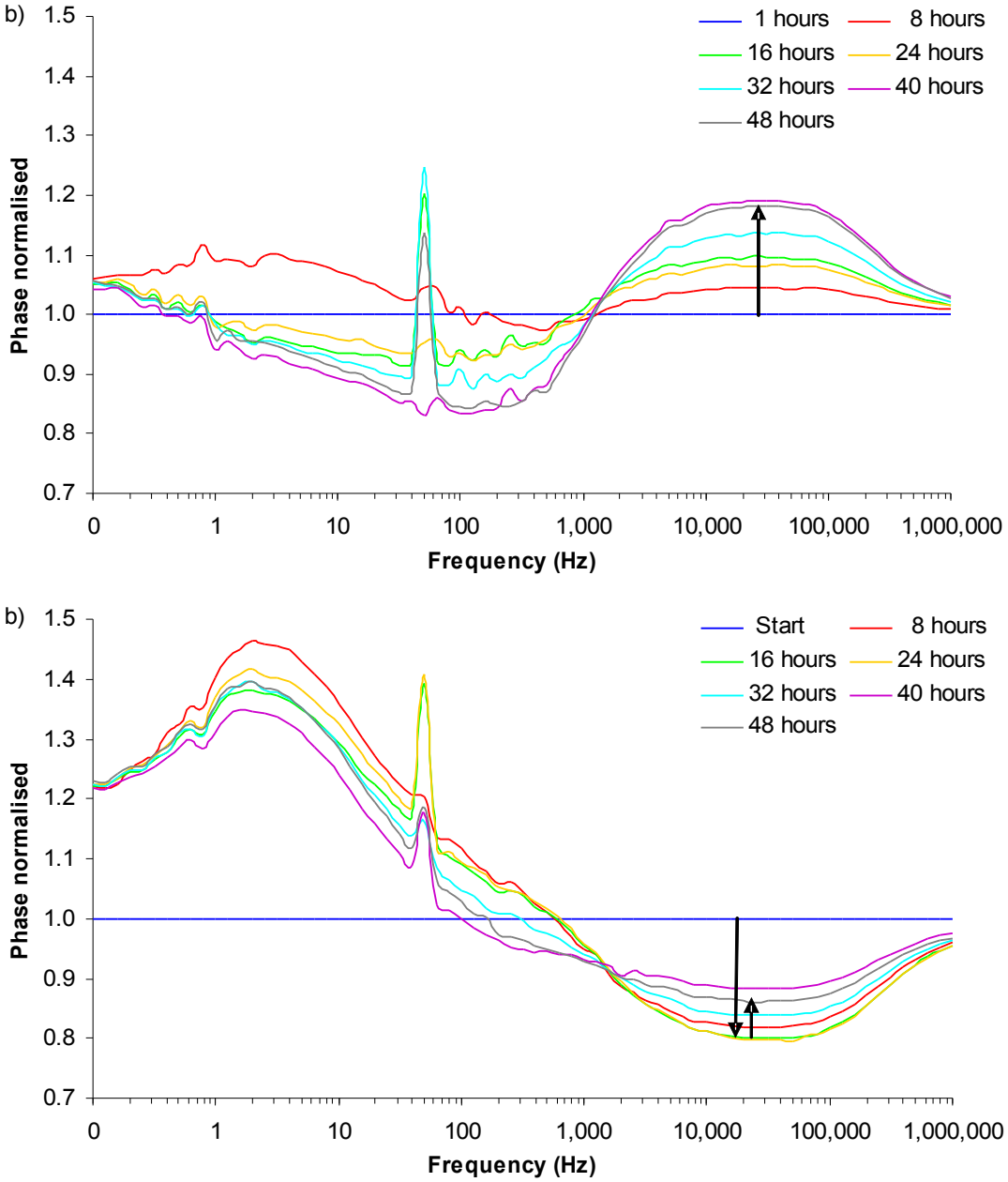

Figure 4-31. The normalised phase profiles for carbon sensors: a) SA082; b) SA081. Black arrows indicate change in magnitude of the phase angle peak.

A similar four scenarios are seen in the normalised resistance and are illustrated in Figures 4-32 and 4-33. The peak or trough occurs between 250kHz and 500kHz in all the samples. The magnitude of the normalised resistance peak decreased in MHB-only, NCTC11964 and SA081 by 0.08, 0.16 and 0.08 respectively. The normalised trough occurs at frequencies where the double layer at the electrode interface primarily defines the impedance. The interface is modelled by a resistor and capacitor in parallel and from the theory in Section 1.5.3 the equation for the resistive part of the impedance, Z', is given in Equation 4-2 where ω is the angular frequency, R_{dl} is the double layer resistance and C_{dl} is the double layer capacitance. For each sample the normalised resistive trough occurs at a fixed frequency over time. Therefore either the double layer resistance and/or capacitance must increase over time to cause the tough to appear in the normalised data.

$$Z' = \frac{R_{dl}}{1 + (\omega R_{dl} C_{dl})^2} \tag{4-2}$$

In the normalised resistance profile of the SA081 cultures a peak occurred at similar frequencies to the trough of the MHB-only indicating that the resistance, Z' increases. The SA081 peak increased for 16 to 17 hours on average by 0.09 and then decreased by 0.06 in the remaining hours of the experiment. This means according to Equation 4-2 the resistor R_{dl} and/or capacitor C_{dl} should decrease at first and then increase. Since this change starts within the first few hours in the SA081 samples the explanation that there are less cells or more damaged cells within the SA082 cultures seems less justified given that it should take time before there is a difference in cell numbers. Possible suggestions are differences in metabolised products or the rate of attachment to the sensor. The possible explanations are discussed further in Section 5.6.2.

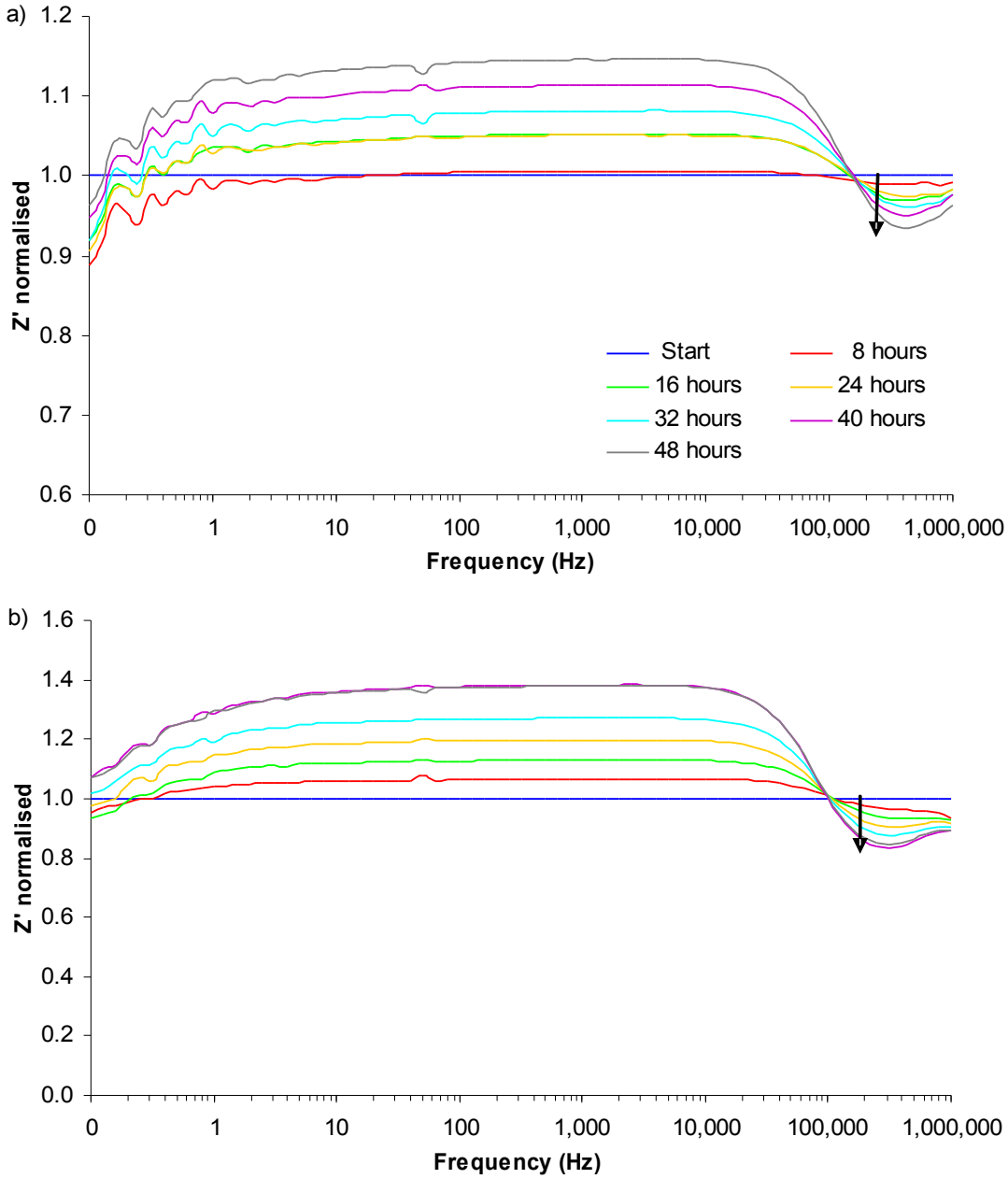

Figure 4-32. The normalised phase profiles for carbon sensors: a) MHB-only control; b) NCTC11964. Black arrows indicate magnitude changes over time.

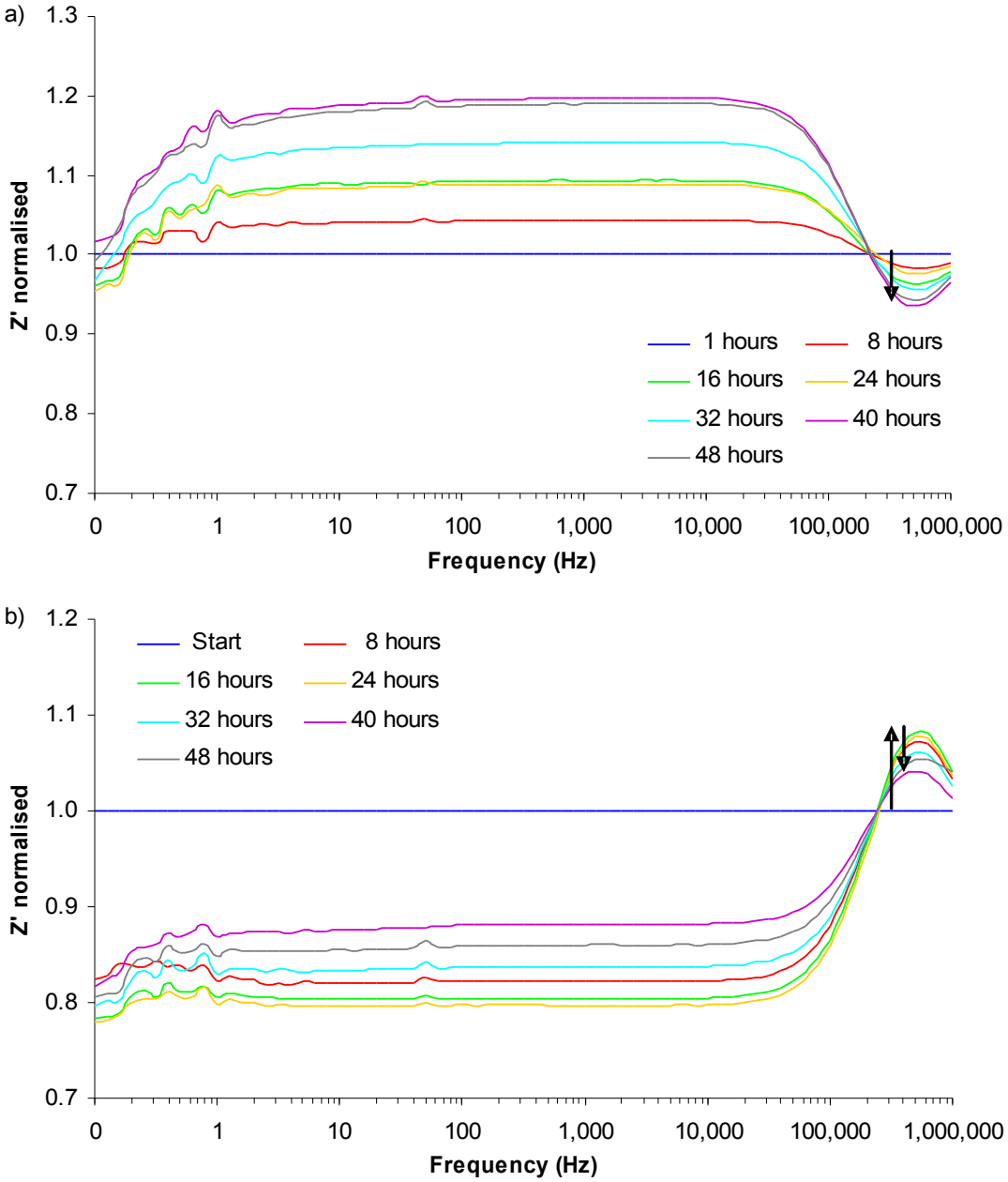

Figure 4-33. The normalised resistance profiles for carbon sensors: a) SA082; b) SA081. Black arrows indicate directional changes over time.

A summary of the normalised peaks or troughs for the carbon sensors with biofilms at 48 hours are listed in Table 4-10. The range of frequencies of the resistance peak are higher for both *Staphylococcus aureus* strains when compared to the media-only. Statistical significant tests were not performed because like the reactance peak discussed in Section 4.5.3 the normalised peaks had a fairly fixed frequency over the 48 hours and therefore a significant difference would only be valid if it could be shown that the *Staphylococcus aureus* strains were causing an immediate change of frequency soon after inoculation. The fixed frequency of the normalised frequency suggests the surface of the carbon electrodes are a significant factor in the properties of the double layer interface and there were insufficient cells to change it.

Table 4-10. The mean normalised peaks and troughs from the biofilm experiments with carbon sensors.

Experiment	48 hour frequency (Hz)	
	Mean	Range
Z' normalised trough		
MHB	$3.8x10^5$	$3.2x10^5$ to $4.0x10^5$
SA081	$5.0x10^5$ (peak)	$5.0x10^5$ to $5.0x10^5$
SA082	$4.8x10^5$	$4.0x10^5$ to $5.0x10^5$
NCTC11964	$3.2x10^5$	$2.5x10^5$ to $4.0x10^5$
Phase normalised peak 1		
MHB	0.64	0.10 to 1.58
SA081	1.91	1.58 to 2.00
SA082	-	-
NCTC11964	-	-
Phase normalised peak 2		
MHB	$1.8x10^4$	$1.6x10^4$ to $2.0x10^4$
SA081	$1.4x10^4$ (trough)	$1.0x10^4$ to $2.5x10^4$
SA082	$2.4x10^4$	$2.0x10^4$ to $4.0x10^4$
NCTC11964	$1.7x10^4$	$1.3x10^4$ to $2.0x10^4$

4.5.5 Equivalent circuits and carbon sensors

An example of the z-plots of carbon sensors are illustrated in Figure 4-35 and it is immediately clear that these carbon sensors compared with the ones used in the suspension experiment (Section 3.3) are far more stable over time. The circuit model selected is the same one used for the suspension experiments and is illustrated again in Figure 4-34. The semicircle at high frequencies caused by the electrode-solution interface is represented by a parallel resistor R_{dl1} and capacitor C_{dl1}. Extrapolating the semicircle until it crosses the resistance axis shows that it will not cross at the origin and therefore there must be a resistor R_s to represent the solution in series with the interface impedance. The reactance at low frequencies is tending towards infinity implies that there is diffusion processes at work which can be represented by the constant phase element CPE_d, as discussed in Section 1.5.3.

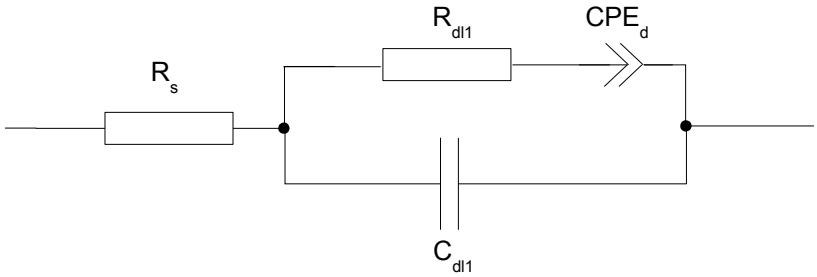

Figure 4-34. The equivalent circuit model for the carbon sensors.

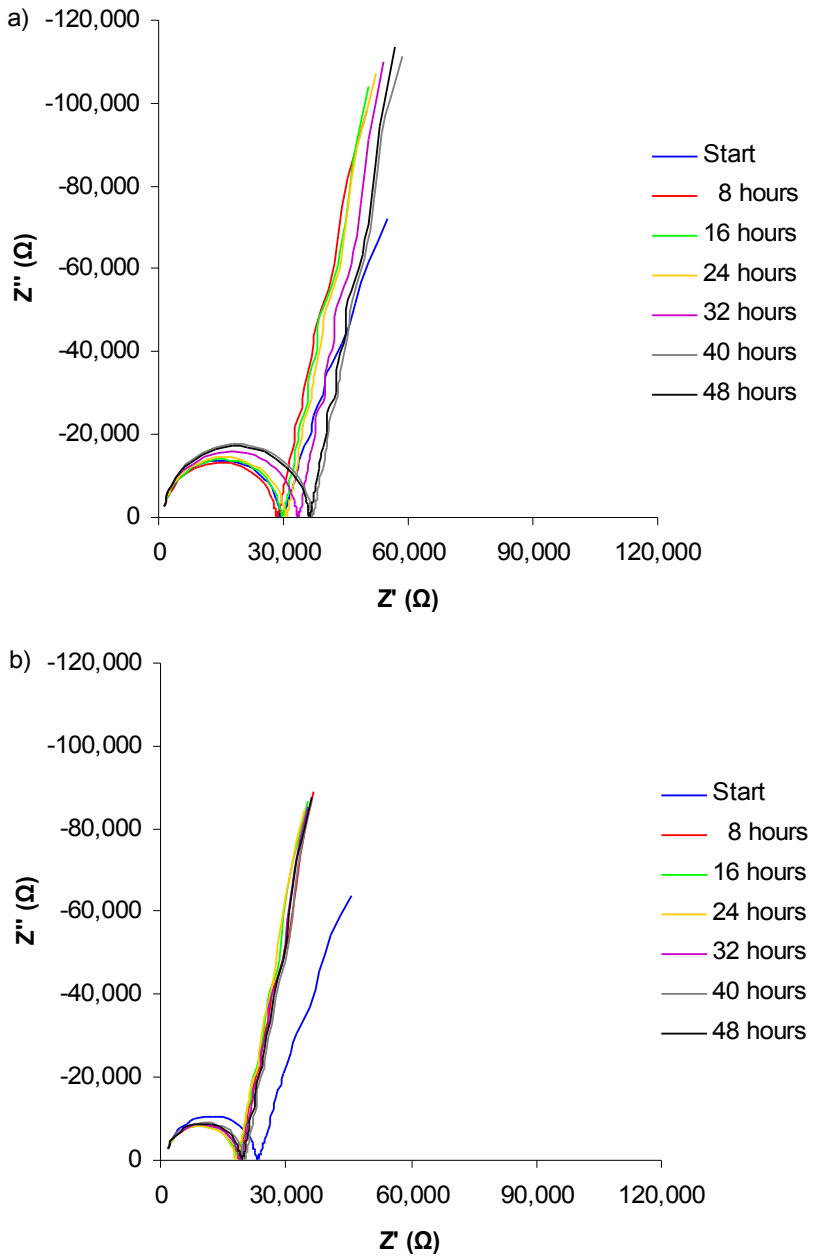

Figure 4-35. The z-plots for the biofilm with carbon sensor experiments: a) MHB-only; b) SA081.

The average component values for the double layer interface over the 48 hours for the biofilm experiment with carbon sensors are illustrated in Figure 4-36. In the MHB-only experiments the double layer resistance, R_{dl1}, rose steadily over time by 3.5kΩ. The R_{dl1} values for SA082 and NCTC11964 also increased by 4kΩ and 12kΩ respectively. These values are in agreement with the changes in the peaks discussed in Sections 4.5.3 and 4.5.4 where the NCTC11964 cells remain suspended in the liquid and there may be less SA082 cells adhered to the electrodes. Therefore it would be expected that the circuit components would be similar to the media. The higher increase with NCTC11964 may be related to the cells not attaching or differences in the products produced by metabolism. The SA081 R_{dl1} component decreases by approximately 4kΩ for the first 24 hours and then increases by 1kΩ for the remaining 24 hours. This agrees with the theory discussed in Sections 4.5.3 and 4.5.4 where it was predicted that the resistance and capacitance must become larger for the resistance peak to decrease.

The C_{dl1} values also indicate that the SA082 and NCTC11964 cultures were most similar to the MHB-only with decreases between $5.1x10^{-13}$ and $5.1x10^{-12}$ F. Again as predicted the SA081 C_{dl1} value is different and increased for the first 24 hours by $1.6x10^{-12}$ F and then decreases by $0.8x10^{-12}$ F for remaining 24 hours.

The diffusional processes at low frequencies are modelled by a constant phase element CPE_d that has two elements CPE_d-T which represents the pseudo-capacitance value and CPE_d-P which measures the closeness to an ideal capacitor. The average values of CPE_d-T and CPE_d-P over the 48 hours are illustrated in Figure 4-37. There are immediate and clear differences between the control system, MHB-only, and all three strains of bacteria. The MHB-only CPE_d-T decreased over the 48 hours by $0.6x10^{-5}$ and the CPE_d-P value increased by 0.07. For the bacterial cultures the general trend for CPE_d-T was a decrease except an increase occurred in both SA081 and SA082 for 8 to 9 hours between 10 and 20 hours in the experimental time. The average increases were $9.4x10^{-7}$ for SA081 and $1.5x10^{-5}$ for SA082. Similarly for NCTC11964 the CPE_d-T value increased by a mean of $1.12x10^{-6}$ over 6

hours between the hours of 8 and 14 in the experimental time. This was repeatable in 5 separate cultures of each strain and is the first indication that the carbon sensors with circuit modelling applied can distinguish the absence and/or growth of bacteria.

A corresponding decrease in the CPE_d-P occurred in all strains. For SA081 and SA082 the decrease occurred for 4 to 5 hours between the experimental hours of 13 to 21 hours with average decreases of $2.4x10^{-3}$ for SA081 and $1.2x10^{-3}$ for SA082. Similarly for NCTC11964 the CPE_d-P value increased by a mean of $3.9x10^{-3}$ over 5 to 6 hours between the experimental hours of 9 and 15 hours. Therefore the growth of bacteria are producing discernible differences in the circuit component values either by metabolised products or the actual cells altering the diffusional processes occurring at the electrode interface. The possible explanations are discussed further in Section 5.5.7.

The mean component values for the start and 48 hour measurements are listed in Table 4-11. The fit at the start and end were all very low at less than 1.1 with standard deviations between 0.04 and 0.27, which indicates an accurate fit of the data. The component errors were also extremely low with all components less than 1.2% except R_s which had errors less than 5.3%. The standard deviation across experimental runs were less than 1.2% for R_s and less than or equal to 0.2% for the remaining components. This indicates that the circuit model fits the data extremely well and given that the changes in the component values matches the predictions discussed in the impedance and normalised impedance section suggests that the model is valid for the carbon sensors in bacterial cultures.

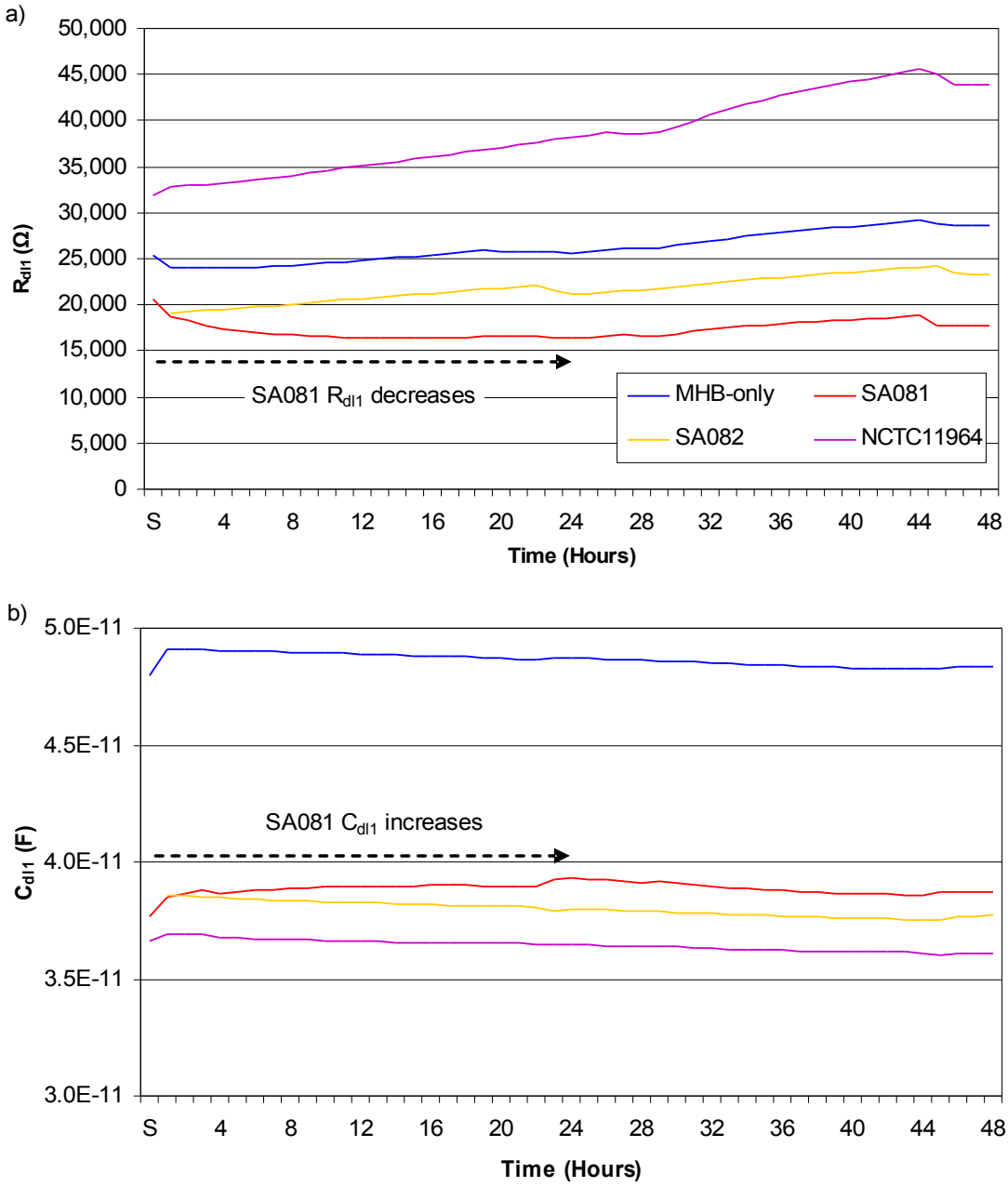

Figure 4-36. The interface parameters over time for the biofilm with carbon sensor experiments. a) R_{dl1} b) C_{dl1}.

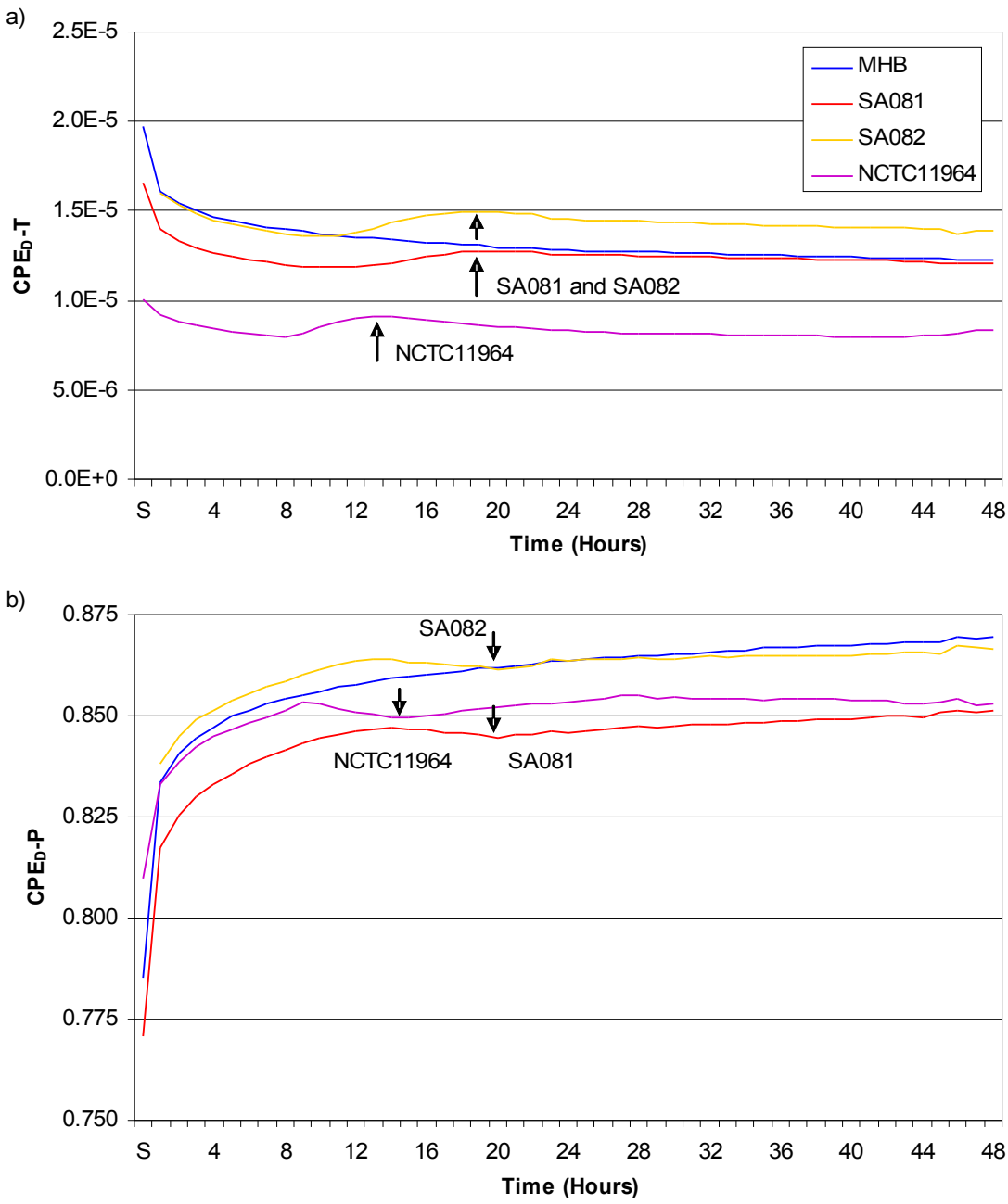

Figure 4-37. The CPE$_D$ parameters over time for the biofilm with carbon sensor experiments. a) CPE$_D$-T value b) CPE$_D$-P value.

Table 4-11. The mean circuit model component values from the biofilm experiments with carbon sensors for the start and 48 hour readings. The numbers in brackets indicate standard deviation.

Experiment	Component Value		Component error (%)	
	Start	48 hour	Start	48 hour
Fit (Weighted sum of squares)				
MHB	0.51 (± 0.27)	0.48 (± 0.10)		
SA081	0.30 (± 0.05)	0.40 (± 0.04)		
SA082	1.08 (± 0.07)	0.49 (± 0.05)		
NCTC11964	0.44 (± 0.15)	0.57 (± 0.12)		
Rs				
MHB	1,134 (± 281)	1,239 (± 59)	3.24 (± 1.14)	3.04 (± 0.35)
SA081	1,391 (± 40)	1,406 (± 34)	2.52 (± 0.21)	2.88 (± 0.14)
SA082	792 (± 79)	1,330 (± 31)	5.27 (± 0.07)	3.06 (± 0.20)
NCTC11964	1,314 (± 38)	1,282 (± 41)	3.16 (± 0.56)	3.50 (± 0.30)
Rdl				
MHB	25,375 (± 2,093)	28,710 (± 4,076)	0.34 (± 0.09)	0.32 (± 0.04)
SA081	20,552 (± 1,612)	17,776 (± 2,183)	0.30 (± 0.02)	0.35 (± 0.02)
SA082	19,052 (± 1,531)	23,370 (± 2,324)	0.49 (± 0.01)	0.33 (± 0.02)
NCTC11964	31,902 (± 7,754)	43,918 (± 11,103)	0.34 (± 0.06)	0.37 (± 0.03)
Cdl				
MHB	$5.3x10^{-11}$ ($\pm$ $1.1x10^{-11}$)	$4.8x10^{-11}$ ($\pm$ $2.3x10^{-12}$)	0.73 (± 0.16)	0.71 (± 0.11)
SA081	$3.8x10^{-11}$ ($\pm$ $2.1x10^{-11}$)	$3.9x10^{-11}$ ($\pm$ $2.1x10^{-11}$)	0.70 (± 0.04)	0.86 (± 0.04)
SA082	$5.1x10^{-11}$ ($\pm$ $2.9x10^{-11}$)	$3.8x10^{-11}$ ($\pm$ $2.1x10^{-11}$)	1.05 (± 0.04)	0.78 (± 0.06)
NCTC11964	$3.7x10^{-11}$ ($\pm$ $2.0x10^{-11}$)	$3.6x10^{-11}$ ($\pm$ $2.0x10^{-11}$)	0.73 (± 0.15)	0.74 (± 0.09)
CPEd-T				
MHB	$1.8x10^{-5}$ ($\pm$ $3.8x10^{-6}$)	$1.2x10^{-5}$ ($\pm$ $1.7x10^{-6}$)	0.82 (± 0.20)	0.77 (± 0.07)
SA081	$1.7x10^{-5}$ ($\pm$ $3.6x10^{-6}$)	$1.2x10^{-5}$ ($\pm$ $3.1x10^{-6}$)	0.62 (± 0.05)	0.66 (± 0.03)
SA082	$1.5x10^{-5}$ ($\pm$ $1.7x10^{-6}$)	$1.4x10^{-5}$ ($\pm$ $1.6x10^{-6}$)	1.18 (± 0.03)	0.75 (± 0.03)
NCTC11964	$1.0x10^{-5}$ ($\pm$ $3.5x10^{-6}$)	$8.3x10^{-6}$ ($\pm$ $3.6x10^{-6}$)	0.76 (± 0.12)	0.88 (± 0.08)
CPDd-P				
MHB	0.80 (± 0.03)	0.87 (± 0.005)	0.58 (± 0.09)	0.47 (± 0.05)
SA081	0.77 (± 0.02)	0.85 (± 0.01)	0.44 (± 0.04)	0.37 (± 0.03)
SA082	0.84 (± 0.01)	0.87 (± 0.01)	0.75(± 0.02)	0.45 (± 0.02)
NCTC11964	0.81 (± 0.01)	0.85 (± 0.01)	0.48 (± 0.07)	0.54 (± 0.07)

4.6 Summary of results – Biofilms

An electrochemical preconditioning procedure was developed that decreased the impedance behaviour at low frequencies of the screen-printed carbon sensors. This was performed to increase the possibility that the sensors would detect the bacteria adhering to the surface.

The formation of biofilms on the electrode surfaces was examined by an alamarBlue assay and by confocal laser scanning microscopy with a LIVE/DEAD *Bac*Light stain. These tests showed that: the growth of bacteria did not result in the formation of mature biofilms that were tens of micrometers in depth; the Ag-AgCl sensors prevented the adhesion and growth of bacteria on the electrode surfaces; and the carbon sensors did not effect the growth of bacteria compared to the control system.

The impedance profiles from the cultures of biofilm growth indicated that the Ag-AgCl sensors did not have discernible differences due to the lack of cell coverage on the electrode surfaces. The carbon sensors had better growth of the cells on the electrode surfaces with large numbers of cell clusters and cell cluster chains with the *Staphylococcus aureus* strains. The SA081 strain developed a greater coverage of viable cells than the SA082 strain. The S*taphylococcus epidermidis* strain NCTC11964 had a poor adherence to the surfaces. These differences in cell adhesion resulted in a number of different impedance profiles over frequency. The NCTC11964 strain had impedance profiles similar to the control system due to the lack of adhesion. Similarly the SA082 strain profiles matched the control system, possibly due to the lack of coverage of the electrodes. There were discernible differences in the impedance profiles of the SA081 strain, particularly in the normalised resistance. These changes are most likely caused by a better coverage of the cells on the electrode surface or production of different chemicals.

The equivalent circuit modelling of the cultures with carbon sensors showed discernible differences between the control system and all three bacterial strains. This could be used as a means of detecting the presence or absence of bacteria. The implications of all the biofilm results are discussed in Chapter 5.

5 Analysis and discussion

The final chapter analyses and discusses the methodology, the knowledge gained from the results and the relevance of the results for achieving the original objective. The conclusion states the main findings, their significance and suggestions for future work.

5.1 Selection of electrode material

The initial experiments involved impedance experiments with different types of electrodes and media, and the growth of bacteria in the presence of different electrode materials. It was important to find an electrode material that had low impedance that would not mask the impedance changes due to the bacteria and a material that did not adversely effect the growth of bacteria otherwise it would be difficult to detect them.

5.1.1 Analysis of electrode materials and media

The impedance curves from the silver-silver chloride (Ag-AgCl) wire electrodes (Figure 3-1) reveal the differences in the number and type of charge carriers in each of the media. The conductivity, σ, of a solution under an electrical field is proportional to the ionic concentration, c, and the mobility, u, of an ion species as shown in Equation 5-1 where F is Faraday's constant and z is the valence number of the ion.

$$\sigma = zFcu \tag{5-1}$$

Thus the total conductivity is the sum of the conductivities of the individual ion species. Conductivity is the reciprocal of resistivity and the solution resistance is proportional to its resistivity as shown in Equation 1-15. Therefore the solution resistance is also proportional to the ionic concentration and ion mobility. Since Solution A has a lower solution resistance, than Mueller-Hinton broth (MHB), it has a higher ionic concentration and/or ions with more mobility. This is due to Solution A containing only ions while the MHB is composed of beef infusion, casein

hydrolysate and starch. The MHB and Solution A combination has a lower resistance than Solution A as it contains a higher concentration of ions due to the combined total of the charge carriers in Solution A and MHB.

The dispersion region(s) as discussed in Section 1.5.3 are mainly caused by the double layer effect at the electrode-solution interface which influences charge transfer resistance and the double layer capacitance. As previously stated the resistance is proportional to the ion concentration and mobility. The capacitance is inversely proportional to the thickness of the double layer as shown by Equation 1-16. The thickness of the double layer, known as the Debye length, k^{-1}, is inversely proportional to the square root of the ionic strength, I, as given in Equation 5-2.

$$k^{-1} \propto \frac{1}{\sqrt{I_s}} \tag{5-2}$$

The ionic strength, I, of a solution is the sum of all ions present and is given by Equation 5-3 where c is the ionic concentration and z is the valence number of the individual ion species.

$$I_s = \frac{1}{2}\sum_{i=1}^{n} c_i z_i^2 \tag{5-3}$$

Therefore the charge transfer resistance is proportional to the concentrations and mobilities of the ions, and the double layer capacitance is proportional to the ionic concentration. Having established that the ion concentration of Solution A is higher than that of MHB, it can be seen that this produces a smaller charge transfer resistance and a smaller capacitance. Hence, the Solution A has the smallest dispersion and MHB has the largest. The MHB and Solution A combination produces a dispersion(s) between Solution A and MHB due to the combined properties of each individual medium. There may also be capacitance within the solutions of MHB, and the MHB and Solution A combination, for example, molecules rotating to orientate themselves within the electric field. However, this is improbable since it generally occurs in the MHz frequency range (Foster & Schwan, 1989).

The impedance of the electrode materials in MHB (Figure 3-2) provide information about their differing physical performance. The magnitude at 0.1Hz of the platinum and silver wire electrodes was a factor of more than 10 times higher when compared with the Ag-AgCl wire electrodes. This is caused by diffusion processes at the electrode surface which produce a pseudo-capacitance effect (Bard & Faulkner, 2001). The decreased capacitance can be seen with the maximum phase angle of the platinum and silver wire electrodes approximately 30^{o} more than the Ag-AgCl wire electrodes.

The Ag-AgCl sensor when compared to the Ag-AgCl wire electrode showed the solution resistance to be 184Ω higher and a maximum magnitude 6.6kΩ higher than the Ag-AgCl wire electrode. These are caused by the difference in layout and structure of the electrodes. The phase angle was only 8^{o} higher than the Ag-AgCl wire electrodes which indicates that the diffusion processes are kept to a minimum.

The carbon sensors produced a high frequency plateau, 15.8kΩ at 10kHz, and this was caused by a high charge transfer resistance, mainly due to the high track resistance of the electrodes. The second dispersion at less than 100Hz and the corresponding phase angle peak were caused by diffusion processes, similarly to the platinum and silver wire electrodes.

5.1.2 Bacterial growth with electrode materials

The final numbers of bacteria after culturing from starting cell densities of approximately $1x10^6$ CFU ml^{-1} indicated that the type of electrode material may have an effect on bacterial growth (Figures 3-3 and 3-4). There was no apparent growth inhibition of the *Staphylococcus aureus* strain, RN4220, with silver wire electrodes. One final count was several orders of magnitude lower than the other two, however this was likely to be caused by an unclean electrode or a reduced inoculation level. The growth of RN4220 was inhibited by the Ag-AgCl wire electrodes and the screen-printed Ag-AgCl sensors on acetate (Ag-AgCl-acetate). On average the final cell numbers with Ag-AgCl wire electrodes and Ag-AgCl-acetate sensors were respectively 10 times and 10,000 times lower than the controls. The *Staphylococcus aureus* strains, RN4220, SA081 and SA082 were not inhibited by the screen-printed Ag-AgCl sensors on the polyethylene substrate (Ag-AgCl-PE100).

Silver ions are well known to inhibit bacterial growth and has been reported to interact with a number of different molecules as described by (Percival *et al.*, 2005). These include: silver ions binding to the cell surface with toxic effects and inhibition of the respiratory transport chain (Bragg & Rainnie, 1974); silver ions interfering with the respiratory chain, collapsing the proton motive force, interfering with specific carriers and inhibiting the uptake and exchange of phosphate (Schreurs & Rosenberg, 1982); silver ions inhibiting the uptake of succinate in membrane vesicles derived from *Escherichia coli* (Rayman *et al.*, 1972); and silver ions have also been shown to effect the production of *Staphylococcus aureus*' exotoxins, although this was strain dependent (Edwards-Jones & Foster, 2002). The role of DNA and silver ion interaction in bacterial growth inhibition remains unclear (Percival *et al.*, 2005). Rosenkranz and colleagues concluded that silver-DNA interaction was not the anti-bacterial mechanism (Rosenkranz & Carr, 1972); (Rosenkranz & Rosenkranz, 1972), whereas Modak and Fox (1973) continued to press the important of DNA interaction. The main mechanism of bacterial growth inhibition by silver ions is generally agreed to be cell membrane damage and damage to associated proteins (Clement & Jarrett, 1994).

In addition to the silver ions, silver salts have been shown to enhance or diminish the mechanism of silver inhibition depending on the concentration of the anions (Gupta *et al.*, 1998); (Silver, 2003). In a medium containing low concentrations of chloride ions the silver ions accumulate in the cells and bind to essential proteins and enzymes (Ghandour *et al.*, 1988). At medium concentrations of chloride ions the silver is precipitated as AgCl and at higher concentrations of chloride ions the silver ions become available again due to the production of $AgCl^{2-}$ (Gupta *et al.*, 1998); (Silver, 2003).

Given the known effects of silver ions on bacteria one possible explanation for the differences in growth in the presence of electrodes is the stability of the electrode materials. The silver wire electrode may be stable and not release silver ions into the media, hence there was no inhibition. The Ag-AgCl wire electrodes and Ag-AgCl-acetate sensors might be less stable than the Ag-AgCl-PE100 sensors and therefore may have released silver ions into the media that caused the inhibition of the bacterial growth. This may or may not have been enhanced by the presence of chloride ions. Other possible explanations for the inhibition are impurities on the Ag-AgCl wire electrodes and chemical impurities from the acetate leaching into the media. The inhibition of bacterial growth by silver ions is further discussed in Section 5.3.1 on the growth of bacteria from lower starting cell densities.

The *Escherichia coli* strain, JM109 had a decreased growth behaviour in the presence of the Ag-AgCl-PE100 sensors with the final cell density on average 1000 times lower than the control. This is in agreement with studies comparing the effects of silver on *Escherichia coli* and *Staphylococcus aureus*. Feng *et al.* (2000) showed that 10 $\mu g\ ml^{-1}$ of silver nitrate on *Escherichia coli* caused the DNA to condense, granules to appear around the cell wall and DNA, and the cytoplasm membrane to detach from the cell walls. The effects on *Staphylococcus aureus* were similar with a detached cytoplasm membrane, however the cells were still intact and the granules were smaller. Jung *et al.* (2008) also concluded that the action of silver was better

against *Escherichia coli* than *Staphylococcus aureus* due to cell membrane degradation and in addition suggested that the silver prevents growth but does not kill the bacteria completely.

There was no apparent inhibition of RN4220 or JM109 with the carbon sensors on the substitute polyethylene substrate (C-PE200). Studies on the bacterial inhibition by carbon have concentrated on activated charcoal which is carbon that has been modified to be very porous. It has been reported that *Escherichia coli* O157:H7 and toxin have been removed by activated carbon in vitro and in vivo (Knutson *et al.*, 2006); (Naka *et al.*, 2001). It appears that the screen-printed sensors are probably not inhibiting the bacterial growth in suspensions of *Escherichia coli* and *Staphylococcus aureus*.

5.1.3 Electrode material conclusion

These experiments provided a simple way to examine the impedance characteristics of electrode materials and the effects of electrode materials on bacterial growth. The results indicated that there are differences in the impedance behaviour of different electrode materials and that the bacterial growth could be affected by the presence of certain electrode types. Improvements to the methodology would be to increase the sample size since three samples was statistically low. In this project the screen-printed sensors were designed as disposable and were discarded after each experiment. There was a limited supply of polyethylene substrate and therefore the number of sensors used in each experiment was kept to a minimum.

It was important to find a suitable material for the infection monitor application in terms of impedance and inhibition. The Ag-AgCl electrodes had the lowest magnitude and phase when considering the whole frequency range from 1MHz to 0.1Hz, plus they do not inhibit the strain of *Staphylococcus aureus* when grown from a high starting cell density. The carbon sensors had no growth inhibition of the *Staphylococcus aureus* strains or the *Escherichia coli* strain, however their impedance characteristics were relatively high. Consequently the Ag-AgCl sensors and the carbon sensors were selected for the impedance experiments.

5.2 Impedance – single suspensions of bacteria

The growth of RN4220 in Mueller-Hinton broth (MHB) with impedance measurements was performed with Ag-AgCl sensors and carbon sensors. The impedance measurements were analysed for two reasons. Firstly to identify differences in the impedance profiles over frequency and/or frequencies that peaks in the profiles occurred at, which then could be used for the detection of bacteria. Secondly, and in conjunction with the equivalent circuit modelling, to examine the changes over time to provide information on the physical processes occurring in the biological system.

5.2.1 Analysis of the Ag-AgCl impedance data

Peaks in the impedance traces over frequency that could differentiate between the absence and presence of bacteria were the main point of interest in the analysis of the data. Peaks in the magnitude, phase angle and reactance traces occurred in the data from the single suspension experiments with the Ag-AgCl sensors (Table 3-2). The resistance peak was poorly defined and occurred at frequencies close to 0.1Hz. The impedance magnitude peak generally decreased over time and occurred at frequencies between the resistance peak and the reactance peak. The reactance peak value increased over time and occurred at frequencies between 1 and 5Hz. There were no discernible differences in these peaks between the control system and the bacterial culture that could be used in a detection system.

The first indication that the signature trace over frequency could be used to differentiate between the absence and presence of bacteria was observed in the phase angle. The phase peak and subsidiary peak (Figure 3-6) relate to two dispersions most probably two different double layers at the electrode-media interfaces. The frequency of these peaks decreased over time in MHB only and may be due to oxidation of the electrode surface producing a change in the capacitance of the double layer. In the RN4220 culture the presence of the cells may affect the double layers, firstly by altering the capacitance of the peak and secondly by decreasing the phase angle on the subsidiary peak. The cells may also be changing the capacitance

of the subsidiary peak, however this would require the cells to decrease the capacitance of the peak and increase the capacitance of the subsidiary peak which seems improbable.

The change in capacitance of the peak requires either the relative static permittivity to decrease, the area to decrease or the distance to increase. Physically a number of situations are possible, the cells could be reducing the area involved in the double layer formation, the cells could be increasing the width of the double layer, or the metabolism of nutrient molecules to smaller and more conductive ones may be altering the double layer characteristics. The physical explanation for the reduction in phase angle of the subsidiary peak requires the double layer resistance to decrease and this may be related to the metabolism of nutrients. An increase in conductivity of bacterial cultures was previously explained by changes to smaller and more highly charged molecules in the media (Firstenberg-Eden & Eden, 1984).

5.2.2 Analysis of the Ag-AgCl normalised impedance peaks

The impedance data was normalised to remove differences in individual sensors and to show relative changes from the starting condition. Again the main interest was peaks in the normalised impedance traces over frequency that could differentiate between the absence and presence of bacteria. In the single suspension experiments the final impedance measurement before inoculation was used as the starting reading in the calculation of the normalised data. This was to ensure all vials were normalised to a measurement performed without bacteria in the medium. The disadvantage was that the sensor had to be removed to perform inoculation which meant that any conditioning on the surface of the electrodes was disrupted.

There was no statistical differences in the normalised peaks between the control system of MHB-only and the bacterial culture of RN4220 (Table 3-3). However the normalised phase angle traces over frequency do have discernible differences due to the presence of bacteria. An example is illustrated in Figure 5-1 for normalised phase plots. The control system, MHB-only shows a peak at 2Hz while one RN4220 culture shows a peak at 20Hz due to the bacterial growth. Unfortunately in another RN4220 culture the peak shows at 2Hz with a secondary peak at 20Hz. The removal of the sensor may have caused the differences between individual normalised plots. If the sensor had not been removed the uneven characteristics at less than 10Hz may not have occurred and there would have been a 100% consistent difference in the normalised phase angle trace due to the bacterial growth. The 20Hz peak does however remain attributable to bacterial growth.

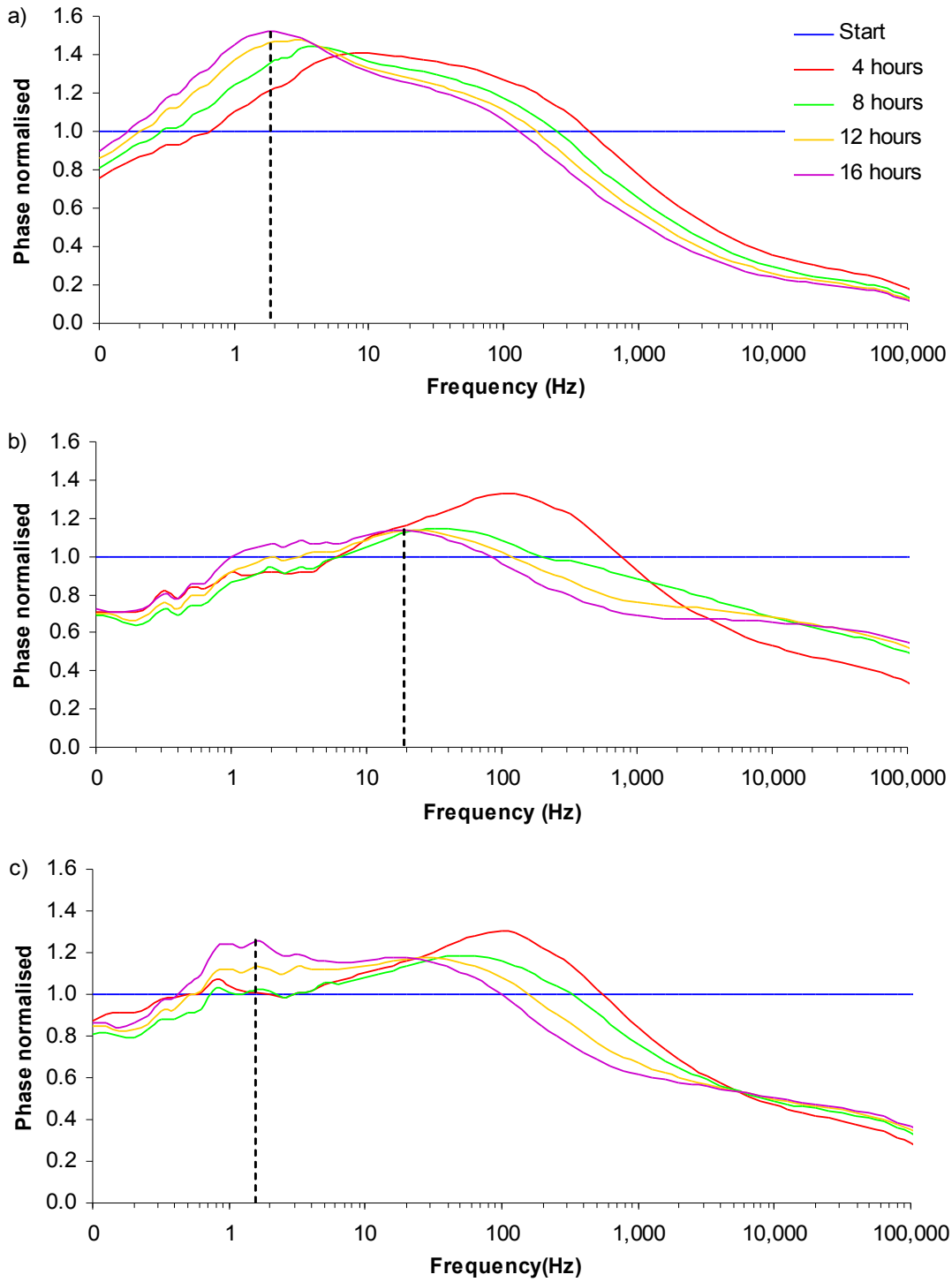

Figure 5-1. Differences in normalised phase peaks: a) MHB only; b) RN4220 culture 1; c) RN4220 culture 2. Dotted line indicates normalised phase peak.

5.2.3 Interpretation of the Ag-AgCl equivalent circuit

The changes over time in the average impedance data of the Ag-AgCl sensors (Table 3-4 and Figure 3-12) have been attributed to possible physical changes in the system. All three resistances, R_s, R_{dl1} and R_{dl2} decrease in the first three hours due to the stabilisation of the electrodes. In MHB only the R_s and R_{dl1} values remain stable which agree with a stable solution resistance and a stable double layer, however the R_{dl2} value rises over time while the actual data indicates a decrease in resistance of the second dispersion. The simulated data does not fit the actual data closely at low frequencies and therefore the R_{dl2} values are compensating to achieve the best fit, hence the lack of agreement. This may indicate that further work needs to be done in developing the circuit model and its components. The decrease in the actual charge transfer resistance may be due to oxidation of the electrode and an increase in charge carriers in the solution, hence increasing the ease at which the charge can transfer to and from the electrodes.

The resistance values for RN4220 culture stabilises for the first three hours and then R_s is stable which agrees with the impedance data. The R_{dl1} component decreases further than without bacteria and is associated with the subsidiary peak which confirms that the decrease in phase angle of the subsidiary peak is associated with a resistance decrease. The R_{dl2} component also decreases further than without bacteria and then rises over time. The oxidation effect could still be valid, however the metabolism by the cells increases the number of ions and converts charge carriers in the media to smaller sizes and more charged (Firstenberg-Eden & Eden, 1984). This will increase the ease of charge transfer, hence the larger decrease in impedance. The increase in the R_{dl2} component in the later half of the experiment may be related to the increased number of cells located within the vicinity of the electrode surface and blocking the areas used for charge transfer.

The mathematical model for bacterial growth produced by Firstenberg-Eden and Eden (1984) and described in Section 1.7.1 is based on bacteria producing ions during growth and after a specified time the increased number of ions produces an increase in the conductance of the system. The point the increase occurs at is called

the detection time. The conductance is governed by the resistance in the system and therefore the charge transfer resistances, R_{dl1} and R_{dl2} , from the Ag-AgCl equivalent circuit show a similar detection points where the resistances decrease below the level of the controls. If a number of parameters, for example, the generation time for the bacteria were known then the numbers of bacteria at the start could be determined by the mathematical model. The intended bacteria monitoring system, described in this thesis, would have unknown samples which would make it difficult to determine the starting cell density. However, the charge transfer resistor values (R_{dl1} and R_{dl2}) over time have discernible differences that could be used for tracking the growth or presence of bacteria in a monitoring system.

The MHB-only capacitance values rise over time which indicates the double layers were altering over time, from for example oxidation of the electrode surface. The capacitance values for RN4220 culture also rise over time with C_{dl2} rising less than in the media only and this relates to the impedance phase peak shifting to a higher frequency, hence the lower capacitance. Felice and colleagues have also suggested that bacterial cells cause additional reactance in the system (Felice *et al.*, 1992); (Felice & Valentinuzzi, 1999).

5.2.4 Analysis of impedance data from the MHB-glucose experiments

The impedance suspension experiments with Ag-AgCl sensors were repeated with 0.2% (v/v) glucose added to the MHB. In comparison to the experiments without glucose there were noticeable differences between the controls and the bacterial cultures in the normalised impedance magnitude data (Table 3-3). The impedance measurements show at 17 hours two normalised impedance magnitude peaks in the MHB-glucose-only experiments, one less than 4Hz and the other between 200 and 1.3kHz (Figure 3-8). In contrast the RN4220-glucose culture shows a third magnitude peak between 2.5k and 6.3kHz. The RN4220-glucose magnitude peak starts with the second peak which disappears between 4 to 9 hours with the third peak appearing one hour later. It has been shown that the available nutrients, including carbon have an influence on the structure and composition of *Staphylococcus aureus* cell walls (Dobson & Archibald, 1978) and it has been

suggested that the metabolism of glucose to lactic acid and then to carbonic acid may produce changes in the impedance of bacterial cultures (Firstenberg-Eden & Eden, 1984). Therefore this additional peak in the normalised impedance trace may be caused by a change in cell structure or due to a metabolised product.

There was also a clear consistent difference in the frequency of the normalised phase angle peak between the control system and bacterial cultures with glucose in the media (Figure 3-9). The normalised phase angle peak for MHB-glucose-only was between 1.62 and 2Hz at 17 hours while the RN4220-glucose peaks were all above 10Hz. This confirms that there is potential for a bacteria monitoring system that uses signature traces over frequency to differentiate between the absence and presence of bacteria, especially the phase angle or the normalised phase angle traces. The availability of nutrients may be restricted in a host (Brown & Williams, 1985) and therefore the signature traces as a result of the bacteria-glucose interaction may not occur in an actual wound.

The equivalent circuit modelling of the impedance measurements for MHB-glucose-only and the RN4220-glucose cultures with Ag-AgCl-PE100 sensors were very similar to those without glucose. This provides further evidence that a suitable circuit model was selected and that the changes over time in the charge transfer resistor values could be used to track the presence of bacterial growth.

5.2.5 Analysis of carbon sensor experiments

The suspension experiments were repeated with carbon sensors, however the high resistance of the electrodes produced a high impedance characteristic and this masked any changes that might have occurred due to the growth of bacteria. In addition the carbon sensors were highly unstable with the maximum resistance increasing for example by 767kΩ and the maximum reactance decreased by 200kΩ over 17 hours. Comparing this to the carbon sensors used in the biofilm experiments, for example, the maximum resistance decreased by 2kΩ and the maximum reactance decreased by 37kΩ. This implies that the suspension experiments with carbon sensors were compromised by unstable electrodes.

The carbon sensors were manufactured on the first of the substitute polyethylene substrates (-PE200). The carbon appeared to bond to this surface while it was unsuitable for the Ag-AgCl ink. Therefore possibly the carbon was released once it was submerged. Alternatively the carbon preconditioning of the sensors for the biofilm experiments removed any loose carbon and made them stable.

5.2.6 Conclusion of the single suspension impedance experiments

These initial impedance measurements of *Staphylococcus aureus* cultures provided information on the physical processes occurring over time and in the presence of bacteria showed discernible differences in the impedance characteristics. The proposed circuit model for Ag-AgCl sensors agrees with many of the suggested physical changes that the impedance measurements indicated and therefore must be close to a good model. However the differences between the simulated data and actual data at low frequencies indicated that either additional components are required or that electrical components cannot accurately model this system at these low frequencies. The most significant finding from the equivalent circuit modelling is that the changes over time in the charge transfer resistor values have the potential to be used in a bacterial detection system. They could indicate the presence of bacterial growth from high cell densities within 5 to 6 hours.

It is difficult to compare this study with the early studies by Ur and Brown (1975), Cady (1975) and Richards *et al.* (1978) due to differences in methodology and equipment. The studies produced changes in impedance that followed the standard bacterial growth curve whereas in this study the data was not analysed for this. In addition Cady (1975) produced characteristic curves over time for a number of different species of bacteria. Firstenberg-Eden and Eden (1984) also produced characteristic curves for different species plus a mathematical model for calculating the starting cell density. The limitations of these systems is that they required controlled conditions to reproduce the curves and parameters known about the bacteria to calculate the cell densities.

In wounds the bacteria will be unknown and the environment uncontrolled, therefore characteristic curves with peaks at unique frequencies would provide a more reliable detection method. These experiments provided the first evidence that the sensors could be used for the detection of bacteria by electrical impedance methods, at least of high cell densities. The frequency of the phase angle peak with Ag-AgCl sensors can be used to detect the presence of bacteria at high cell densities after 12 hours. If alternative species were tested and the frequency of the phase angle peak occurred at a different frequency to the one the *Staphylococcus aureus* strain produced, then the system could have the potential to differentiate bacterial species. The frequency of the normalised phase peak could also be used if the ripples at low frequencies could be eliminated. Another application would be a laboratory based system which could have a more controlled environment and use glucose to enhance the discernible differences between the absence or presence of bacteria.

A number of changes and improvements to the methods were instigated in subsequent experiments. Firstly lower inoculation densities were used because in some clinical scenarios it would be useful to detect lower numbers of cells. In the parallel suspension experiments the test vials housing the cultures and sensors were modified to avoid removing the sensor for inoculation. Finally before the biofilm experiments the carbon sensors were made more stable because their unstable characteristics had possibly negated any discernible differences.

5.3 Suspensions – Lower inoculation densities

The starting cell densities of approximately $1x10^6$ CFU ml^{-1} in the single suspension experiments was deemed to be possibly too high for some clinical applications, for example, bacterial levels of $1x10^4$ or $1x10^5$ CFU per tissue gram are often quoted as the critical colonisation before an infection begins (Bowler *et al.*, 2001). Therefore further bacterial growth experiments and impedance experiments were performed with lower starting cell densities to investigate whether the electrode material was suitable for lower densities and that the impedance could still detect the bacteria.

5.3.1 Bacterial growth with lower inoculation densities

Despite the strains of *Staphylococcus aureus* growing normally in the presence of Ag-AgCl-PE100 sensors from a single colony, growth rates were variable when grown from different cell densities from approximately $1x10^2$ to $1x10^5$ CFU ml^{-1} (Figure 3-19). It was hypothesised that the concentration of silver ions released was possible too great for the smaller number of cells at inoculation to establish normal growth rates. A number of experiments were performed to try and establish whether this hypothesis was correct.

The growth of all three strains of *Staphylococcus aureus* with pre-washed electrodes reached the control growth levels (Figure 3-20). This could suggest that an electrochemical stabilisation occurred where silver ions were released into the media used for pre-washing and then normal growth occurred after inoculation in fresh media. Alternatively the pre-washing removed any chemical impurities, for example, solvents used in the manufacturing of the sensors.

The bacteria grown previously with Ag-AgCl sensors had low growth levels when grown in the presence of Ag-AgCl sensors for a second time (Figure 3-21). This probably indicates that when the bacteria grow to the same cell numbers as the controls they are not becoming resistant to the silver ions. Silver resistant bacteria have been found in environments containing silver, for example burn units (Silver *et al.*, 1999), however exposure times tend to be significantly longer then the 24 hours used in this investigation. The cells might even be damaged hence the low growth

rates with the second electrode. This observation is in accordance with Feng *et al.* (2000) who concluded that the *Staphylococcus aureus* cell membranes were damaged, although the cells were still intact.

The mechanisms and effects of silver on bacteria were discussed in Section 5.1.2 and the experiments from lower starting densities could indicate that the ratio of silver ion concentration to cell numbers is higher, hence the apparent inhibition of growth. Other explanations are the release of chemical impurities, and possible clumping of bacteria leading to a higher inoculation density than perceived. The differences in individual electrode pairs could be caused by the old screen-printing mask used in the manufacturing procedure where the mesh defining the electrode outline was beginning to fill in at the edges of some of the electrodes.

5.3.2 Analysis of parallel suspension impedance experiments

These impedance experiments were performed to investigate the effect on the signature traces of lower starting cell densities, glucose concentration and pre-washing of the Ag-AgCl sensors. There was wide variation in the final cell densities of RN4220 after 16 hours with all the varied parameters (Figure 3-22). They are several possible explanations for the differences in cell densities observed. In all three experimental runs the RN4220-glucose-0.2% culture reached the levels of control which could be related to a glucose concentration for an optimum growth rate. The pre-washed sensors reached the control levels in two of the three experimental runs possibly indicating that pre-washing is a solution to the inhibition. The one pre-washed sensor that did not achieve the control levels of growth may have been poorly washed. Another possibility for the range of cell densities is that the impedance measurements were having a detrimental effect on the bacterial growth which was explored further in a subsequent experiment.

The differences in the final cell densities irrespectively of the media type or the preparation of the sensor highlighted that the discernible differences in the phase angle signature traces over frequency between the absence and presence of bacteria occurs at a critical cell density. That is in the 7 of the 24 vials where the density

reached in excess of $5x10^7$ CFU ml^{-1} by comparing the phase angle signature traces, the vials with high cell densities could be differentiated from low cell densities and media only (Figure 3-25). The comparison of the frequency of the phase angle peak was less reliable than comparing the signature traces. In six of the eight vials that reached in excess of $8.5x10^6$ CFU ml^{-1} had peaks occurring at frequencies above 13Hz giving a 91.3% agreement with a proposed difference in phase angle peak frequency once the critical cell density is reached (Table 3-6). The two vials that disagree could either be due to variations in electrode pairs or a false final cell density. In addition the effect of the bacteria growing from a lower density may affect how the electrodes behave, for instance, if the low frequency phase peak becomes established before the bacteria reach high densities then the phase peak may not shift back to the high frequency.

As explained in Section 3.5.2 there was two types of phase angle profiles for the starting measurement (Figure 3-24) which produced differences in the normalised impedance magnitude profiles (Figures 3-27 and 3-28). Given that in the single impedance experiments, in a media of only Mueller-Hinton broth, no significant differences were seen in the normalised magnitude plots these contrasting start measurements had little effect. The possible explanation for these differences were that two different batches of sensors were used in the parallel suspension experiments. Plausible causes for the batches of sensors being different are: the sensors are now on the substitute polyethylene (-PE300); the sensors have not been kept for a year in a box; and the Ag-Ag-Cl ink was not brand new. If these Ag-AgCl sensors were to be used in a bacterial monitoring system then the impedance characteristics would have to be repeatability. Therefore the creation of a consistent manufacturing procedure would be essential.

The equivalent circuit modelling of the parallel suspension impedance data shows similar changes over time when compared with the single suspensions (Figure 3-2- and Table 3-7). The resistors, R_{dl1} and R_{dl2} that represent the double layer resistance both decrease more in the presence of cell densities greater then $5x10^7$ CFU ml^{-1} than those with no bacteria or less than this critical density. This confirms that changes of

the interface impedance are probably caused by the presence of large numbers of cell densities or their corresponding large volume of products from metabolism. The decrease in the resistor values occurred after 8 to 9 hours compared with 5 to 6 hours in the single experiments which highlights the lower starting cell density and time required to reach the critical point where changes are observed.

5.3.3 Analysis of the influence of impedance measurements on growth

All the strains of *Staphylococcus aureus* were grown with and without impedance measurements to discover whether the measurements had an effect on their growth. The strain RN4220 appears to grow as expected without impedance measurements, however not with impedance measurements which could indicate that either the measurements are causing more silver to be released into the media or the electric current is damaging the cell membranes. Inhibition of bacteria by electrical stimulation generally uses constant currents or high voltage pulsed currents for prolonged periods, for example, hours or days (Kloth, 2005). Also an alternating current did not inhibit *Escherichia coli* compared with a direct current (Rowley, 1972). Therefore it would seem unlikely that the alternating current that is applied for approximately 2 minutes every hour has an effect.

The clinical strains, SA081 and SA082, grew to expected levels in some vials and not in others (Figure 3-31), similar to the bacterial growth experiments (Figure 3-19). In samples 3 and 4 for SA082 the growth did not reach control levels with or without impedance measurements. The starting cell densities were 80 to 760 CFU ml^{-1} less than in samples 1 and 2 which may indicate there was a critical cell density at approximately 1000 CFU ml^{-1} where cell densities below this will not grow as expected. The explanations given for RN4220 could also be valid, however the cell membranes of the SA082 strain could be more robust hence their ability to grow to expected growth levels with impedance measurements in 50% of the experiments.

The impedance peaks and the normalised peaks were similar to the parallel suspension experiments. Again the phase angle signature traces over frequency could detect the presence of cell densities over $5x10^7$ CFU ml^{-1} (Figure 3-22) while the

frequency of the phase angle peak was less reliable (Table 3-7). The phase peaks for two of the RN4220 test vials indicate that they should contain a high cell density, however the final count disagrees. The equivalent circuit modelling of the two SA082 cultures that reached final cell densities in excess of $5x10^7$ CFU ml^{-1} also showed that once a critical cell number is reached the double layer resistances decrease with a corresponding decrease in the double layer capacitors. The importance of this is that the signature traces and circuit modelling can indicate the presence of high cell densities for multiple strains of *Staphylococcus aureus.*

5.3.4 Conclusion of lower inoculation density experiments

As previously discussed in Section 5.1.2 silver ions can inhibit bacterial growth. The silver ions could be damaging cells which then have to repair themselves, slowing metabolic rates, or by killing a percentage of cells over time. This effect is more apparent at lower inoculation densities due to the increased ratio of cell numbers to concentration of inhibiting substance. Therefore silver ions are a strong candidate for the variation in final cell densities. Other explanations have previously been described in Section 5.1.2.

The impedance experiments showed that the the growth of multiple strains of *Staphylococcus aureus* produced a change in frequency of the phase angle peak once the cell densities exceeded $8.5x10^6$ CFU ml^{-1} or a change in the phase angle profiles over frequency when cell densities exceeded $5x10^7$ CFU ml^{-1}. These densities are in accordance with earlier studies of bacteria growth with impedance (Eden & Eden, 1984). Unfortunately the differences in the frequencies of peaks from low inoculation densities was less reliable due to more false negatives and positives. The signature traces over frequency are more reliable to indicate the absence and/or presence of bacteria, however this would require a control system to compare traces. This would not be possible in an actual wound, while the signature traces could be used in a laboratory based detection system.

General issues to consider that might produce better results are to pre-wash the sensors, treat the electrodes by electrochemical procedures to try and stabilise them, and reduce the number of impedance measurements performed. This could ensure that all the sensors produce the same level of inhibition and have the same impedance characteristics.

Another consideration is whether in an actual wound detecting $5x10^7$ CFU ml^{-1} would be adequate or actually be a late warning system given that infections are more likely to occur at cell densities greater than $1x10^5$ CFU per gram of tissue (Bowler *et al.*, 2001). Correlations between swap cultures and tissue biopsies have been shown, for example, $1x10^5$ CFU per gram of tissue is equivalent to approximately $5.9x10^5$ CFU per swap of a square centimetre (Levine *et al.*, 1976). However, it is still unclear how bacteria levels per tissue gram or per cm^2 would relate to a detection system that indicates $5x10^7$ CFU ml^{-1}. The levels of bacteria in a wound must be evaluated with other important factors, including bacterial virulence and host resistance (Schultz *et al.*, 2003). Therefore valuable information given by an infection monitoring system for wounds could be to indicate, like semi-quantitative swaps, the growth between light (1+) and profuse (4+) cultures (Bowler *et al.*, 2001). This would provide information to the healthcare personnel that could be used in addition to other factors to select the most appropriate treatment options. The bacterial levels in a wound are further complicated by the present of biofilms, which are discussed in Section 5.5.

5.4 Carbon preconditioning

The performance of carbon electrodes can be improved by electrochemical preconditioning (Blaedel & Jenkins, 1974); (Blaedel & Mabbott, 1978); (Cui *et al.*, 2001); (Gonon *et al.*, 1981); (Wang *et al.*, 1996). Methods vary between positive potentials, potential cycling between positive and negative amplitudes and AC waveforms. The amplitude and duration of applied potentials also varied. Most studies examined the performance improvement by cyclic voltammetry. Cui et al. (2001) investigated the impedance of screen-printed carbon sensors after applying positive potentials between 1 and 2 volts and for durations between 0.5s and 20 minutes. The electrode interface consisting of the double layer was reduced by increasing the applied potential and time, however the diffusional processes became more pronounced.

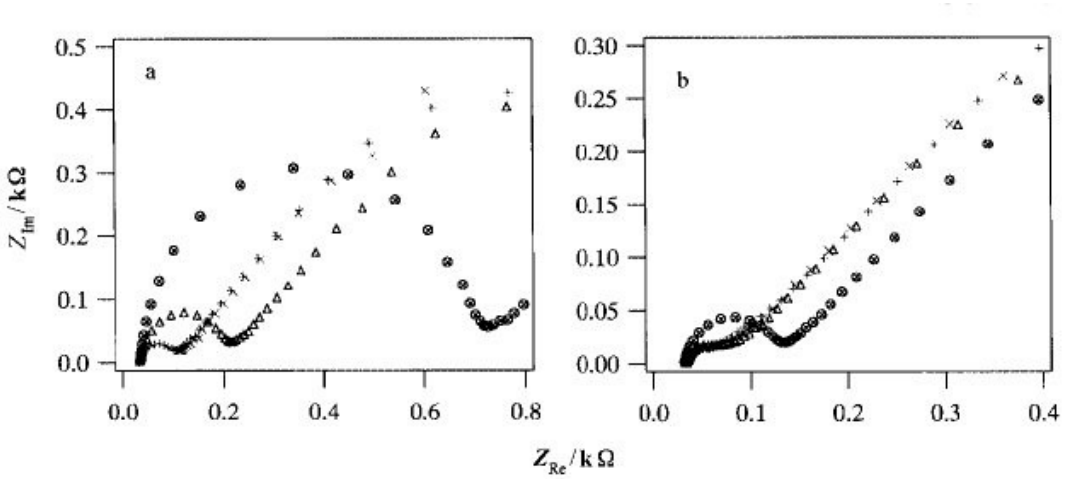

Figure 5-2. Example of impedance plots after preconditioning. Screen-printed carbon sensors preconditioned in a saturated NA2Co3 solution for: a) 30s; b) 5 minutes with different applied potentials: ⊗) 1.2; Δ) 1.4; ×)1.6V; +) 2.0V. Image taken from Cui *et al.*, 2001 and reproduced with the permission of The Royal Society of Chemistry.

The carbon sensors used in the suspension experiments had very high impedances compared with the Ag-AgCl sensors and therefore preconditioning of the carbon surfaces was investigated to modify the electrode surface and reduce this impedance. Carbon tipped sensors were also investigated as their shorter length of carbon meant they had lower impedance characteristics before preconditioning.

5.4.1 Selection of carbon sensor type

Initially the preconditioning was performed with cyclic voltammetry which appeared to modify the impedance behaviour of the carbon tipped sensors on acetate (C-tip-acetate) more than the carbon sensors on acetate (C-acetate) (Tables 4-1 and 4-2). Initially the C-tip-acetate was selected for the preconditioning experiments, however conversion on to the polyethylene substrate (-PE300) highlighted a number of issues. The current manufacturing method was unable to accurately reproduce sensors with the same length of carbon tip before the silver track started plus a thinner layer of carbon was being deposited on the polyethylene substrate.

The consequences of this were a wide variation in the impedance behaviour between sensors (Figure 4-4). The length of the carbon tip was related to the initial impedance before preconditioning, the longer the tip the higher the track resistance and hence impedance. The carbon ink had a high resistance per millimetre and hence a very small difference in length could cause a large difference in resistance. A higher starting impedance meant a higher impedance after preconditioning as well.

In addition to the lack of consistency between individual sensors the preconditioning of the C-tip-acetate sensors was causing the depth of the carbon tip to decrease which caused the impedance at higher frequencies to increase (Figure 4-3). The thinner depth of carbon tip on the polyethylene substrate exaggerated this increase in impedance. Given these findings the carbon tipped sensors were abandoned and efforts concentrated on pure carbon sensors.

5.4.2 Analysis of carbon preconditioning

The preconditioning procedure was modified to use a square-wave which would provide more energy per time as it is always at its maximum voltage. Also the equipment to produce a square-wave is simpler than for cyclic voltammetry which has implications for commercial manufacturing procedures. The parameters time, voltage, period and media type were investigated to find the optimum impedance behaviour.

The scanning electron microscope (SEM) micrographs (Figure 4-7) before and after preconditioning of pure carbon sensors show that the honeycomb structure was removed to leave the surface a uniform roughness. The honeycomb structure was probably caused by the mesh that the ink passes through in the screen printing process, leaving its imprint on the ink. The changes in the surface structure affect the impedance characteristics and modelling the data with an equivalent circuit provides an interpretation of this effect (Table 4-5). The CPE_d component in the equivalent circuit models the diffusion processes. The preconditioning changes the diffusion characteristics of the system. The CPE_d is related to a capacitor and has two values: the CPE_d-T value is a measure of the reactance and is effected by surface area, distance and permittivity of materials; and the CPE_d-P value is a measure of how close the component is to a real capacitor, hence is a measure of the leakage current.

In the optimum preconditioning procedure the CPE_d-T value increased by 9.58×10^{-6}, hence the surface area must increase or the distance must decrease. The CPE_d-P decreased by 0.19 due to the preconditioning, implying that more diffusion is occurring and transporting the charge carriers to the electrode. The more uniform roughness after preconditioning could decrease the distance and allow more diffusion as illustrated in Figure 5-3.

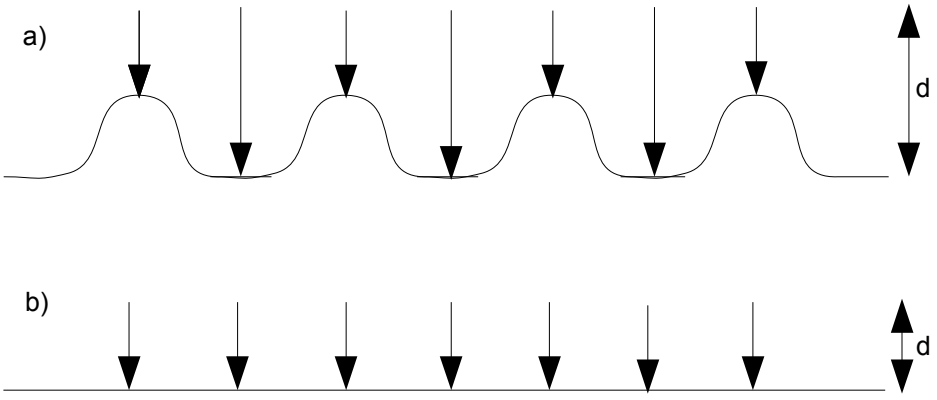

Figure 5-3. Diffusion length change caused by preconditioning. Arrows represent the diffusion and d the diffusion distance. The smooth line for the surface structure does not imply the actual surface was smooth.

The optimum preconditioning was achieved when the correct level of energy was delivered to remove the honeycomb structure and no more. Removing more carbon would reduce the thickness of the electrode and increase the impedance of the electrodes. The time and voltage parameters of the preconditioning procedure control the energy delivered to the electrode. Therefore too low a voltage or too short a time will not provide sufficient energy while too high a voltage or too long a time will remove too much carbon. This is shown in the results with the impedance decreasing and then increasing as the voltage and time were increased (Table 4-3).

The effect of the period of the square-wave was limited except at the optimum of 120s. Too short a period may reduce the build up of energy in the carbon while too long a period causes the electrode surface to be worn down quicker. The Mueller-Hinton broth (MHB) created a lower impedance than the KCl on the C-PE300-v2 sensors. This could be related to molecules becoming adsorbed on to the surface or absorbed though any pores in the surface. These molecules would allow easier transfer of charge from the liquid to the electrode.

5.4.3 Conclusion of carbon preconditioning

Electrochemical preconditioning is a simple way to alter the impedance characteristics of the carbon sensors. The impedance component caused by diffusional processes was reduced by the preconditioning procedure. The impedance behaviour of the carbon electrode in Cui *et al.* (2001) after preconditioning appeared to be a trade off between the impedance of the double layer and the diffusional processes. In comparison the preconditioning procedure described in this thesis reduced the impedance component caused by the diffusional processes and had little effect on the double layer impedance. It is unclear which would be the optimum impedance behaviour for the detection of biofilms because changes due to bacteria were seen in both the double layer impedance and the diffusional processes (Figures 4-36 and 4-37).

5.5 Biofilm growth with different sensor types

A study of the growth of biofilms on the Ag-AgCl sensors and on the preconditioned carbon sensors was conducted to find the level of biofilm growth on the electrodes. The formation of biofilms on sensors (without impedance measurements) was analysed with an alamarBlue assay and imaged using confocal laser scanning microscopy with a LIVE/DEAD *Bac*Light stain. The *Bac*Light experiments were repeated, this time with impedance measurements at the start and end for Ag-AgCl sensors and every hour for carbon sensors to find whether the impedance measurements affected the growth of bacteria.

5.5.1 The alamarBlue assay

Various methods have been employed to quantify biofilms including: dry weight of biofilm (Apilanez *et al.*, 1998); removal of biofilm by sonication and subsequent plate counting (Benard *et al.*, 2009); digital counting from microscopy images (Harris *et al.*, 2004); percentage surface coverage (Kinnari *et al.*, 2008); and XXT assays (Smith & Hunter, 2008). The alamarBlue assay was developed for antimicrobial susceptibility testing (Baker *et al.*, 1994) and has been used to quantitatively evaluate the proliferation of bacteria in a number of studies (Baker & Tenover, 1996); (Collins & Franzblau, 1997); (Hugo *et al.*, 1991); (McBride *et al.*, 2005). In the biofilm experiments the alamarBlue assay was used to semi-quantify the proliferation of bacteria on the electrode surfaces against the control surfaces.

A limitation of the alamarBlue assay was it did not account for the position of cells on the surface, for example were the bacteria on the top or bottom sides of the polyethylene substrates. This was clearly shown when comparing the results from surfaces grown in the petri dish with those grown in the 24-well plates (Figure 4-9). The alamarBlue reduction with the control surfaces from the 24-well plates indicated that there should have had a greater number of cells than the control surfaces from the petri dishes. However, the microscopy images did not appear to show an obvious increase in cell numbers. Therefore the 24-well plates may have forced more of the

bacteria to grow on the underside of the surfaces due to the smaller surface area of the well. Alternatively the cells from the 24-well plates were in a different metabolic state and metabolised the alamarBlue dye at a faster rate.

5.5.2 Confocal laser scanning microscopy

The confocal laser scanning microscopy with the LIVE/DEAD *Bac*Light stain allowed the position of the cells to be visualised, the structure of the biofilms to be studied, and determined whether the cells were alive or dead. The diversity of biofilms was described in Section 1.1.3 and it was expected that a three-dimensional biofilm would grow on the control surface, the polyethylene substrate. An example of a dense *Staphylococcus aureus* biofilm is illustrated in Figure 5-4.

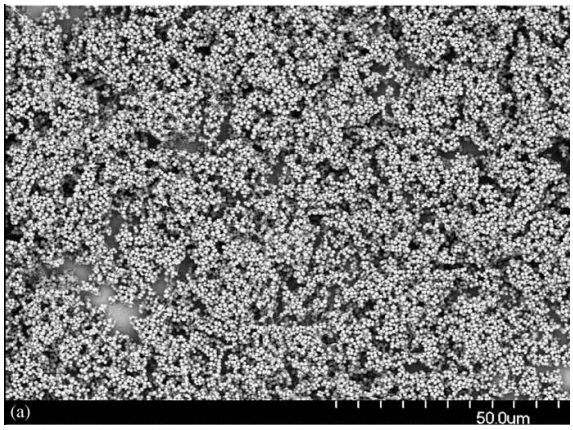

Figure 5-4. An example of a *Staphylococcus aureus* biofilm on a smooth titanium surface. The scale bar represents 50μm. Image taken from Harris *et al.*, 2004 and reproduced with the permission of Elsevier.

The methodology used in these biofilm experiments had a number of limitations. The large surface areas being examined, 169mm^2 for the square surface and 14mm^2 for two electrode tips are vast areas to scan under the microscope. Therefore it would seem likely that it would be possible to easily miss certain features. A small volume of liquid remained on the surface which could have contained loose bacteria, hence the number of washes was increased for the carbon sensor experiments. When there were very few bacteria in view the auto-exposure of the microscope equipment was configured very high and this often caused the computer software to stall, hence no

image was possible. It was found near the end of the experiments that in some cases the exposure could be set manually and still achieve a good image. Many of the Ag-AgCl sensor images were of poor quality due to electrostatic forces making a small volume of excess liquid into micro-droplets on the electrode surface. This caused the light to bend and blur the images.

In addition to these minor issues the quantification of the bacteria numbers or the area they covered was not performed since the images clearly show there was a large scale variation across the surfaces and between surfaces. Extrapolating this data to quantify either the surface area or the electrode area would lead to a meaningless answer since the ratio of dense to sparse areas was unknown. Visual scanning of the surfaces with the microscope showed that there were probable more sparse areas than dense areas.

5.5.3 Biofilm growth on polyethylene control surfaces

The *Staphylococcus aureus* strains, SA081 and SA082, were grown with the polyethylene substrate as a control (Figures 4-15 and 4-16). After 24 hours and 48 hours the base of the petri dish and the controls were covered with a set of round colonies all equidistant from each other. However these colonies remained in the liquid when the surfaces were removed and even disintegrated into a suspension. The images indicated that there were high density monolayers and a few three-dimensional towers, particularly after 48 hours compared with 24 hours. The controls in the 24-well plates contained more clusters of bacteria and cluster chains. None of the micrographs showed a dense three-dimensional structure across a large surface area.

Similar biofilms with confluent growth areas containing dense cell clumps and areas containing few cells have been observed on polymer surfaces. For example, a *Staphylococcus aureus* biofilm on a titanium surface coated in polyethylene glycol (Harris *et al.*, 2004) and the SA082 strain on the polyethylene control surface are illustrated in Figure 5-5. The bacteria on the coating of polyethylene glycol formed clumps that were 10 to 50μm wide that were irregularly spaced across the surface

(Harris *et al.*, 2004). The clumps after 24 hours of growth were not too dissimilar to the clumps after only 2 hours and it was suggested that there were few sites for initial attachment and there was not a great proliferation of cells after attachment or that weakly attached bacteria were washed off the surface during the rinsing stage before the images were captured.

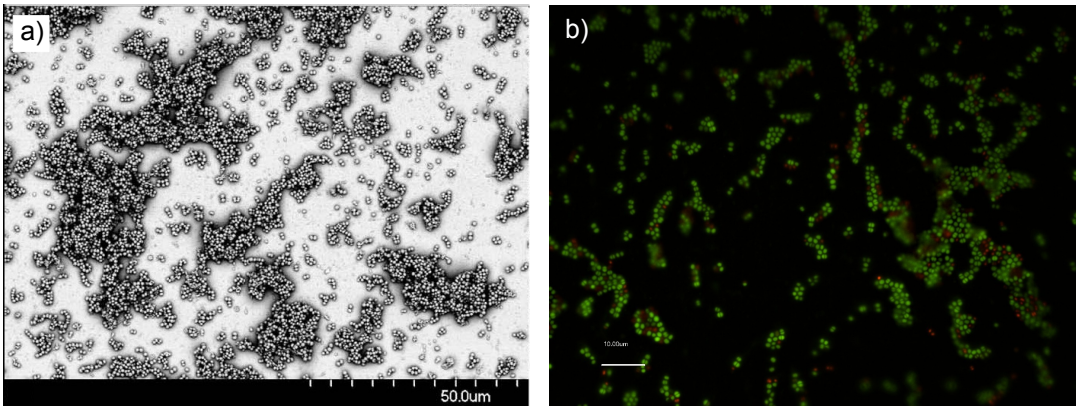

Figure 5-5. Comparison of *Staphylococcus aureus* biofilms on polymer surfaces: a) Titanium surface with polyethylene glycol coating after 24 hours and the scale bar represents 50µm. Image taken from Harris *et al.*, 2004 and reproduced with the permission of Elsevier; b) SA082 on the control surface after 48 hours and the scale bar represents 10µm.

The clumps on the polyethylene control surface were 2 to 30µm wide, however they appeared to be only in a monolayer unlike on the polyethylene glycol coating. Smith and Hunter (2008) grew biofilms for 24 hours and also only achieved monolayers with *Staphylococcus aureus*. The ability of different strains to grow biofilms on stainless steel, polyethylene and glass was also examined, finding that some strains produced better biofilms than others. Other studies grew biofilms for a week to produce significant biofilms (Muñoz-Berbel *et al.*, 2006) or required glucose in the media to produce biofilms several micrometers thick (Boles & Horswill, 2008). Therefore there are a number of possible explanations for the lack of a dense three dimensional biofilm on the control surfaces. Firstly *Staphylococcus aureus* can form biofilms containing only clusters and therefore a dense layer of cells to form should not always be expected. Secondly the bacterial strains used may have had poor biofilm capabilities, the ability to form biofilms may have been lost through

subculturing (Cook *et al.*, 2000b) or a longer time may have been required to allow the maturation of the biofilm. Finally the environmental conditions may not have been suitable.

5.5.4 Biofilm growth on Ag-AgCl sensors

The numbers of bacteria in the petri dishes multiplied and formed visible colonies on the base of the petri dish similarly to the control surfaces. However the colonies were not visible on the Ag-AgCl electrode tips. The colonies on the edges of the surface containing the electrode tip were removed in the washing process. The mean values from the alamarBlue assay with Ag-AgCl sensors indicated a nearly 40% decrease in cell numbers compared with the controls (Figure 4-8). A decrease was expected given the previous growth reduction in the suspension experiments. The decrease was probably not more than 40% due to the bacteria on the rest of the sensor surface away from the actual electrodes and possibly on the reverse side of the surface. There was no statistical significant difference between the control and sensor surfaces which is related to the variation in bacteria adhered to individual surfaces.

The micrographs from the confocal laser scanning microscopy clearly show very little growth on the actual electrode tips (Figures 4-15 to 4-18). There were very few cells and more dead cells on the electrode tips with and without impedance measurements. The bacteria must be most likely sensing the presence of the silver or silver chloride and deciding to grow elsewhere in the petri dish. The lack of cell coverage on the electrode has implications for the use of Ag-AgCl electrodes in a detection system because to produce a detectable impedance change requires the electrode interface to be altered by the presence of cells.

As previous described in Section 5.1.2 silver ions can have a biocidal effect on bacteria. Studies in vitro have also shown that surfaces that release silver ions can reduce bacterial adhesion and the formation of biofilms (Ahearn *et al.*, 1995); (Ewald *et al.*, 2006) while bacteria can adhere to surfaces that do not readily release silver ions and this is often followed by death of a proportion of the cells (Ahearn *et al.*, 1995); (Cook *et al.*, 2000b). Studies in vivo of the ability of silver coated medical

devices to reduce bacterial adherence and the subsequent infection have had contrasting outcomes. There have been reports of reductions in infection rates with silver impregnated cuffs on catheters (Boswald *et al.*, 1999); (Maki *et al.*, 1988) and also no statistical differences were found in infection rates with or without silver impregnated cuffs (Babycos *et al.*, 1993); (Dahlberg *et al.*, 1995). Possible explanations for the surfaces not reducing colonisation include the silver ions are released rapidly and then the biofilms form (Ewald *et al.*, 2006), the length of time catheters are in place in vivo is generally longer than in vitro tests which allows the biofilms to grow slowly over time or the in vivo biological fluids, for example chloride ions, inactive the silver (Gupta *et al.*, 1998).

The possibility of a biofilm forming on a surface containing silver with the correct environmental conditions is important for the development of the infection monitor. In an actual wound the Ag-AgCl sensors may not inhibit the bacteria as they did with the in vitro experiments described in this thesis and create a repeatable and reliable change in the impedance due to the biofilm formation. The next step in the development process could be to create an in vitro environment that mimics the actual wound conditions to re-test the formation of biofilms on the Ag-AgCl sensors.

5.5.5 Impedance analysis of the Ag-AgCl sensors with biofilms

Impedance measurements at the start and end of the experiments for both the control and the bacterial cultures were very similar (Figure 4-25). This was also evident in the frequencies that the peaks occurred at (Table 4-6) with there being no significant differences. In the biofilm experiments with Ag-AgCl sensors impedance measurements were only performed at the start and after 48 hours to reduce the possibility of enhanced growth inhibition by the measurements as possibly observed in the suspension experiments (Figure 3-31). This made it more difficult to interpret the physical processes over time as the change between the start and end may have occurred gradually or in a short time frame.

Differences in the impedance and normalised impedance profiles of the *Staphylococcus aureus* strain SA082 with the Ag-AgCl sensors occurred in comparison to the control system, MHB-only and the SA081 strain (Figure 4-24 to 4-26). There were significant differences between the peaks of SA082 and MHB-only in both the magnitude and reactance peaks (Table 4-6). However there were overlapping frequencies between the frequency ranges which would make them potentially unreliable in a detection system. The most prominent difference appeared in the normalised phase angle trace where the MHB-only and the strain SA081 had two peaks, the first between 0.2 and 1.2Hz, and the second between 9.5 to 37.8Hz. The strain SA082 had only the second peak (Figure 4-26). It was not apparent in the micrographs that the strain SA082 had a greater number of cells than SA081 on the surface that might account for these impedance differences.

The differences in the impedance profiles between strains may be related to proteins or other organic molecules. It has been shown that proteins that are absorbed onto electrode surfaces can effect the interface impedance. A variety of effects have been reported and the differences are probably related to the methods employed. Insulin adsorption onto a platinum electrode decreased the charge transfer resistance due to the oxidation processes (Wright *et al.*, 2004). Human serum albumin and immunoglobulin G adsorption onto a gold electrode formed a proteinaceous layer which decreased the interface capacitance and increased the charge transfer resistance as electron transfer was blocked (Moulton *et al.*, 2004). A variety of proteins adsorbed onto gold-plated copper, stainless steel and platinum electrodes caused the capacitance to increase and the charge transfer to decrease as the protein concentration increased (Smiechowski *et al.*, 2006).

It has been reported that lineages of *Staphylococcus aureus* have a unique combination of surface proteins (Sung *et al.*, 2008) and there are differences between the expression and secretion of proteins (Sibbald *et al.*, 2006). Therefore one possible explanation to the differences seen in the impedance profiles is that the two strains are producing different proteins which are affecting the interface impedance in

different ways. Other possibilities are that each sensor had to be connected manually to the impedance equipment which may have caused the loose bacteria in the dishes to be stirred up, creating a dense cell concentration in the vicinity of the electrodes.

The hypothesis of the impedance profiles producing unique signature traces for the absence and presence of a biofilm was based on the assumption that with a dense biofilm the interface of the electrode with the fluid becomes the biofilm. The lack of cell coverage on the electrodes meant that this expected change in impedance profiles was less likely to occur. The discernible differences observed with one of the *Staphylococcus aureus* strains suggests that the detection of bacteria with Ag-AgCl sensors by electrical impedance techniques is still achievable and also it might detect a low number of cells. As discussed in Section 5.5.4 the wound environment may create conditions more suitable for biofilm growth which in turn would increase the likelihood of signature traces from multiple strains of *Staphylococcus aureus*.

5.5.6 Biofilm growth on carbon sensors

The presence of visible colonies of the two *Staphylococcus aureus* strains on the carbon electrode tips was in contrast to the lack of visible colonies on the Ag-AgCl sensors, however these colonies were also removed in the washing process. The alamarBlue assay indicated that there was no statistical significant differences between the *Staphylococcus aureus* controls and the carbon sensors (Figure 4-13). The micrographs from the confocal laser scanning microscopy agreed with both the control and sensor surfaces containing a large number of cell clusters or cluster chains (Figures 4-19 to 4-22). This implies that the carbon probably does not inhibit the growth of these bacteria and the reasons for the lack of a dense biofilm are similarly to those described for the control surface, the polyethylene surface, in Section 5.5.3.

In contrast the NCTC11964 did not form colonies on the control surfaces or the sensor surfaces and more cells remained suspended in the liquid. The alamarBlue assay indicates that the carbon surfaces had a statistical significant difference on the numbers of bacteria on the sensor surface compared with the control (Figure 4-13).

The micrographs showed that very few cells formed on either the control or the sensor surfaces (Figure 4-23). All the data suggests that this strain of *Staphylococcus epidermidis* was probably poor at adhering to surfaces and forming biofilms.

As for the polymer surfaces described in Section 5.5.3, clumps of staphylococci species have been observed on carbon surfaces with examples illustrated in Figure 5-6. On three types of heart valve leaflets made of pyrolytic carbon there were clumps of *Staphylococcus aureus* in confluent growth areas and significant cell free areas (Benard *et al.*, 2009). Small clumps of *Staphylococcus aureus* on an amorphous carbon surface were observed after only 90 minutes (Kinnari *et al.*, 2008) and *Staphylococcus epidermidis* formed bacterial aggregations with extracellular matrix on an amorphous carbon surface, however their were very few cell numbers (Katsikogianni *et al.*, 2006). *Staphylococcus aureus* has also been shown to be more adherent when compared to *Staphylococcus epidermidis* on a polymer-like carbon coating on polyethylene terephthalate (Wang *et al.*, 2004) and on pyrolytic carbon heart valve leaflets (Kinnari *et al.*, 2008).

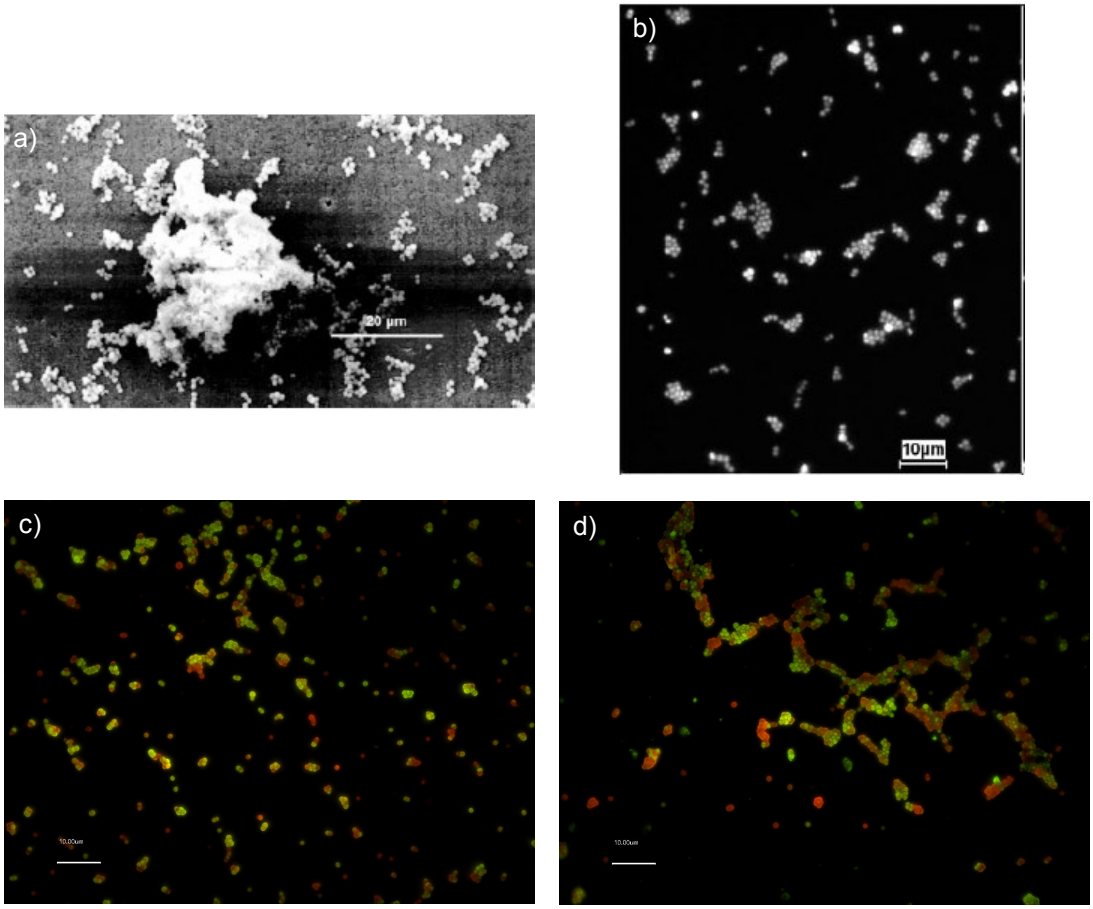

Figure 5-6. Comparison of *Staphylococcus aureus* biofilms on carbon surfaces: a) Two days old biofilm developed on silicon pyrolytic carbon heart valve leaflet from St Jude Medical. The scale bar represents 20µm. Image taken from Benard *et al.*, 2009 and reproduced with the permission of John Wiley and Sons; b) Cells attached to a diamond-like carbon surface after 90 minutes. The scale bar represents 10µm. Image taken from Kinnari *et al.*, 2008 and reproduced with the permission of John Wiley and Sons; c) and d) SA082 on carbon electrode tip of a C-PE300-v2 sensor surface after 48 hours. The scale bar represents 10µm.

Similarly to the polymer surfaces *Staphylococcus aureus* may form biofilms in aggregated clumps rather than a dense uniform layer on carbon surfaces. Again in an actual wound the adhered bacteria on the carbon electrodes might proliferate more and increase the surface coverage which would be better for detection purposes by electrical impedance techniques.

5.5.7 Impedance analysis of the carbon sensors with biofilms

The impedance profiles and normalised impedance profiles over frequency show differences between the *Staphylococcus aureus* strain SA081 and the control system, MHB-only. The strain SA082 and the *Staphylococcus epidermidis* strain NCTC11964 appeared very similar to the MHB-only data. This difference in the profiles was noticeable in the reactance peak whose magnitude decreases initially and then increased in all five separate SA081 cultures whereas in the MHB-only, SA082 and NCTC11964 the peak increased steadily over time (Figures 4-29 and 4-30). The normalised phase profiles and resistance profiles of SA081 clearly showed that the relative changes of the magnitudes of their peaks changed in opposite directions to the controls and other strains (Figures 4-31 to 4-34).

The cells of strain NCTC11964 were not attaching to the sensors as observed by the turbid media and the lack of cells in the micrographs. The most probably explanation is that this strain has been subcultured too much and has lost the ability to adhere to surfaces (Cook *et al.*, 2000b). As previously described in Section 5.5.5 a discernible difference in the impedance profiles is less likely to occur when cell coverage of the electrodes is low, hence the similarities between the MHB-only and the NCTC11964 traces.

The *Staphylococcus aureus* strain SA082 with Ag-AgCl sensors had distinct impedance profiles compared with the controls, where as with the carbon sensors it was the strain SA081. Firstly a difference in cell coverage of the electrodes might cause a difference given that there was a critical density in the suspension experiments. The micrographs in Section 4.4.2 indicate that the SA081 cells probably have a better coverage and less of them were dead compared to SA082. The cell coverage might have been enhanced by the proliferation of loose colonies on the surface of the electrodes, however loose colonies occurred in both strains which makes it less likely that these colonies had an effect on the different impedance profiles.

The evidence that other factors are involved is that the changes in the impedance profiles of SA081 are evident within the first few hours of the experiments. This is probable too early for a substantial difference in cell coverage between the strains unless the SA081 had a faster adhesion rate. If this was the case you might expect a similar change in the impedance profiles of SA082 to occur later which did not happen.

Other possible explanations for the differences include the ones described for the Ag-AgCl sensors. The two strains might be producing different proteins and the SA081 proteins have a enhanced interaction with the carbon electrodes compared with SA082 proteins. There may be evidence of this in the equivalent circuit modelling where the double layer resistance R_{dl1} of SA081 decreases for the first 24 hours compared with increases in the SA082 cultures and control system (Figure 4-36). A decrease in the charge transfer resistance due to protein adsorption has been reported (Smiechowski *et al.*, 2006); (Wright *et al.*, 2004). Another difference between the strains may be the composition of the extracellular matrix. Studies have suggested the *Staphylococcus aureus* extracellular matrix consists of proteins, DNA and polysaccharide (Boles & Horswill, 2008); (Izano *et al.*, 2008); (Mann *et al.*, 2009); (O'Neill *et al.*, 2007) or ones that are not reliant on polysaccharides (Boles *et al.*, 2010); (O'Neill *et al.*, 2007). The microscopy of the biofilms on the sensors did not investigate the presence of the extracellular matrix and therefore it is unknown whether the two strains produced different extracellular matrices.

A non-biological explanation for the different profiles may have been caused by the sensors themselves where the electrodes used in the SA081 experiments had a lower track resistance which could have been under a critical threshold where detection was possible. The mean track resistances were 10.7kΩ for SA081, 11.9kΩ for SA082, 14.0kΩ for NCTC11964 and 12.7kΩ for MHB. The electrodes used for the SA082 and NCTC11964 were marginally higher than those used in the SA081.

Comparison of the frequencies that the peaks occurred at in the impedance profiles of the biofilm experiments with carbon sensors was difficult due to the relationship between the starting frequency and the final frequency. As stated in Section 4.4.3 the SA081 samples had higher final frequencies of the reactance peak than the control system, however the starting frequencies were also higher. Therefore it was concluded that there were no significant differences in the frequencies of the peaks between the media only and all the strains of bacteria. Similarly to the suspension experiments the comparison of the impedance profiles over time might provide a more reliable method for detecting the presence of bacteria, as a supposed to the frequency of the peaks within the profiles.

The equivalent circuit modelling of the carbon sensors provided further information on the physical processes occurring within the cultures. The component of interest is the CPE_d which models the diffusional processes at the electrode interface. The general trend in the CPE_d values in all experiments was a decrease for the CPE_d-T value and increase for the CPE_d-P value (Figure 4-37). These changes could be caused by the the leakage of the pseudo-capacitance reducing due to the adsorption of molecules onto the electrode surface or redox reactions reducing the number of molecules involved in the diffusion. The change in the CPE_d-T is linked to the change in the CPE_d-P, for example the adsorption of molecules could change the surface area or distance involved in the pseudo-capacitance.

There were discernible differences in the CPE_d-T and CPE_d-P values over time in all fifteen cultures containing bacteria and in none of the media only cultures. There was a rise for a number of hours in the CPE_d-T value with a corresponding dip in the CPE_d-P value (Figure 4-37). There are a number of possible suggestions for the cause of these directional changes in the CPE_d values. Firstly the change is related to the growth of bacteria and could be due to the increase in ions or metabolic products that are produced during growth. The process reduces and stops when the bacteria reach their maximum density. Alternatively it is related to the proliferation of the cell colonies on the surface of the electrodes until they reach their maximum density, however it was not visually obvious whether this occurred with the strain

NCTC11964 strain. The importance of this highlights that equivalent circuit modelling of the impedance data over time from carbon electrodes can differentiate between the absence and presence of bacterial growth. This technique also appears to be valid for multiple species and strains.

5.5.8 Biofilm experiment conclusion

The biofilm experiments were performed to investigate the growth of biofilms on the sensors and any corresponding changes in the impedance measurements. This is important for the detection of bacteria in a wound because evidence is increasing on the formation of biofilms in wounds (Deva *et al.*, 2007); (James *et al.*, 2008); (Kirketerp-Moller *et al.*, 2008). Biofilms are the natural growth structure in other ecosystems and therefore a sensor in an actual wound may well become covered with a biofilm. This could result in a discernible change in the impedance measurements and indicate the presence of a biofilm or that there are significant levels of bacteria in the wound.

The main finding from the microscopy was that the bacteria appeared not to dense biofilms on any of the surfaces tested, the polyethylene substrate, the Ag-AgCl electrodes or the carbon electrodes. Very few cells were adhered to the Ag-AgCl electrodes, most probably due to the bacteria preferring to grow elsewhere. On the polyethylene surface and on the carbon surfaces cell clusters and cell cluster chains formed, possibly adhered to edges or fissures on the surfaces. As discussed in Sections 5.5.4 and 5.5.6 *Staphylococcus aureus* strains can form biofilms with dense cell clusters and sparse areas. Therefore the cell coverage of SA081 and SA082 on the surfaces studied were not too distance from some mature biofilm structures except that the clusters were not three dimensional structures.

The lack of a significant cell coverage of the sensors has implications for impedance measurements. The potential for discernible differences increases as the cell coverage increases across the sensor as it becomes the interface of the electrode. Muñoz-Berbel *et al.* (2007) showed that changes within equivalent circuit modelling components due to the bacterial adhesion of cell densities above $1x10^4$ CFU ml^{-1}

were related to attachment time and cell concentration. Therefore the impedance technique is capable of detecting relatively small concentration of bacteria within a short time frame. This was seen as the impedance measurements indicated that despite the lack of cell coverage both types of sensor have the potential to detect the presence of bacteria.

The downside was that only one of the *Staphylococcus aureus* strains produced discernible differences on each of the electrode types. For the Ag-AgCl sensor, SA082 produced a different normalised phase profile compared with the control system. Confusingly it was the strain SA081 which produced discernible differences, particularly in the normalised phase and resistance, with the carbon sensors. A detection system for wounds would have to work reliably for all strains, however these results highlight that a good cell coverage may not be necessary for indicating the presence of bacteria. This could be important in an actual wound as the biofilms that form reside in the wound bed, not particularly attached to a well-defined solid surface (James *et al.*, 2008); (Kirketerp-Moller *et al.*, 2008). In addition to the attachment the bacteria may form dense clusters in wounds, as illustrated in Figure 5-7. This means the sensors probably require the ability to detect clusters rather than dense layers of bacteria. The bacteria in wound biofilms may also proliferate more readily and negate the issues of inhibition by the Ag-AgCl sensors and only detecting certain strains.

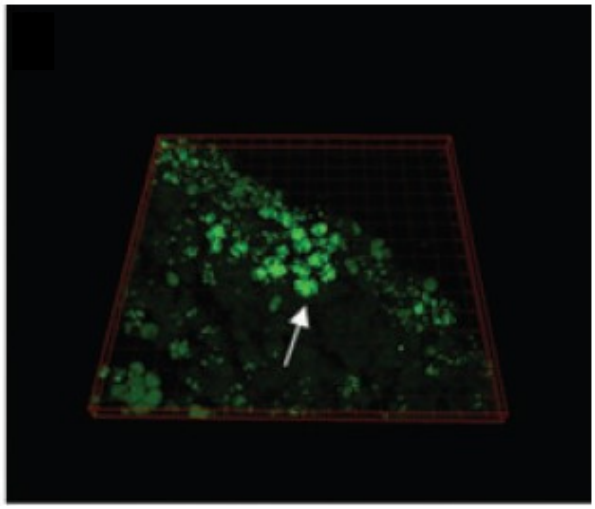

Figure 5-7. *Pseudomonas aeruginosa* in a tissue biopsy from an infected chronic wound. The arrow points at bacterial aggregates. Image taken from Werthen *et al.*, 2010 and reproduced with the permission of John Wiley and Sons.

Biofilms can be monitored by impedance as shown by Dheilly *et al.,* (2008). The resistance increased during biofilm growth and maturation of *Pseudomonas aeruginosa* and then decreased as the biofilm detached. The circuit modelling with carbon sensors also showed that the growth of bacteria can be monitored, however it is unclear whether this was due to bacterial adhesion or the proliferation of loose bacteria. This study on biofilms has shown that impedance measurements can monitor the presence of bacteria and that for the specific application of monitoring for infection in wounds a more realistic wound environment is required to test the sensors. It would also be valuable to select a strain that creates a substantial biofilm and one that does not to compare the ability of the sensors to monitor different scenarios.

5.6 Conclusion

The care of wounds is costly and time-consuming. Bacteria infect wounds and delay healing by changing the chemical balance within wounds. This increases wound costs, decreases patient welfare and is generally a significant burden on society. One of the major difficulties in wound management is that it is necessary to remove dressings to check for potential infections which leads to an increased risk of contamination by bacteria. If an infection is suspected then the general treatment begins with removal of the dead tissues to allow sampling of the base of the wound. Broad spectrum antibiotics may be given at this stage while the sample is processed. Samples are cultured and reports issued stating the main species of bacteria present and a semi-quantitative indication of the growth level between light to heavy. This allows treatment to be adjusted to target the bacteria present.

One of the main areas of research to improve wound management focuses on faster techniques to detect bacteria from the samples. The three main contenders are microfludic devices with biosensors, electronic noses and molecular techniques. Electronic noses show promise firstly in detecting the presence of bacteria (Aathithan *et al.*, 2001); (Parry *et al.*, 1995) and secondly in differentiating common pathogens in single species cultures (Lai *et al.*, 2002); (Trincavelli *et al.*, 2010). The main limitation foreseen in a detection system for wound samples is the ability to differentiate species in cultures containing multiple species. If this is not possible, then the individual species would have to be isolated from the sample which would significantly increase the time for detection. The other issue with the electronic noses is that the equipment is currently not small or portable (Lai *et al.*, 2002), which would mean the samples would have to be processed in a laboratory rather than at point of care.

There are a vast number of different types of biosensors each with their own advantages and disadvantages. The main advantage is their speed with possible detection of 1000 CFU ml^{-1} within 40 minutes (Gau *et al.*, 2001). A possible disadvantage is that many use antibodies that target specific species and therefore are

not designed for samples of multiple species. Also many require a strict procedure to be followed including washing steps. This might require the use of a laboratory and technical expertise. To provide a point of care device for a wound would require a device that accepts samples taken from the wounds and processes them to provide information on the bacterial contents of the sample. These types of devices may be possible in the future with microfluidic devices containing the sensors and related processes (Lazcka *et al.*, 2007). In general the main difficulty with these technologies is converting laboratory ideas into commercial products (Deisingh & Thompson, 2004).

Molecular techniques will probably become the most useful technology because of their ability to differentiate between species within a single device due to their unique genes (Deisingh & Thompson, 2002). This would require preprocessing to extract the DNA and therefore currently would not be a point of care device. In terms of wound management the main disadvantage of all these technologies is that they all require samples from wounds. As previously stated this requires wound dressing to be removed which damages healing tissues and increases the risk of infection.

The advantage of the real-time infection monitor for wounds described in this thesis would be that it could be placed underneath the wound dressing, monitor for bacteria and provide information directly at the point of care. Screen-printed electrodes are easy and cheap to manufacture and can be created on flexible materials suitable for use on the body. Electrical impedance techniques require no additional chemicals to create a response, provide significant information with a single measurement and are relatively easy to perform. This thesis has presented the methods, findings and conclusions of the preliminary study of an infection monitor for wounds using screen-printed sensors and electrical impedance techniques.

The objectives of this project were to investigate the potential use of electrical impedance in detecting bacteria, indicating bacterial levels and differentiating species. The main achievement is the discovery that screen-printed Ag-AgCl sensors produce signature impedance traces at cell densities greater than $5x10^7$ CFU ml^{-1} for

a number of strains of *Staphylococcus aureus* in suspension. This indicates that this technique has potential for detecting the absence and presence of bacteria. The impedance traces produced using screen-printed Ag-AgCl and carbon sensors were also shown to have potential in detecting the presence or adhesion of bacteria in stationary fluids. More relevant results could be obtained by creating an artificial wound environment, which may allow the formation of a more significant biofilm, to test the sensor capabilities. The growth of a number of different species of bacteria can be monitored by equivalent circuit modelling.

Some indication of bacterial levels was achieved as only bacteria in excess of $5x10^7$ CFU ml^{-1} can be detected in suspension. Equivalent circuit modelling can indicate when the bacteria are proliferating above this density and when the proliferation slows. The ability to differentiate multiple species present at one time was not fully investigated because of the limited growth in the biofilm experiments.

In terms of an infection monitor for wounds the implications of these results are that the detection and indication of bacterial levels are still achievable. For an effective addition to wound management the impedance data obtained from an infection monitor would have to be related to the semi-quantitative swab results that indicate the bacterial growth levels from light (1+) to profuse (4+), as described in Section 5.3.4. An even more beneficial addition to wound management would be to relate the data to the four levels of infection defined by the European Wound Management Association and listed in Table 1-4 (European Wound Management Association (EWMA), 2006). Each level of infection has a treatment strategy and if the infection monitor could indicate these levels then the treatment could be selected before the dressing is removed. This in turn would reduce costs, improve the management of wounds and most importantly increase the well-being of the patient. This will rely upon finding a relationship between these growth levels or infection stages and the percentage surface coverage of the biofilm on the electrodes.

At this stage in the development of an infection monitor for wounds it is too early to tell whether it could differentiate species and if it could, whether it would be reliable with biofilms containing multiple species. Once a wound was defined as infected a sample would still have to be taken to discover the anti-susceptibilities of the species to enable the correct antibiotics to be given. Therefore if the infection monitor could detect the species it may well enhance the speed of identification and anti-susceptibility by the hospital microbiology laboratory.

5.6.1 Future work

Suggestions for future work are:

- Adapt the conditions or bacteria to produce three-dimensional biofilms.
- Miniaturise the electrodes to increase the probability that the bacteria would cover the electrode, resulting in an impedance change.
- Create an array of miniature sensors which would also increase the probability of detecting bacteria in low density clusters.
- Investigate alternative species commonly isolated in wounds, for example *Pseudomonas aeruginosa* and streptococci species.

If these suggestions were successful in detecting the bacteria then a portable instrument to perform the measurements in vivo and provide a clear indication of the condition of the wound to the patient or carer could be developed. The Ag-AgCl sensors had an inhibiting effect on the bacteria at low cell densities which could be utilised in alternative applications that require electrodes to be kept clean from biofouling or reduce the levels of bacteria. A further alternative line of research would be to investigate the combination of the moisture sensor with a bacterial reduction facility.

References

Aathithan, S., Plant, J.C., Chaudry, A.N., French, G.L. (2001) 'Diagnosis of bacteriuria by detection of volatile organic compounds in urine using an automated headspace analyzer with multiple conducting polymer sensors.' *Journal of Clinical Microbiology*. **39**(7):2590-2593.

Abdel-Hamid, I., Ivnitski, D., Atanasov, P., Wilkins, E. (1999) 'Highly sensitive flow-injection immunoassay system for rapid detection of bacteria.' *Analytica Chimica Acta*. **399**(1-2):99-108.

Abu Al-Soud, W., Radstrom, P. (1998) 'Capacity of nine thermostable DNA polymerases to mediate DNA amplification in the presence of PCR-inhibiting samples.' *Applied and Environmental Microbiology*. **64**(10):3748-3753.

Ahearn, D.G., May, L.L., Gabriel, M.M. (1995) 'Adherence of organisms to silver-coated surfaces.' *Journal of Industrial Microbiology*. **15**(4):372-376.

Amos, A.F., McCarty, D.J., Zimmet, P. (1997) 'The rising global burden of diabetes and its complications: estimates and projections to the year 2010.' *Diabetic Medicine*. **14**(S5):S7-S85.

Apilanez, I., Gutierrez, A., Diaz, M. (1998) 'Effect of surface materials on initial biofilm development.' *Bioresource Technology*. **66**(3):225-230.

Appelgren, P., Bjornhagen, V., Bragderyd, K., Jonsson, C.E., Ransjo, U. (2002) 'A prospective study of infections in burn patients.' *Burns*. **28**(1):39-46.

Babycos, C.R., Barrocas, A., Webb, W.R. (1993) 'A prospective randomized trial comparing the silver-impregnated collagen cuff with the bedside tunneled subclavian catheter.' *Journal of parenteral and enteral nutrition*. **17**(1):61-63.

Baker, C.N., Banerjee, S.N., Tenover, F.C. (1994) 'Evaluation of alamar colorimetric MIC method for antimicrobial susceptibility testing of Gram-negative bacteria.' *Journal of Clinical Microbiology*. **32**(5):1261-1267.

Baker, C.N., Tenover, F.C. (1996) 'Evaluation of alamar colorimetric broth microdilution susceptibility testing method for staphylococci and enterococci.' *Journal of Clinical Microbiology*. **34**(11):2654-2659.

Bard, A.J., Faulkner, L.R. (2001) 'Electrochemical methods: Fundamentals and applications.' 2nd edition. Wiley.

Benard, L., Litzler, P.Y., Cosette, P., Lemeland, J.F., Jouenne, T., Junter, G.A. (2009) 'Proteomic analysis of *Staphylococcus aureus* biofilms grown in vitro on mechanical heart valve leaflets.' *Journal of Biomedical Materials Research Part A*. **88A**(4):1069-1078.

Bishop, S.M., Walker, M., Roger, A.A., Chen, W.Y.J. (2003) 'Importance of moisture balance at the wound-dressing interface.' *Journal of Wound Care*. **12**(4):125-128.

Bjarnsholt, T., Kirketerp-Moller, K., Jensen, P.O., Madsen, K.G., Phipps, R., Krogfelt, K., Hoiby, N., Givskov, M. (2008) 'Why chronic wounds will not heal: a novel hypothesis.' *Wound Repair and Regeneration*. **16**(1):2-10.

Blaedel, W.J., Jenkins, R.A. (1974) 'Steady-state votammetry at glassy carbon electrodes.' *Analytical Chemistry*. **46**(13):1952-1955.

Blaedel, W.J., Mabbott, G.A. (1978) 'Pyrolytic carbon-film electrode.' *Analytical Chemistry*. **50**(7):933-936.

Bockris, J.O., Reddy, A.K.N. (1970) 'Modern electrochemistry. An introduction to an interdisciplinary area.' 1st edition. London Macdonald & Co.

Bodenstein, M., David, M., Markstaller, K. (2009) 'Principles of electrical impedance tomography and its clinical application.' *Critical Care Medicine*. **37**(2):713-724.

Boles, B.R., Horswill, A.R. (2008) 'Agr-mediated dispersal of *Staphylococcus aureus* biofilms.' *PLOS Pathogens*. **4**(4):e1000053.

Boles, B.R., Thoendel, M., Roth, A.J., Horswill, A.R. (2010) 'Identification of genes involved in polysaccharide-independent *Staphylococcus aureus* biofilm formation.' *PLOS One*. **5**(4):e10146.

Boswald, M., Lugauer, S., Regenfus, A., Braun, G.G., Martus, P., Geis, C., Scharf, J., Bechert, T., Greil, J., Guggenbichler, J.P. (1999) 'Reduced rates of catheter-associated infection by use of a new silver-impregnated central venous catheter.' *Infection*. **27**(S1):S56-S60.

Bowler, P.G., Davies, B.J. (1999) 'The microbiology of infected and noninfected leg ulcers.' *International Journal of Dermatology*. **38**(8):573-578.

Bowler, P.G., Duerden, B.I., Armstrong, D.G. (2001) 'Wound microbiology and associated approaches to wound management.' *Clinical Microbiology Reviews*. **14**(2):244-269.

Bragg, P.D., Rainnie, D.J. (1974) 'Effect of silver ions on respiratory-chain of *Escherichia-coli*.' *Canadian Journal of Microbiology*. **20**(6):883-889.

Breidenbach, W.C., Trager, S. (1995) 'Quantitative culture technique and infection in complex wounds of the extremities closed with free flaps.' *Plastic and Reconstructive Surgery*. **95**(5):860-865.

Bridier, A., Dubois-Brissonnet, F., Boubetra, A., Thomas, V., Briandet, R. (2010) 'The biofilm architecture of sixty opportunistic pathogens deciphered using a high throughput CLSM method.' *Journal of Microbiological Methods*. **82**(1):64-70.

Brook, I., Frazier, E.H. (1998) 'Aerobic and anaerobic microbiology of chronic venous ulcers.' *International Journal of Dermatology*. **37**(6):426-428.

Brown, M.R.W., Williams, P. (1985) 'The influence of environment on envelope properties affecting survival of bacteria in infections.' *Annual Review of Microbiology*. **39**(1):527-556.

Cady, P. (1975) 'Rapid automated bacterial identification by impedance measurement.' In *New approaches to the identification of microorganisms*. Heden, C. & Illeni, T. (Eds.). p73-99.

Casalinuovo, I.A., Di Pierro, D., Coletta, M., Di Francesco, P. (2006) 'Application of electronic noses for disease diagnosis and food spoilage detection.' *Sensors*. **6**(11):1428-1439.

Chaby, G., Senet, P., Vaneau, M., Martel, P., Guillaume, J.C., Meaume, S., Teot, L., Debure, C., Dompmartin, A., Bachelet, H., Carsin, H., Matz, V., Richard, J.L., Rochet, J.M., Sales-Aussias, N., Zagnoli, A., Denis, C., Guillot, B., Chosidow, O. (2007) 'Dressings for acute and chronic wounds - A systematic review.' *Archives of Dermatology*. **143**(10):1297-1304.

Chin, G.A., Diegelmann, R.F., Schultz, G.S. (2005) 'Cellular and molecular regulation of wound healing.' In *Wound healing*. Falabella, A.F. & Kirsner, R.S. (Eds.). p17-37.

Church, D., Elsayed, S., Reid, O., Winston, B., Lindsay, R. (2006) 'Burn wound infections.' *Clinical Microbiology Reviews*. **19**(2):403-434.

Clement, J.L., Jarrett, P.S. (1994) 'Antibacterial silver.' *Met Based Drugs*. **1**(5-6):467-482.

Cole, K.S. (1928) 'Electric impedance of suspension of spheres.' *Journal of General Physiology*. **12**(1):29-36.

Cole, K.S. (1932) 'Electric phase angle of cell membranes.' *Journal of General Physiology*. **15**(6):641-649.

Collins, L.A., Franzblau, S.G. (1997) 'Microplate alamar blue assay versus BACTEC 460 system for high-throughput screening of compounds against Mycobacterium tuberculosis and Mycobacterium avium.' *Antimicrobial Agents and Chemotherapy*. **41**(5):1004-1009.

Cook, H., Stephens, P., Davies, K.J., Harding, K.G., Thomas, D.W. (2000a) 'Defective extracellular matrix reorganization by chronic wound fibroblasts is associated with alterations in TIMP-1, TIMP-2, and MMP-2 activity.' *Journal of Investigative Dermatology*. **115**(2):225-233.

Cook, G., Costerton, J.W., Darouiche, R.O. (2000b) 'Direct confocal microscopy studies of the bacterial colonization in vitro of a silver-coated heart valve sewing cuff.' *International journal of antimicrobial agents*. **13**(3):169-173.

Cooper, R., Lawrence, J. (1996) 'The prevalence of bacteria and implications for infection control.' *Journal of Wound Care*. **5**(6):291-295.

Costerton, J.W., Geesey, G.G., Cheng, G.K. (1978) 'How bacteria stick.' *Scientific American*. **238**(1):86-95.

Costerton, J.W., Stewart, P.S., Greenberg, E.P. (1999) 'Bacterial biofilms: A common cause of persistent infections.' *Science*. **284**(5418):1318-1322.

Costerton, W., Veeh, R., Shirtliff, M., Pasmore, M., Post, C., Ehrlich, G. (2003) 'The application of biofilm science to the study and control of chronic bacterial infections.' *Journal of Clinical Investigation*. **112**(10):1466-1477.

Crowther, J.R. (2001) 'The ELISA guidebook.' 2nd edition. Humana Press.

Cui, G., Yoo, J.H., Lee, J.S., Yoo, J., Uhm, J.H., Cha, G.S., Nam, H. (2001) 'Effect of pre-treatment on the surface and electrochemical properties of screen-printed carbon paste electrodes.' *Analyst*. **126**(8):1399-1403.

Cunliffe-barnes, T. (1945) 'Healing rate of human skin determed by measurement of the electrical potential of experimental abrasions.' *American Journal of Surgery*. **69**(1):82-88.

Dahlberg, P.J., Agger, W.A., Singer, J.R., Yutuc, W.R., Newcomer, K.L., Schaper, A., Rooney, B.L. (1995) 'Subclavian hemodialysis catheter infections - a prospective, randomized trial of an attachable silver-impregnated cuff for prevention of catheter-related infections.' *Infection control and hospital epidermiology*. **16**(9):506-511.

Daltrey, D.C., Rhodes, B., Chattwood, J.G. (1981) 'Investigation into the microbial-flora of healing and non-healing decubitus ulcers.' *Journal of Clinical Pathology*. **34**(7):701-705.

Dang, C.N., Prasad, Y.D.M., Boulton, A.J.M., Jude, E.B. (2003) 'Methicillin-resistant *Staphylococcus aureus* in the diabetic foot clinic: a worsening problem.' *Diabetic Medicine*. **20**(2):159-161.

Davies, C.E., Hill, K.E., Newcombe, R.G., Stephens, P., Wilson, M.J., Harding, K.G., Thomas, D.W. (2007) 'A prospective study of the microbiology of chronic venous leg ulcers to reevaluate the clinical predictive value of tissue biopsies and swabs.' *Wound Repair and Regeneration*. **15**(1):17-22.

Deisingh, A.K., Thompson, M. (2002) 'Detection of infectious and toxigenic bacteria.' *Analyst*. **127**(5):567-581.

Deisingh, A.K., Thompson, M. (2004) 'Biosensors for the detection of bacteria.' *Canadian Journal of Microbiology*. **50**(2):69-77.

Deva, A.K., Ngo, Q., Vickery, K. (2007) 'Role of bacterial biofilms in chronic wounds.' *Wound Repair and Regeneration*. **15**(6):A149.

Dheilly, A., Linossier, I., Darchen, A., Hadjiev, D., Corbel, C., Alonso, V. (2008) 'Monitoring of microbial adhesion and biofilm growth using electrochemical impedancemetry.' *Applied microbiology and biotechnology*. **79**(1):157-164.

Dobson, C.B., Archibald, A.R. (1978) 'Effect of specific growth limitations on cell wall composition of *Staphylococcus aureus* H.' *Archives of Microbiology*. **119**(3):295-301.

Donlan, R.M. (2002) 'Biofilms: Microbial life on surfaces.' *Emerging Infectious Diseases*. **8**(9):881-890.

Dowd, S.E., Sun, Y., Secor, P.R., Rhoads, D.D., Wolcott, B.M., James, G.A., Wolcott, R.D. (2008) 'Survey of bacterial diversity in chronic wounds using pyrosequencing, DGGE, and full ribosome shotgun sequencing.' *BMC Microbiology*. **8**(43):1-15.

Drew, P.J., Posnett, J., Rusling, L. (2007) 'The cost of wound care for a local population in England.' *International Wound Journal*. **4**(2):149-155.

Eden, G., Eden, R. (1984) 'Enumeration of microorganisms by their dynamic AC conductance patterns.' *IEEE Transactions on Biomedical Engineering*. **31**(2):193-198.

Edwards-Jones, V., Foster, H.A. (2002) 'Effects of silver sulphadiazine on the production of exoproteins by *Staphylococcus aureus*.' *Journal of Medical Microbiology*. **51**(1):50-55.

Ewald, A., Gluckermann, S.K., Thull, R., Gbureck, U. (2006) 'Antimicrobial titanium/silver PVD coatings on titanium.' *Biomedical Engineering Online*. **5**(22):1-10.

European Wound Management Association (EWMA) (2004) 'Position document: Wound bed preparation in practice.' London, MEP Ltd. p1-5.

European Wound Management Association (EWMA) (2006) 'Position Document: Management of wound infection.' London: MEP Ltd. p1-6.

Falanga, V. (1993) 'Chronic Wounds - Pathophysiologic and experimental considerations.' *Journal of Investigative Dermatology*. **100**(5):721-725.

Felice, C.J., Valentinuzzi, M.E., Vercellone, M.I., Madrid, R.E. (1992) 'Impedance bacteriometry - Medium and interface contributions during bacterial-growth.' *IEEE Transactions on Biomedical Engineering*. **39**(12):1310-1313.

Felice, C.J., Valentinuzzi, M.E. (1999) 'Medium and interface components in impedance microbiology.' *IEEE Transactions on Biomedical Engineering*. **46**(12):1483-1487.

Feng, Q.L., Wu, J., Chen, G.Q., Cui, F.Z., Kim, T.N., Kim, J.O. (2000) 'A mechanistic study of the antibacterial effect of silver ions on *Escherichia coli* and *Staphylococcus aureus*.' *Journal of Biomedical Materials Research*. **52**(4):662-668.

Firstenberg-Eden, G., Eden, G. (1984) 'Impedance microbiology.' 1st edition. Wiley, New York.

Flanagan, M. (2003) 'The philosophy of wound bed preparation in clinical practice.' Smith and Nephew Medical. p1.

Flemming, H.C., Wingender, J. (2010) 'The biofilm matrix.' *Nature Reviews Microbiology*. **8**(9):623-633.

Foster, K., Schwan, H. (1989) 'Dielectric properties of tissues and biological materials: A critical review.' *Critical Reviews in Biomedical Engineering*. **17**(1):25-104.

Foulds, I.S., Barker, A.T. (1983) 'Human-skin battery potentials and their possible role in wound-healing.' *British Journal of Dermatology*. **109**(5):515-522.

Frolund, B., Palmgren, R., Keiding, K., Nielsen, P.H. (1996) 'Extraction of extracellular polymers from activated sludge using a cation exchange resin.' *Water Research*. **30**(8):1749-1758.

Gadepalli, R., Dhawan, B., Sreenivas, V., Kapil, A., Ammini, A.C., Chaudhry, R. (2006) 'A clinico-microbiological study of diabetic foot ulcers in an Indian tertiary care hospital.' *Diabetes Care*. **29**(8):1727-1732.

Garcia-Aljaro, C., Muñoz-Berbel, X., Muñoz, F.J. (2009) 'On-chip impedimetric detection of bacteriophages in dairy samples.' *Biosensors and bioelectronics*. **24**(6):1712-1716.

Gardner, S.E., Frantz, R.A., Schmidt, F.L. (1999) 'Effect of electrical stimulation on chronic wound healing: a meta-analysis.' *Wound Repair and Regeneration*. **7**(6):495-503.

Gau, J.J., Lan, E.H., Dunn, B., Ho, C.M., Woo, J.C.S. (2001) 'A MEMS based amperometric detector for *Escherichia coli* bacteria using self-assembled monolayers.' *Biosensors and Bioelectronics*. **16**(9-12):745-755.

Ghandour, W., Hubbard, J.A., Deistung, J., Hughes, M.N., Poole, R.K. (1988) 'The uptake of silver ions by *Escherichia-coli*-K12 - Toxic effects and interaction with copper ions.' *Applied Microbiology and Biotechnology*. **28**(6):559-565.

Goldstein, E.J.C., Citron, D.M., Nesbit, C.A. (1996) 'Diabetic foot infections. Bacteriology and activity of 10 oral antimicrobial agents against bacteria isolated from consecutive cases.' *Diabetes Care*. **19**(6):638-641.

Gomez, R., Bashir, R., Sarikaya, A., Ladisch, M.R., Sturgis, J., Robinson, J.P., Geng, T., Bhunia, A.K., Apple, H.L., Wereley, S. (2001) 'Microfludic biochip for impedance spectroscopy of biological species.' *Biomedical Microdevices*. **3**(3):201-209.

Gomez, R., Bashir, R., Bhunia, A.K. (2002) 'Microscale electronic detection of bacterial metabolism.' *Sensors and Actuators B-Chemical*. **86**(2-3):198-208.

Gonon, F.G., Fombarlet, C.M., Buda, M.J., Pujol, J.F. (1981) 'Electrochemcial treatement of pyrolytic carbon-fiber electrodes.' *Analytical Chemistry*. **53**(9):1386-1389.

Gordois, A., Scuffham, P., Shearer, A., Oglesby, A. (2003) 'The healthcare costs of diabetic peripheral neuropathy in the UK.' *The Diabetic Foot*. **6**(2):62-73.

Griffiths, H., Thornton, K., Clements, C., Burge, T., Kay, A., Young, A. (2006) 'The cost of a hot drink scald.' *Burns*. **32**(3):372-374.

Gupta, A., Maynes, M., Silver, S. (1998) 'Effects of halides on plasmid-mediated silver resistance in *Escherichia coli*.' *Applied and Environmental Microbiology*. **64**(12):5042-5045.

Hagan, D. (1990) 'Electrical measurement of bacterial-growth.' *Process Biochemistry*. **25**(1):R4-R5.

Harding, K.G., Morris, H.L., Patel, G.K. (2002) 'Science, medicine, and the future - Healing chronic wounds.' *British Medical Journal*. **324**(7330):160-163.

Harris, C.M., Kell, D.B. (1985) 'The estimation of microbial biomass.' *Biosensors*. **1**(1):17-84.

Harris, C.M., Todd, R.W., Bungard, S.J., Lovitt, R.W., Morris, J.G., Kell, D.B. (1987) 'Dielectric permittivity of microbial suspensions at radio frequencies - a novel method for the real-time estimation of microbial biomass.' *Enzyme and Microbial Technology*. **9**(3):181-186.

Harris, L.G., Tosatti, S., Wieland, M., Textor, M., Richards, R.G. (2004) '*Staphylococcus aureus* adhesion to titanium oxide surfaces coated with non-functionalized and peptide-functionalized poly(L-lysine)-grafted-poly(ethylene glycol) copolymers.' *Biomaterials*. **25**(18):4135-4148.

Hasan, A., Murata, H., Falabella, A., Ochoa, S., Zhou, L., Badiavas, E., Falanga, V. (1997) 'Dermal fibroblasts from venous ulcers are unresponsive to the action of transforming growth factor-beta 1.' *Journal of Dermatological Science*. **16**(1):59-66.

Hause, L.L., Komorowski, R.A., Gayon, F. (1981) 'Electrode and electrolyte impedance in the detection of bacterial-growth.' *Annals of Internal Medicine*. **28**(5):403-410.

Hemington-Gorse, S.J., Potokar, T.S., Drew, P.J., Dickson, W.A. (2009) 'Burn care costing: the Welsh experience.' *Burns*. **35**(3):378-382.

Heym, B., Rimareix, F., Lortat-Jacob, A., Nicolas-Chanoine, M.H. (2004) 'Bacteriological investigation of infected pressure ulcers in spinal cord-injured patients and impact on antibiotic therapy.' *Spinal Cord*. **42**(4):230-234.

Higuchi, R., Dollinger, G., Walsh, P.S., Griffith, R. (1992) 'Simultaneous amplification and detection of specific DNA-sequences.' *Bio-technology*. **10**(4):413-417.

Hope, T.A., Iles, S.E. (2004) 'Technology review: The use of electrical impedance scanning in the detection of breast cancer.' *Breast Cancer Research*. **6**(2):69-74.

Hopf, H.W., Ueno, C., Aslam, R., Burnand, K., Fife, C., Grant, L., Holloway, A., Iafrati, M.D., Mani, R., Misare, B., Rosen, N., Shapshak, D., Slade, J.B., West, J., Barbul, A. (2006) 'Guidelines for the treatment of arterial insufficiency ulcers.' *Wound Repair and Regeneration*. **14**(6):693-710.

Health Protection Agency (2006) 'Susceptibility testing.' National Standard Method BSOP 45 Issue 2. http://www.hpastandardmethods.org.uk/pdf_sops.asp

Health Protection Agency (2008) 'Introduction of the preliminary identification of medically important bacteria.' National Standard Method BSOPID 1 Issue 1.4. http://www.hpastandardmethods.org.uk/pdf_sops.asp

Health Protection Agency (2009a) 'Investigation of skin, superficial and non-surgical wound swaps.' National Standard Method BSOP 11 Issue 5. http://www.hpastandardmethods.org.uk/pdf_sops.asp

Health Protection Agency (2009b) 'Investigation of abscessses and deep-seated wound infections.' National Standard Method BSOP 14 Issue 5. http://www.hpastandardmethods.org.uk/pdf_sops.asp

Hugo, E.R., McLaughlin, W.R., Oh, K.H., Tuovinen, O.H. (1991) 'Quantitative enumeration of acanthamoeba for evaluation of cyst inactivation in contact-lens care solutions.' *Investigative Ophthalmology and Visual Science*. **32**(3):655-657.

Illingworth, C.M., Barker, A.T. (1980) 'Measurement of electrical currents emerging during the regeneration of amputed fingertips in children.' *Clinical Physics And Physiological Measurement*. **1**(1):87-89.

Izano, E.A., Amarante, M.A., Kher, W.B., Kaplan, J.B. (2008) 'Differential roles of poly-N-acetylglucosamine surface polysaccharide and extracellular DNA in *Staphylococcus aureus* and *Staphylococcus epidermidis* biofilms.' *Applied and Environmental Microbiology*. **74**(2):470-476.

James, G.A., Swogger, E., Wolcott, R., Pulcini, E.D., Secor, P., Sestrich, J., Costerton, J.W., Stewart, P.S. (2008) 'Biofilms in chronic wounds.' *Wound Repair and Regeneration*. **16**(1):37-44.

Jensen, P.O., Bjarnsholt, T., Phipps, R., Rasmussen, T.B., Calum, H., Christoffersen, L., Moser, C., Williams, P., Pressler, T., Givskov, M., Hoiby, N. (2007) 'Rapid necrotic killing of polymorphonuclear leukocytes is caused by quorum-sensing-controlled production of rhamnolipid by *Pseudomonas aeruginosa*.' *Microbiology-SGM*. **153**():1329-1338.

Johnstone, C.C., Farley, A., Hendry, C. (2007) 'The physiological basics of wound healing.' *Nursing Standard*. **22**(9):Suppl: 3-10.

Jung, W.K., Koo, H.C., Kim, K.W., Shin, S., Kim, S.H., Park, Y.H. (2008) 'Antibacterial activity and mechanism of action of the silver ion in *Staphylococcus aureus* and *Escherichia coli*.' *Applied and Environmental Microbiology*. **74**(7):2171-2178.

Kaltenboeck, B., Wang, C. (2005) 'Advances in real-time PCR: Application to clinical laboratory diagnostics.' *Advances in Clinical Chemistry*. **40**(1):219-259.

Karatan, E., Watnick, P. (2009) 'Signals, regulatory networks, and materials that build and break bacterial biofilms.' *Microbiology and Molecular Biology Reviews*. **73**(2):310-347.

Katsikogianni, M., Spiliopoulou, I., Dowling, D.P., Missirlis, Y.F. (2006) 'Adhesion of slime producing *Staphylococcus epidermidis* strains to PVC and diamond-like carbon/silver/fluorinated coatings.' *Journal of Materials Science-Materials in Medicine*. **17**(8):679-689.

Kell, D.B., Davey, C.L. (1990) 'Conductimetric and impedimetric devices.' In *Biosensors: a practical approach*. Cass, A.E. (Ed.). p125-154.

Kingsley, A. (2001) 'A proactive approach to wound infection.' *Nursing Standard*. **15**(30):50-58.

Kinnari, T.J., Soininen, A., Esteban, J., Zamora, N., Alakoski, E., Kouri, V.P., Lappalainen, R., Konttinen, Y.T., Gomez-Barrena, E., Tiainen, V.M. (2008) 'Adhesion of staphylococcal and Caco-2 cells on diamond-like carbon polymer hybrid coating.' *Journal of Biomedical Materials Research Part A*. **86A**(3):760-768.

Kirketerp-Moller, K., Jensen, P.O., Fazli, M., Madsen, K.G., Pedersen, J., Moser, C., Tolker-Nielsen, T., Hoiby, N., Givskov, M., Bjarnsholt, T. (2008) 'Distribution, organization, and ecology of bacteria in chronic wounds.' *Journal of Clinical Microbiology*. **46**(8):2717-2722.

Kloth, L.C. (2005) 'Electrical stimulation for wound healing: a review of evidence from in vitro studies, animal experiments, and clinical trials.' *International Journal of Lower Extremity Wounds*. **4**(1):23-44.

Knutson, H.J., Carr, M.A., Branham, L.A., Scott, C.B., Callaway, T.R. (2006) 'Effects of activated charcoal on binding *E-coli* O157 : H7 and Salmonella typhimurium in sheep.' *Small Ruminant Research*. **65**(1-2):101-105.

Kuehn, B.M. (2007) 'Chronic wound care guidelines issued.' *JAMA-Journal of the American Medical Association*. **297**(9):938-939.

Kumar, S., Ashe, H., Fernando, D.J. (1994) 'The prevalence of foot ulceration and its correlates in Type 2 diabetic patients: a population study.' *Diabetic Medicine*. **11**(5):480-483.

Lai, S.Y., Deffenderfer, O.F., Hanson, W., Phillips, M.P., Thaler, E.R. (2002) 'Identification of upper respiratory bacterial pathogens with the electronic nose.' *Laryngoscope*. **112**(6):975-979.

Lazcka, O., Del Campo, F.J., Muñoz, F.X. (2007) 'Pathogen detection: A perspective of traditional methods and biosensors.' *Biosensors and Bioelectronics*. **22**(7):1205-1217.

Lee, S.H., Park, T.H. (2010) 'Recent advances in the development of bioelectronic nose.' *Biotechnology and Bioprocess Engineering*. **15**(1):22-29.

Levine, N.S., Lindberg, R.B., Mason, A.D., Pruitt, B.A. (1976) 'The quantitative swab culture and smear: a quick, simple method for determining the number of viable aerobic bacteria on open wounds..' *Journal of Trauma-Injury Infection & Critical Care*. **16**(2):89-94.

Lim, T.S., Mwipatayi, B.P., Murray, R., Sieunarine, K., Abbas, M., Angel, D. (2006) 'Microbiological profile of chronic ulcers of the lower limb: A prospective observational cohort study.' *ANZ Journal of Surgery*. **76**(8):688-692.

Lobmann, R., Schultz, G., Lehnert, H. (2005) 'Proteases and the diabetic foot syndrome: Mechanisms and therapeutic implications.' *Diabetes Care*. **28**(2):461-471.

Louie, T.J., Bartlett, J.G., Tally, F.P., Gorbach, S.L. (1976) 'Aerobic and anaerobic bacteria in diabetic foot ulcers.' *Annals of Internal Medicine*. **85**(4):461-463.

Mack, D., Davies, A.P., Harris, L.G., Rohde, H., Horstkotte, M.A., Knobloch, J.K.M. (2007) 'Microbial interactions in *Staphylococcus epidermidis* biofilms.' *Analytical and Bioanalytical Chemistry*. **387**(2):399-408.

Maki, D.G., Cobb, L., Garman, J.K., Shapiro, J.M., Ringer, M., Helgerson, R.B. (1988) 'An attachable silver-impregnated cuff for prevention of infection with central venous catheters - a prospective randomised multicenter trial.' *American Journal of Medicine*. **85**(3):307-314.

Mangram, A.J., Horan, T.C., Pearson, M.L., Silver, L.C., Jarvis, W.R. (1999) 'Guideline for prevention of surgical site infection, 1999.' *American Journal of Infection Control*. **27**(2):97-132.

Mann, E.E., Rice, K.C., Boles, B.R., Endres, J.L., Ranjit, D., Chandramohan, L., Tsang, L.H., Smeltzer, M.S., Horswill, A.R., Bayles, K.W. (2009) 'Modulation of eDNA release and degradation affects *Staphylococcus aureus* biofilm maturation.' *PLOS One*. **4**(6):e5822.

Martini, F.H. (2006) 'Fundamentals of anatomy and physiology.' 7th edition. Pearson Benjamin Cummings.

McBride, J., Ingram, P.R., Henriquez, F.L., Roberts, C.W. (2005) 'Development of colorimetric microtiter plate assay for assessment of antimicrobials against Acanthamoeba.' *Journal of Clinical Microbiology*. **43**(2):629-634.

McColl, D., Cartlidge, B., Connolly, P. (2007) 'Real-time monitoring of moisture levels in wound dressings in vitro: an experimental study.' *International Journal of Surgery*. **5**(5):316-322.

McColl, D., MacDougall, M., Watret, L., Connolly, P. (2009) 'Monitoring moisture without disturbing the wound dressing.' *Wounds UK*. **5**(3):94-99.

Modak, S.M., Fox, C.L. (1973) 'Binding of Silver Sulfadiazine to Cellular Components of Pseudomonas-Aeruginosa.' *Biochemical Pharmacology*. **22**(19):2391-2404.

Moulton, S.E., Barisci, J.N., Bath, A., Stella, R., Wallace, G.G. (2004) 'Studies of double layer capacitance and electron transfer at a gold electrode exposed to protein solutions.' *Electrochimica Acta*. **49**(24):4223-4230.

Mousa, H.A.L. (1997) 'Aerobic, anaerobic and fungal burn wound infections.' *Journal of Hospital Infection*. **37**(4):317-323.

Muñoz-Berbel, X., Muñoz, F.J., Vigués, N., Mas, J. (2006) 'On-chip impedance measurements to monitor biofilm formation in the drinking water distribution network.' *Sensors and Actuators B-Chemical*. **118**(1-2):129-134.

Muñoz-Berbel, X., Vigués, N., Jenkins, A.T.A., Mas, J., Muñoz, F.J. (2008) 'Impedimetric approach for quantifying low bacteria concentrations based on the changes produced in the electrode-solution interface during the pre-attachment stage.' *Bioelectronics*. **23**(10):1540-1546.

Murray, P.R., Rosenthal, K.S., Pfaller, M. (2005) 'Medical microbiology.' 5th edition. Elsevier Mosby.

Naka, K., Watarai, S., Tana, Inoue, K., Kodama, Y., Oguma, K., Yasuda, T., Kodama, H. (2001) 'Adsorption effect of activated charcoal on enterohemorrhagic *Escherichia coli*.' *Journal of veterinary medical science*. **63**(3):281-285.

National Burn Care Review (2001) 'Standards and strategy for burn care: a review of burn care in the British Isles.' National Burn Care Review Committee. p3.

Neu, T.R., Manz, B., Volke, F., Dynes, J.J., Hitchcock, A.P., Lawrence, J.R. (2010) 'Advanced imaging techniques for assessment of structure, composition and function in biofilm systems.' *FEMS Microbiology Ecology*. **72**(1):1-21.

Noble, P.A. (1999) 'Hypothetical model for monitoring microbial growth by using capacitance measurements - a minireview.' *Journal of Microbiological Methods*. **37**(1):45-49.

Noble, P.A., Dziuba, M., Harrison, D.J., Albritton, W.L. (1999) 'Factors influencing capacitance-based monitoring of microbial growth.' *Journal of Microbiological Methods*. **37**(1):51-64.

O'Neill, E., Pozzi, C., Houston, P., Smyth, D., Humphreys, H., Robinson, D.A., O'Gara, J.P. (2007) 'Association between methicillin susceptibility and biofilm regulation in *Staphylococcus aureus* isolates from device-related infections.' *Journal of Clinical Microbiology*. **45**(5):1379-1388.

Olsvik, O., Popovict, T., Skjerve, E., Cudjoe, K.S., Hornes, E., Ugelstad, J., Uhlen, M. (1994) 'Magnetic separation techniques in diagnostic microbiology.' *Clinical Microbiology Reviews*. **7**(1):43-54.

Parry, A.D., Chadwick, P.R., Simon, D., Oppenheim, B., McCollum, C.N. (1995) 'Leg ulcer detection identifies beta-haemolytic streptococcal infection.' *Journal of Wound Care*. **4**(9):404-406.

Pasche, S., Angeloni, S., Ischer, R., Liley, M., Lupranoe, J., Voirin, G., Vincenzini, P.D.D. (2009) 'Wearable biosensors for monitoring wound healing.' In *Advances in science and technology. Vol. 50*. Vincenzini, P. & De Rossi, D. (Eds.). p80-87.

Percival, S.L., Bowler, P.G. (2004) 'Biofilms and. their potential role in wound healing.' *Wounds-a Compendium of Clinical Research and Practice*. **16**(7):234-240.

Percival, S.L., Bowler, P.G., Russell, D. (2005) 'Bacterial resistance to silver in wound care.' *Journal of Hospital Infection*. **60**(1):1-7.

Peromet, M., Labbe, M., Yourassowsky, E., Schoutens, E. (1973) 'Anaerobic Bacteria Isolated from Decubitus Ulcers.' *Infection*. **1**(4):205-207.

Plowman, R., Graves, N., Griffin, M.A.S., Roberts, J.A., Swan, A.V., Cookson, B., Taylor, L. (2001) 'The rate and cost of hospital-acquired infections occurring in patients admitted to selected specialties of a district general hospital in England and the national burden imposed.' *Journal of Hospital Infection*. **47**(3):198-209.

Pollack, S.V. (1984) 'The wound healing process.' *Clinics in Dermatology*. **2**(3):8-16.

Posnett, J., Franks, P.J. (2007) 'The costs of skin breakdown and ulceration in the UK. (Skin Breakdown. The silent epidemic).' Nephew Foundation. p6-12.

Prescott, L.M., Harley, J.P., Klein, D.A. (2002) 'Microbiology.' 5th edition. McGraw Hill.

Pruitt, B.A., McManus, A.T., Kim, S.H., Goodwin, C.W. (1998) 'Burn wound infections: Current status.' *World Journal of Surgery*. **22**(2):135-145.

Rayman, M.K., Sanwal, B.D., Lo, T.C.Y. (1972) 'Transport of succinate in *Escherichia-coli* .2. Characteristics of uptake and energy coupling with transport in membrane preparations.' *Journal of Biological Chemistry*. **247**(19):6332.

Reilly, J., Stewart, S., Allardice, G.A., Noone, A., Robertson, C., Walker, A., Coubrough, S. (2008) 'Results from the Scottish National HAI prevalence survey.' *Journal of Hospital Infection*. **69**(1):62-68.

Richards, J.C.S., Jason, A.C., Hobbs, G., Gibson, D.M., Christie, R.H. (1978) 'Electronic measurement of bacterial-growth.' *Journal of Physics E-Scientific Instruments*. **11**(6):560-568.

Rigaud, B., Hamzaoui, L., Frikha, M.R., Chauveau, N., Morucci, J.P. (1995) 'In-vitro tissue characterization and modeling using electrical-impedance measurements in the 100 Hz-10 MHz frequency-range.' *Physiological Measurement*. **16**(3A):A15-A28.

Rigaud, B., Morucci, J.P., Chauveau, N. (1996) 'Bioelectrical impedance techniques in medicine .1. Bioimpedance measurement - Second section: Impedance spectrometry.' *Critical Reviews in Biomedical Engineering*. **24**(4-6):257-351.

Robson, M.C., Krizek, T.J. (1973) 'Predicting skin-graft survival.' *Journal of Trauma-injury Infection and Critical Care*. **13**(3):213-217.

Robson, M.C., Duke, W.F., Krizek, T.J. (1973) 'Rapid bacterial screening in treatment of civilian wounds.' *Journal of Surgical Research*. **14**(5):426-430.

Robson, M.C., Barbul, A. (2006) 'Guidelines for the best care of chronic wounds.' *Wound Repair and Regeneration*. **14**(6):647-648.

Robson, M.C., Cooper, D.M., Aslam, R., Gould, L.J., Harding, K.G., Margolis, D.J., Ochs, D.E., Serena, T.E., Snyder, R.J., Steed, D.L., Thomas, D.R., Wiersma-Bryant, L. (2006) 'Guidelines for the treatment of venous ulcers.' *Wound Repair and Regeneration*. **14**(6):649-662.

Rosenkranz, H.S., Carr, H.S. (1972) 'Silver sulfadiazine effect on the growth and metabolism of bacteria.' *Antimicrobial Agents and Chemotherapy*. **2**(5):367-372.

Rosenkranz, H.S., Rosenkranz, S. (1972) 'Silver sulfadiazine interaction with isolated DNA.' *Antimicrobial Agents and Chemotherapy*. **2**(5):373-383.

Rowley, B.A. (1972) 'Electrical current effects on *Escherichia-coli* growth-rates.' *Proceedings of the Society for Experimental Biology and Medicine*. **139**(3):929+.

Rowley, B.A., McKenna, J.M., Chase, G.R., Wolcott, L.E. (1974) 'Influence of electrical current on an infecting microorganism in wounds.' *Annals of the New York Academy of Sciences*. **238**(Oct11):543-551.

Rutkove, S.B. (2009) 'Electrical impedance myography: Background, current state, and future directions.' M*uscle and Nerve*. **40**(6):936-946.

Safarik, I., Safarikova, M., Forsythe, S.J. (1995) 'The application of magnetic separations in applied microbiology.' *Journal of Applied Bacteriology*. **78**(6):575-585.

Santucci, S.G., Gobara, S., Santos, C.R., Fontana, C., Levin, A.S. (2003) 'Infections in a burn intensive care unit: experience of seven years.' *Journal of Hospital Infection*. **53**(1):6-13.

Schierle, C.F., De la Garza, M., Mustoe, T.A., Galiano, R.D. (2009) 'Staphylococcal biofilms impair wound healing by delaying reepithelialization in a murine cutaneous wound model.' *Wound Repair and Regeneration*. **17**(3):354-359.

Schreurs, W.J.A., Rosenberg, H. (1982) 'Effect of Silver Ions on Transport and Retention of Phosphate by Escherichia-Coli.' *Journal of Bacteriology*. **152**(1):7-13.

Schultz, G.S., Sibbald, R.G., Falanga, V., Ayello, E.A., Dowsett, C., Harding, K., Romanelli, M., Stacey, M.C., Teot, L., Vanscheidt, W. (2003) 'Wound bed preparation: a systematic approach to wound management.' *Wound Repair and Regeneration*. **11**(2):1-28.

Shedden, L., Connolly, P., 2009. World Wide Patent Application (WO/2009/136157).

Sibbald, M.J.J.B., Ziebandt, A.K., Engelmann, S., Hecker, M., de Jong, A., Harmsen, H.J.A., Raangs, G.C., Stokroos, I., Arends, J.P., Dubois, J.Y.F., van Dijl, J.A. (2006) 'Mapping the pathways to staphylococcal pathogenesis by comparative secretomics.' *Microbiology and molecular biology reviews*. **70**(3):755+.

Silley, P., Forsythe, S. (1996) 'Impedance microbiology - A rapid change for microbiologists.' *Journal of Applied Bacteriology*. **80**(3):233-243.

Silver, S., Gupta, A., Matsui, K., Lo, J. (1999) 'Resistance to Ag(I) cations in bacteria: Environments, genes and proteins.' *Metal-Based Drugs*. **6**(4-5):315-320.

Silver, S. (2003) 'Bacterial silver resistance: molecular biology and uses and misuses of silver compounds.' *FEMS Microbiology Reviews*. **27**(2-3):341-353.

Smiechowski, M.F., Lvovich, V.F., Roy, S., Fleischman, A., Fissell, W.H., Riga, A.T. (2006) 'Electrochemical detection and characterization of proteins.' *Biosensors and Bioelectronics*. **22**(5):670-677.

Smith, K., Hunter, I.S. (2008) 'Efficacy of common hospital blocides with biofilms of multi-drug resistant clinical isolates.' *Journal of Medical Microbiology*. **57**(8):966-973.

Smyth, E.T.M., McIlvenny, G., Enstone, J.E., Emmerson, A.M., Humphreys, H., Fitzpatrick, F., Davies, E., Newcombe, R.G., Spencer, R.C. (2008) 'Four country healthcare associated infection prevalence survey 2006: overview of the results.' *Journal of Hospital Infection*. **69**(3):230-248.

Sopwith, W., Hart, T., Garner, P. (2002) 'Preventing infection from useable medical equipement: a systematic review.' *BMC Infectious Diseases*. **2**(4):1-10.

Steed, D.L., Attinger, C., Colaizzi, T., Crossland, M., Franz, M., Harkless, L., Johnson, A., Moosa, H., Robson, M., Serena, T., Sheehan, P., Veves, A., Wiersma-Bryant, L. (2006) 'Guidelines for the treatment of diabetic ulcers.' *Wound Repair and Regeneration*. **14**(6):680-692.

Stewart, G.N. (1899) 'The charges produced by the growth of bacteria in the molecular concentration and electrical conductivity of culture media.' *Journal of Experimental Medicine*. **4**(2):235-243.

Stone, L.L., Dalton, H.P., Haynes, B.W. (1980) 'Bacterial debridement of the burn eshar: The in vivo activity of selected organisms.' *Journal of Surgical Research*. **29**(1):83-92.

Stoodley, P., Debeer, D., Lewandowski, Z. (1994) 'Liquid flow in biofilm systems.' *Applied and Environmental Microbiology*. **60**(8):2711-2716.

Suehiro, J., Yatsunami, R., Hamada, R., Hara, M. (1999) 'Quantitative estimation of biological cell concentration suspended in aqueous medium by using dielectrophoretic impedance measurement method.' *Journal of Physics D-Applied Physics*. **32**(21):2814-2820.

Suehiro, J., Noutomi, D., Shutou, M., Hara, M. (2003a) 'Selective detection of specific bacteria using dielectrophoretic impedance measurement method combined with an antigen-antibody reaction.' *Journal of Electrostatics*. **58**(3-4):229-246.

Suehiro, J., Shutou, M., Hatano, T., Hara, M. (2003b) 'High sensitive detection of biological cells using dielectrophoretic impedance measurement method combined with electropermeabilization.' *Sensors and Actuators B-Chemical*. **96**(1-2):144-151.

Suehiro, J., Ohtsubo, A., Hatano, T., Hara, M. (2006) 'Selective detection of bacteria by a dielectrophoretic impedance measurement method using an antibody-immobilized electrode chip.' *Sensors and Actuators B-Chemical*. **119**(1):319-326.

Sung, J.M.L., Lloyd, D.H., Lindsay, J.A. (2008) '*Staphylococcus aureus* host specificity: comparative genomics of human versus animal isolates by multi-strain microarray.' *Microbiology-SGM*. **154**():1949-1959.

Tentolouris, N., Jude, E.B., Smirnof, I., Knowles, E.A., Boulton, A.J.M. (1999) 'Methicillin-resistant *Staphylococcus aureus*: an increasing problem in a diabetic foot clinic.' *Diabetic Medicine*. **16**(9):767-771.

Tentolouris, N., Petrikkos, G., Vallianou, N., Zachos, C., Daikos, G.L., Tsapogas, P., Markou, G., Katsilambros, N. (2006) 'Prevalence of methicillin-resistant *Staphylococcus aureus* in infected and uninfected diabetic foot ulcers.' *Clinical Microbiology and Infection*. **12**(2):186-189.

Trill, H. (2006) 'Diagnostic technologies for wound monitoring.' PhD thesis. Cranfield University.

Trincavelli, M., Coradeschi, S., Loutfi, A., Soderquist, B., Thunberg, P. (2010) 'Direct identification of bacteria in blood culture samples using an electronic nose.' *IEEE Transactions on Biomedical Engineering*. **57**(12):2884-2890.

Turner, P.G., McClennan, A.G., Bates, A.D., White, M.R.H. (1997) 'Instant notes in molecular biology.' 1st edition. Bios Scientific Publisher Ltd.

Turner, A.P.F., Magan, N. (2004) 'Electronic noses and disease diagnostics.' *Nature Reviews Microbiology*. **2**(2):161-166.

Ur, A., Brown, D.F.J. (1975) 'Monitoring of bacterial activity by impedance measurements.' In *New approaches to the identification of microorganisms*. Heden, C. & Illeni, T. (Eds.). p63-71.

Vaneau, M., Chaby, G., Guillot, B., Martel, P., Senet, P., Teot, L., Chosidow, O. (2007) 'Consensus panel recommendations for chronic and acute wound dressings.' *Archives of Dermatology*. **143**(10):1291-1294.

Vindenes, H., Bjerknes, R. (1995) 'Microbial colonization of large wounds.' *Burns*. **21**(8):575-579.

Vuong, C., Saenz, H.L., Gotz, F., Otto, M. (2000) 'Impact of the agr quorum-sensing system on adherence to polystyrene in *Staphylococcus aureus*.' *Journal of Infectious Diseases*. **182**(6):1688-1693.

Wang, J., Pedrero, M., Sakslund, H., Hammerich, O., Pingarron, J. (1996) 'Electrochemical activation of screen-printed carbon strips.' *Analyst*. **121**(3):345-350.

Wang, J., Huang, N., Yang, P., Leng, Y., Sun, H., Liu, Z.Y., Chu, P.K. (2004) 'The effects of amorphous carbon films deposited on polyethylene terephthalate on bacterial adhesion.' *Biomaterials*. **25**(16):3163-3170.

Weber, S.A., Watermann, N., Jossinet, J., Byrne, J.A., Chantrey, J., Alam, S., So, K., Bush, J.O., Kane, S., McAdams, E.T. (2010) 'Remote wound monitoring of chronic ulcers.' *IEEE Transactions on Information Technology in Biomedicine*. **14**(2):371-377.

Werthen, M., Henriksson, L., Jensen, P.O., Sternberg, C., Givskov, M., Bjarnsholt, T. (2010) 'An in vitro model of bacterial infections in wounds and other soft tissues.' *APMIS*. **118**(2):156-164.

Whitney, J., Phillips, L., Aslam, R., Barbul, A., Gottrup, F., Gould, L., Robson, M.C., Rodeheaver, G., Thomas, D., Stotts, N. (2006) 'Guidelines for the treatment of pressure ulcers.' *Wound Repair and Regeneration*. **14**(6):663-679.

Wimpenny, J.W.T., Colasanti, R. (1997) 'A unifying hypothesis for the structure of microbial biofilms based on cellular automaton models.' *FEMS Microbiology Ecology*. **22**(1):1-16.

Wong, M.L., Medrano, J.F. (2005) 'Real-time PCR for mRNA quantitation.' *Biotechniques*. **39**(1):75-85.

Woodward, A.M., Jones, A., Zhang, X.Z., Rowland, J., Kell, D.B. (1996) 'Rapid and non-invasive quantification of metabolic substrates in biological cell suspensions using non-linear dielectric spectroscopy with multivariate calibration and artificial neural networks. Principles and applications.' *Bioelectrochemistry and Bioenergetics*. **40**(2):99-132.

Wright, J.E.I., Cosman, N.P., Fatih, K., Omanovic, S., Roscoe, S.G. (2004) 'Electrochemical impedance spectroscopy and quartz crystal nanobalance (EQCN) studies of insulin adsorption on Pt.' *Journal of Electroanalytical Chemistry*. **564**(1-2):185-197.